Synthrocytes:
Synthetic erythrocytes to substitute animal red blood cells in hemagglutination assays for global influenza surveillance

Ana Sánchez Cano

Doctoral Thesis

Synthrocytes:

Synthetic erythrocytes to substitute animal red blood cells in hemagglutination assays for global influenza surveillance

Ana Sánchez Cano

Director: Dr. Eva Baldrich Rubio

Tutor: Dr. Jordi Mas Gordi

Diagnostic Nanotools Group

Vall d'Hebron Research Institute

PhD program in Biotechnology

Department of Genetics and Microbiology – Faculty of Biosciences

Universitat Autònoma de Barcelona

2023

Abstract

Influenza viruses cause annually seasonal flu epidemics with an important morbidity and mortality, as well as a high economical cost worldwide. The severity of the annual influenza epidemic is proportional to the degree of immune protection of the population, which is related to the high change rate of the viral envelope of these viruses. Since annual vaccination is the main prevention measure, the high antigenic drift obliges to the annual reformulation of the vaccine composition. Accordingly, global virological surveillance of circulating influenza viruses is required in order to collect genetic and antigenic information necessary to determine the vaccine composition yearly, a task that is coordinated globally by the World Health Organization (WHO) and to which laboratories from all over the world contribute.

The hemagglutination inhibition assay (HAI) is one of the methods recommended by the WHO for the antigenic characterization of circulating influenza viruses and for the titration of specific neutralizing antibodies (Ab) against them, two tasks that are crucial for the annual recommendation of the vaccine composition. HAI is based on the fact that influenza binds to red-blood cells producing their agglutination and changing their sedimentation pattern, a behaviour that is prevented in the presence of specific anti-influenza Ab. HAI is a relatively simple and economical assay, but it has to be carried out with fresh erythrocytes. This is a biological reagent that is variable, unstable and difficult to obtain in large quantities for worldwide distribution, and that is acquired independently by each laboratory, which introduces lots of intra- and inter-laboratory variability in the results produced.

The main objective of this PhD Thesis was the development of a synthetic reagent that could substitute animal erythrocytes in the HAI assays. As it will be shown, a reagent called "**synthrocyte**" has been developed, which mimics the differential sedimentation displayed by animal RBCs in the absence and in the presence of agglutinating agents in <25 min. By the end of this Thesis work, synthrocytes could bind the 4 influenza seasonal subtypes (A(H1N1)pdm09, A(H3N2), B/Yamagata and B/Victoria), producing changes in sedimentation that resembled those generated by erythrocytes in 30-60 min, and entailing a protocol and level of handling similar to those in classical HAI assays. Moreover, synthrocytes were reproducible and more stable than their animal counterparts, could be lyophilized for long-term storage, and were mass-producible.

This work laid the first stone for the creation of a new research line that has continued beyond this Thesis with the contribution of other Team Members. We envisage that the results summarized here, and those that followed and will follow, will pave the way to achieve the worldwide standardization of HAI tests with minimal equipment or training requirements and facilitate inter-laboratory result evaluation.

Agradecimientos

Si pudiese dedicar tan solo unas palabras a cada una de las personas que han contribuido a que esta tesis sea posible, éste sería sin duda el capítulo más largo. Con esta tesis he aprendido muchas cosas, científica y personalmente, pero sin duda las lecciones más importantes me las llevo de las personas que habéis caminado a mi lado durante este (a veces duro) camino. No puedo resumir todos los recuerdos y experiencias que he vivido durante estos años en estas pocas páginas, pero siempre estaréis en mi memoria y corazón, formando parte de lo que soy hoy en día.

Quiero empezar estos agradecimientos con mi lab, “mi DINA”. Han sido muchas horas juntos en nuestro pequeño rincón, trabajando al máximo y filosofando entre centrífugas. Hemos compartido muchísimas aventuras, alegrías y frustraciones, que con vuestra compañía siempre se viven mejor.

Por supuesto, a Eva, mi directora, por todo su apoyo y guía durante estos años. Gràcies per confiar en mi per dur a terme aquest projecte tan maco anomenat sintròcit. Per convertir-me en una millor científica i ensenyar-me tantes coses, tot i que m’hagi resistit a l’electroquímica. Per la teva paciència infinita amb els meus deadlines extensibles i les planificacions impossibles, per ajudar-me a convertir els contratemps en oportunitats i ensenyar-me una altra forma de veure les coses.

A todo el Team Sintrocito. A Erica, por ser la primera en acompañarme en la aventura y darle más color a este proyecto y a todo el mundo que tuviera la suerte de estar cerca de ti. A María, por aportar ese toque de calma y realidad que a veces nos hace falta. A Hari, por ser un soplo de aire fresco con tu inagotable energía y cariño. Este proyecto no podría estar en mejores manos.

Al resto de compañeros del lab, A Judit (tot i que per mi sempre seràs team sintròcit), per preocupar-te sempre d’alimentar-me bé. A Gisela, por mostrarme que se puede alcanzar velocidad supersónica haciendo ensayos con partículas magnéticas y por dejarme formar parte de un proyecto tan apasionante. A Kevin, por las risas y discusiones de fútbol aderezados con dramas filosóficos sobre el futuro. A Briza, por ser la mamá del laboratorio y la ternura personificada, ojalá haber podido trabajar más tiempo contigo. A Helena, nuestra DINA de adopción, por siempre escuchar con tu sonrisa imborrable.

A Andrés y Nieves, por vuestro apoyo incondicional y por acordaros siempre de mí.

También a todo el equipo de virus respiratorios del servicio de microbiología del Hospital Vall d’Hebrón. A Cristina, por nuestras charlas en la campana de cultivos y tu voluntad y ganas de ayudarme infinitas. A Andrés, por tus consejos y propuestas locas que hicieron nacer este proyecto. A Tomás, por confiar en nosotras y hacer que esta tesis fuese posible.

Aquesta tesi tampoc seria el que és sense el meu altre laboratori, a BioSystems. Gràcies Petraki per donar-me l’oportunitat de formar part d’aquest equip. A Pere, per donar-me la confiança i llibertat per compaginar ambdues coses amb els meus horaris impossibles. A Olga, per la teva calma, guia i suport constant. A Núria, pel teu esperit reivindicatiu. A Ana

Belén, por tener paciencia infinita cuando me dejo (otra vez) el lavador encendido. A Paola, por hacerme reir con tus interpretaciones alternativas. A Ana, por ayudarme a verme con otros ojos más amables y ser siempre esa voz de apoyo. A tot l'equip de Customer i Bussiness, Elena, Qi, Coral, Gemma i Bruno, per la vostra companyia i ànims tot aquest temps. A Caterina, per resoldre tots els meus dubtes sobre liofilitzadors i tenir sempre noves propostes. A Pedro, por no poner nunca mala cara pese a hacerte esperar para poner el liofi. Y a todas las docenas de personas que me han dado apoyo desde BioSystems en esta andanza.

No quiero olvidarme de todas las personas que me acompañaron en mi aventura estadounidense. A Tania, por tus paseos de los martes por el parque. To Dr. Henry, for giving me the opportunity of working with your team in the frenzied COVID project. Thank you, Chuck, for worrying about me during hard times. To Isabelle, for being my main pillar during the pandemic and my internship, for helping me re-discover the mountains and sharing your amazing recipes. Also, together with Been, for breaking the lab record for staying late while sharing delicious dinners.

También quiero agradecer la ayuda del Dr. Iván Sanz y a Javi, por dejarnos probar nuestros sintrocitos en un entorno real y enseñarnos cómo funciona un Centro Nacional de Gripe.

Y por supuesto, toda la gente que me ha acompañado fuera de las paredes de los laboratorios. A mis padres, por su apoyo cuando decidí cambiar la estabilidad por un reto. A mi hermana, por darme siempre esos abrazos cuando más falta me hacen. A mis tíos y tías, primos y primas, a todos los Sánchez, los Cano, los Rodríguez y los Murillo por ilusionarse más por mis logros que yo misma. En especial a mi tío Josa, sin ti nunca me hubiera interesado por la ciencia, ni mucho menos me hubiera planteado seguir este camino. Gracias por ser mi inspiración.

A los Merofantas, Joaquín, Cris, Isma, Lluís, Sergio y Ángel, por confiar siempre en mí. Porque mi primera pandemia siempre será la del CODA. Por fin podremos acabar la campaña del Fenris y volver a morir escalando por rutas "fáciles", esta vez en Suiza.

A mis Viejóvenes, Rocío, Ainoa y Fanny, las primeras en celebrar mi inicio en este reto que ha sido el doctorado, y las que siempre habéis estado ahí apoyándome, incluso cuando no quería. Gracias por los momentos y risas necesarias para hacerme desconectar, por todos los ánimos y paciencia infinita.

Y finalmente a Jonás, por todo, por apoyarme en los momentos más bajos y poner en valor mis momentos más altos. Por ser el compañero perfecto para compartir este camino, los miedos y las ilusiones (y hasta la bibliografía). Porque sin tus ánimos y apoyo inagotables nunca me hubiera tirado a la piscina para cumplir mi sueño.

List of abbreviations

α-	Anti-
ø	Diameter
µP	Homogenized stained microparticles
4PL	Four parameter logistic curve
Ab	Antibodies
Ag	Antigen
AU	Absorbance unit
Av	Avidin
BM	Bovine mucin
BPL	Beta-propiolactone
BS3	Bis[sulfosuccinimidyl] suberate
BSA	Bovine serum albumin
BSL-3	Biosafety level 3
DMSO	Dimethyl sulfoxide
EDC	1-ethyl-3-(3-dimethylaminopropyl) carbodiimide hydrochloride
ELISA	Enzyme Linked Immunosorbent Assay
ERL	Essential Regulatory Laboratories
FBS	Fetal bovine serum
Gal	Galactose
GIP	WHO Global Influenza Program
GISRS	Global Influenza Surveillance and Response System
Glc	Glucose
GlcNAc	N-acetyl-glucosamine
Gly	Glycine
GYPA	Glycophorin A
H	Hemagglutinin
HA	Hemagglutination assay
HAI	Hemagglutination inhibition assays
HAU	Hemagglutination unit
hgr	High-growth reassortant
HRP	Horseradish peroxidase
Ip	Isoelectric point
LDH	Lactate dehydrogenase
LOD	Limit of detection
LOQ	Limit of quantification
M2	Matrix-2-protein
MAA	*Maackia amurensis* lectin
MDCK	Madin-Darby Canine Kidney
MP	Magnetic particles
N	Neuraminidase
n-Ab	Neutralizing antibodies
NaN_3	Sodium azide
Neu5Ac	5-N-acetylneuraminic acid
Neu5Gc	5-N-glycolylneuraminic acid

NeuAv	Neutravidin
NI	Neuraminidase inhibition assay
NIC	National Influenza Center
PAA	Poly(acrylic acid)
PBS	Phosphate-buffered saline
PEG	Polyethylene glycol
PLA	poly(lactic acid)
PM	Porcine mucin
pLDH	PAN *Plasmodium* lactate dehydrogenase
PfLDH	*Plasmodium falciparum* lactate dehydrogenase
RBCs	Red blood cells
RBD	Receptor-binding domain
RDE	Receptor destroying enzyme
ReLEG	Red de Laboratorios Autonómicos de Gripe”
RSV	Respiratory syncytial virus
RT	Room temperature
SA	Sialic acid
SA-BSA	Sialic acid conjugated chemically to BSA
SARI	Severe acute respiratory infection
SEM	Scanning electron microscope
SL	Sialyllactose
SLN	Sialyllactosamine
SN	Supernatant
SNA	*Sambuccus nigra* lectin
StrepAv	Streptavidin
Sulfo-NHS	N-hydroxysulfosuccinimide
SynAU	Synthrocyte agglutination unit
THF	Tetrahydrofuran
TMB	3,3′,5,5′-tetramethylbenzidine Liquid Substrate
WGA	Wheat germ agglutinin
WHO	World Health Organization
WHO CCs	WHO Collaborating Centers

Index

Chapter 1

State of the art

Chapter 1. State of the art

1.1 Influenza

Influenza (also known as “flu”) is an acute respiratory illness caused by influenza viruses. It can produce mild to severe illness, and at times can even lead to death. Annual seasonal influenza epidemics infect every year up to 20% of the population during the colder months, which has a huge impact in the national Health Systems and global economy.[1]

Most people with influenza present upper-respiratory-tract symptoms that include cough, sore throat and nasal discharge, which often occur suddenly in combination with other systemic symptoms such as fever, myalgia, fatigue or muscle aches.[2] Although not severe, these symptoms usually disrupt daily activities, including work or school attendance, and in some cases, they even require medical care. Some people are more prone to suffer complications, particularly people over 65 years, young children, pregnant women and people with certain chronic conditions. These serious complications include pneumonia, myocarditis and encephalitis among others, and may result in death. The World Health Organization (WHO) estimates that between 290.000 and 650.000 people die of respiratory diseases linked to seasonal influenza each year worldwide, and that up to 72.000 of these deaths occur in the European Region.[1,3]

This entails important expenses for the countries and their National Health Systems in preventive policies, vaccination campaigns, medical leaves, absenteeism, and a significant decrease in productivity.

1.1.1. Classification and nomenclature of influenza viruses

Influenza viruses belong to the *Orthomyxoviridae* family and can be divided into 4 types, named influenza A, B, C and D viruses. Types A and B are responsible for global epidemics and are referred to as seasonal influenza viruses. Influenza A viruses generally cause most of the seasonal influenza infections and have the highest rates of morbidity and mortality.[4] Moreover, all the influenza pandemics registered to date were caused by these types of viruses. Besides humans, influenza A viruses also infect many avian and mammalian species, including ducks, geese, pigs and horses, among others,[5] and it is well known that their primary reservoir are aquatic birds.[6] Influenza B viruses, on the other hand, infect humans almost exclusively and use to cause minor localized outbreaks that occur some weeks later than influenza A epidemics,[7] but have never been associated with a pandemic before.[8] Influenza C viruses infect humans and some animals, causing asymptomatic or mild upper respiratory symptoms and minor localized outbreaks.[9] Finally, influenza D viruses mainly affect cattle and swine populations. Although Ab against influenza D viruses have been reported in people exposed to cattle, it is unclear if they can infect and cause disease in humans.[10]

Influenza A viruses are further classified into subtypes according to the combinations of their hemagglutinin (H) and neuraminidase (N) proteins (Figure 1.1). There are 18 different H

subtypes and 11 N subtypes, numbered from H1 to H18 and N1 to N11, respectively. Currently, more than 130 different combinations have been found in nature, most of them in avian species, except for H17N10 and H18N11 that were only found in bats,[11] and there are potentially many more.

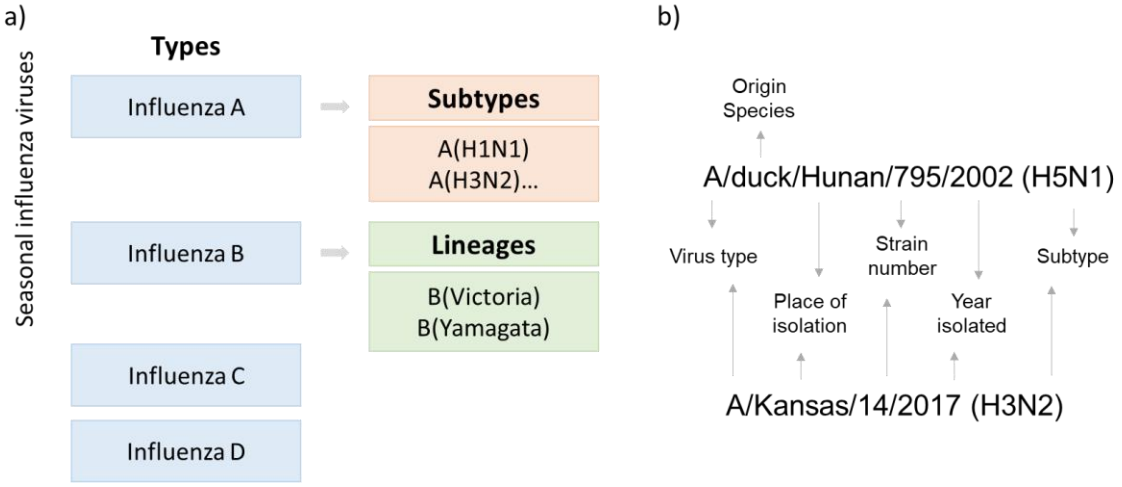

Figure 1.1 | a) Influenza virus classification. Influenza A and B viruses are responsible for most of the human infections and for seasonal flu epidemics. Influenza A viruses are further classified into subtypes depending on their H and N composition, while influenza B are further classified into B/Victoria or B/Yamagata lineages. **b)** Examples of the nomenclature used for naming influenza A virus isolates.

Influenza B viruses, on the other hand, are not classified into subtypes but divided into two antigenically distinct lineages: B/Victoria and B/Yamagata. These two lineages have been co-circulating worldwide since 1985 and their dominance alternated over time across different geographic locations and seasons.[12] However, B/Yamagata-lineage has not been isolated since March 2020, and some authors consider it extinct as a result of a combination of its slow antigenic and genetic changes and the suppressive conditions of the COVID-19 pandemic.[13,14]

Due to the large number of different influenza viruses identified, it was necessary to define an international criterion for their naming. In 1979 the WHO accepted a nomenclature system that considered the antigenic type, the host of origin, the geographic origin, the strain number and the year of collection.[15] For example, A/duck/Hunan/795/2002 refers to an influenza virus of antigenic type A, from duck origin, isolated in Hunan with the strain number 795 in 2002. If the virus has a human origin, the name of the host is omitted, as in A/Kansas/14/2017. For influenza A viruses they also considered the H and N subtypes, which are indicated in parentheses at the end. Hence, these two viruses would be named as A/duck/Hunan/795/2002 (H5N1) and A/Kansas/14/2017 (H3N2), respectively.

1.1.2. Structure and genome

Influenza viruses are enveloped viruses with a spherical or filamentous shape. Freshly isolated virions are often filamentous and turn more spherical with the successive passages when grown in cultured cells or in embryonated eggs.[16] Spherical virions often reach 100 nm in diameter, while filamentous forms usually exceed 300 nm in length.[17,18]

Influenza A and B viruses' genomes contain eight single-stranded RNA segments that encode transcripts for at least 12 viral proteins.[2] Of them, matrix-2 protein (M2), H and N are exposed on the surface of the envelope and confer the antigenic characteristics to the viral particle.[16] While H and N are glycoproteins found in a molar ratio of approximately four to one in the viral membrane, M2 forms pH-regulated proton selective ion channels and is expressed at lower concentration (in a ratio of 1 per 10-100 H molecules).[17] Figure 1.2 shows a scheme of the viral particle with these surface proteins.

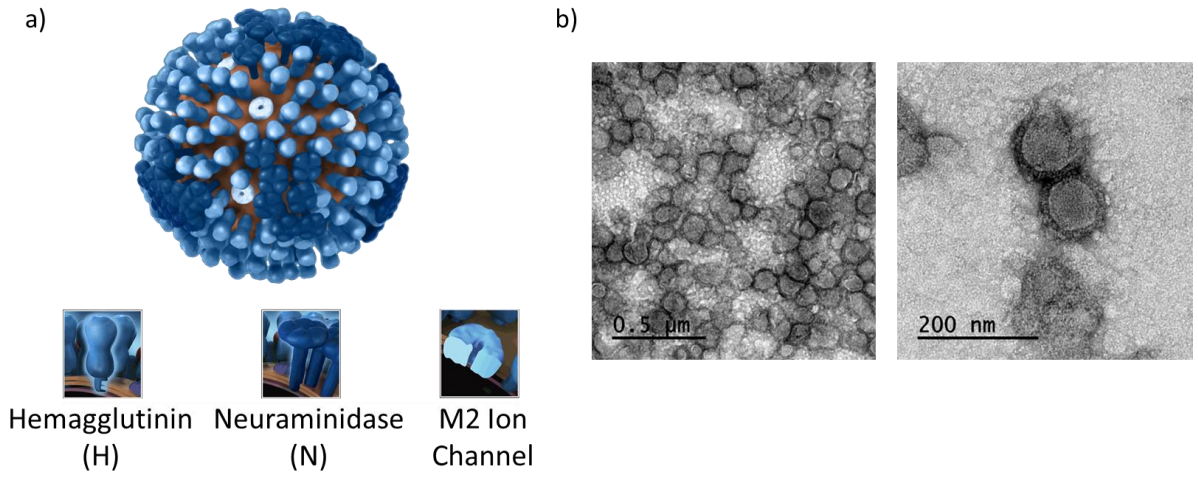

Figure 1.2 | a) Structure of influenza virus virion, obtained from[19] **b)** TEM micrography of some of the viruses employed for this thesis (A/NewCaledonia/20/99 (H1N1)).

H is the dominant glycoprotein in the surface of influenza A and B viruses and is responsible for the recognition and binding to the cells of the upper respiratory tract of the host. Its structure is homotrimeric, consisting of three identical monomers, each one displaying a globular head domain that contains a receptor binding site specific for sialic acid (SA).[20] During infection, H attaches to the host sialylated glycan receptors and initiates the viral entry. Although the avidity of a single H trimer for SA is in the order of 10^{-3} M Kd values, a remarkably weak union,[21,22] it has been defended that simultaneous binding of multiple H trimers increases the avidity 10^4 to 10^6-fold.[16] Moreover, virion morphology is also an important factor for the binding, with spherical viral particles binding cells better than the filamentous ones.[18]

N, on the other side, is the glycoprotein in charge of the release of the viral particles from infected cells. It removes the terminal SA present on cellular receptors from the dying cell that are bound to H to promote the release of the new virions and their spread in the respiratory tract. Moreover, it also prevents the H-mediated aggregation of the virions by desialylating H and other glycolipids on the virion surface.[23]

1.1.3. Host-Receptor binding

As defined above, H binds to the SA on the host cell surface and initiates the entry of the viral particle. Accordingly, H protein is a key determinant for host specificity and its evolution over time is crucial for the virus to expand or modify its host tropism, as it happens with the adaptation of avian and swine influenza A viruses to humans.[24] SA are a diverse family of

sugars consisting of a nine-carbon backbone that are typically attached to the terminal position of N- and O-linked glycans.[25] SA can have a variety of structural arrangements depending on the groups and the type of linkage they exhibit, but always display negative charge and hydrophilicity, which plays a part in its multiple biological roles.[26] As depicted in Figure 1.3a, the most common mammalian SA has the carbon 5 (C5) substituted with an acetamido to form 5-N-acetylneuraminic acid (Neu5Ac), an hydroxyacetamide to form 5-N-glycolylneuraminic acid (Neu5Gc), or a hydroxyl moiety to form deaminoneuraminic acids.[27] It is well known that H attaches to terminal Neu5Ac. However, this has to be linked to a galactose (Gal) through an α2,6 or α2,3 linkage, followed by a Glucose (Glc) or a N-acetyl-glucosamine (GlcNAc) residue through a β-1,4 linkage, to allow H binding.[28] These SA-coupled disaccharides are also named as Sialyllactose (SL) and Sialyl-N-acetyllactosamine (SLN), respectively (Figure 1.3b).

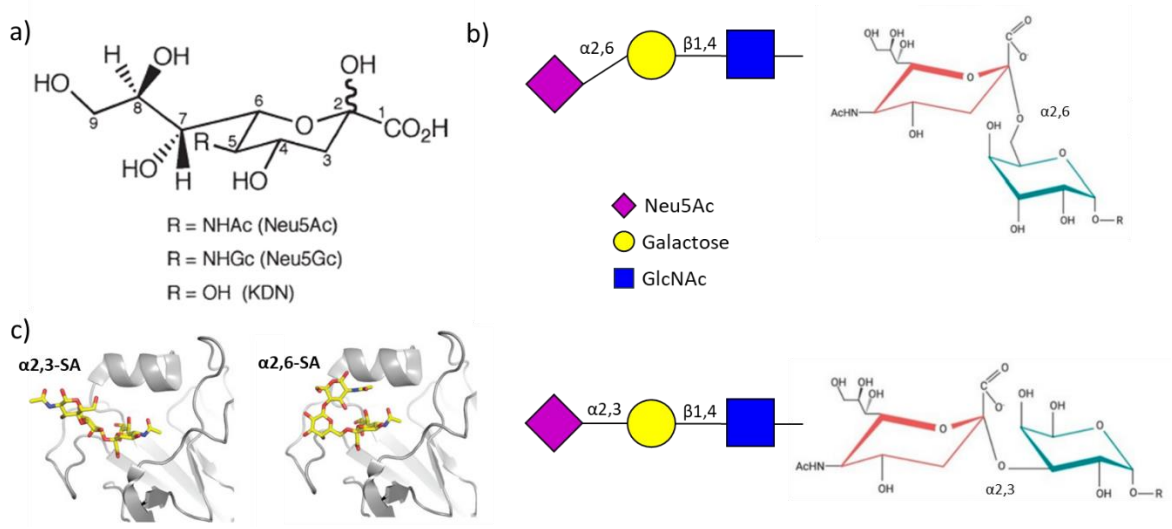

Figure 1.3 | a) Structural diversity of mammalian sialic acids, depending on the modification of the C5.[27] **b)** Scheme of SA recognized by influenza viruses, which are generally linked via α2,6- (top) or α2,3- (bottom) linkages to a galactose.[26] **c)** Binding of α2,3- (left) and α2,6- (right) linked SA to H protein (in grey). While α2,3-receptor binds through an extended configuration, α2,6-linked binds through a folded conformation.[29]

Rogers and Paulson were the first to demonstrate that influenza viruses exhibited different host tropism depending on the host species they had been isolated from, a work that started with H3 viruses[30] and followed with H1 and H2 influenza A viruses.[31,32] It was later revealed that human-adapted influenza A and influenza B viruses generally prefer α2,6- linked SA,[27,33] which are expressed predominantly on the apical surface of the upper respiratory epithelia in humans.[34] Avian influenza A viruses, on the contrary, prefer α2,3- linkages, which are largely expressed in the gut and respiratory tract of birds and in the alveolar and bronchiolar region of humans.[26,34,35] These changes in the binding preference are related to the configuration that adopts the SA, which binds differently into the HA pocket (Figure 1.3c).[36] Nevertheless, the general categorization of influenza viruses as α2,3 or α2,6 - preferred binding depending on their host origin is an oversimplification. Some studies have shown that individual strains of influenza viruses exhibit a wide variation of glycan binding profiles.[16,37] Moreover, some

studies suggest that the sequence and structure of the glycans adjacent to the Neu5Ac also affects the affinity of influenza viruses,[38] and not just this linkage.

One of the characteristics of new emerging human-adapted influenza A viruses is that they suffer a change in H glycan binding preference, shifting from avian to human receptor tropism.[39,40] Although it is commonly assumed that adaptation of avian influenza A viruses to bind α2,6 linkages is the main driver to produce pandemics, it is not the only significant issue involved in breaking the inter-species barrier.[24,40] Others, such as the ability to transcribe and replicate the RNA genome efficiently[41] or the absence of previous immunity for the novel virus in the global population, are also key elements to generate pandemics. However, it is important to note that all strains that effectively propagated in the human population exhibited α2,6 preference or at least combined α2,3 and α2,6 binding affinity.[24] It is true that some recent avian influenza viruses (H5N1) isolated from human samples show α2,3 preference,[42] which is associated with increased pathogenicity due to the presence of α2,3 in the human lower respiratory tract. The lack of increased recognition of α2,6 in these strains is a factor to explain the low transmissibility between humans of these viruses.

On another note, previous studies showed that affinity of influenza viruses grown *in vitro* could be subjected to adaptations to the method of culture used. In other words, human influenza viruses grown in embryonated eggs could change their receptor tropism to α2,3 through the multiple passages to adapt to the dominance of α2,3-linkages in eggs.[43,44] Some of these mutations have minimal impact in H antigenicity, while others can alter it significantly.[45] Thus, this should be taken into consideration when analyzing the binding preferences of influenza viruses, which should have suffered the fewest passages possible.

1.1.4. Antigenic shift and antigenic drift

The severity of each seasonal influenza epidemic is proportional to the degree of protective immune status of the population. This is in turn related to the degree of change in the virus antigenic components because influenza A and B viruses mutate, and thus evolve, at a high rate. These changes occur due to two major mechanisms: the antigenic drift and the antigenic shift.

Antigenic drift is a process that results of the accumulation of small and gradual changes that introduce alterations in the key epitopes of the surface proteins of the virus. These changes take place through mutations in the viral genome during the replication cycle of the virus, and are of particular importance when they affect H and N proteins, the main antigens on the viral surface. Usually, these small changes produce viruses that are closely related to one another, but the changes can accumulate over time and produce viruses that are antigenically different, and therefore, that could escape the host preexisting immunity.[46] Occasionally, a single change in a relevant antigenic location on the H is enough to result in antigenic drift.[47,48]

The new influenza strains produced by antigenic drift are the primary reason why the composition of flu vaccines needs to be updated annually, and also why a person becomes susceptible to many influenza infections over a lifetime. Older influenza viruses are generally replaced by new drifted variants, although the rate of replacement depends on the virus

subtype. Influenza A(H1N1) and specially B viruses tend to co-circulate for a longer time, while A(H3N2) have a faster substitution rate.[49,50]

Antigenic shift is a less frequent and more dramatic change that usually ends with the emergence of novel influenza A viruses that differ from the previously circulating ones and that possess pandemic potential. The antigenic shift occurs when the new influenza A virus exhibits either a new H protein or a new combination of H and N proteins that can infect humans. There are different mechanisms by which this antigenic shift could happen.[51] The most common is a process of genetic reassortment, in which two influenza viruses co-infect a host at the same time and swap viral RNA segments. This process could occur directly (such as a simultaneous infection of two human influenza viruses in a patient) or through an intermediate animal host (such as pigs), in which influenza viruses from different species could co-exist and cause the reassortment more easily (Figure 1.4b (ii)).

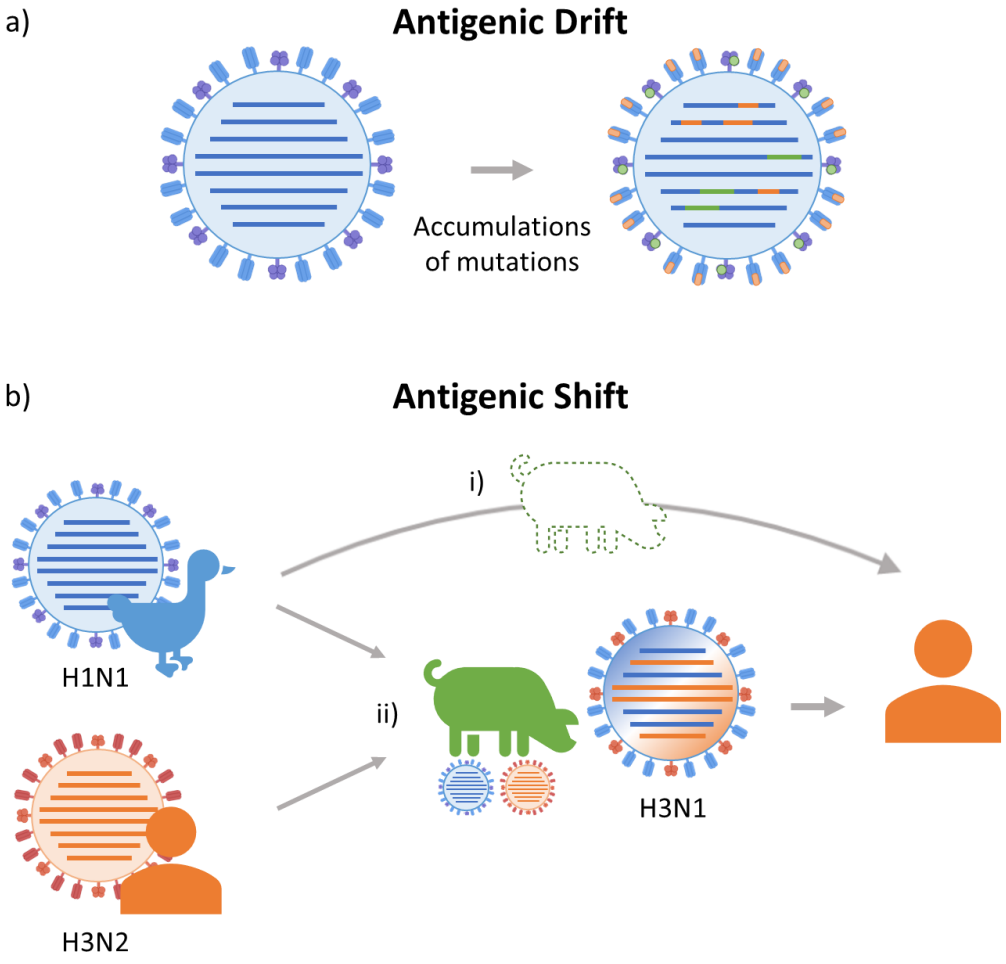

Figure 1.4 | Scheme of antigenic drift and shift mechanisms. a) In antigenic drift, the virus accumulates over time nonsynonymous substitutions in diverse genes such as the ones encoding for H and N proteins. b) Diverse mechanisms that produce antigenic shift. i) Direct transmission from one species to another, or through an intermediate vessel (swine in the image). ii) Gene reassortment, after two antigenically distinct influenza viruses (that can infect originally two different species) co-infect a pig. Because influenza virus is segmented, it can lead to gene reassortment and produce a new virus that contains characteristics from both parental strains (such as H from one and N from the other).

This co-existence is feasible thanks to the expression of both α2,6 and α2,3 receptors in the respiratory epithelial cells of swine and some avian species such as turkeys.[26,52] Antigenic shift can also happen when viruses from certain animals undergo a mutation that makes possible to infect humans directly (or through an intermediate species), without undergoing genetic reassortment, although it is less common (Figure 1.4b (i)).[53]

If the novel influenza A virus generated by antigenic shift has the ability to sustain chains of human-to-human transmission and a significant part of the population does not have Ab against it, it can potentially cause a pandemic outbreak. In fact, since 1900 this phenomenon has caused at least four pandemics, all originated by influenza A virus subtypes H1N1, H2N2 or H3N2 that were reassorted with influenza viruses of avian origin. In the case of the two A(H1N1) pandemics, swine influenza A viruses were also involved in this antigenic shift.[54]

1.1.5. Pandemic and seasonal influenza

Seasonal influenza epidemics are a relatively predictable annual event, which causes a consistent disease burden year after year. Currently, influenza A(H1N1)pdm09 and A(H3N2) viruses circulate among people worldwide, together with B/Victoria (and until recently, B/Yamagata).

Influenza A viruses are usually the predominant viruses each season, although there is not a clear prevalence between A(H1N1) and A(H3N2) viruses. Severity also varies each year depending on the strain characteristics (receptor affinity, immunological trigger capacity and replication efficiency, among others) and the immunologic state of the population (similarity to previous strains and the appropriateness of the annual influenza vaccine).

Table 1.1 | Estimates of the predominant influenza viruses each season between 2012 and 2020 in the United States and Europe.[55,56]

Season	Predominant viruses	
	Europe	USA
2012-2013	B	A/H3N2
2013-2014	A/H1N1pdm09	A/H1N1pdm09
2014-2015	A/H3N2	A/H3N2
2015-2016	A/H1N1pdm09, B	A/H1N1pdm09
2016-2017	A/H3N2	A/H3N2
2017-2018	B	A/H3N2
2018-2019	A/H1N1pdm09, A/H3N2	A/H1N1pdm09, A/H3N2
2019-2020	A/H1N1pdm09, A/H3N2	A/H1N1pdm09, B

For influenza pandemic outbreaks, four have been documented since 1900. It is thought that wild waterfowl are the main reservoir for the spread of potential pandemic influenza viruses. When multiple avian viruses infect a bird and undergo genetic reassortment, they occasionally

display the ability to infect humans and, if the human population is not protected immunologically, the new virus may cause pandemic outbreaks.

The first of these four pandemics occurred in 1918 and was identified popularly as the “Spanish flu”. Although there is no global consensus on where it originated due to its almost simultaneous appearance in North America, Europe and Asia, it seemingly arose in the United States in March 1918 and was propagated by the American army during the First World War.[57] It was also the most severe, with an estimated 500 million people infected (one third of the world’s population) and around 50 million deaths worldwide during the pandemic. This virus was an A(H1N1) strain closely related to what is called “classic swine” influenza virus. One of its characteristics was the ability to produce infection of both human and swine, although it is yet to be resolved if the virus spread from swine to human or vice versa. Nevertheless, the sequence analysis carried decades later suggested that at least some of the genes derived from an avian-like influenza virus that did not circulate widely in humans or swine prior to the pandemic, which could contribute to its elevated virulency.[58] Regarding the SA binding preference, isolates with a dual α2,3/α2,6 affinity and α2,6 preference were identified from clinical material. Further analysis showed higher transmissibility of the α2,6-binding preference viruses, but not appreciable difference in virulence.[51,59]

The next pandemic influenza virus emerged in East Asia in February 1957, and was isolated for the first time in Singapore.[60] Morbidity and mortality of this pandemic, known as the “Asian Flu”, was significantly lower than the previous one, yet it produced between 1 and 4 million deaths.[61] This was caused by an A(H2N2) virus originated by antigenic shift after reassortment between wild duck influenza A viruses and some circulating human A(H1N1) viruses genes.[62] A(H2N2) viruses showed a low rate of genetic and antigenic evolution (specially H2)[63] and retained the preference for avian-like α2,3-linked SA receptors.[64] The pandemic remitted by 1958, but the virus remained circulating in humans for 11 years, until it was displaced in 1968 by the emergence of new H3N2 viruses.[65] Although the H2N2 subtype has actually disappeared from humans, wild birds still act as a reservoir for it. Reemergence of these viruses represent a potential thread due to the absence of humoral immunity in subjects born after 1968, caused by their lack of exposure to H2N2 subtype viruses.[63]

It is suspected that the A(H3N2) virus responsible for the subsequent 1968 pandemic derived in part from the 1957 A(H2N2) virus, which had been evolving through antigenic shift. This A(H3N2) virus comprised two genes derived from low pathogenicity avian influenza A virus, including H3, but maintained the N2 from the 1957 A(H2N2) virus (among other six genes).[62] The H3 protein contained two mutations that altered its receptor specificity to bind preferentially α2,6-linked SA[66,67] and facilitated human-to-human transmission, producing a rapid worldwide expansion that caused an estimated 1 million deaths worldwide.[68] Despite this, this pandemic was considered a mild outbreak, since the immunity developed with the previous A(H2N2) pandemic protected the population to a certain extent. The 1968 pandemic also received the name of “Hong Kong pandemic” because of its first isolation in Hong Kong in July 1968. Since then, this subtype continued circulating worldwide as a seasonal influenza A virus, associated with more severe illness than those caused by influenza A(H1N1) viruses.[68]

The last recorded influenza pandemic occurred in 2009. It was caused by an A(H1N1)pdm09 virus that was first identified in Mexico and in the United States.[69] Because this virus was very different from the A(H1N1) viruses that were circulating at the time of the pandemic, the suffix "pdm09" was added to its nomenclature to distinguish it and its successive derived viruses. Serological studies showed that young people did not possess immunity against this new strain, while one third of people over 60 years had Ab against it, suggesting that the virus did not derive from the contemporary seasonal A(H1N1) but was related to a previous A(H1N1) (Figure 1.5).

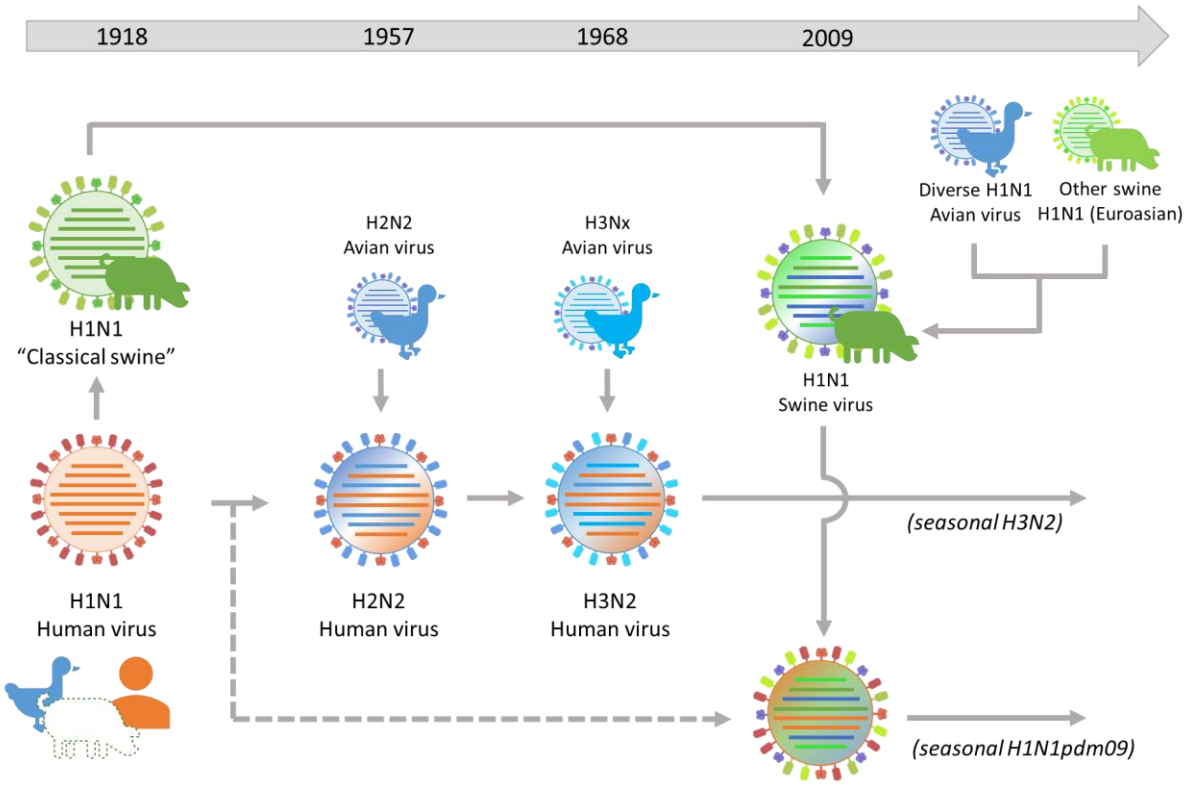

Figure 1.5 | Reassortment events related to historic pandemic influenza A viruses in the last 110 years, based on [70]. The 1918 A(H1N1) probably originated from multiple reassortments between avian, human and swine viruses or by direct zoonotic transmission. This A(H1N1) continued to circulate until 1957, when it presumably reassorted with an avian A(H2N2) virus. Subsequent reassortments in 1968 with an A/H3NX virus are pointed as the origin of the H3N2 virus that has caused seasonal epidemics ever since. A(H1N1) was introduced again in the human population in 1977, where it co-circulated with A(H3N2) until the emergence of H1N1pdm09. This virus originated after multiple reassortment events between avian, swine and human influenza viruses.

In fact, genetic analysis established a connection with three influenza viruses that circulated in pigs, which could be traced back to the 1918 A(H1N1) pandemic virus.[71,72] Other genes from the A(H1N1)pdm09 virus had their origin in the "triple-reassortant" lineage, a variant that included genes from human, swine and avian influenza viruses.[69] Although this virus contained genes derived from diverse swine influenza viruses, exposure and transmission from pigs were not detected.

The “swine flu”, as commonly called, produced between 151.000 and 575.00 deaths worldwide along 2009, according to the estimations.[73] Moreover, contrary to typical seasonal influenza viruses, these deaths occurred mostly in children and young adults instead of in older age groups (>65 years).[69] Nowadays, other strains derived from the A(H1N1)pdm09 continue to circulate and constitute one of the current seasonal flu viruses.

In summary, influenza comprises a diverse group of viruses with unique characteristics. Among others, their ability to infect a diversity of host species (including birds, swine, humans, dogs, horses and other mammalian species) depending on their affinity for the different SA-based host receptors. Another characteristic is their high mutation rate, which often produces antigenic changes that allow the virus to escape the immune protection, even that induced by vaccination, or cause changes in the SA-affinity that facilitate inter-species transmission. Finally, the simultaneous co-infection of the host cells by various influenza virus (of different subtype or even host-species origin) can produce the emergence of new reassorted influenza viruses with a devastating pandemic potential, as has happened before.[74]

In consequence, monitoring the multiple changes and adaptations that influenza viruses undergo is essential to mitigate the effects of the seasonal epidemics and reduce the pandemic menace.

1.2. Influenza virus global surveillance

Apart of its role to anticipate pandemics, epidemiologic and virologic surveillance of influenza viruses is essential to produce effective influenza virus vaccines. By now, vaccination is the main measure available to lessen the impact of influenza epidemics, but viral antigenic drift imposes vaccine annual reformulation (and risk-population annual revaccination). This obliges to the antigenic characterization of circulating influenza viruses, which is carried by an international surveillance network coordinated by the WHO Global Influenza Program (GIP).

1.2.1. Global Influenza Surveillance and Response System (GISRS)

Since its creation in 1952, the WHO’s Global Influenza Surveillance and Response System (GISRS) monitors continuously the changes occurred in influenza viruses that circulate around the world, conducts risk assessment and recommends risk management measures. In this way, GISRS acts as a global network for surveillance of influenza evolution and epidemiology, monitoring also the impact of the annual vaccination in the disease spreading and severity. With this information, it develops plans to prepare the response to the seasonal epidemics and zoonotic influenza. Moreover, GISRS also establishes alerts when novel influenza viruses and other respiratory pathogens emerge.

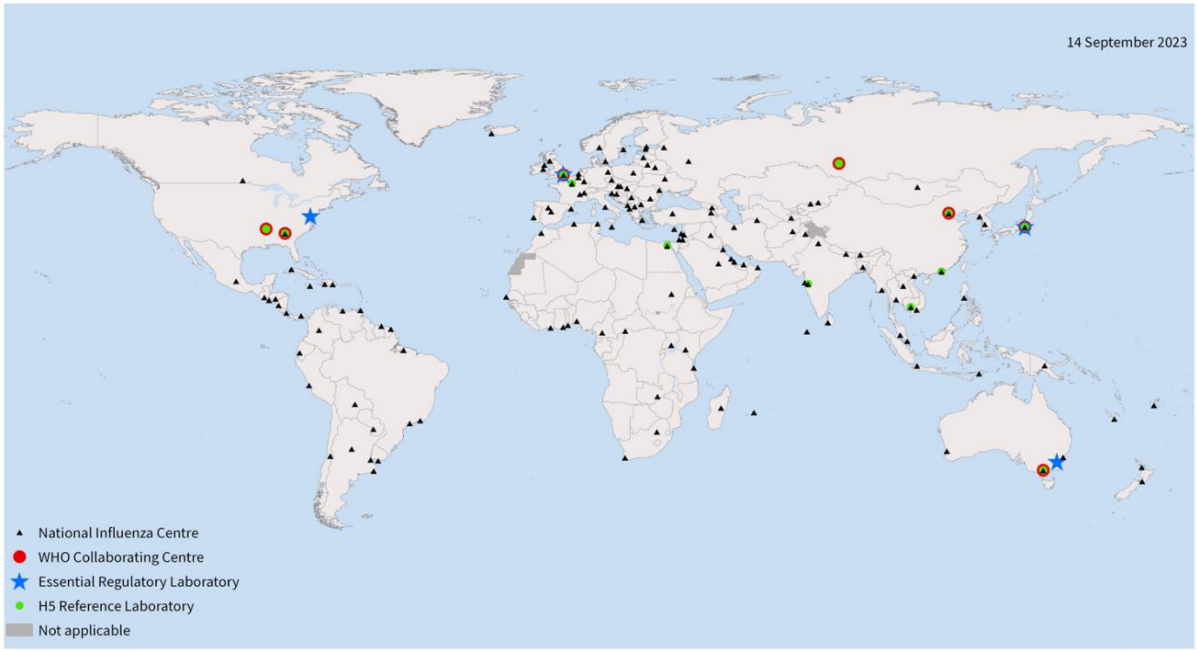

Figure 1.6 | Distribution of the laboratories that are part of the GISRS network,[75] in charge of worldwide influenza surveillance.

The GISRS consists currently of 158 national institutions distributed across 129 countries.[75,76] They are divided into:

- **144 National influenza centers (NICs**). They collect virus specimens from patients with influenza-like illness, acute respiratory infection or severe acute respiratory infection (SARI). These samples are then used to perform primary virus isolation and preliminary analysis and identification by molecular methods, virus culture and/or immunological methods. In general, NICs attempt to differentiate between influenza A and influenza B viruses and to determine their subtype or lineage using reference reagents provided by the WHO. Then, they ship representative samples of the isolated viruses to the WHO Collaborating Centers, including the influenza A viruses that cannot be typed or subtyped at the NICs.[77]

- **7 WHO Collaborating Centers (WHO CCs)**. They perform further analysis of the samples gathered by the NICs, including advanced genetic and antigenic characterization. The WHO recommendation on the influenza vaccine composition for the Northern and Southern hemisphere is made twice a year based on these results. Moreover, WHO CCs are also in charge of the production of reference reagents and the publication of all the data gathered through portals such as FluNet.[78,79]

- **4 WHO Essential Regulatory Laboratories (ERLs)**. These institutions are associated with national regulatory agencies and are the primary information resource on issues related to influenza vaccines. They facilitate and/or perform serological studies on sera obtained from individuals after influenza vaccination and help in the standardization, development and regulation of influenza vaccines and the reagents required for their evaluation.[80]

- **13 WHO H5 Reference Laboratories**. A specific H5 Reference Laboratory Network was established in 2004 to monitor particularly avian influenza A(H5N1) infections in humans and to define influenza pandemic preparedness. They collect specimens and virus isolates of A(H5N1) and other influenza subtypes with the potential to cause human infections (from animals and human sources) and perform advanced genetic and antigenic analysis, together with serological studies, in the local region where these were isolated. They also monitor the antiviral susceptibility of these viruses.[81]

In short, GISRS operates through efficient sharing of influenza viruses and surveillance information, and provision of technical support and updated reagents by and to GISRS members. It is estimated that, every year, more than 5000 influenza viruses are thoroughly characterized by the GISRS network.[82] The work is done continuously around the year so that there is always an overall image of the antigenic and genetic characteristics of the contemporary influenza viruses and their general evolution. This information has a big relevance for public health, but is dependent on the quality and representativeness of the isolates and clinical specimens shared by NICs and other laboratories with the WHO CCs.

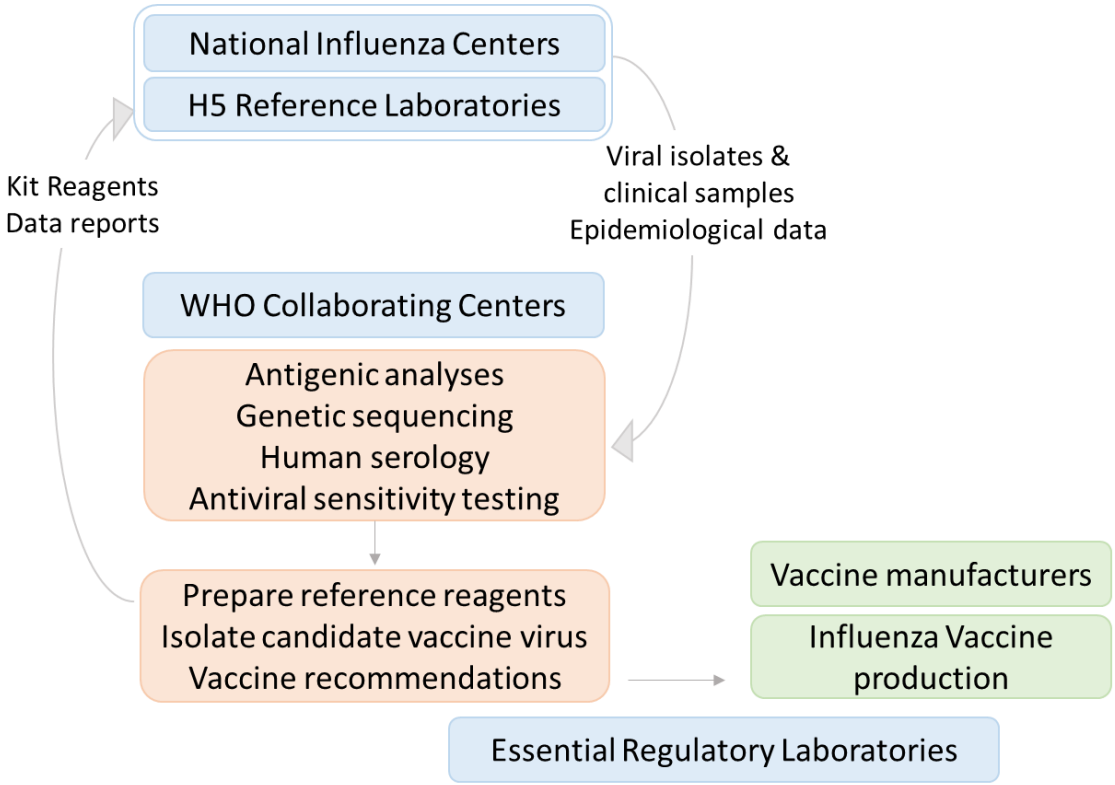

Figure 1.7 | GISRS workflow for influenza surveillance and vaccine formulation recommendation. NICs and other reference laboratories ship viral isolates and clinical specimens to WHO CCs after performing a preliminary analysis. There, WHO CCs further characterize the viruses and produce reference antigens and candidate vaccine viruses, besides gathering all the data together and publishing it in portals such as FluNet. With all this information, they recommend the composition for next season influenza vaccine.

1.2.2. Local influenza monitoring

The European Influenza Surveillance Network (EISN, former European Influenza Surveillance System) was established in 1996.[83] Its role is similar to the GISRS, but centered in Europe. This network, comprising mostly NICs of the GISRS, covers 29 countries and is coordinated by three European institutes. One of the coordinating centers is the Worldwide Influenza Center at the Francis Crick Institute, in London (UK), which is the WHO CC in charge of the European region.

In Spain, flu surveillance uses diverse systems and information resources, which allow monitoring the flu activity at a national level and in each autonomous community. One of them is the sentinel surveillance network, which covers at least 1% of the population of each autonomous community and collects microbiologic and epidemiologic data from a representative part. This provides a comprehensive view of the disease evolution and the circulating viruses for each season.[84]

To conduct this surveillance, physicians who collaborate with the sentinel network collect samples from patients that present symptoms compatible with flu and send them to the designated laboratory of the corresponding autonomous community. Altogether, these laboratories form the “Red de Laboratorios Autonómicos de Gripe” (ReLEG). Samples from patients with SARI that required hospitalization in a sentinel hospital are also collected. Such samples are analyzed by reverse transcription polymerase chain reaction (RT-PCR) for flu, COVID-19 and, if possible, for respiratory syncytial virus (RSV). When positive for flu, samples are genetically sequenced to monitor variants. If the center/hospital does not count with the facilities or equipment necessary, samples are sent to the “Centro Nacional de Microbiología” (CNM) for this analysis. Optimally, this study should distinguish between influenza A and B viruses and, in the case of A viruses, the subtype (H1, H3 and H5). However, the correct detection of the virus may be conditioned by the sample quality, transport to the reference laboratory, and storage before realizing the analysis.[84]

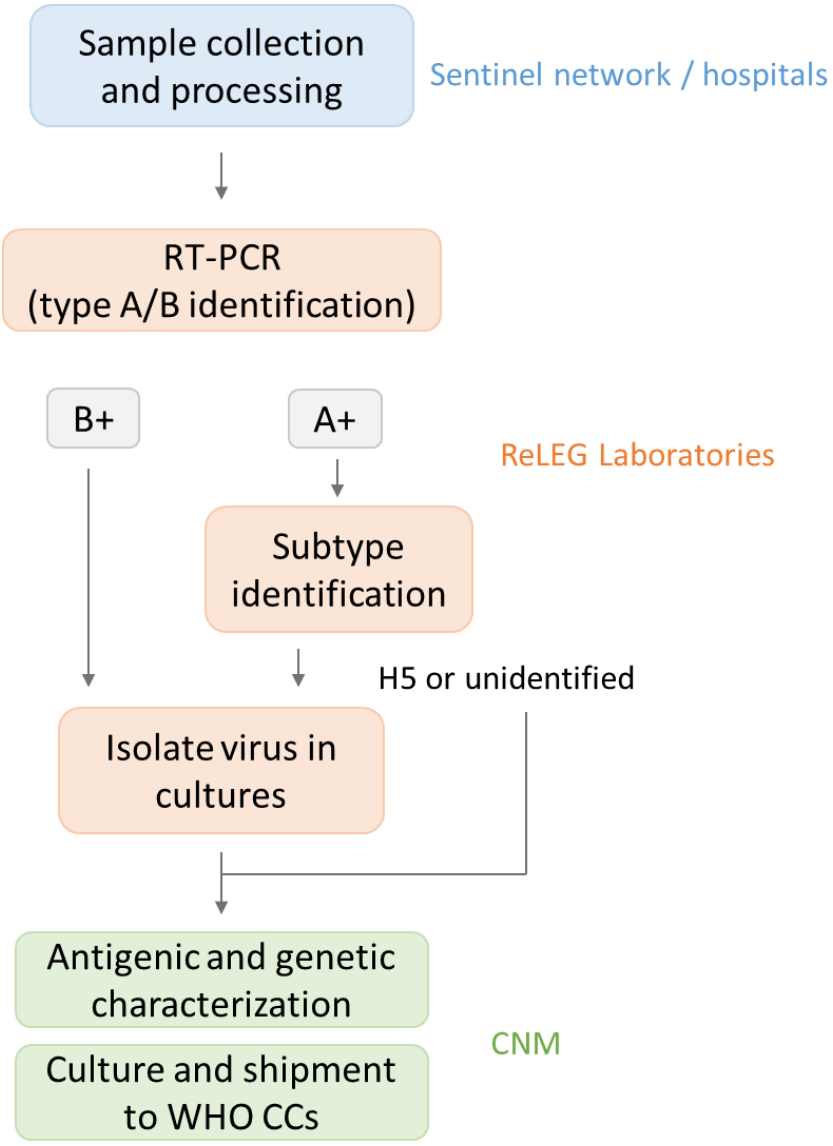

Figure 1.8 | Workflow for influenza virus sample handling by ReLEG and Spanish NICs. Samples collected by the sentinel network are preliminary analyzed in ReLEG to type and subtype the virus and, when possible, the virus present are isolated. The successfully isolated viruses and the unclassifiable ones (such as non-seasonal virus types) are sent to the CNM for further antigenic and genetic characterization. There, some of these viruses are cultured and sent to the WHO CCs at least twice per epidemic season.

It is important to note that the number of samples collected is different depending on the week of the year. In summer (from week 21 to 39 in the north hemisphere), samples are not collected routinely by the sentinel physicians, but confirmed influenza infections from hospital laboratories are still notified. If the network detects a higher incidence that could be indicative of a pandemic/non-typical epidemic, the sentinel centers maintain the surveillance as the rest of the year. In the epidemic season (from week 40 to week 20 in the north hemisphere), a representative selection of the circulating viruses (in the form of isolated viruses or respiratory samples), collected on different time points of the epidemic, are sent to the CNM to be antigenically and genetically characterized. Then, this information and some representative

samples are shipped to the London WHO CC for further characterization. In general, it is advised to send samples to the WHO CC at least twice per epidemic season. The first shipment should include viruses isolated in autumn-winter (beginning of the season), and the other should proceed by the end of January (end of the season). Besides, the samples obtained during the inter-epidemic season (in summer) and those considered unclassifiable should also be sent for further analysis.[84]

The protocol described here applies to Spain, but other countries follow similar processes to obtain, analyze and share samples. With all this information, the GISRS is able to monitor globally influenza changes (produced by antigenic drift) and the emergence of new subtypes or variants (produced by antigenic shift), and then design and develop plans and strategies for prevention and/or mitigation of the disease burden.

1.2.3. Vaccine strain adaptation and production

Due to the constantly evolving nature of influenza viruses, every flu season is different. Therefore, it is necessary to readjust annually the strains that compose the vaccine in order to achieve the desirable effectiveness.

Since 1973, the WHO has provided formal recommendations for the composition of influenza vaccines based on the information provided by GISRS. Twice a year, the WHO organizes technical consultations with an advisory board of experts that consider the surveillance data of the recently circulating viruses and recommend the strains suitable to be included in the influenza vaccine for the following influenza season. These meetings are held in February and September to define the northern and southern hemisphere vaccine composition, respectively. These recommendations are generally followed by the national vaccine regulatory agencies and by the pharmaceutical companies when they design and produce the influenza vaccines.[85]

1.2.3.1. Selection of candidate vaccine viruses (CVVs)

Detecting and identifying antigenically drifted seasonal influenza viruses is not the only function of WHO CCs. They are also responsible for selecting and producing the candidate vaccine viruses (CVVs). The wild-type influenza viruses that circulate in nature do not always grow well *in vitro* and are not always suitable to mass-fabricate vaccines in the short timeframe available. CVVs are flu viruses generally produced by reassortment of circulating influenza strains with laboratory-adapted influenza strains that grow to high titers in eggs, and which will be later used by vaccine manufacturers to mass produce the flu vaccines. CVVs are designed taking into account the influenza specimens collected over the previous year and should reflect the antigenic characteristics of the circulating viruses. To ensure this, these viruses are grown in embryonated eggs or cell cultures and submitted to precise genetic and antigenic analysis. CVVs are also employed to carry serologic studies on sera obtained from people of all age groups and from different geographical areas, both before and after flu vaccination.[86] These studies are useful to determine each season if the immunological response elicited by that year's reassortant vaccine is protecting the population against the current circulating influenza viruses.[82] Sometimes, these experiments reveal that previous vaccines are already effective

against some of the new circulating strains, which means that vaccine composition does not need to be updated completely. An example is the B/Yamagata virus strain, which has remained unchanged in the vaccine since the 2013/14 season.

Both the antigenic and serological studies cited above are mostly performed using hemagglutination inhibition assays (HAI). To carry these assays, researchers need, not only the CVV under study, but also batteries of reference antisera displaying Ab against selected influenza strains. Such sera are often produced in ferrets, because influenza elicits in them an immunological response very similar to that produced in humans. Precisely because ferrets are susceptible to circulating influenza viruses,[87] they must be kept in appropriate facilities to avoid prior exposure to the virus. The animals are then infected under laboratory conditions with the selected influenza strain, and convalescent antiserum is obtained. The antiserum produced contains Ab specific against the influenza strain used for the infection, and can be employed as a sensitive reagent in HAI for detecting antigenic variations between reference and tested influenza viruses and establishing similarities between them.[82] This antiserum is also used in HAI assays to characterize new CVVs and determine if they display the antigenicity recommended by the WHO for the next season vaccine virus, and therefore choosing the vaccine composition.

Besides these antigenic tests, it is necessary to perform impurity and exclusivity tests to guarantee that each CVV preparation only contains the virus intended and no other viruses, bacteria or fungi.[88] Moreover, confirming that the CVVs do not kill chicken embryos is key to use them in vaccine mass production, which is usually carried in embryonated eggs.[82,89]

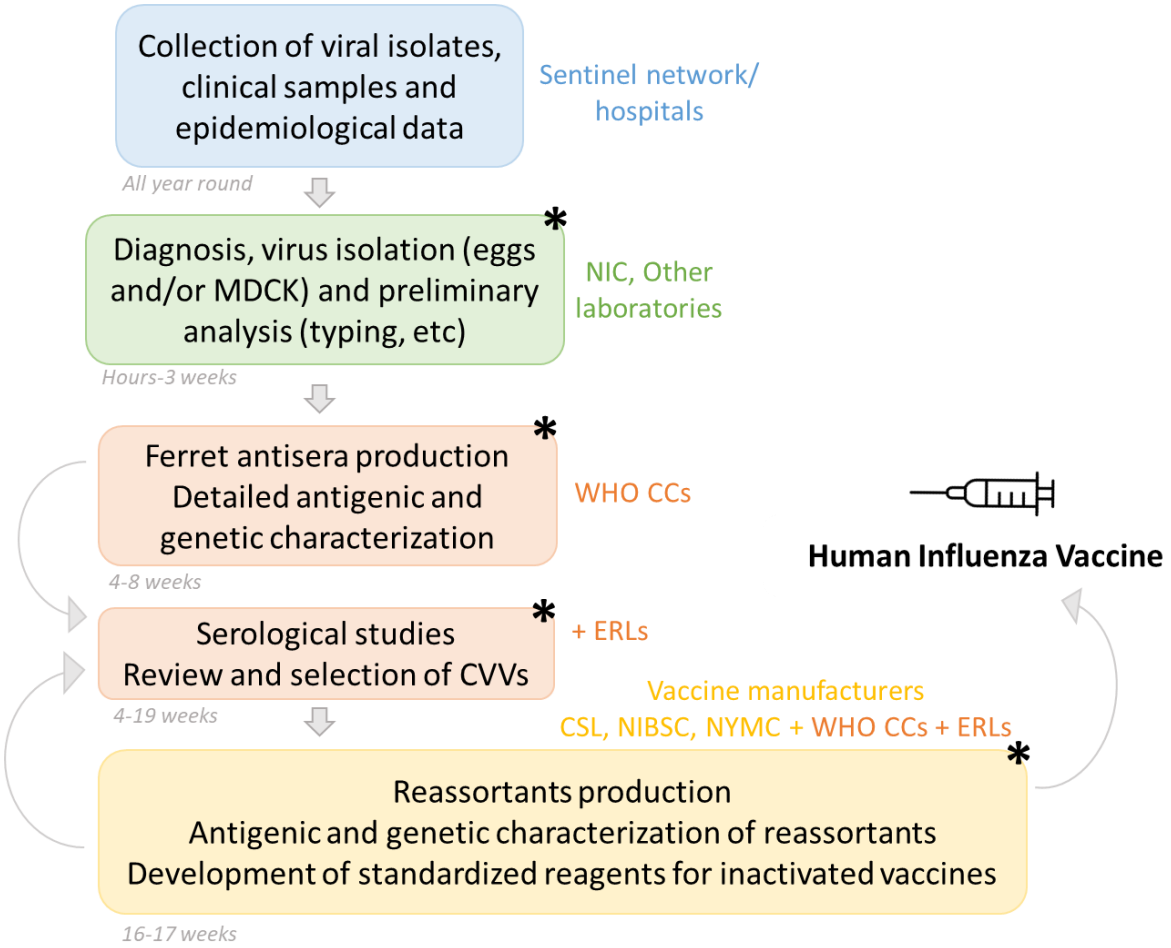

Figure 1.9 | Process of influenza vaccine virus selection and development. Steps involving HAI assays are marked with an asterisk.[82]

One major challenge of selecting these CVVs is the time-pressure. CVVs must be prepared and available early enough for the manufacturers to mass produce influenza vaccines in time for the flu season, which usually requires 6-8 months depending on the type of vaccine. Some years influenza viruses start circulating later than usual, and this hinders the timely selection of the suitable candidates for the vaccine.

1.2.3.2. Production of CVVs

Once the strains are selected, vaccine manufacturers begin the manufacturing process to include newly selected flu strains. Historically, vaccine viruses were isolated and grown in chicken eggs to facilitate their mass production. This presents an important problem for influenza A(H3N2) viruses, which grow poorly in eggs.[90] Furthermore, it is known that growing human influenza viruses in eggs can cause changes in their antigenicity due to virus adaptation[43,44,91] reducing the similarity of the vaccine viruses to the circulating ones. To avoid this, the WHO recently authorized the growth of influenza vaccine viruses in mammalian cultured cells (Madin-Darby Canine Kidney, MDCK)[92] and also the use of recombinant flu vaccines. Accordingly, the WHO recommends two different vaccine compositions if the viruses are produced in eggs or in cultured cells.[93]

Nevertheless, in order to produce the required quantities of influenza vaccine on time, manufacturers produce hybrid viruses called “high-growth reassortants” (hgr). These viruses have 2 genes encoding the H and N surface proteins from the recommended virus and 6 “backbone” genes from another established egg-adapted strain (like A/Puerto Rico/8/34) to improve the growth in eggs.[94] Before these hgr are used in vaccine production processes, they need to pass additional antigenic characterization using HAI assays to guarantee that all the process (the reassortment and the growth in eggs/cells) maintains the antigenic characteristics of the selected viruses.[88] Ferret antisera raised against these viruses are employed in these assays.

For this season (2022-2023), at least 29 different CVVs have been developed and are available for influenza vaccine manufacturing.[95]

1.2.3.3. Vaccine production

Influenza vaccines can be classified depending on diverse features. For example, they can be sorted according to the virus production technology employed (egg-based, cell-based or recombinant) or according to the type of active substance (inactivated influenza vaccine, attenuated influenza vaccine, and recombinant H vaccine).[85] Another classification is based on the number of strains present in the seasonal vaccine. We can distinguish between quadrivalent vaccines (that contain 4 strains; H1N1, H3N2, B/Yamagata and B/Victoria) and trivalent vaccines (without B/Yamagata). Each year, the 3 or 4 strains are individually evaluated and selected.

Plenty of companies produce their own influenza vaccine (Seqirus, Sanofi and GlaxoSmithKline, among others), always based on the WHO recommendations. Although CVVs are available, sometimes these companies develop their own reassortants from a wild type virus or *de novo* by molecular techniques. In this case, the new reassortant must also be genetically and antigenically characterized, including a demonstration of its antigenic similarity to the WHO recommended strain (generally by HAI).[88]

The process for vaccine production is depicted in Figure 1.10. For cultured-based vaccines, once the virus is grown, it undergoes a process of harvesting, filtration and purification, which is followed by virus inactivation or disruption depending on the type of vaccine. Then, H and N antigens for each production batch are characterized, usually using specific antisera obtained from a WHO CC and performing HAI tests. Genetic characterization of the H and N genes and comparison to the CVVs is also recommended. Moreover, it must be ensured that the inactivation process does not affect the antigenicity of the influenza vaccine virus.

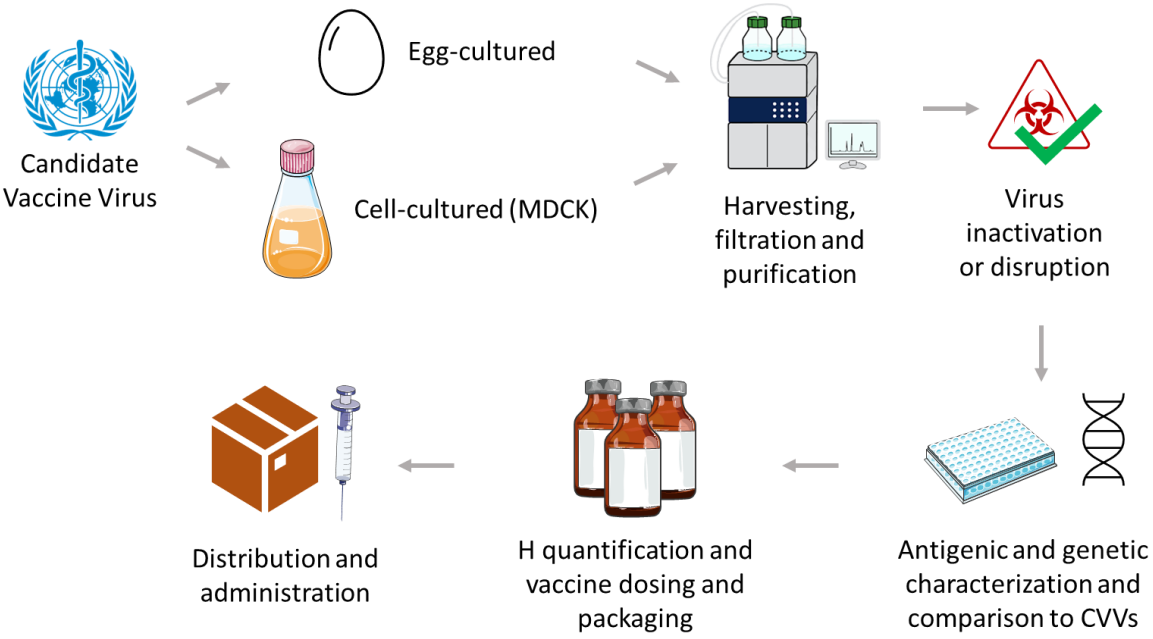

Figure 1.10 | Production process of influenza vaccines from CVVs recommended by the WHO, using egg or cell-cultured process.[85]

Finally, the amount of H protein should be quantified using the immunological single radial immunodiffusion ssay (the current gold standard) to measure the potency of the inactivated influenza vaccines and standardize their content.[88]

After the vaccine production, it is necessary to distribute and administer the vaccine prior to the beginning of the influenza season, starting with the immunologically compromised population.

To sum up, the production of influenza vaccines is a long and highly regulated process that must be performed within 6-8 months to allow for the timely production of the annual seasonal influenza vaccines. Figure 1.11 shows how the process is distributed around the year and how it compares with the incidence of the flu season in the northern hemisphere.

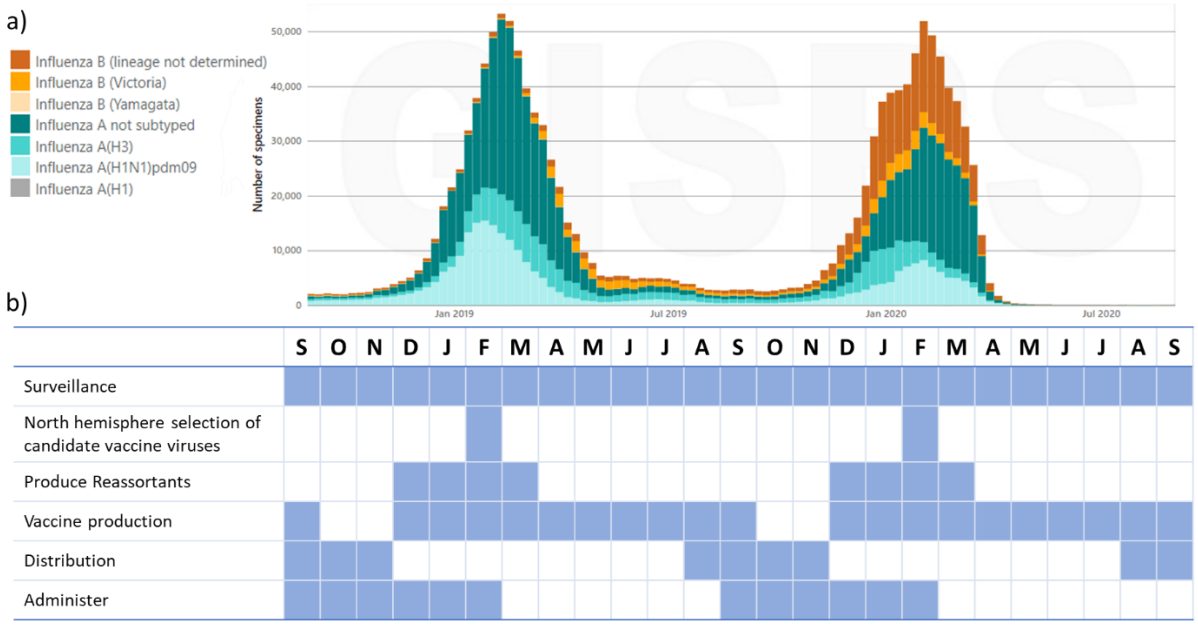

Figure 1.11 | a) Flu incidence in the northern hemisphere between September 2018 and September 2020 (two seasons), data obtained from FluNet.[79] **b)** Timeline of influenza vaccine development with the different phases detailed.

This process entails multiple steps, being the antigenic characterization of the viruses (both CVVs and contemporary circulating strains) a central pillar of it.

1.3. Antigenic characterization

As previously stated, antigenic analysis is key to monitor influenza evolution and to select strains for producing influenza vaccines. Initial typing of influenza virus isolates is usually performed by commercially available multiplexed immunofluorescence.[96] A number of methods may be used next to antigenically characterize those viruses. Basically, these methods rely on categorizing the H and N proteins on the virus surface, generally by comparison with known influenza viruses.

One of them is the hemagglutination inhibition assay (HAI). HAI allows determining the antigenic resemblance of an isolated virus to a known reference virus by using controlled antisera that contain Ab against specific influenza subtypes. In this way, HAI is employed for subtyping and for determining antigenic characteristics of influenza viral isolates. This is one of the reference methods that the WHO CCs employ to monitor every season the circulating influenza viruses, it is also widely used during the production of CVVs to assess their antigenic characteristics, and will be discussed in detail in the next sections.

Other techniques have been described for chemical, physical and biological characterization of H antigens, including Western Blot, SDS-PAGE electrophoresis, matrix assisted laser desorption/ionization-mass spectrometry (MALDI/MS), transmission electron microscopy (TEM) and dynamic light scattering (DLS).[88]

N activity is usually analyzed by neuraminidase inhibition assay (NI). This assay was first described by Warren in 1959,[97] and was later modified by Aymard-Henry *et al* in 1973.[98] This

technique is based in the fact that binding of specific Ab to NA results in the inhibition of its enzymatic activity.[99] NI is performed in microtiter plates and starts with the incubation of the virus isolate with selected subtype-specific reference antisera. Then, a sialylated protein, such as fetuin, is added. If the viral neuraminidase is active, it will release quantities of free Neu5Ac from fetuin. This free Neu5Ac is converted to β-formyl pyruvic acid due to the oxidation produced by a periodate reagent added to the plate. Next, arsenite reagent and thiobarbituric acid are added and consecutively boiled to release a pink-reddish product. Color intensity is then measured spectrophotometrically and should be proportional to the potency of the N. However, in the presence of homologous antiserum, N is inhibited, Neu5Ac is not released, and the reaction does not happen.

Molecular methods (such as RT-PCR) could also be employed to characterize H and N. Nevertheless, the information they provide is complementary to the HA/HAI techniques and not a direct replacement.

1.3.1. Hemagglutination assay

The hemagglutination assay (HA) is a classical method used worldwide in a broad range of applications. This assay is often used for quantification of viruses or bacteria under controlled conditions and is necessary for the production of some vaccines and antigens *in vitro.* HA is employed as well as a tool for screening the cell cultures or the egg amnio-allantoic fluid on which the influenza viruses are usually grown from respiratory patient samples.[100,101] However, HA by itself is not an identification assay, because there are diverse pathogens (such as influenza,[102] paramyxoviruses,[103] rubivirus,[104] adenovirus,[105,106] and certain bacteria[107] able to produce hemagglutination with similar results. In contrast, when the assay is modified to perform an inhibition hemagglutination assay (HAI), it allows both pathogen identification and characterization, and also titration of anti-pathogen neutralizing Ab.[108]

HA and HAI were originally described by Hirst in 1942 based on the ability of influenza viruses to bind to red blood cells (RBCs), causing hemagglutination and altering RBC sedimentation.[102] Normally, free RBCs sediment in the wells of microtiter plates and form a visible pellet at the bottom. This is related to the fact that the abundant sialylated glycoproteins of the RBC surface give the individual cell a negatively charged surface. This creates a repulsive electric zeta potential between cells that prevents the RBCs to interact with each other and agglutinate[109]. In this way, individual cells settle down over time, roll across the plate bottom, and concentrate around the center of the well. The produced pellets have different shapes depending on the animal origin of the RBCs and the type of microtiter plate used (a tight button for avian RBCs in V-shaped plates and a halo for the mammalian ones in U-shaped plates; Figure 1.12a).

However, when the RBCs are incubated in the presence of influenza virus, the H proteins exposed on the virus surface recognize and bind the SA residues of the RBCs surface. This interaction is driven by a combination of hydrophobic, electrostatic, and hydrogen bonds, which counteract the repulsion between the RBCs. If influenza viruses bind simultaneously to multiple RBCs, they produce their agglutination and form a lattice structure that prevents RBCs sedimentation. These agglutinated RBCs remain cloudy in the wells without displaying any

pellet (Figure 1.12b). This process is called hemagglutination and can be easily observed by the naked eye, without using any equipment, although it requires some experience and can be subjected to different criteria depending on the type of erythrocytes employed.

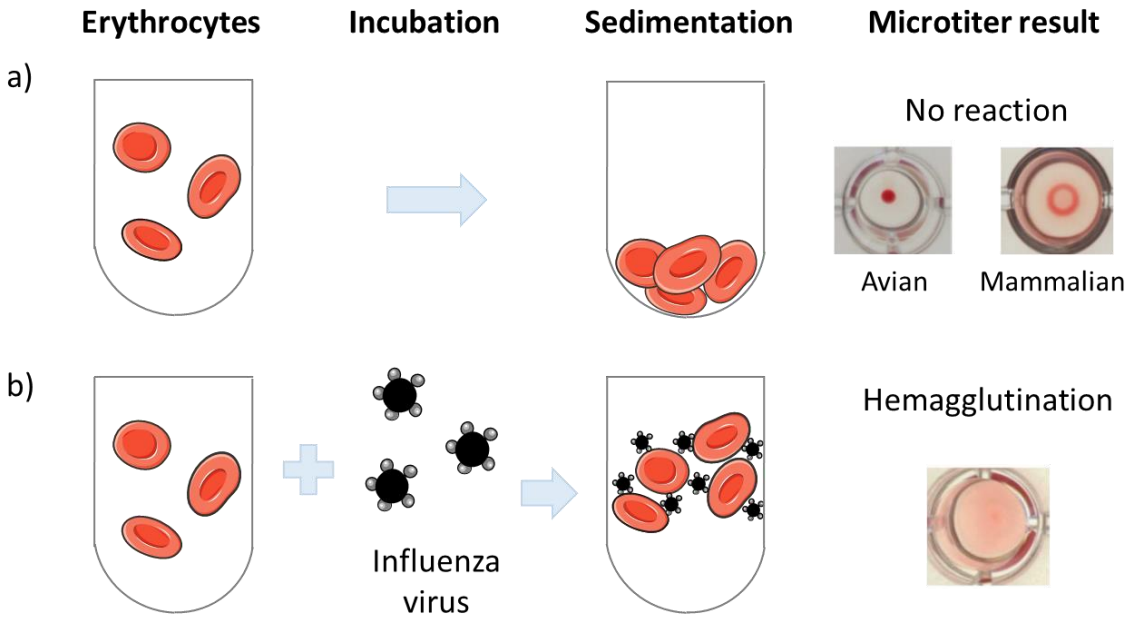

Figure 1.12 | a) RBCs sediment in the microwell and produce two types of pellets depending on the RBCs origin and the type of microtiter plate used (V-plate, avian RBCs; U-plate, mammalian RBCs). **b)** In the presence of influenza virus, RBCs hemagglutinate and prevent the pellet generation.

To perform HA assays, dilutions of virus-containing samples are mixed with a fixed amount of RBCs. Then, the virus titer is determined based on the highest minimal sample dilution that produces a change in RBCs sedimentation pattern and is recorded in HA units (HAU). In this way, a HAU does not correspond to an absolute concentration of virus, but instead describes the amount of a certain virus preparation needed to agglutinate a fixed amount of a standardized RBC suspension.[110] By convention, the last well in the HA titration where complete hemagglutination occurs contains 1 HAU.

1.3.2. Characteristics of RBCs in hemagglutination

As described before, human influenza viruses bind preferentially to α2,6 linked SA, while avian influenza viruses prefer α2,3 linked SA. Accordingly, the choice of the erythrocytes used in the HA and HAI assays varies depending on the characteristics of the tested virus. In this respect, the content, type and proportion of SA is different in RBCs of different animal species. For example, dog erythrocytes contain an estimate of $72x10^6$ SA residues/erythrocyte, while rabbit erythrocytes contain only $3x10^6$ residues/erythrocyte, 24-times less.[111]

Not only the total amount of SA diverges, but also the proportion between α2,6 and α2,3 linked SA present in the glycoproteins and glycolipids of the erythrocyte surface. Table 1.2 shows a summary of the distribution of different types of SA among diverse animal RBCs, revealed by diverse studies using lectins that recognize specifically these types of linkages (*Maackia amurensis* lectin for α2,3 and *Sambucus nigra* lectin for α2,6). For example, horse RBCs

display almost exclusively α2,3 linked SA, which is useful for characterizing avian (A(H5N1)) and equine influenza viruses due to their preference for α2,3-linked SA. Nevertheless, horse RBCs display mainly Neu5Gcα2,3Gal instead of Neu5Acα2,3Gal,[112] which could explain why, in some comparative studies, they leaded to lower HA titers but higher HAI titers than other alternatives. Again, this makes them the preferred option for HAI titration against avian viruses.[113]

Table 1.2 | Comparation of the amount of α2,3- and α2,6-linked SA described in RBCs depending on their animal origin.[112,114] ***** Contain mainly NeuGc instead of NeuAc.

RBCs Origin	α2,3	α2,6
Chicken	++	+
Turkey	+	++
Pigeon	+/-	++
Human	++	++
Guinea Pig	+	++
Horse*	++	+/-
Pig*	+	++
Sheep	++	-
Cow*	++	+/-

Both turkey and chicken erythrocytes are a popular selection for performing seasonal influenza HA and HAI due to their availability, faster settling time, and clearer inhibition patterns, because both are small and nucleated cells that display rapid sedimentation.[114,115] However, turkey RBCs contain both types of receptors (α2,3 and α2,6), although with a higher content of α2,6, which allow them to recognize more influenza H3 viruses.[116,117] This trend has changed recently, since some strains of influenza viruses (specially A(H3N2)) have reduced or even lost their ability to bind to turkey RBCs in the later years,[117,118] making them less useful for determining HA and HAI titers. As described previously in Section 1.1.3, this is related to changes occurred in amino acids around the receptor pocket of the H protein, which could produce this effect in the binding preference of the virus. On the other hand, these same viruses retained their binding to guinea pig RBCs.[119] Therefore, for the analysis of viruses with high α2,6 affinity or in early passages during growth *in vitro*, guinea pig RBCs are often required to obtain acceptable titers in HA assays.[115]

It is worth noting that even when using a certain type of RBCs, such as from a fixed animal species, there may be differences in the sensitivity of the RBCs depending on the individual animal they were obtained from[114]. Moreover, it is well known that, in each RBC preparation, the amount of SA is also affected by aging. Some studies showed that, as erythrocytes grow old, the amount of SA exposed on surface can drop by 20-30%, which decreases the surface negative charge and may be related to senescence and survival of RBCs.[120–122]

Other differences between species include RBC shape and diameter, among other morphological parameters. Mammal RBCs are anucleated cells with a size ranging from 7.5 to 8.7 µm in diameter in humans.[123] Guinea pig RBCs show a mean diameter of 7.1 µm, while sheep, pig and horse RBCs are smaller with mean diameters ranging from 4.9 to 6.2 µm.[124] The absence of the nucleus produces a thinner central region, which confers the biconcave shape typical in most of the mammalian erythrocytes. Bird RBCs, on the other hand, contain an oval nucleus and present a more elliptical shape. Their diameter can range between 10-15 µm in length and 6-9 µm width depending on the bird species,[125,126] making them larger than mammalian erythrocytes. Due to these morphological differences, some HA settings, such as the type of plates (U-bottomed or V-bottomed) and the sedimentation times, should be adapted for each RBC species. This also includes the way to interpret the pellets when hemagglutination does or does not occur. Table 1.3 shows a summary of these adaptations when working with mammalian and avian cells.

Table 1.3 | Changes in the HA protocol according to the type of RBCs. Avian RBCs are bigger due to the nucleus presence, and therefore require less time to sediment. When using V-plates with avian RBCs, it is also recommended to tilt the plate to differentiate easily between agglutinated and non-agglutinated wells, while this is not required for mammalian RBCs.

RBCs Origin	Plate type	Sedimentation time	Tilting required
Avian	V-bottom	30 min	Yes
Mammal	U-bottom	60 min	No

To sum up, using erythrocytes from different hosts can be a fast way to evaluate the receptor specificity of influenza viruses. H binding depends on the type of SA and the linkage that connects it to the oligosaccharide.[112] By exploiting these characteristics, combined with the diverse distribution of SA on the surface of RBCs of different species, we can study influenza virus specificity and detect potential changes that could lead to interspecies transmission. However, unavoidable RBC intra-host differences could introduce some variability in these HA results.

1.3.3. Hemagglutination inhibition assay (HAI)

Although HA can provide useful information, its lack of specificity and the potential changes in H tropism make it insufficient to subtype the different influenza viruses. Therefore, a HAI assay is usually performed after HA.

HAI test involves 3 different elements: Ab, influenza virus and RBCs. When a sample containing a certain influenza virus is pre-incubated with Ab that show affinity for that virus, the Ab recognizes the virus and binds to it. If this blocks the virus H, it does no longer bind to RBCs. Consequently, hemagglutination is inhibited and RBCs sediment, forming the characteristic sedimentation pattern (Figure 1.13a). On the contrary, if the Ab had been raised against a strain completely different from the one in the sample, recognition does not take place, the Ab does not block H in the influenza virus, and HA happens (Figure 1.13b).

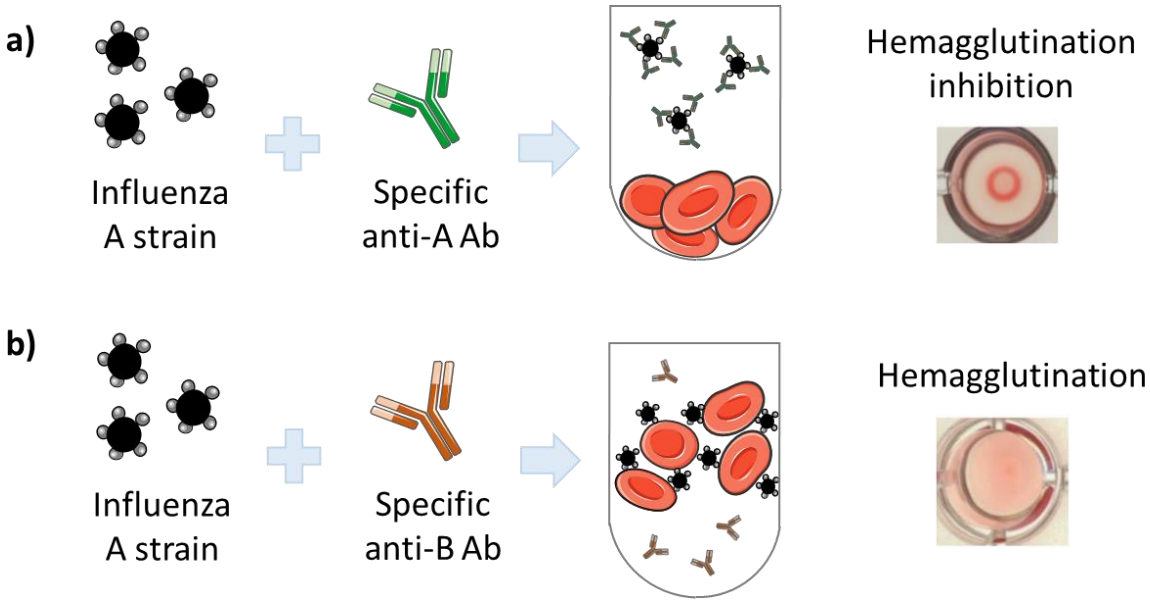

Figure 1.13 | a) When influenza virus is incubated with specific Ab against the same strain (or a strain antigenically similar), it causes the inhibition of RBC agglutination, thus producing the sedimentation pattern. **b)** If the Ab have been produced against a completely different strain, they will not block the interaction between the virus and the RBCs and hemagglutination will happen.

This method has two main applications: the antigenic characterization of isolated viruses and as a tool for serological analysis (to evaluate vaccine response or for epidemiological studies). Depending on the target application, a combination of reference viruses or reference antisera are used to perform HAI (Figure 1.14).

Most of these reference viruses are inactivated for safety reasons, generally using beta-propiolactone (BPL), a process often used in vaccine virus inactivation as well. Working with inactivated viruses facilitates their handling, because BSL-3 facilities are not required.[127] Other alternatives have been described for inactivating influenza viruses, including the use of heat, formalin, Triton X-100, UV-radiation and H_2O_2, among others.[127–129]

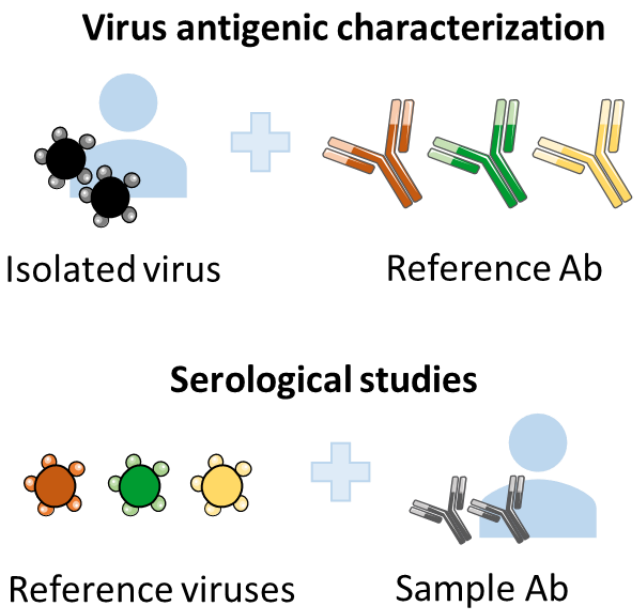

Figure 1.14 | Schematic of two of the main applications for HAI assays. The viral antigenic characterization requires incubation of reference Ab with virus isolated from patient samples and grown in eggs or cell culture. Serological studies, on the contrary, are generally performed incubating reference viruses with serum samples obtained pre and post vaccination. In both cases, results are always compared to a reference panel that combines reference Ab and reference viruses that function as controls.

Although some studies showed that BPL treatment reduces the HA titer,[127,128] it is still the preferred method due to its widespread use in industrial settings for inactivation of multiple pathogens, disinfection, and sterilization of some components such as plasma or tissue for transplants.[130]

For the antisera, they are produced by infecting immunological naïve animals, normally ferrets, goats or sheep, with the reference virus. It has been known for long that HAI tests can be affected by non-specific inhibitors and agglutinins naturally present in the sera.[131,132] There are many serum treatments used to remove non-specific inhibitors, including heat treatment and treatment with either kaolin, periodate or receptor destroying enzyme (RDE) from *Vibrio cholerae* (which has neuraminidase activity),[133,134] among others.[131,135]

Of these, the WHO recommends employing preferentially the RDE treatment for all the serums to be used in HAI assays. This is especially important for the sera from ferrets, which are extensively used at CCs to antigenically characterize the viruses obtained locally or through NICs, due to their higher content of non-specific inhibitors compared to other species.[131] Once the RDE has destroyed most of the non-specific inhibitors, it must be inactivated at 56ºC prior to the use of the treated sera in HAI assays.

Apart from the non-specific inhibitors, non-specific agglutinins must also be removed from the sera. These agglutinins could interact directly with the RBCs causing HA, and thus false negative results in HAI tests, even in the presence of specific anti-influenza Ab. To solve this, it is recommended to perform sera pre-adsorption with an excess of RBCs from the same

species that is going to be used in the assay.[115] Moreover, in some cases (such as when using horse RBCs for serologic detection of Ab against some avian influenza viruses), it is suggested to perform first RBCs adsorption and then RDE treatment, because new non-specific inhibitors may be introduced into the serum during the adsorption step.[136]

HAI has diverse advantages that explain their extended use. It is relatively inexpensive and rapid: results can be obtained in about 2 h. No special equipment or facilities are needed to perform the assay. Moreover, different types of samples are allowed (serum, plasma, allantoic fluid and cell culture supernatant, among others). HAI assays are also very versatile, because they can be set up to detect either Ab or viruses depending on the reagents employed.[137] Still, they present some disadvantages, such as the need to pre-treat serum samples to remove nonspecific agglutinins and potential inhibitors, the need to titrate and adjust the biological reagents each time the assay is performed, or the subjective interpretation of the test results that can be biased by worker training and experience, among others. Nevertheless, HAI still remains being one of the reference assays for global influenza surveillance.

1.3.3.1. Antigenic characterization of isolated viruses by HAI

One of the main uses of HAI is measuring the degree of antigenic similarity between a test virus and a known reference virus, using for this a reference antiserum with Ab against that reference virus. This characterization is employed by the WHO to monitor the changes that are taking place in circulating viruses and to compare them to those included in the vaccines.

To perform a HAI assay for virus antigenic characterization, each reference antiserum is diluted across the microtiter plate and incubated with a fixed amount of the virus-containing test sample or a reference virus for 15 to 90 min, depending on the protocol employed.[138,139] Test samples use to be respiratory samples obtained from patients, which have been spiked in embryonated eggs or cell cultures to amplify the virus so that it reaches titers high enough to be studied by HAI. The amount of sample, and thus test virus dilution, needed has been previously obtained during a HA titration and is in general equivalent to 4 HAU per 25 µL.[115] Then, RBCs, diluted to a standard concentration, are added to the wells. The plate is then incubated for other 30-60 min, depending on the type of RBCs used, to allow RBC to sediment. If the Ab in a reference antiserum, that resulted from animal immunization with a certain reference virus, can recognize and bind the influenza virus present in a sample obtained from an ill patient, this indicates that both viruses display some antigenic similarity. By determining which reference antiserum dilutions inhibit the hemagglutination of the RBCs in the presence of the test and reference viruses, we can compare RBC tropism and Ab-binding affinity and specificity for the two viruses (Figure 1.15). This is, the fewer the amount of Ab required to prevent hemagglutination (thus the higher the dilution of the reference antiserum), the higher the antigenic similarity between the two viruses compared. In this context, the highest dilution of the antiserum that results in hemagglutination inhibition is considered the HAI titer for that test virus.

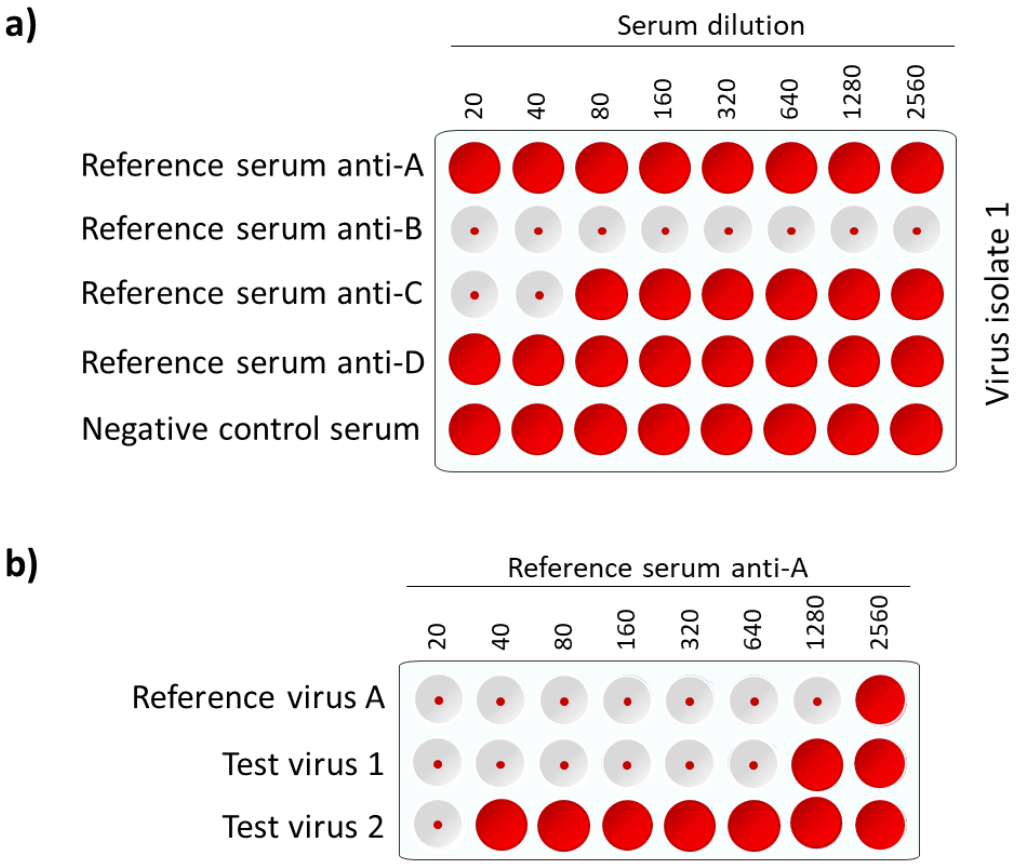

Figure 1.15 | Two ways of performing HAI assay for virus antigenic characterization. In HAI assays, both virus and RBCs are added at a fixed concentration. **a)** In this example, different reference anti-sera are sequentially diluted and incubated with the same fixed amount of virus from isolate 1. As can be seen, reference serum anti-B produces a total inhibition of the hemagglutination, while serum anti-A and D produces none. This indicates that Virus 1 is from the same type or subtype as reference virus B. Virus 1 also presents some cross-reaction with reference serum anti-C. Controls (reference virus for each anti-serum) should always be added to allow comparation. **b)** In this configuration, the assay is carried in parallel for a reference strain (A) and two test viruses using the same reference antiserum (anti-A) submitted to serial dilution. This reference virus has a HAI titer of 1280, because the greatest dilution of antiserum that still blocks hemagglutination from occurring is 1:1280. At this dilution, the Ab in the antiserum are still capable of recognizing and binding to the antigens on the virus, inhibiting virus-induced RBC hemagglutination. In contrast, in the presence of less Ab, the virus produces hemagglutination. When test virus 1 is compared to the reference virus, they differ in HAI titer by only one dilution (a 2-fold difference) and therefore they display antigenic similarity. However, test virus 2 differs by five dilutions (a 32-fold difference) and should be considered as a completely different strain.

It is considered that two influenza viruses are antigenically similar if their HAI titers differ by two-well dilutions (4-fold dilution) or less.[140] Figure 1.15 shows an example of a HAI assay where one of the tested viruses is considered similar to the reference one (Virus 1), with just a 2-fold difference (1 dilution) in titer. Virus 2 clearly differs antigenically because it shows a 32-fold difference (5 dilutions) with the reference virus. This indicates that test virus 2 is probably a completely different strain or even subtype of influenza virus.

This information is helpful to determine, for example, if the individual components of the vaccine need to be updated each year. If a reference antiserum, produced by infecting ferrets with one of the influenza strains included in the vaccine of the previous season, can target and neutralize effectively a virus of the same subtype circulating the following season, that circulating virus will be considered antigenically similar to the strain used in the vaccine. If a similar result is obtained for the whole set of circulating and vaccine-included viruses, the vaccine may not need to be changed that year. On the contrary, if the ferret antiserum does not neutralize one or more of the circulating flu viruses, it will be concluded that the circulating virus has undergone significant antigenic drift and therefore this component needs to be updated in the next vaccine.

1.3.3.2. Serologic studies using HAI

Direct virus antigenic characterization is the main use for HAI assays at the GISRS, but they can also be helpful to carry out serological studies. Serological tests are a fundamental tool in epidemiological and immunological studies, as well as for evaluation of the Ab response following vaccination.

Serological analysis are not ordinarily used for influenza diagnosis, because virus isolation is usually faster and produces more accurate results. In addition, most human sera contain Ab to influenza viruses due to prior infections or vaccinations, and therefore diagnosis of individual cases using only one-time point serum extraction is unreliable. Nevertheless, serology can be useful in certain situations, such as when the identification of the virus by direct isolation is not feasible (because clinical specimens are unobtainable or when appropriate facilities for virus isolation are not available). This is also the method of choice to study the immunological response of a population group after vaccination or after infection with influenza virus. In this case, serology testing requires the analysis of paired serum samples (pre- and post-vaccination; acute and convalescent). Then, seroconversion is assessed based on the titer of specific anti-influenza Ab detected 2-3 weeks after the infection, which should have increased 4-fold or more to be considered significant. This may allow to establish the diagnosis of influenza infection in cases when the direct attempts to detect the virus have been negative.[115]

When used for this application, HAI follows the same principle as for the antigenic characterization, but using reference viruses instead of reference antisera. These viruses are usually controlled strains produced by the WHO (for example, CVVs or the components of the WHO Influenza Reagent Kit) or influenza virus strains grown in the laboratory and previously characterized. The Influenza A reference antigens in the WHO Influenza Reagent Kit are BPL inactivated whole viruses also suitable for serological diagnosis, but influenza B antigens need to be ether-treated. This is necessary due to the low sensitivity to Ab rises of influenza B whole viral antigens.[115,141] Although ether treatment increases the sensitivity, it also reduces the specificity of HAI when performing the assay with serum samples against influenza B.[142,143] Therefore, the WHO Influenza Reagent Kit provides BPL-inactivated B reference antigens for antigenic characterization and ether-treated antigens for serological purposes.

As previously, paired serums require to be pretreated using RDE and RBC pre-adsorption to eliminate nonspecific inhibitors and nonspecific agglutinins. Then, HAI test can be carried out following the same protocol as in antigenic characterization of viral isolates.

The HAI titer of a serum sample is defined as the inverse of the highest serum dilution where RBCs show complete inhibition, i.e. where cells are not agglutinated. In general, the starting dilution is 1:10, and therefore the lower detection limit of the Ab titer in this assay is 10.[115] An Ab titer higher than 40 is commonly considered an indication of seroprotection against that specific virus. Beyond this threshold, there is at least a 50% reduction in the possibility of contracting influenza infection.[110,144] This protection increases in correlation with the titer, although the progressive benefits for titers higher than 100 are less significant.[145]

As previously stated, it is recommended to state the immune protection based on seroconversion. This is especially useful to evaluate vaccination effectiveness, where the titers of the pre-vaccinated serum and 30-days post-vaccination serum are compared. A 4-fold titer increase indicates the achievement of seroprotective titers.[146] In the case of negative pre-vaccination serums, the minimum titer to be considered seroconversion is 40. Nonetheless, this criterion should be adjusted depending on the age of the cohort, where children and elders require different thresholds due to their immunological state.

1.3.3.3. HAI versus other serological methods

Complement fixation and enzyme immunoassays can also be used for serological diagnosis. Complement fixation is easier to perform than HAI, but it does not distinguish between virus subtypes, and ELISA entails longer and more complex handling.[96] Hence, the gold standard techniques for detecting anti-influenza Ab and to differentiate between subtype- and strain-specific Ab are the neutralization and the HAI assays.[115] The neutralization assay (also called microneutralization assay when performed in 96-well plates) is a highly sensitive and precise test that detects specifically neutralizing Ab to influenza viruses. The assay is based on the assumption that neutralizing Ab present in a test serum will block the H protein, preventing virus binding to the host cell surface and inhibiting infection. To carry the assay, serially diluted serum is pre-incubated with a standardized amount of influenza virus, as it happens in the HAI procedure. Then, MDCK cells are added and incubated overnight to allow infection to occur. Next day, cells are fixed and detection of influenza nucleoprotein in infected cells is performed through an ELISA.

One characteristic of this technique is that it detects functional strain-specific Ab against the viral H protein. Furthermore, it uses infectious viruses instead of inactivated antigens, which should facilitate assay implementation in response to the emergence of a novel virus or in a pandemic setting. On the other side, it requires the use of high-level facilities in the case of highly pathogenic strains, which hinders the establishment of these techniques in many laboratories. Other disadvantages includes a considerable inter-laboratory variability due to discrepancies in their reference protocols and the internal procedure to determine the endpoint of the assay,[135] and their laborious and time consuming process, which requires at least two days to yield results.

Compared to the HAI assay, microneutralization identifies functional n-Ab and is more sensitive than HAI, especially for low-titer seroconversions.[135] However, it is less specific in elderly adults, because some of the neutralizing Ab produced by previous exposure to influenza viruses will target conserved regions of the H, common between different subtypes of influenza A viruses,[147] and requires more time and complex equipment to be performed.

1.3.4. Limitations of hemagglutination inhibition assay

The importance of the HAI assays for influenza surveillance is evident. HAI is a key method to obtain antigenic information of the circulating viruses and to determine whether a vaccine made using a specific set of viral strains will protect the population against the circulating viruses or not. It is a widespread technique used in most of the laboratories that comprise the GISRS, but still has some limitations that impact its potential use and result reliability.

A few of these limitations are directly related to circulating virus isolation and growth efficiency. For example, as stated before, respiratory samples from patients do not display virus titers high enough to be studied directly by HAI and are normally grown first in eggs. However, a considerable proportion of recent influenza A(H3N2) viruses do not grow well in eggs, and are also more prone to suffer egg-related adaptations than other influenza viruses. This not only worsens the matching between the vaccine and the current A(H3N2) circulating viruses, but also reduces the amount of virus available to perform the antigenic characterization after egg-growth. To solve this, primary isolation is now being performed using MDCK cells in many centers. Moreover, this cell line was modified to increase the amount of α2,6-linked SA in their surface (MDCK SIAT1),[148] because current A(H3N2) viruses bind preferentially to these SA residues. Nevertheless, there is still a reduction in the HA titer obtained from isolates grown in cell culture compared with egg-grown isolates.[115]

Another issue is the ability of different influenza viruses to agglutinate RBCs obtained from different animal species. The changes in the viral H molecule sometimes alter receptor affinity, and this may translate into a loss of sensitivity when using certain RBCs. This is especially important in the most recent A(H3N2) viruses,[149,150] and also in some strains during the early growth passages.[117] This handicap makes it necessary to use different types of RBCs to obtain satisfactory HA titers for the whole set of circulating influenza viruses, because RBCs from different species have different SA-residue composition. Turkey RBCs are generally the primary option to perform HAI, but for difficult influenza strains it is recommended to use guinea-pig RBCs, which have demonstrated more sensitivity for human influenza viruses.[115] Even though, there are still some A(H3N2) viruses that cannot be characterized through HAI due to the low HA titer they produce in the culture step. For these cases, a new assay that requires less virus was developed, called High-content Imaging-based micro-Neutralization Test (HINT),[151] but its use is still not widespread.

1.3.4.1. The challenge of method standardization

One of the most important limitations of HAI analysis is the lack of standardization between laboratories. The results obtained from HAI assays by the different GISRS members must be analyzed globally, integrating the data from multiple laboratories distributed around the world in order to reach a consensus for the vaccine composition and to detect the emergence of new influenza viruses. In this context, HAI result variability hinders the comparability of the results obtained and impacts ultimately the vaccine effectiveness. The limited reproducibility of HAI assays between laboratories has always been a concern, with titers that could vary up to 128-fold for some specimens tested in parallel in diverse laboratories.[152] This high variability is mainly caused by two parameters: the lack of protocol harmonization and the use of biological reagents difficult to standardize.

Regarding protocol unification, since 1994 different international studies have been carried out to assess the extent of the problem.[153] In fact, "Immunological Assay Standardisation and Development for use in Assessments of Correlates Of Protection for Influenza Vaccines" was the main topic for the 10th Innovative Medicines Initiative (IMI) call in 2013.[154] Moreover, multiple attempts to standardize the technique have been made, for example, by the creation of diverse global partnerships such as CONSISE in 2011 (Consortium for the Standardization of Influenza Seroepidemiology,[155] and FLUCOP in 2015.[156]

Some of the identified variables with a significant impact in the assay variability included the amount of virus added, the viral culture system (eggs or cultured cells), the initial serum dilution and the duration of the RDE treatment, the duration and temperature of the serum-virus incubation and for the serum-virus-RBCs settling.[152,157,158] Moreover, the age and origin of the RBCs and the concentration employed in HAI assays showed the highest variability across laboratories.[139]

Another issue noted by many of these authors was that, despite the availability of common HAI protocols, most laboratories used their own assay procedures.[158] Nevertheless, diverse studies that attempted to unify the protocol reported that, even with detailed harmonization, interlaboratory variability was not significantly improved.[159] One of the suggested explanations was that some of the most critical reagents, such as the RBCs, were obtained from different sources in the different laboratories. Later studies showed that when the key reagents were obtained from the same source, variability was reduced.[157]

The biological reagents used in the HAI assay are difficult to standardize. To help with the standardization of influenza surveillance assays worldwide, the WHO distributes to the requesting centers (through the International Reagent Resource (IRR) of the Centers for Disease Control and Prevention (CDC, Atlanta, USA)) a kit that contains most of the reagents needed for HAI virus typing, subtyping and antigenic characterization, with the exception of RBCs. Accordingly, RBCs are obtained by each laboratory independently. Apart from providing intra- and inter-laboratory variability, using unstable fresh RBCs forces the experimentalist to titrate and adjust the different kit components each time a HAI test is performed, which constitutes another inconvenience of this technique.

1.3.4.2. RBCs drawbacks

RBCs are one of the main reagents needed for HAI and HA assays, but also one of the main causes for the assay high variability. Logistical issues and their short-life impede the centralized production and distribution of RBCs from a common source to all the laboratories performing HAI for influenza surveillance. Diverse studies highlighted the importance of standardizing the RBCs. One of the most recent was the last FLUCOP report, which surveyed the variation in the RBCs usage protocols in 11 laboratories. This study showed that RBCs were one of the main sources of variability in HAI assays due to the differences in the type, age (days from bleeding) and concentrations employed, as well as for the procedures to obtain them.[139] These differences also entailed the RBCs counting protocols (which could be based on packed volume estimate, hematocrit, autocell count or photometer) and the number of washing steps prior to their use in HAI, which differed between 1 and 4 washes.

This study selected fresh turkey RBCs (1 to 5 days old) as the optimal setting for HAI assays. This brings forward one of the main drawbacks of RBCs: their short shelf-life. RBCs should be obtained regularly because they begin to hemolyze after 5-7 days from the bleeding, causing inaccuracies in HA/HAI assays.[121] Accordingly, RBCs should be discarded after 1 week to avoid false results. This same characteristic is what makes erythrocytes difficult to obtain commercially and/or in large quantities for worldwide distribution. In our experience, when RBCs are commercially purchased through suppliers, they often arrive too close to their expiration date, or even after it, which hinders the performance of the assays (Figure 1.16).

Figure 1.16 | Commercial RBCs received the same day of the expiration date. Hemolysis of the RBCs can be easily observed in the supernatant of the bottle, even prior its opening. Another option is to employ glutaraldehyde-stabilized RBCs, which are also commercially available.[160] This treatment helps to extend the RBCs shelf-life while preserving the erythrocyte antigenicity, but few studies have evaluated this treatment impact in HA and HAI assays.[161] Although results seem promising, their performance after a prolonged storage period is not demonstrated yet. This, together with its considerable higher price, makes the use of this material not common for influenza surveillance.

Besides the lack of stability, RBCs also require multiple and cumbersome pre-wash steps to prepare them each time they are extracted or when hemolysis has occurred.[115] Then, RBCs have to be normalized using a counting protocol that, as stated before, is not well standardized across the laboratories.[139]

Moreover, the titration of the reference viruses by HA is always necessary previous to any HAI tests to ensure that the virus still recognizes successfully the remaining RBCs, which consumes resources and time.

Another major drawback of using fresh RBCs is the need to use and bleed regularly caged animals, which entails ethical concerns. Increasingly stringent regulations related to animal welfare are being established globally, which hampers the collection of this required reagent.

RBCs should be collected from specific pathogen-free or specific Ab-negative animals, and even the sex of the animal must be considered. For example, some studies suggest that the hormones present in hen's blood can decrease the reproducibility of the test, an effect expected to be common across the different species.[137] Due to this requirement, many laboratories decide to obtain the RBCs through their own stabled animals or through arrangements with nearby animal facilities instead of purchasing them using traditional commercial suppliers. This increases further the variability of RBCs acquisition price and characteristics across the laboratories.

Moreover, as explained in Section 1.3.2, RBCs from different animal species must be used depending on the virus affinity. For example, as a generalization, avian influenza viruses recognize better the α2-3 linked SA, and thus are better analyzed using horse RBCs, which contain more of this type of SA-linked residue. When focused on human influenza viruses, A(H3N2) viruses are traditionally analyzed using guinea pig RBCs, while turkey RBCs are recommended for the rest of the seasonal influenza viruses.

1.3.4.3. Alternatives to RBCs

HAI assays are essential for influenza virus surveillance and vaccine or antigen (Ag) production, despite their multiple drawbacks. Most of them could be prevented by the standardization of the protocols and substitution of RBCs, one of their main variability sources. Multiple attempts have been made in this direction, usually substituting RBCs with synthetic particles coated with specific antigens or Ab.

These synthetic particles can be made of different materials, including latex, silica, polymers or even gold nanoparticles. Latex particles are one of the most common approaches. In general, coated-latex beads could clump together in the presence of the appropriate Ag or Ab, mimicking the hemagglutination assay. An example of this application for serological studies was developed by Esmail and colleagues, who designed an agglutination-based test where blue latex particles coated with receptor-binding domain (RBD) or nucleocapsid protein recognized anti-SARS-CoV-2 Ab with high sensitivity.[162] They compared these modified particles to RBCs conjugated with the same SARS-CoV-2 antigens. In both cases, the assay was performed on cards, and although agglutination could be observed by the naked eye, it was difficult to distinguish the degree of agglutination without using image analysis, especially in the latex particles. Many serological assays based on latex agglutination use this type of readout in cards.[163,164] Other approaches kept the sedimentation of the particles in microplates as a reading method, more like classical HAI assays. S. Hosaka, for example, employed dyed poly(glycidyl methacrylate) microparticles with a diameter of 2 to 4 μm covered with BSA and achieved a sedimentation rate and sediment shape nearly equal to those of RBCs.[165] Moreover, these particles could also change the sedimentation pattern when agglutinated with anti-BSA antisera, producing the same hazy bottom than RBCs.

On the other side, latex and gold nanoparticle agglutination tests based on Ab have been previously developed to detect influenza H.[166–168] In these examples, particles were coated with reference antisera, which could produce variability between particle and antisera production batches. Moreover, these assays required spectrophotometric reading to obtain

the results. Although all these methods were sensitive and relatively fast, they relied on Ab recognition. As described in section 1.1.3, influenza viruses present a high diversity on H, which mean that implementing such an immunoassay would require producing specific beads for each influenza strain tested, which would make the assay cumbersome and expensive.

To avoid this issue, multiple strategies that employ influenza receptors instead of Ab have been developed. One of the most used is the incorporation of SA glycans to different types of particles, including gold nanoparticles.[169–172] This incorporation could be achieved through chemical conjugation to the surface or embedding the SA during the particle production process. One of the common strategies for detecting influenza viruses consists of using α2-3 and α2-6 SA, generally in form of SL or SLN, or even as larger ramified derivatives. The studies have shown that employing SA with ramifications and multiple SA-terminals per molecule, which allows for the simultaneous binding of multiple H trimers, increased the sensitivity of the assays. Some of these SA-coated nanoparticles are even employed as influenza virus infection inhibitors in antiviral therapy.[173,174]

Albeit the multiple approaches described above have been defended by their authors as feasible alternatives to HA and HAI, most of them require substantial changes compared to the standard HA/HAI methodology, often requiring additional instrumentation for obtaining the results (such as spectrophotometry,[170,172] biolayer interferometry,[171] or surface plasmon resonance,[175,175] which are not always available in laboratories of low-income countries.

Chapter 2

Objectives

Chapter 2. Objectives

The overall aim of this PhD Thesis was the development of a synthetic reagent that could substitute animal erythrocytes in the HA/HAI assays used currently for global influenza surveillance. This reagent, called "**synthrocytes**", should mimic the differential sedimentation displayed by animal RBCs in the absence and in the presence of agglutinating agents, but be more stable, reproducible, and potentially mass-produced, without requiring considerable changes in the existing protocol for HAI assays. This should contribute to worldwide standardization of HAI tests with minimal equipment or training requirements and facilitate inter-laboratory result evaluation.

To ensure the transferability of the developed protocols, commercially available materials and well-established techniques have been used wherever possible. Moreover, because this work was envisioned as a potentially marketable product, some decisions during the development were conditioned by their economic impact and not only by their scientific performance.

In order to accomplish the general thesis aim, the work targeted four specific objectives over time, which are detailed next:

1. Development of synthrocytes with the capacity to bind influenza viruses and change the sedimentation pattern upon binding, to be used to perform HA- and HAI-like assays.

    1.a. Production of the first proof-of-concept made with naturally sialylated proteins.

    1.b. Use of synthetic receptors for improving synthrocyte sensitivity and reproducibility.

    1.c. Development of a multiplexed synthrocyte using a battery of receptors on surface to achieve recognition of the main 4 seasonal influenza types.

2. Explore synthrocyte industrialization feasibility by optimizing strategies for synthrocyte long-term stabilization and production scale-up.

3. Reduce the variability of synthrocyte agglutination assays through automatization and objectivation of results readout.

4. Identification of new alternative applications for the developed technology.

The accomplishments achieved during this thesis have been organized in 10 chapters plus annexes. Chapter 3 describes the reagents, materials and procedures employed during this work. Chapters 4 to 9 describe the experimental results obtained and their corresponding discussion. More specifically, chapters 4 and 5 present the design and development of the different synthrocyte versions produced, starting with the selection of the synthrocyte components and the optimization of their production protocol. Chapter 6 describes the stability studies, lyophilization procedure and production scale-up, which were performed under the supervision of Dr. Pere Carulla during a 12-month stage in the company Biosystems. These tasks overlapped over time with those described in Chapters 4-5. Chapter 7 shows the results of the first technology field validation carried in the National Influenza Center of Valladolid. Chapter 8 presents two different approaches explored for quantification and automation of

synthrocyte agglutination assays, including a microfluidic device developed during a 5-month internship carried out in Dr. Henry's group in Colorado State University (USA). Two alternative applications for the technology developed in this work are explored in Chapter 9. The general conclusions and future work are presented in Chapter 10.

Finally, Annex 1 includes a copy of the manuscript published summarizing part of the results of this Thesis and Annex 2 displays copies of the scientific articles with results obtained during this Thesis, often as part of the training received, but not included in this dissertation.

This work started thanks to the Explora project BIO2015-72401-EXP, funded by the Spanish Ministry of Economy, which enabled the design and development of the first proof-of-concept of synthrocytes. Following this preliminary study, synthrocytes were improved and tested for other applications in the context of projects IU68-017255/2019PROD00086 (*Agència de Gestió d'Ajuts Universitaris i de Recerca* (AGAUR), *Departament d'Empresa i Coneixement, Generalitat de Catalunya; Projectes Producte*), DTS20/00093 (*Instituto de Salud Carlos III*; *Proyectos de Desarrollo Tecnológico en Salud*), and LCF/TR/CC21/52490005 (La Caixa Foundation; Consolidate). Projects IU68-017255/2019PROD00086 and LCF/TR/CC21/52490005 supported also patentability and market studies, intellectual property protection and helped to determine regulatory and economical requirements for synthrocyte realistic implementation.

The whole thesis was possible thanks to a predoctoral fellowship IFI18/00020 "Doctorados IIS-Empresa en Ciencias y Tecnologías de la Salud" (i-PFIS), granted by *Instituto de Salud Carlos III,* cofounded by the European Regional Development Fund, and two contracts supported by projects BIO2015-72401-EXP and LCF/TR/CC21/52490005. The 5-month stage in Colorado University (USA) was supported by a mobility fellowship M-AES from *Instituto de Salud Carlos III* (MV19/00036).

The technology described in this Thesis, including the synthrocytes and their utilization in agglutination assays, have been protected through the following patent request:

> Reagents and fast methods for pathogen characterization and serology testing Autores: Eva Baldrich Rubio, Ana Sánchez Cano, Andrés Antón Pagarolas, Cristina Andrés Vergés. José Raúl Herance Camacho, Tomás Pumarola Suñé.
>
> European Patent EP19382496.8, 13 June 2019, Oficina Española de Patentes y Marcas
>
> International Patent PCT/EP2020/066292, 12 June 2020, European Patent Office, The Hague
>
> Fundació Hospital Universitari Vall d'Hebron - Institut de Recerca (VHIR)

Chapter 3

Materials & Methods

Chapter 3. Materials and Methods

3.1. Reagents, Chemicals, and Biocomponents

3.1.1. Microparticles

Diverse types of microparticles were employed in this Thesis, comprising a range of sizes, materials, densities and reactive groups exposed on surface. They are summarized in Table 3.1.

Table 3.1 | Properties of tested microparticles. "*ns*", stands for not stated by the provider.

Provider	Particle	Material (colour)	Density (g/ccm)	Surface	Diameter (µm)	Reference
Micromod (Germany)	Sicastar – blue	Silica (blue)	1.8	NH_2	10	73-01-104
					5	73-01-503
					3	73-01-303
				COOH	5	Custom-made
	PLA-blue Sicastar	Poly(D,L-lactic acid) (blue)	1.0	NH_2	30	54-01-304
					2	54-01-203
					0.5	54-01-502
	Sicastar-M	Magnetic silica (brown)	2.5	NH_2	1.5	39-01-153
	Sicastar-M-CT	Cluster-typed magnetic silica (brown)	2.5	NH_2	6	59-01-603
Bangs Laboratories (USA)	ProMag 3	Polymer and iron oxide (brown)	1.6	COOH	2.75	PMC3N
	ProMag HP 3	Polymer and iron oxide (brown)	1.4	COOH	3.13	PMC3HP
Invitrogen (USA)	Dynabeads M-270 Amine	Polystyrene with magnetic material	ns	NH_2	2.70	14307D

3.1.2. Receptor candidates

Over the course of this thesis, multiple receptor candidates (natural and synthetic) have been tested for their potential influenza-binding capacity.

3.1.2.1. Naturally sialylated proteins

The characteristics of all the proteins used for influenza recognition are described in Table 3.2.

Table 3.2 | Characteristics of the proteins evaluated. ns, not stated by the provider. *Reports indicate that GYPA has a carbohydrate content ranging 40-80%[176] and accounts for 75% of the total sialic acid exhibited on the RBCs membrane.[177,178] ** Experimental results shown that Trnsf has a pI of 5.7 approximately.[179]

Provider	Protein	Ref.	Abbrev.	Origin	SA content	MW (kDa)	Isoelectric point (pI)
Sigma-Aldrich (Spain)	Glycophorin A	G5017	GYPA	Human erythrocyte membrane	ns*	50-80	5.9-6.3
	Bovine Mucin	M3895	BM	Submaxillary glands	9-24%	~ 1000	3
	Porcine Mucin	M2378	PM	Stomach mucus	<1.2%	~ 1000	3.5
	Fetuin	F3004	Fet	Fetal Bovine Serum	5-8%	48.4	3.3,3.2-3.8
	Human Transferrin	T3309	Trnsf	Human	ns	76-81	ns (5.7)**
	Bovine Serum Albumin	A7030	BSA	Bovine Serum	ns	66	4.7-5.3
Thermo Fisher (USA)	Avidin	21121	Av	Egg	ns	67-68	10
	Neutravidin	31000	NeuAv	Egg	Deglycosylated	60	6.3

Unless otherwise recommended by the provider, proteins were aliquoted immediately after being received, and were stored at -20ºC in isofreeze color-changing racks. Lyophilized proteins received in high volume were stored in powder and the required weight was freshly resuspended before each use.

Neutravidin (NeuAv) and BSA were used as negative controls for diverse experiments.

3.1.2.2. Synthetic receptors

Synthetic receptors that comprised various types of SA were analyzed. Below is a table with the description of their molecular structure (Table 3.3).

Table 3.3 | Description of the different SA mentioned in this work**.**

Name	Abbrev.	Nomenclature	Scheme
3'-Sialyllactose	3'-SL	Neu5Ac(α2-3)Gal(β1-4)Glc	
6'-Sialyllactose	6'-SL	Neu5Ac(α2-6)Gal(β1-4)Glc	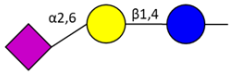
3'-Sialyl-N-acetyllactose	3'-SLN	Neu5Ac(α2-3)Gal(β1-4)GlcNAc	
6'-Sialyl-N-acetyllactose	6'-SLN	Neu5Ac(α2-6)Gal(β1-4)GlcNAc	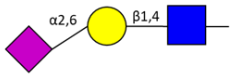
N-Acetyllactose	N-Ac	Gal(β1-4)GlcNAc	

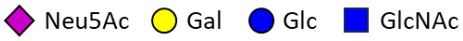

These SA were obtained commercially from two different providers, modified with different reactive groups, linkers and/or protein carriers to facilitate their conjugation on top of the particles. Table 3.4 shows the different combinations employed in this work.

Table 3.4 | Characteristics of the SA molecular derivatives tested.

Provider	Ref.	Provider's terminology	SA	Linker/carrier	Abbrev.
Glycotech (USA)	01-038	3'-Sialyllactose-PAA-biotin	3'-SL	PAA-biotin	$[3'\text{-SL}]_3$-PAA-b
	01-039	6'-Sialyllactose-PAA-biotin	6'-SL	PAA-biotin	$[6'\text{-SL}]_3$-PAA-b
	01-060	6'-Sialyl-N-acetyllactosamine-PAA-biotin	6'-SLN	PAA-biotin	$[6'\text{-SLN}]_3$-PAA-b
Dextra (UK)	NH316	Glycyl-6'-sialyllactose	6'-SL	Gly (-NH2)	6'-SL-NH2
	NGB1706	6'-Sialyllactose-biotin	6'-SL	Biotin	6'-SL-b
	NGP0706	6'-Sialyllactose-BSA	6'-SL	BSA	6'-SL-BSA
	NGP0702	3'-Sialyllactose-BSA	3'-SL	BSA	3'-SL-BSA
	NGP0301	3'-Sialyl-N-acetyllactosamine-BSA	3'-SLN	BSA	3'-SLN-BSA
	NGP0201	N-Acetyllactosamine-BSA	None	BSA	N-Ac-BSA

PAA: Poly(acrylic acid); BSA: Bovine serum albumin

In the synthetic receptors with PAA-biotin, the SA is incorporated to a polyacrylamide matrix thereby creating a 30-kd multivalent polymer. Unless otherwise stated, approximately every 5th amide group of the polymer chain is N-substituted with biotin in a 4:1 ratio. The final content of this polymer is approximately 5% mol biotin and 10% mol SA.

In the synthetic receptors with BSA, the SA is incorporated in the BSA surface through a 3-carbon spacer.

3.1.3. Lectins

Lectins are glycoproteins usually obtained from plant sources that have a carbohydrate-binding capacity. They bind with high specificity to sugar moieties present in glycoproteins or in free monosaccharide and glycan structures. In the presence of human RBCs, this may produce hemagglutination. Each lectin has its own recognition pattern, some of them being very restrictive, and displays a different hemagglutination activity. The hemagglutination activity is expressed as the lowest concentration needed to agglutinate a 2% suspension of human erythrocytes after 1 h incubation at 25°C.

Three different lectins purchased from Sigma-Aldrich were employed to simulate the virus-induced agglutination. Their characteristics are shown in Table 3.5.

Table 3.5 | Summary of the lectins employed in this work.

Lectin	Ref.	Abbrev.	Recognition	Hemagglutination activity
Wheat germ agglutinin	L9640	WGA	N-acetyl-β-D-glucosamine oligomers and Neu5Ac	<20 µg/mL
Sambuccus nigra lectin	L6890	SNA	Mostly α-Neu5Ac(α2-6)Gal, and Neu5Ac(α2-6)GalNAc	≤4 µg/mL
Maackia amurensis lectin	L8025	MAA	Mostly Neu5Ac(α2-3)GalNAc	<10 µg/mL

3.1.4. Influenza viruses

All influenza viruses used in this work had been inactivated by the producer using beta propiolactone treatment (BPL). This treatment modifies chemically the nucleic acids and amino acids of the virus and produces a loss of the infectivity capability.[130,180] The inactivated influenza viruses used for developing the first version of synthrocytes were provided by Hytest (Finland). Apart from BPL inactivation, these viruses had been purified using ultracentrifugation with sucrose gradient from allantoic fluid of 10 days old embryonated eggs. The final preparations contained also 0.09 % sodium azide (NaN_3) and 0.005 % thimerosal and their concentration was estimated by the supplier. The references for these viruses are found in the following table.

Table 3.6 | Inactivated virus from Hytest.

Strain	Subtype/Lineage	Ref.
A/New Caledonia/20/99	H1N1	8IN73-3
A/Solomon Islands/03/06	H1N1	8IN73-4
A/Taiwan/1/86	H1N1	8IN73
A/Beijing/262/95	H1N1	8IN73-2
A/Brisbane/10/07	H3N2	8IN74-4
A/Panama/2007/99	H3N2	8IN74-1
B/Victoria/504/00	B/Yamagata	8IN75-3

WHO reference viral antigens were obtained through the Influenza Reagent Resource (IRR, Influenza Division, WHO collaborating center for the surveillance, epidemiology and control of Influenza; Centers for Disease Control and Prevention, Atlanta), which corresponded to the viruses included in the WHO Influenza Reagent Kit for Influenza Isolates of the seasons 2018-

21. These vials contained BPL-inactivated virus in allantoic fluid containing 0.01% of NaN_3. A summary of all the viruses employed and their corresponding season are listed below.

Table 3.7 | WHO reference viral antigens used in this work. The season in which each strain was included in the kit is also indicated.

Subtype/Lineage	Strain	Ref.	Year
H1N1pdm09	A/California/07/2009 NYMC X-179A	FR-1184	2013-2015
	A/Michigan/45/2015 NYMC X-275	FR-1605	2018-2019
	A/Brisbane/02/2018	FR-1665	2019-2020
		FR-1730	2020-2021
	A/Indiana/02/2020	FR-1773	2021-2022
H3N2	A/Singapore/INFIMH-16-0019/2016	FR-1606	2018-2019
	A/Kansas/14/2017	FR-1666	2019-2020
		FR-1731	2020-2021
	A/Tasmania/503/2020 cln2	FR-1783	2021-2022
B/Yamagata	B/Phuket/3073/2013	FR-1609	2018-2019
		FR-1669	2019-2020
		FR-1734	2020-2021
		FR-1777	2021-2022
B/Victoria	B/Colorado/06/2017	FR-1607	2018-2019
		FR-1667	2019-2020
	B/Washington/02/2019	FR-1732	2020-2021
		FR-1775	2021-2022
H5N1	A/Egypt/N03072/2010 PR8-IDCDC-RG29	FR-1073	-
	A/Vietnam/1203/2004 PR8-IBCDC-RG/GLP	FR-919	-
	A/Chicken/Vietnam/NCVD-016/2008 PR8-IDCDC-RG12	FR-907	-
H7N9	A/Anhui/01/2013	FR-1248	-
H9N2	A/Hong Kong/33982/2009 PR8-IDCDC-RG26	FR-916	-

3.1.5. Antiserums

The WHO Influenza Reagent Kit for identification of influenza isolates contained each year reference antiserums against each of the viral types included in the kit. These serums were made of pooled hyperimmune antiserum produced in goats against representative influenza viruses that circulated at the time the reagent was manufactured. A description of all the reference antiserums employed in this work can be found in the following table.

Table 3.8 | Reference antiserums from the WHO Influenza Reagent Kit for identification of influenza isolates. The season where each strain was included in the kit is also indicated.

Subtype/Lineage specificity	Ref.	Year
H1N1pdm09	FR-1611	2018-2019
	FR-1682	2019-2020
	FR-1736	2020-2021
	FR-1779	2021-2022
H3N2	FR-1612	2018-2019
	FR-1683	2019-2020
	FR-1737	2020-2021
	FR-1780	2021-2022
B/Yamagata	FR-1614	2018-2019
	FR-1685	2019-2020
	FR-1739	2020-2022
B/Victoria	FR-1613	2018-2019
	FR-1684	2019-2020
	FR-1738	2020-2022
Negative control sera	FR-1377	2018-2022

3.1.6. RBCs

Commercial chicken, turkey and guinea pig RBCs were employed in this Thesis. Chicken and guinea pig RBCs were obtained from Innovative Grade US Origin (USA). Turkey RBCs were obtained from Rockland (USA). In all the cases, RBCs were received as washed pooled cells at concentrations ranging from 5 to 10% cells/mL. Before using them, cells were washed once to eliminate the buffer and the hemolyzed residues, and to work with a concentrated 100% erythrocytes stock.

Human RBCs were obtained locally from residual whole blood samples from anonymized O- individuals. Approval from the ethical committee was not required for this obtainment. Isolation and preparation of these RBCs are described in Section 3.10.1.

3.1.7. Buffers

All buffer solutions were prepared with milli-Q water and all reagents were of the highest available grade. The composition of these solutions is described in Table 3.9:

Table 3.9 | Composition of the buffered solutions used in this work.

Abbrev.	Composition	pH
PBS	11.9 mM sodium phosphate, 137mM NaCl, 2.7 mM KCl	7.4
PBST	PBS, Tween20 0.05 %	7.4
TBS	25 mM Tris, 140 mM NaCl, 3.0 mM KCl	7.4
MES	150 mM 2-(N-morpholino)ethanesulfonic acid	5.4

3.1.8. Enzyme Linked Immunosorbent Assay (ELISA) reagents

All ELISA assays were performed using 96-well high-binding microtiter plates purchased from Corning (Ref. 9018). A summary of the Ab and reagents used for the ELISA development is shown in Table 3.10. The blocking of the plate after physisorption of the capture molecule was performed using a commercial BSA-based buffer (Reagent Diluent Concentrate 2, R&D Systems). The primary Abs required for the ELISAs were purchased from Hytest (Finland). Each Ab had been produced in mouse and specifically recognized a different type/subtype of influenza based on the H protein. Secondary Ab was an anti-mouse IgG conjugated to horseradish peroxidase (HRP; Sigma Aldrich). ELISA detection was performed colorimetrically, using a ready-to-use solution of 3,3′,5,5′-tetramethylbenzidine Liquid Substrate (TMB; Sigma Aldrich) that contains hydrogen peroxide (H_2O_2) as a substrate. This solution was stored at 4°C and protected from light, as recommended by the provider, but it was temperated before its utilization. The stop solution employed was 1 M H_2SO_4.

Table 3.10 | Summary of the reagents used in ELISA.

Reagent	Provider	Ref.	Description	Dilution
Blocking solution	R&D Systems	DY995	10x PBS with 10% BSA	1:10 in H2O
Primary Ab	Hytest	3AH1	Influenza A Hemagglutinin H1 Ab	1:10000
		3HG3	Influenza A Hemagglutinin H3 Ab	1:5000
		3BH9	Influenza B Hemagglutinin Ab	1:10000
Secondary Ab	Sigma-Aldrich	A9044	Anti-mouse IgG peroxidase-labeled Ab (Ab-HRP)	1:30000
Enzyme substrate	Sigma-Aldrich	T4444	3,3′,5,5′-tetramethylbenzidine liquid substrate (TMB)	Ready-to-use
Stop solution	Fisher Scientific	12933634	H_2SO_4	1 M

3.1.9. Other reagents

For the particle-dying process, reactive blue (Ref. A12911, Alfa Aesar), dimethyl sulfoxide (DMSO, Ref. BP231, Fisher Scientific) and tetrahydrofuran (THF, Ref. 401757, Sigma Aldrich) were employed.

For cross-linking, reagents used included glutaraldehyde (Ref. 354400, Merck), 1-ethyl-3-(3-dimethylaminopropyl) carbodiimide hydrochloride (EDC) (Ref. 22980, Fisher Scientific), bis(sulfosuccinimidyl)suberate (BS3, Ref. 21580, Thermo Fisher) and Poly(ethylene glycol) diamine (PEG-diamine, Ref. 753084, Sigma-Aldrich).

BSA (Ref. A9074), Tween20 (Ref. P1379) and cholera filtrate (Ref. C8772, used as a receptor-destroying enzyme (RDE) to treat sera for hemagglutination inhibition assay) were obtained from Sigma-Aldrich.

3.1.10. Other applications specific reagents

For malaria detection, PAN *Plasmodium* lactate dehydrogenase (pLDH) monoclonal Ab (Ref. C01834M) were purchased from Biospacific (USA), and recombinant LDH from *Plasmodium falciparum* (PfLDH, Ref. A3005) was provided by CTK biotech (USA).

For SARS-CoV-2 detection, stabilized trimeric spike protein from SARS-CoV-2 was purchased from ExcellGene (Switzerland) and casein was purchased from Sigma-Aldrich (Ref. C5679).

3.2. Instrumentation

Several agitation equipment were used to perform the bead conjugation process and to optimize the agglutination assay.

- Rotator: Mini Lab Roller rotator (Labnet International, USA). This compact equipment displayed a 15-cm wheel that could be placed either in vertical or horizontal position, and that rotated at a fixed speed of 24 rpm. For this work, the wheel was always placed horizontally.

- Vortex Genie 2 (Scientific Industries, USA). This robust vortex agitator accommodated a wide platform that held up to 24 Eppendorf tubes. Vibration speed could be regulated between approximately 600 and 3200 rpm.

- Thermal Shake *lite* (VWR). Microtube shaking incubator with temperature control from 0 to 105°C. Agitation speed could be regulated between 300 and 1500 rpm.

- PS-M3D (Grant-bio). Multifunction 3D rotator with reciprocating, vortexing and orbital shaking. The turning angle is between 0 and 30° with adjustable speed between 1 and 100 rpm. The orbit diameter is 22 mm.

Centrifugations were carried using a Heraeus Fresco 21 centrifuge (Thermo Scientific). This is a refrigerated centrifuge with a capacity of 24 microtubes (1.5-2 mL) and a maximum speed of 14.800 rpm.

A FLUOstar Omega (BMG Labtech) microplate reader was employed to perform the quality control of colored particles and to interpret spectrophotometrically HA/HAI sedimentation patterns. This equipment can perform UV/Vis spectrometric reading from either the top or the bottom of the well. Moreover, it can also scan the wells forming a matrix that collects more than 900 data points per well.

Pictures of the microtiter plates with HA/HAI results were taken using a digital camera (Sony G Exmor R 20.4) or a mobile phone camera (Xiaomi MiA3). Illumination and placement of the plate was kept constant when possible. Usually, full-row images were taken (this is, each picture showed the 12 wells of the plate). When detail was required, two pictures of each row were taken to enhance the definition and to keep the wells centered (in this case, each picture contained 6 wells).

3.3. Characterization of receptor candidates by ELISA

ELISA was used to assess the ability of receptor candidates to recognize different influenza virus types before conjugating them to the beads. In order to do this, the different proteins and SA synthetic receptors were used as plate-bound capture agents (Figure 3.1).

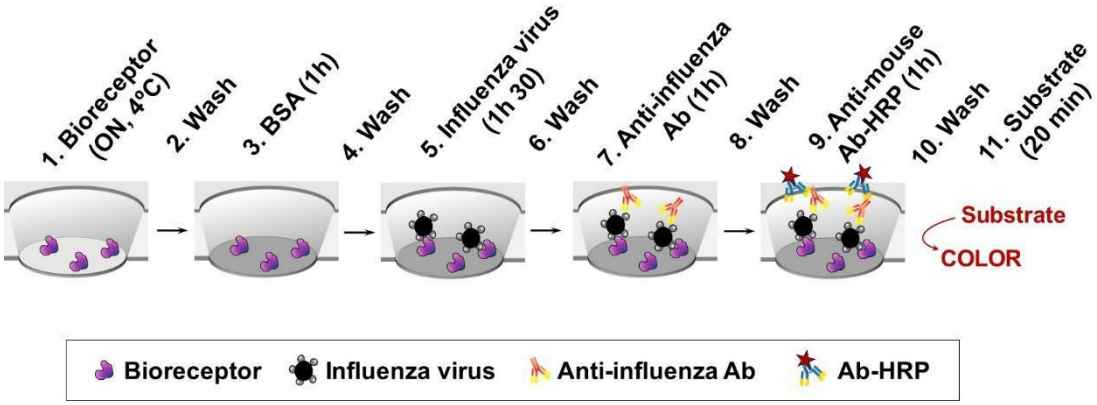

Figure 3.1 | Scheme of the ELISA procedure to evaluate the receptor candidates. The receptors were adsorbed in the plates and acted as a capture agent for the viruses. Then, the viral attachment was detected using a primary anti-hemagglutinin Ab followed by secondary-HRP-labeled Ab. Finally, the TMB substrate was added and the result read spectrophotometrically at 450 nm.

Unless otherwise stated, incubations were performed using 100 µL/well, with the plate covered with an adhesive seal to prevent evaporation, and were always followed by three consecutive washes using 200 µL/well of PBST. To start with, 50 µL/well of the receptor was immobilized in a 96-well high-binding plates overnight at 4°C. The optimal concentration for each receptor was previously established by performing a titrate with 2-fold dilution series of the receptor (prepared in PBS). Then, the plates were washed and were blocked for 1 h at room temperature (RT) with 200 µL/well of PBS-BSA 1% to prevent non-specific binding. Three consecutive incubations followed, with the corresponding washing steps in-between, the first with decreasing concentrations of the influenza virus strain of interest (90 min at 34°C); the second with primary Ab (diluted in PBS-BSA 1%; 60 min at RT); and the third with an HRP-labeled secondary Ab (diluted in PBS-BSA 1%; 60 min at RT). Finally, the plate was washed 4 times and was incubated with TMB substrate solution for 20 min (100 µL/well). This ready-to-use TMB was color-less. HRP catalyzed the oxidation of TMB coupled to the reduction of H_2O_2, which produced a half-oxidized blue product. When the stop solution was added (50 µL/well of 1 M H_2SO_4), the reaction produced fully oxidized TMB with a yellow color that was read spectrophotometrically at 450 nm.

3.4. Selection of beads displaying agglutination-dependent sedimentation

3.4.1. Microparticle chemical crosslinking

Two different strategies were used for the chemical crosslinking of the microparticles, depending on the reactive group exposed on their surface (NH_2 or COOH). In both cases, particles were washed once with PBS and then serially diluted with PBS in a microtiter plate with or without the corresponding crosslinker. For aminated particles, we employed a 2.5 mM solution of BS3, an homobifunctional crosslinker composed of two hydroxysuccinimide (NHS) ester groups separated from each other by an 11.4 A spacer arm. This reagent binds amine-to-amine from different particles, promoting agglutination (Figure 3.2). Carboxylated particles were incubated with a mixture of EDC (4 mg/mL) and PEG-diamine (0.05 or 0.5 mg/mL) to activate the carboxyl groups and to produce agglutination, respectively.

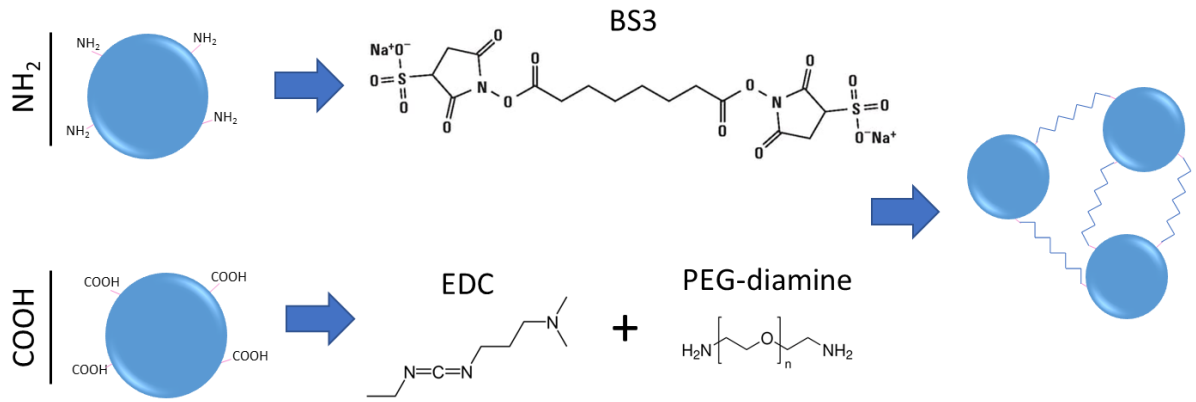

Figure 3.2 | Microparticle chemical-induced agglutination. Aminated particles were crosslinked using BS3, which reacts directly with the amine-terminals on the particle surface. Carboxylated particles, on the other hand, require first COOH-activation by EDC. Then, the two terminal amines of the PEG-diamine react to the activated carboxyl groups and produce agglutination.

Particles were allowed to settle down in the microplates at RT while taking pictures every 5 min. For amine particles, 10 min were enough to see differences, while for carboxyl particles it was required at least 30 min before noticing changes in the sedimentation pattern.

3.4.2. Study of well shape and agitation conditions in microparticle sedimentation

Since RBCs of different animal origin sediment differently in diverse bottomed plates, here, sedimentation of 5 and 10 µm Sicastar particles was studied using three types of microtiter plates: U-bottom (Ref. NUNC262162), V-bottom (Ref. NUNC249662) and flat-bottom (Ref. NUNC269787).

The effect of the agitation was also studied. Amine Sicastar 5 µm particles were incubated under different types of agitation or in static during 15 min, with concentrations of BS3 ranging from 2.5 mM to 0.07 mM. The types of shaking included vortex fast mixing (Vortex Genie 2,

600 rpm) and orbital agitation at either 10 or 30 rpm (PS-M3D). Then, images of the plates were taken after 15 min.

3.5. Particle custom-dyeing protocol and quality control

Particles of diverse colors were commercially available when we started this development, but they were subjected to a high batch-to-batch variability that affected color vividness specifically. Standardization of the bead color intensity was achieved by developing our own custom protocol for particle staining, using colorless Sicastar microparticles (Figure 3.3). This process was optimized mostly by another team member, together with the quality control required to ensure that each batch of custom-dyed particles displayed color and concentration within certain acceptable ranges.

Briefly, a 150 mM dilution of reactive blue dye was prepared in DMSO. This preparation was then diluted 1:100 in THF to obtain a final concentration of 1.5 mM. After that, as-received microparticles were homogenized, were mixed with the 1.5 mM reactive blue dilution in a 1:1 (v/v) ratio (usually, 500 µL of each), and were incubated for 1 h at RT with rotation. Particles were washed once with THF and twice with MiliQ water. Then, the final volume of the particle suspension was adjusted to match the initial volume.

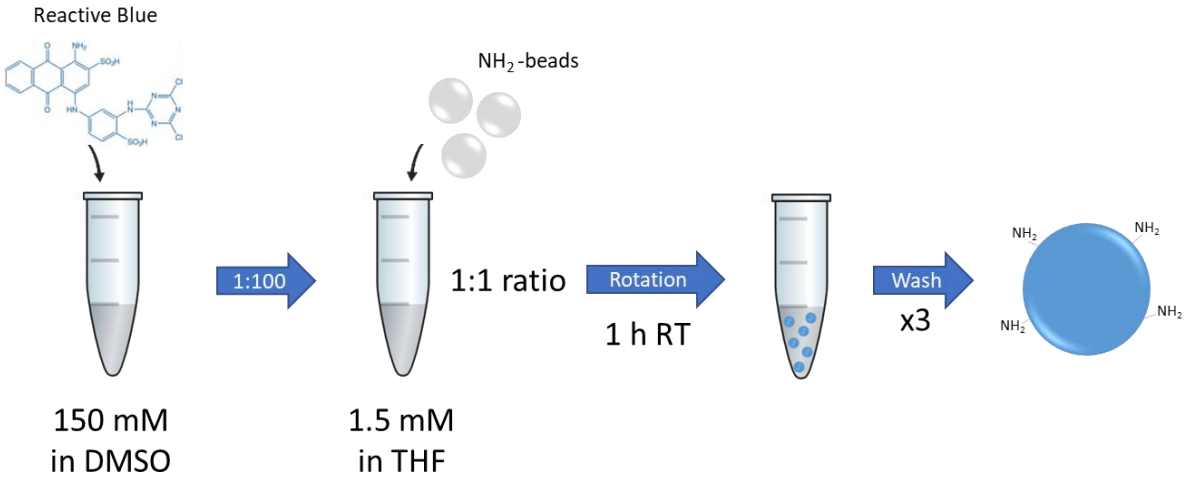

Figure 3.3 | Schematic of the microparticle custom-dyeing protocol.

The quality control of custom-dyed particles consisted of absorbance measurement by spectrophotometry. For this, 3 µL of the homogenized stained particles (µP) and 3 µL of the supernatant (SN, after sedimenting the custom-dyed beads) were collected and measured spectrophotometrically at 604 nm. Then, the % of dyeing rate was calculated as follows:

$$\frac{\text{Abs } \mu P}{\text{Abs } \mu P + \text{Abs SN}} \text{x } 100$$

It was established that the % of dyeing rate should range between 95 and 100%, which indicated that most of the dye was permanently bound to the particles and was not being released to the supernatant anymore. Lower percentages indicated that particles were still releasing dye to the supernatant and thus required more washes.

3.6. Bead chemical modification

The incorporation of the receptors onto the particles can be accomplished by diverse methods. The coupling strategy must take into consideration the reactive groups on the surface of the particles and the available groups in the receptor. Here, receptors were bound directly using chemical crosslinkers (glutaraldehyde or EDC) or indirectly through biotin-NeuAv affinity binding. Unless otherwise stated, all incubations were carried out in Eppendorf tubes, at RT, protected from light, and under end-to-end mixing using a Mini Lab Roller rotator. For washes, particles were centrifuged for 3 min at 100 xG and resuspended in the appropriate buffer.

3.6.1. Direct modification

This type of coupling was employed for all the sialylated protein receptors and for synthetic receptors that contained a SA residue with a terminal -NH_2 available (SA-NH_2) or that were bound to a BSA carrier (SA-BSA). Conjugation with glutaraldehyde was employed for amine-bearing particles and EDC was used for carboxylated beads. The first produced the best results and will thus be described in more detail.

3.6.1.1. Conjugation of aminated particles using glutaraldehyde

A two-step incubation protocol was used for this type of conjugation (Figure 3.4). Sicastar blue particles (12.5 mg, equivalent to 250 µL of the as-received 50 mg/mL stock) were washed once with PBS and were incubated in rotation in 0.5 mL of glutaraldehyde 6% for 30 min. Glutaraldehyde-activated beads were washed with 1 mL of PBS and were incubated for 2 h in 0.5 mL of PBS with the appropriate amount of receptor (Table 3.11). This step was performed under agitation at 950 rpm in a thermoshaker (Thermal Shake Lite).

Modified beads were then centrifuged, the supernatant was removed, and the beads were incubated in rotation for 30 min with 1 mL of a TBS, 1% BSA blocking buffer. The resulting synthrocytes were washed once more with PBS and were finally resuspended in PBS, 0.02% BSA, 0.1% NaN_3 and stored at 4°C.

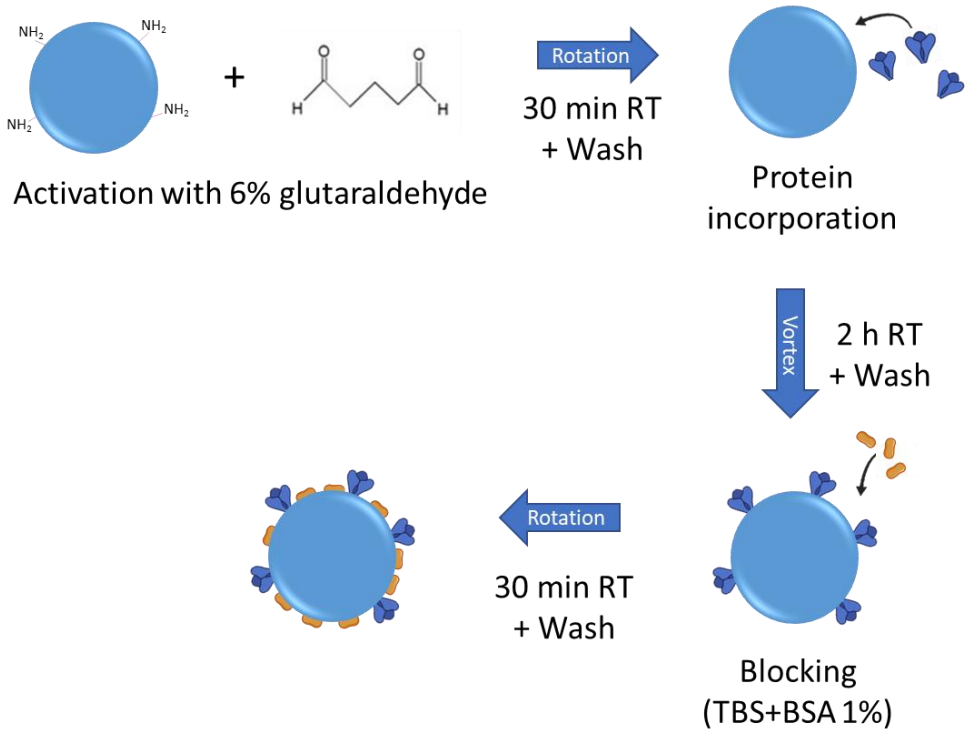

Figure 3.4 | Schematic of the two-step glutaraldehyde conjugation protocol for aminated particle modification with receptors.

Table 3.11 | Summary of the amount of protein required for each conjugation depending on the receptor employed.

Receptor	Quantity for conjugation
GYPA, BM, PM, Av, NeuAv, Fet, Trnsf	150 µg
SA-BSA	60-80 µg
Malaria panAb LDH	25 µg
SARS-CoV-2 Trimeric Spike	20 µg

This protocol was optimized thoroughly during this work. Parameters depicted in Table 3.12, such as the amount of receptor, volumes, number of washes, incubation times, types of blockings, buffer pH, type of agitation and storage buffer were optimized. The protocol described here includes the final selected conditions for direct conjugation with glutaraldehyde.

Table 3.12 | Summary of the different conditions optimized during this work, including the range evaluated for each of them.

Conditions optimized	Range tested	Optimal
Number of washes pre-conjugation	1-3	1
Incubation volumes	250-1000 µL	500 µL
Conjugation incubation time	30 min – 4 h	2 h
Type of agitation	Rotation, vortex (950-1500 rpm)	Vortex-type (950 rpm)
Conjugation buffer pH	6-8	7.4
Number of washes post-conjugation	0-2	1
Number of washes post-blocking	1-3	1
Types of blocking	Physical blocking: BSA, casein, dry-milk Chemical blocking: TBS, ethanolamine	BSA + TBS
Storage buffer	0.01%-1% BSA	0.02% BSA

3.6.1.2. Conjugation of carboxylated particles using EDC

Carboxylated Sicastar blue particles (25 mg, equivalent to 500 µL of the as-received 50 mg/mL stock) were washed twice with 1 mL of MES 0.5 M (pH = 4.5). Then, particles were incubated in 0.5 mL of MES, 20 mM EDC and 69 mM N-hydroxysulfosuccinimide (sulfo-NHS) for 45 min. EDC-activated particles were washed once with PBS and were incubated for 3 h with 200 µg of the sialylated protein dissolved in PBS. After that, particles were washed once with PBS and blocked using 1 mL of TBS, 1% BSA for 30 min. Finally, the conjugated beads were washed thrice with PBS and were stored with 0.1% BSA.

3.6.2. Indirect modification

Although direct conjugation was the main coupling strategy employed during this thesis, other approaches were evaluated. Biotin-NeuAv affinity binding can act as an amplifier of the available active area. This is because NeuAv is a tetrameric protein that display 4 biotin-binding sites, increasing 3 or 4 times (theoretically) the number of receptor-binding moieties on the surface, although this process is not completely efficient (Figure 3.5). The main disadvantage of this strategy was that it was useful only to bind biotinylated receptors. Accordingly, it was used for receptors that could be biotinylated in the laboratory, and this strategy was also useful to incorporate commercial biotinylated synthetic receptors, such as biotinylated SA $[SA]_3$-PAA-b and 6'-SL-b employed in this work.

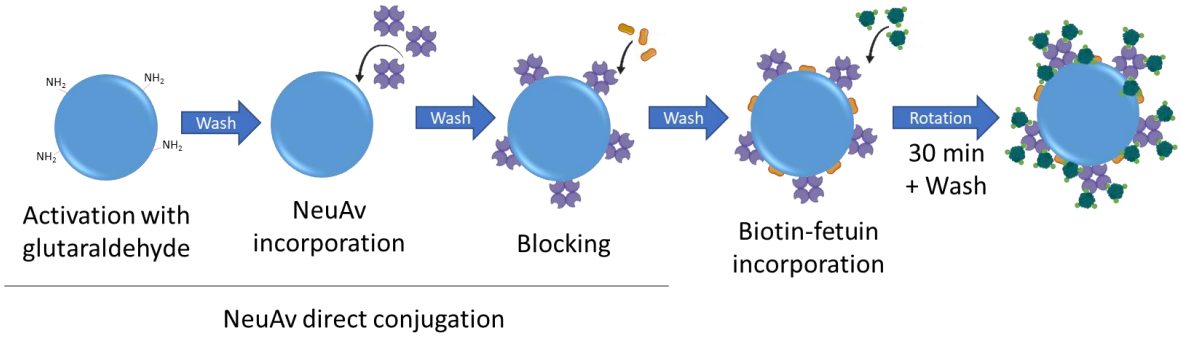

Figure 3.5 | Schematic of the indirect conjugation protocol, which consist in combining particles conjugated with NeuAv (by direct conjugation) and biotinylated fetuin.

3.6.2.1. Preparation of NeuAv-conjugated beads

Amine Sicastar particles were directly conjugated with NeuAv following the protocol described in Section 3.6.1.1. StrepAv direct conjugation was also tested during the optimization of this work following the same protocol, although NeuAv was finally chosen.

3.6.2.2. Preparation of biotinylated fetuin

The main biotinylation reagent employed for this protocol was Biotin-XX, SSE (6-((6-((Biotinoyl)Amino)Hexanoyl)amino)Hexanoic Acid, Sulfosuccinimidyl Ester, Sodium Salt; Ref. B6352; Thermo Fisher). This biotin presents a succinimidyl ester group that reacts with amines, a sulfonate group that provides water solubility, and a 14-atom spacer that enhances the accessibility of biotin to the relatively deep biotin-binding sites of NeuAv.

A solution of Biotin-XX, SSE 2.5 mg/mL was prepared in MiliQ water immediately before its utilization. Different molar ratios (biotin:fetuin) were used during the optimization, ranging from 5:1 to 18:1 of molar excess. The appropriate volume of the Biotin-XX solution was added to 150 µg of fetuin and the mixture was incubated for 2 h in rotation at RT.

Next, the conjugate was purified using a desalting column PD MiniTrap G-25 (GE Healthcare, Ref. 28-9180-07) and eluted with 1.5 mL of PBS. Fractions of 200 µL were recovered and analyzed with a Nanodrop Spectrophotometer 2000 (Thermo Scientific) at 280 nm. Finally, fractions containing the biotinylated protein were combined and concentrated using a centrifugal filter K Amicon Ultra-0.5 50K (Merck, Ref. UFC510024). The conjugate was measured again spectrophotometrically and diluted with PBS to the desired concentration to store it at 4ºC.

3.6.2.3. Modification of NeuAv-conjugated beads with biotinylated receptors

NeuAv-conjugated beads were incubated in rotation with the biotinylated receptor for 30 min to promote their affinity binding. Finally, particles were washed twice with PBS and were resuspended in PBS, 0.1% BSA, 0.1% NaN_3 and stored at 4°C.

3.7. Synthrocyte standardization and lyophilization

After conjugation, modified beads were counted using a Neubauer chamber and adjusted to a final concentration of ~$1.1x10^8$, ~$9.5x10^8$ beads/mL or ~$2x10^9$ beads/mL for 10, 5 and 3 µm particles, respectively, to produce standardized ***synthrocyte stocks***. These were stored in solution at 4°C using the correspondent storage buffers described in Section 3.6. Before being used, synthrocytes were diluted with PBS to produce the appropriate ***synthrocyte working suspensions*** (see later in the text).

For long-term storage, particles were lyophilized. A number of excipients were tested during lyophilization optimization (Table 3.13).

Table 3.13 | Summary of the different excipients tested for lyophilization and their tested range.

Excipient	Ref.	Provider	Tested concentration
BSA	A9647	Sigma-Aldrich	5 g/L - 40 g/L
Sodium Azide	111500	DC Fine Chemicals	0.1%
Trehalose	108216	Sigma-Aldrich	5 g/L - 40 g/L
Lactose	36889	Fisher Scientific	10 g/L - 40 g/L
Sucrose	131621	Panreac	5 g/L - 40 g/L

The final composition of the lyophilization buffer included 11.6 g/L of BSA and 0.1% of NaN_3 in PBS. Usually, 125 µL of standardized synthrocytes and 375 µL of lyophilization buffer were distributed in each 5 mL glass vial during the optimization process. For the final lyophilization format, the amount was increased to 350 µL of synthrocytes and 850 µL of buffer in each vial. These vials were reconstituted with 5 mL of PBS to produce ready-to-use synthrocyte working suspensions, which covered the requirements of one full microtiter plate.

The lyophilization process was performed using industrial equipment at Biosystems facilities. The lyophilizing recipe employed (temperature and cycles) is confidential and will not be disclosed here.

3.8. Synthrocyte Agglutination (SynA) Assay

Synthrocyte agglutination was achieved here by diverse means, including the use of lectins and different influenza viruses. In all cases, a dilution series of the agglutinating agent was prepared in a microtiter plate; synthrocytes, diluted to produce working suspensions, were added; and the mixtures were incubated at room temperature until sedimentation pattern interpretation. Unless otherwise stated, U-bottomed microplates (NUNC) were employed for all the assays involving synthrocytes.

Parameters such as dyeing and BSA blocking efficiency affected particle sedimentation and determined the amount of particles per well needed to carry SynA. Accordingly, this parameter had to be re-optimized along synthrocyte development and after each methodological improvement. Table 3.14. summarizes how synthrocyte working suspensions were prepared and the amount of particles needed per well for the main production paths that will be described in the work.

Table 3.14 | Amount of particles needed per well for the main synthrocyte production paths. The table compares de stock dilution needed to produce the different working suspensions, and the corresponding amount of synthrocyte stock needed per well in each case.

Type of particles	Amount of stock/well	Amount of beads/well	Working suspension (stock dilution)
Commercially-dyed	7.5 µL	375 µg	1/6.66
Custom-dyed	5 µL	250 µg	1/10
Lyophilized	3.5 µL	175 µg	1/14.3

3.8.1. Lectin-mediated SynA

A 10-fold serial dilution of the corresponding lectin (from 0.01 to 100 µg/mL in PBS) was prepared in a 96-well plate (final volume of 50 µL/well). Then, 50 µL of synthrocyte working suspension were added, mixed by pipetting and incubated for 10 to 25 min at RT before sedimentation evaluation.

The three lectins used for these experiments and their corresponding carbohydrate-binding tropism are described in Section 3.1.3.

3.8.2. Influenza virus mediated SynA

For influenza mediated SynA, 50 µL/well of PBS were added to each microplate row. Then, 50 µL of the influenza Ag was added to the first well and a serial 2-fold dilution was performed across the row, from well 1 to 11 as shown in Figure 3.6. The starting virus dilution corresponded to a 2 titer and the last one to 2048. The last well in the row did not contain virus and was used as a negative control. Then, 50 µL of synthrocyte working suspension were incorporated to all the wells and incubated at RT (for 10 min for 10 and 5 µm synthrocytes, and for 25 min for 3 µm synthrocytes). Finally, images of the wells were taken.

The agglutination titer was defined as the highest virus dilution able to produce visible agglutination and was considered to contain 1 Synthrocyte Agglutination Unit (SynAU).

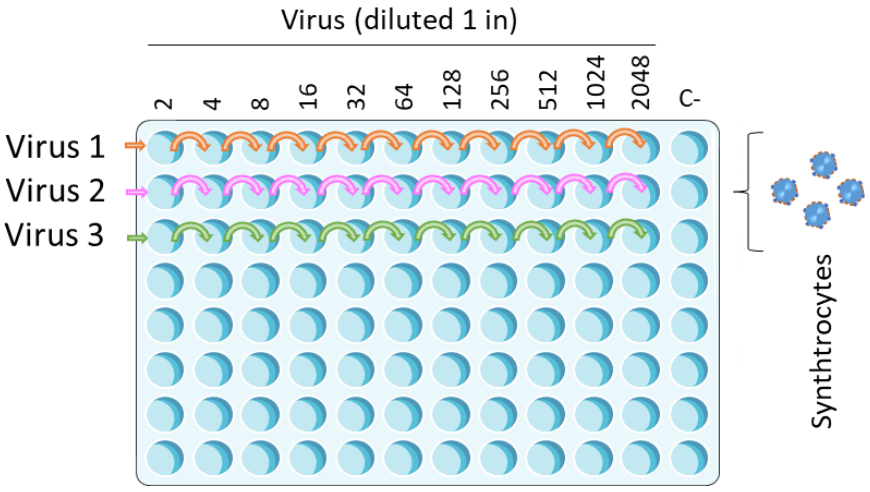

Figure 3.6 | Schematic of SynA protocol. In this example, 3 different viruses are tested. After adding 50 µL of PBS to all the wells, each virus is diluted in a serial 2-fold dilution to column 11, leaving well 12 with just PBS as a negative control. Then, 50 µL of synthrocyte working suspension are added and allowed to sediment for 10 to 25 min depending on the synthrocyte size.

3.8.3. Agglutination assessment by microscopy

To confirm lectin- and virus-induced agglutination, 2 µL of the synthrocyte stock solution were mixed with 22 µL of lectin or virus and incubated for 30 s on a glass slide. Then, the slide was covered and gently swung for 2 min. Finally, it was observed by microscopy (20×) using a Nikon TE2000 microscope.

3.9. Synthrocyte Agglutination Inhibition Assay (SynAI)

Along this work, diverse reagents were used to produce synthrocyte agglutination inhibition. As explained in Section 1.3.3, inhibition would happen if agglutination occurred in the presence of binders that display affinity for the agglutinating agent tested (for instance, Ab recognizing specifically the influenza virus strain present). Moreover, these Ab should block the ability of the viral H to interact with their SA receptor in order to prevent the agglutination, thus should be neutralizing Ab (n-Ab). Such n-Ab are present in the serum of infected and vaccinated individuals, but can be also produced in animal hosts (such as ferrets or goats) and through hybridoma technology (i.e., as monoclonal n-Ab). Here, we disclose the different protocols used depending on the source of Ab employed. In all the cases, the protocols were based on the ones provided by the WHO,[115] and adjusted following our hospital recommendations.

3.9.1. Agglutination inhibition by n-Ab

Commercial n-Ab were employed in the initial steps to confirm that the inhibition of the agglutination was specific, and before testing more complex sera (Section 3.9.2). Two monoclonal Ab specific for influenza A hemagglutinin were tested (Antibodies Online, Germany). The first one was raised against A/New Caledonia/20/99 (Ref. ABIN1605067), the other against A/Taiwan/1/86 (Ref. ABIN284533), both influenza A(H1N1) viruses.

To perform the analysis, 10-fold dilutions of each n-Ab were prepared in the wells of a U-plate (50 µL/well in PBS). Then, 50 µL/well of a 2.5 mg/mL dilution of A/New Caledonia/20/99 virus were added to each well, gently mixed and incubated for 30 min at RT. Finally, 50 µL/well of the synthrocyte working suspension were incorporated and images were taken after 10 min.

3.9.2. Agglutination inhibition by serums

This section includes the process required to work with WHO reference antiserums and with serum obtained from vaccinated and control donors and volunteers. In all the cases, serums were pretreated to remove nonspecific inhibitors of hemagglutination and nonspecific agglutinins that occur naturally in sera. These interferences could produce false positive and negative HAI/SynAI results, respectively.

3.9.2.1. Serum pre-treatment

To remove nonspecific inhibitors, serums must undergo a treatment with receptor destroying enzyme (RDE). This sialidase is extracted from *Vibrio cholerae* cultures and was purchased as a lyophilized powder from Sigma-Aldrich (Ref. C8772). 100 µL of each serum were mixed with 300 µL of RDE (reconstituted in 5 mL sterile water) and were incubated for 16 h at 37°C. Then, the RDE was inactivated by incubating the mixture at 56°C for 30 min. Finally, 600 µL of PBS were added to each serum to obtain a final 1/10 serum dilution.

Next, serums were pre-adsorbed with synthrocytes to remove nonspecific agglutinins. For this, the RDE-treated serum (1 mL after the 1/10 dilution) was incubated with 190 µL of stock synthrocytes for 40 min. To avoid modifying the serum dilution, synthrocytes were centrifuged and the supernatant was removed before adding the serum. After each 10 min, particles were mixed by inversion to favor the adsorption of nonspecific agglutinins. Finally, the mixture was centrifuged, and the supernatant was collected. This treated serum could be directly stored at -20°C. If the serums were to be used in HAI, this process was performed using RBCs instead of synthrocytes, as described in Section 3.10.3.

3.9.2.2. SynAI procedure

The first step for SynAI was performing a SynA assay following Section 3.8.2 to obtain the titer for each virus considered. Then, the virus was diluted to a final concentration equivalent to 2 or 4 SynAU/25 µL. A back-titration was next done using this Ag dilution to confirm if this was the dilution needed or should be amended.

Serial 2-fold dilutions of each serum (25 µL/well) were prepared across a plate between wells 1 and 7. 25 µL of each serum was also added to well 8 as a non-specific agglutination control. A fixed dilution of the virus (2 or 4 SynAU/25 µL/well) was added to wells 1-7 and 25 µL of just PBS to well 8, and the mixtures were incubated for 30 min at RT. Afterwards, 50 µL of synthrocyte working suspension were incorporated to all the wells and incubated for 10 min for 10 µm particles or for 25 min for 3 µm particles to allow them to sediment. Images were taken and the pattern was analyzed to determine the SynAI titer. The SynAI titer was the reciprocal of the highest serum dilution at which the agglutination was inhibited.

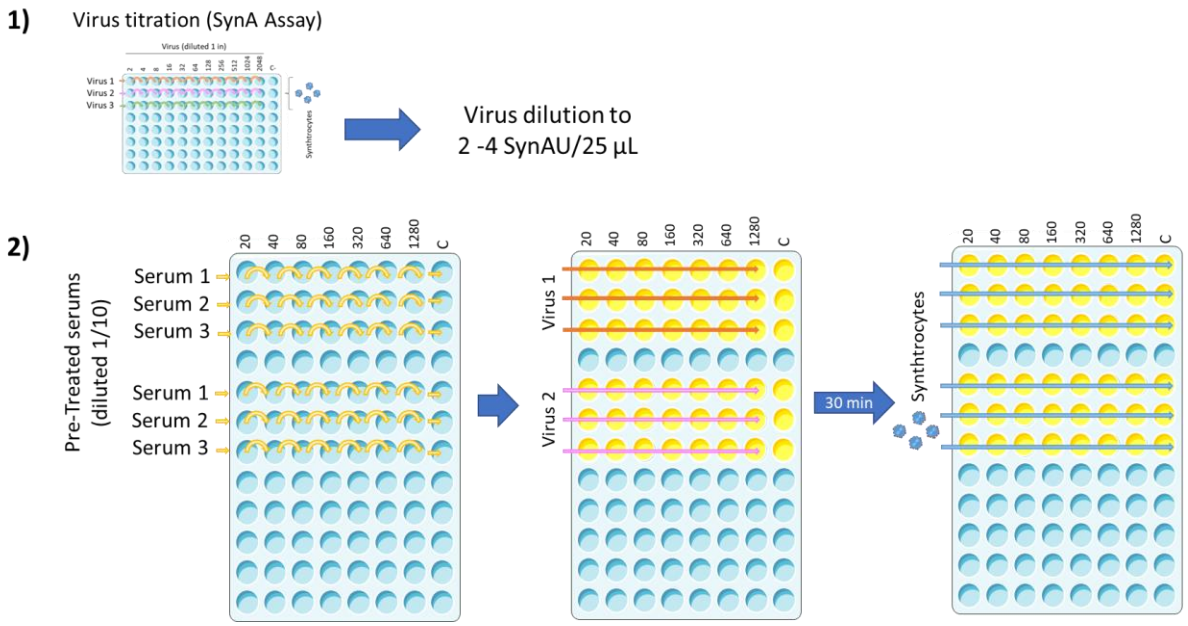

Figure 3.7 | Schematic of SynAI protocol. First, SynA is performed to determine the appropriate virus dilution for each virus. In this example, 3 different serums are tested for anti-influenza Ab against 2 different viral strains. Each serum is diluted 2-fold from column 1 to 7, adding serum directly to column 8 too. Then, 25 µL of each virus dilution are added to all the wells in a row except for well 8, that just adds PBS. After 30 min of incubation at RT, 50 µL of synthrocyte working suspension are added and allowed to sediment for 10 to 25 min depending on the synthrocyte size.

The nonspecific inhibitors are not always completely removed by RDE treatment and their presence can give false positives. Occasionally some viral isolates can be highly sensitive to this, and will be recognized because they have high SynAI titers to more than one antiserum in the test. To solve this, serum can be heat-inactivated again (56ºC for 30 min) or alternative methods such as trypsin-heat-periodate can be used.[115]

3.10. Hemagglutination and Hemagglutination Inhibition Assay (HA & HAI)

3.10.1. RBCs preparation and standardization

When the RBCs source was whole blood, for example in RBCs from human origin, RBCs were isolated by centrifugation of 10 mL of blood (5 min at 500G, without break). After the centrifugation, plasma and the leukocyte layer were removed by carefully pipetting. Then, 50 mL of PBS were added to wash the cells and the process was repeated 3 more times before using them. After the last washing, PBS was completely removed to concentrate the erythrocytes to a 100% stock. Such processed RBCs were stored and used in less than 4 days unless otherwise specified.

Commercial isolated RBCs were also washed 4 times using the same procedure. In cases where the supplier indicated that RBCs had been already washed, only two cycles of washes were performed.

Before using them in HA and HAI assays, the amount of RBCs needed for the experiments was diluted with PBS to a 0.5% or 0.75% working dilution (for avian or mammalian RBCs, respectively).

3.10.2. HA

The procedure to prepare the microplate and to dilute the virus was the same as described in Section 3.8.2 for SynA assays. The type of microplate varied depending on the type of RBCs. Avian RBCs required V-bottomed plates while mammalian RBCs employed U-bottomed microplates to produce the appropriate sedimentation profiles. After virus dilution, 50 µL of the standardized RBCs working dilution were incorporated to all the wells, gently mixed and incubated at RT for 30 min for avian RBCs or 60 min for mammalian RBCs to allow them to settle down. Finally, images of each well were taken. V-bottomed plates were also tilted to produce a tear-shape pattern to assess agglutination. Table 3.15 shows a summary of the procedures and results interpretation depending on the RBCs animal origin.

Table 3.15 | Differences in the HA and HAI procedure and interpretation depending on the RBCs origin.

Origin RBC	Dilution	Plate	Incubation Time	Sedimented pattern
Mammal	0.75 %	U-bottom	60 min	
Avian	0.5 %	V-bottom	30 min	

The agglutination titer was defined as the highest dilution that produced visible agglutination. The last agglutinated well was considered to contain 1 HAU.

3.10.3. HAI

Serums were pretreated before performing HAI following a protocol similar to the one described in Section 3.9.2.1. RDE treatment was exactly the same, but serum for HAI was adsorbed using RBCs. For each mL of diluted and RDE-treated serum (1/10), 50 µL of packed RBCs (100%) were added, gently mixed and incubated at 4°C for 1 h, mixing by inversion every 15 min. Finally, the mixture was centrifuged and the supernatant was collected for the posterior HAI.

Serial 2-fold dilutions of each serum (25 µL/well) were mixed with the corresponding dilution of the virus (25 µL/well) and incubated for 30 min at RT. Afterwards, 50 µL of standardized RBCs working dilution were incorporated and incubated for 30 to 60 min depending on the type of RBCs. Images were taken and the pattern was analyzed to determine the HAI titer. The HAI titer was the reciprocal of the highest serum dilution at which the agglutination was inhibited.

3.11. Laminated microfluidic device for agglutination detection

3.11.1 Materials

Diverse device designs were developed along this work. All of them were made using the materials described in the following table.

Table 3.16 | Summary of the materials required to produce the laminated devices.

Material	Provider	Ref.
Polyester film (100 µm thick)	3M	PP2500
Double-sided adhesive (50 µm thick)	3M	467MP
Filter paper Grade 4 CHR	Whatman plc	3001-917
Filter paper Grade 1 CHR	Whatman plc	3004-917

3.11.2. Capillary-flow device fabrication

All the models produced during the optimization were manually assembled following the same process, but the number of layers and channels varied depending on the design. This section describes the process to produce the final version of the device.

This laminated microfluidic device was produced by assembling 4 layers of hydrophilic polyester film intercalated with 3 layers of double-sided adhesive. Each layer displayed series of patterns, which were designed using CorelDRAW and cut with a CO_2 laser cutter, in order to create upon assembly 3D microfluidic channels, inlets and outlets. A piece of filter paper was inserted at the detection zone to separate agglutinated from non-agglutinated beads, and a waste pad was placed over the end of the device to create a passive pump for the fluidic system.

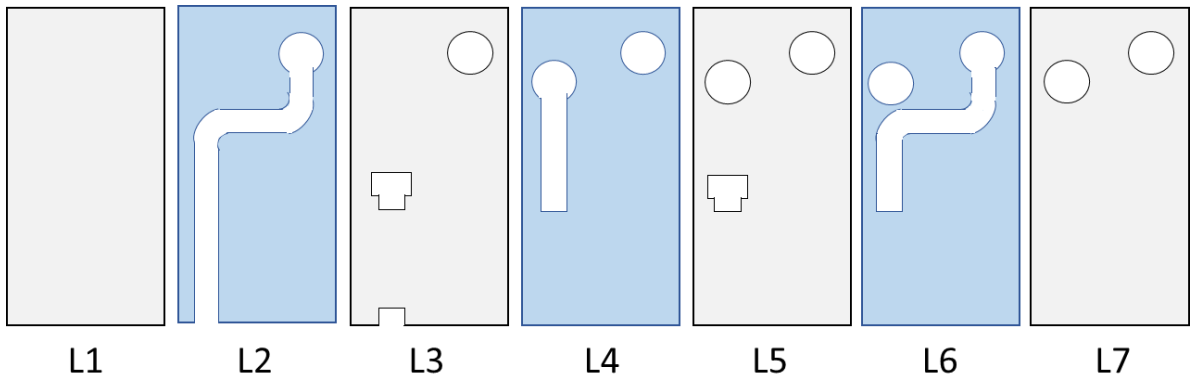

Figure 3.8 | Schematic of the different layers that integrated the final device design. In grey, layers made of polyester film; in blue, double-sided adhesive layers. For more details reefer to Chapter 8.

3.11.3. Device operation

Synthrocytes and sample were mixed in a 1:3 (v:v) proportion in an Eppendorf. 10 µL of this mixture were added to the device sample inlet. Then, the device was placed vertically for 5 min to facilitate sample-synthrocyte incubation under flow conditions and transfer towards the incubation valve. After that, 80 µL of washing buffer (PBS) were added to the buffer-inlet. Buffer arrival to the incubation valve prompted synthrocyte/solution flow in direction to the detection zone. Here, synthrocyte aggregates were retained by the filter paper, while free synthrocytes passed across. The process was considered finished once all the PBS had been pulled by the passive pump and the flow stopped (approximately 20 min after start).

3.11.4. Colorimetric band quantification

Pictures of the synthrocyte band (at the detection zone) were taken once the flow stopped. Then, ImageJ software was employed for their analysis. Images were inverted and converted to 8-bit greyscale, selecting a rectangular area before the filter paper on the detection zone. Integrated density of the selected area (the product of area x mean grey value) was calculated automatically by the software from the menu “Analyze”. Data was usually fitted with a 4 parameter logistic regression (4PL) using GraphPad.

Chapter 4

Synthrocytes proof-of-concept with naturally sialylated glycoproteins

Chapter 4. Synthrocytes proof-of-concept with naturally sialylated glycoproteins

HA and HAI assays are reference serological techniques used worldwide for a number of different applications. Among others, HA and HAI are employed for virus antigenic characterization, determination of immunity to recent infection or vaccination, and monitoring of vaccine production. These applications are an essential part of the global virological surveillance of influenza viruses and are vital to establish the annual reformulation of the flu vaccine.

HA and HAI are relatively simple, fast (generate results in hours), inexpensive and do not require sophisticated equipment nor a challenging training for the operators. All these characteristics contribute to make HA and HAI widely accepted. However, these methods have a major drawback: they have to be carried out in fresh erythrocytes. This biological reagent displays a short shelf-life (<2 weeks) and is hard to mass-produce, being the main source of variability in HA-based assays.[139] Moreover, erythrocytes must be obtained from different animal species, such as turkey, chicken or guinea pig, depending on the virus that is going to be analyzed.[114] For this, animals must be held in animal facilities under strict rules and RBCs need to be extracted frequently. Thus, ethics and animal welfare become another concern for these assays.

The necessity for a standardized method is evident and is regularly requested by the WHO. However, the different attempts to harmonize HA/HAI have not been successful. For instance, unifying the protocols used in the different laboratories, which usually diverge, could not circumvent the fact that RBCs are a difficult reagent to standardize. Efforts to produce an artificial material that could fully mimic the properties of native human RBCs, including size, biconcave shape, deformability, and oxygen-carrying capacity, entailed complex and expensive manufacturing steps.[181,182] Trakarnsanga *et al* produced stable and immortalized cell lines able to provide a continuous supply of RBCs obtained *in vitro*, but their production was complex and required genetic manipulation through lentiviral transduction.[183]

Another strategy consisted on fully changing the technique, substituting HA/HAI by a novel method. Some examples include using glycan-functionalized gold nanoparticles to produce a colorimetric agglutination method for influenza identification;[184] or using gold electrodes modified with sialic acid receptors and either a quartz crystal microbalance or an electrochemical sensor to detect influenza viruses.[185] Other approaches include using molecular methods instead of HA to detect the viral nucleic acid,[186] and ELISA or neutralization assays to substitute HAI.[114] Nonetheless, none of the methods proposed as HA or HAI alternatives provide the same antigenic characterization as the classical technique. Moreover, most of them are more expensive or time-consuming, and might require providing appropriate training and measuring equipment to all the laboratories of the global network, which would be expensive.

The objective of this doctoral Thesis was to create *synthrocytes,* a synthetic reagent able to substitute fresh erythrocytes in HA and HAI assays, in order to facilitate method standardization. This chapter describes the production of the first *synthrocyte* proof-of-

concept, for its application in monitoring and surveillance of influenza viruses. Fundamentally, synthrocytes comprise two parts. On the one hand, a colored microparticle, which mimics erythrocyte size and density and provides the sedimentation capacity. On the other hand, a (bio)receptor incorporated on the particle surface, which gives the ability to bind the virus. Work included the selection of both, the optimization of microparticle surface bioengineering, and synthrocyte testing in the presence of a battery of influenza viruses and virus-binding antiserums provided as WHO reference materials.

4.1. Identification of beads displaying agglutination-dependent differential sedimentation.

The differential sedimentation displayed by agglutinated and non-agglutinated erythrocytes depends on different physicochemical factors. Their size, density, shape, and surface charge has been shown to be crucial for the sedimentation to occur.[109] Here, work started with the identification of microparticles capable of producing different sedimentation patterns when free or agglutinated.

For this, a battery of commercial microparticles displaying a range of materials, sizes and densities were tested. The properties of all these particles are summarized in Table 3.1 (Chapter 3.1.1). Beads were serially diluted in PBS with or without a chemical cross-linker that produced their agglutination, and were allowed to settle down in the wells of a microtiter plate for 20 min. For particles that displayed amino groups on the surface, a homobifunctional amino-to-amino crosslinker, bis(sulfosuccinimidyl)suberate (BS3), was employed (Figure 3.2). For particles with carboxyl groups, these were activated with EDC to create amine-reactive groups, followed by diamine-PEG addition to produce agglutination. As it can be observed in Figure 4.1, only two of the amine beads changed their sedimentation pattern upon agglutination, Sicastar-blue 5 and 10 µm in diameter. Both particles were silica based, blue-stained, spherically shaped, and had a density of 1.8 g/ccm. They thus exhibited characteristics close to those of human erythrocytes, which have 7-9 µm diameter and a density of 1.11 g/ccm.[123,187] In the absence of BS3, a dilution 1:8 of the 5 µm Sicastar-blue stock (equivalent to 625 µg/well) sedimented, forming a halo at the bottom of the well that reminded that observed for mammalian erythrocytes. The presence of the cross-linker prevented the sedimentation of the beads. This effect was also observed in Sicastar-blue 10 µm, but only for 1:2 and 1:4 dilutions (equivalent to 1.25 and 2.5 mg/well). Sicastar-blue 3 µm also showed a differential sedimentation pattern when agglutinated or not, but the results were not reproducible during the series of test performed.

Overall, when the number of Sicastar-blue particles per well was too high, agglutination failed to induce changes in the sedimentation pattern. However, low particle concentrations did not produce sediments observable by the naked eye.

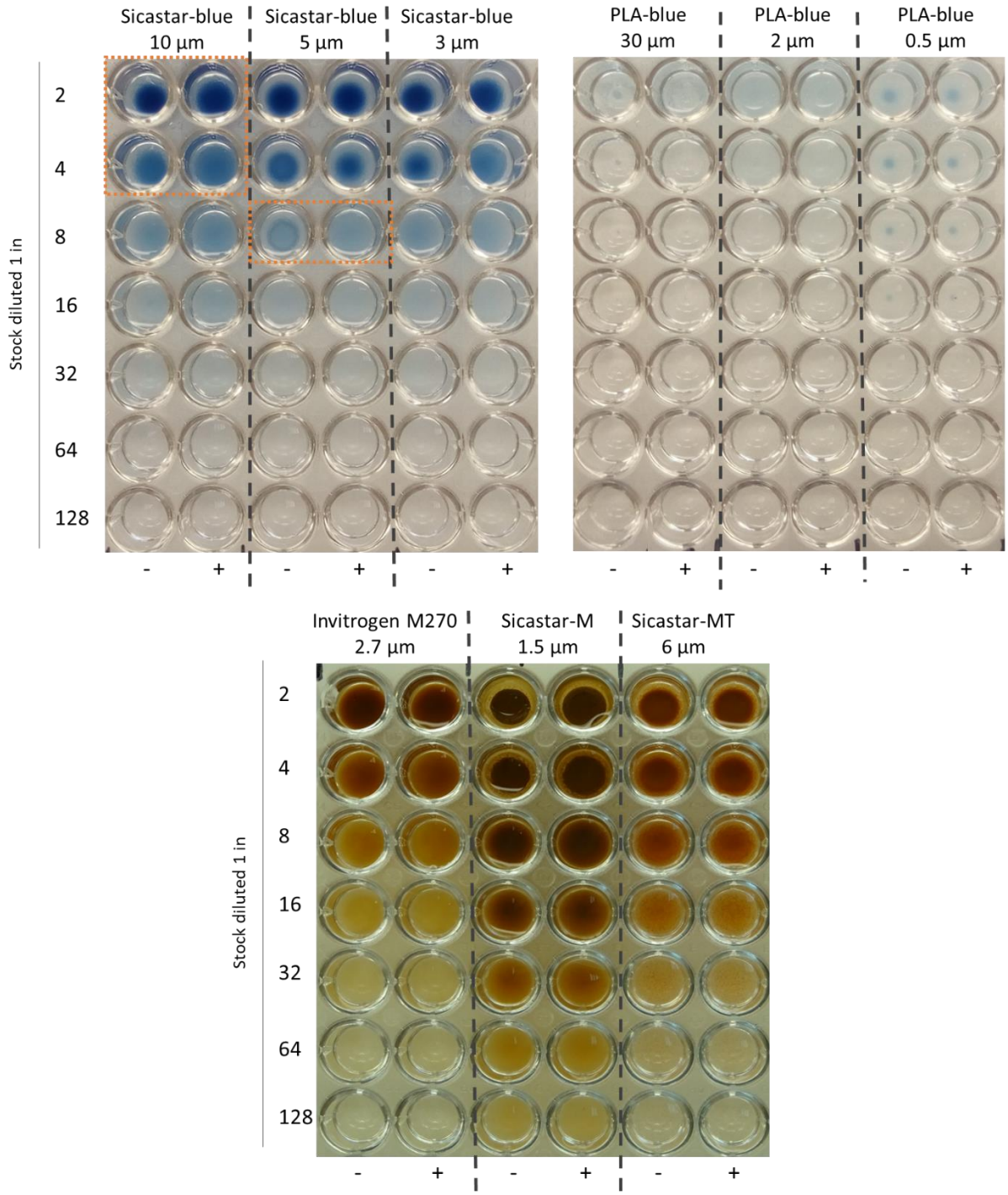

Figure 4.1 | Examples of the sedimentation patterns of nine types of commercial microbeads displaying amino groups on surface (Table 3.1, Chapter 3.1.1). Beads were serially diluted 1:2 with PBS, were chemically crosslinked using an agglutinating agent (BS3, 2.5 mM) and were allowed to settle down in U-shaped wells. Squares highlight the changes in sedimentation observed.

In contrast, the rest of amine-bearing particles tested did not display erythrocyte-like sedimentation. PLA particles, which are made of polymer, exhibited extremely faint pellets that needed hours to form (over 24 h for 0.5 µm beads). Three types of magnetic particles (MP) were also tested, but differences between agglutinated and non-agglutinated particles were only significant when using magnets, which increased the complexity of the assay. In consequence, these particles were discarded.

For evaluation of carboxylated MP, beads were activated using EDC and subsequently cross-linked using PEG-diamine. As can be seen in Figure 4.2, free and agglutinated particles displayed the same sedimentation pattern. The only difference was observed between non activated and EDC-activated particles, which could be explained by higher electrostatic repulsion between as-received carboxylated particles.

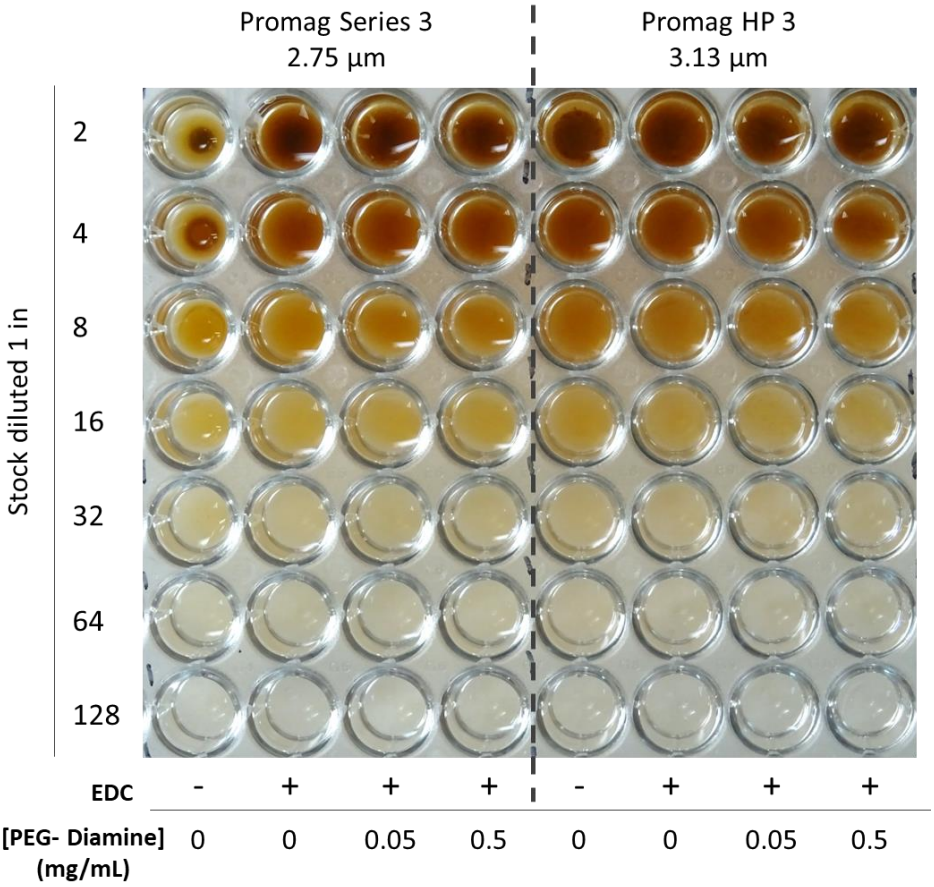

Figure 4.2 | Sedimentation of two types of beads displaying carboxyl groups on the surface (Table 3.1, Chapter 3.1.1). Beads were serially diluted with PBS prior or after activation with EDC ("-" and "+", respectively) and incubation in the absence or presence of different concentrations of PEG-diamine as a crosslinker. Beads were then allowed to settle down in U-shaped wells. No differences could be appreciated between free and agglutinated particles.

Once 5 and 10 µm Sicastar-blue beads had been selected, they were further characterized.

The SEM images of both types of particles revealed a well-defined spherical shape with a relatively smooth surface (Figure 4.3). They also presented a range of sizes instead of a totally homogeneous composition. For 10 µm beads, size ranged between 4 and 12 µm, and for 5

μm particles the range was between 3 and 7 μm. Results were consistent with the information provided by the commercial supplier (size range 7.5-12.5 and 3.5-6.5 μm for Sicastar-blue 10 and 5 μm, respectively). Furthermore, some particles were shattered, revealing an inner core made of the same material (Figure 4.3c). This inner structure is probably related to the manufacturing method which, although not revealed by the supplier, is presumably based in a core-shell synthesis strategy.

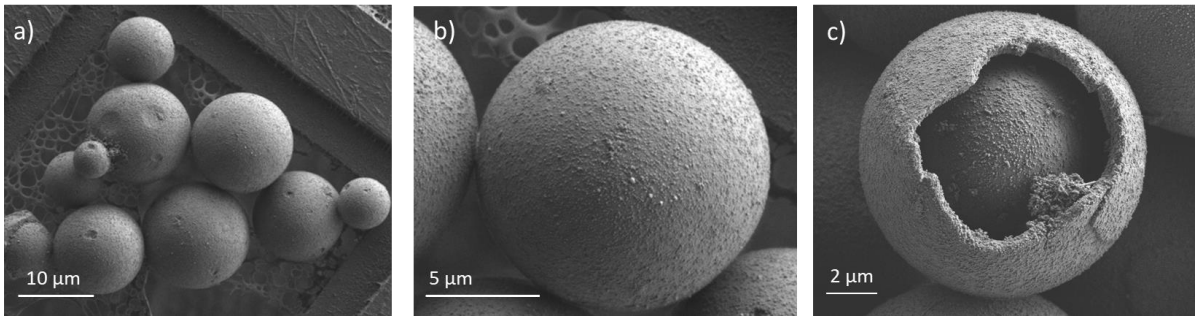

Figure 4.3 | Exemple of SEM images of Sicastar-blue particles (10 μm). **a)** Differences in particle size could be observed **b)** Amplification of the surface. **c)** Inside of a broken particle.

Sedimentation of Sicastar-blue 5 and 10 μm beads was next tested in three types of microtiter plates, which had flat-, U-, or V-bottomed wells. In classical HA and HAI test, erythrocytes from different species require different bottomed wells. Mammalian discoidal RBCs, which are enucleated, work better in U-bottomed wells, where they form broad ring-like sediments. In contrast, spherical nucleated avian RBCs are used in V-bottomed plates, in which they form a tight button. As shown in Figure 4.4a, differences in sedimentation between agglutinated and non-agglutinated Sicastar 5 μm particles were only evident in U-shaped wells, in which they formed ring-like sediments. For Sicastar 10 μm, the changes could be observed in both U- and V-shaped wells, where they formed rings and tight pellets, respectively, but the assay was more sensitive and easier to interpret visually in U-shaped wells. In contrast, no distinction could be made between free and agglutinated beads in flat-bottomed plates in none of the cases.

The effect of agitation in particle sedimentation was also evaluated. Aminated Sicastar 5 μm particles were incubated during 15 min with decreasing concentrations of BS3 either in static or with different types of agitation. Results are shown in Figure 4.4b. Under static conditions, the particles settled down forming ring-like pellets without BS3 or with BS3 concentrations below 0.15 mM, changing the sedimentation pattern for BS3 concentrations spanning 0.31-2.5 mM. Vortex agitation was discarded because it produced sedimentation in all the wells independently of BS3 presence. This could indicate that fast agitation difficulted the agglutination and/or promoted particle collaborative rolling across the well bottom and towards the center of the well. Incubation in an orbital shaker at 30 rpm also promoted the sedimentation, although to a lower extent and only for BS3 concentrations above 0.63-1.25 mM, depending on the replicate. Finally, incubation in the orbital shaker at 10 rpm increased the sensitivity slightly, and SB3 could be detected down to 0.15 mM. However, the improvement was not significant enough to include new equipment and modify the established

protocol with RBCs. Other parameters, such as cross-linker length, were studied, but did not affect the performance of the assay.

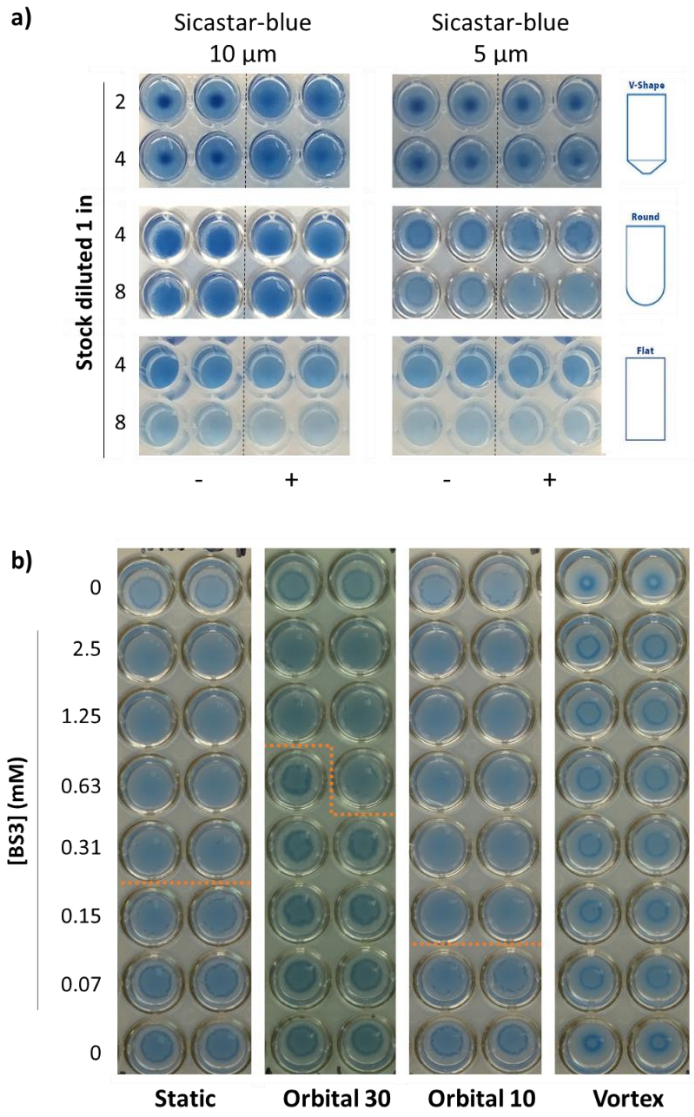

Figure 4.4 | Effect of the shape of the well and agitation type in sedimentation assays. **a)** Aminated Sicastar beads were diluted in PBS containing or not BS3 ("+" and "-", respectively) and were allowed to settle down for 10 min in either V-, U- or flat-bottomed wells before taking a picture. Two bead dilutions are shown for each assay condition, including two replicates of each. In V-shaped wells, beads settled down forming thigh buttons, while in U-shaped they formed ring-like sediments that could only be appreciated with 5 µm particles. No distinction could be made between free and agglutinated beads in flat-bottomed plates in none of the cases **b)** Sicastar 5 µm particles (750 µg per well) were incubated with decreasing concentrations of BS3 (2 replicates per concentration) and were allowed to settle down for 15 min without agitation or submitted to different types of agitation: orbital shaker at 30 rpm, orbital shaker at 10 rpm, and vortex at 600 rpm. Harsh agitation methods, like vortexing, produced sedimentation of all the particles. Gentle agitation ameliorated slightly the sensitivity, but the improvement was not worth the addition of the required equipment.

4.2. Selection of influenza-binding bioreceptors

Influenza viruses interact with erythrocytes through the H protein of the viral envelop. Specifically, H can recognize and bind the SA residues exposed on the surface of the RBCs membrane. Each virus has different affinity for different sialic acids, depending on its preferred host cell. For example, human influenza viruses preferably bind to SA linked to a terminal galactose in α2,6 bond, while avian viruses prefer an α2,3 bond, which are the most frequent in the epithelial cells of the upper respiratory tract of the corresponding host species. Accordingly, binding of influenza viruses to erythrocytes of one or another species depends on the presence of naturally glycosylated proteins that display on surface appropriate sialic acids. For example, while human influenza viruses are usually studied by HA/HAI using erythrocytes from guinea pig or human, avian influenza viruses use to be studied on horse or chicken erythrocytes. Here, production of synthrocytes was initially founded in the utilization of naturally glycosylated proteins displaying a high content of SA on surface.

In this section, we studied the ability of four highly sialylated proteins of commercial origin to bind influenza viruses. The characteristics of these proteins are described in Table 3.2 (Section 3.1.2.1). Each of them had a different sialic acid composition (both in content and in oligosaccharide type). Neutravidin (NeuAv), a deglycosylated protein, was used in parallel as a negative control.

A sandwich ELISA was developed to assess the affinity of influenza virus for each receptor. A full description of the process is explained in Chapter 3.3. In brief, a dilution series of the sialylated bioreceptor candidate was first immobilized on the surface of the plate (Figure 4.5. Next step was blocking with BSA to prevent non-specific adsorption, followed by an incubation with a serial dilution of the virus. Finally, indirect immunodetection was done, which included three serial incubations with an Ab specific for the virus, a secondary Ab labelled with the enzymatic tag HRP, and a chromogenic enzymatic substrate. Color evolution was finally measured spectrophotometrically. As it can be observed, color intensity was proportional to the amount of virus bound by the bioreceptor candidate. Binding increased slightly also with the amount of protein immobilized on surface. For example, maximal binding of A(H1N1) A/NewCaledonia/20/99 was observed for GYPA immobilized on plate at a concentration of 10 µg/mL, signal attained saturation for 20 µg/mL in the case of BM, avidin and neutravidin, but PM had to be used at 40 µg/mL and even then, the signal obtained was low.

Time and temperature of the virus incubation step were also optimized. Virus binding was efficient at RT and only improved slightly at 34ºC for high virus concentrations (Figure 4.6a). Binding was fast and occurred in about 30 min, although it improved if incubation was extended to 90 min (Figure 4.6b).

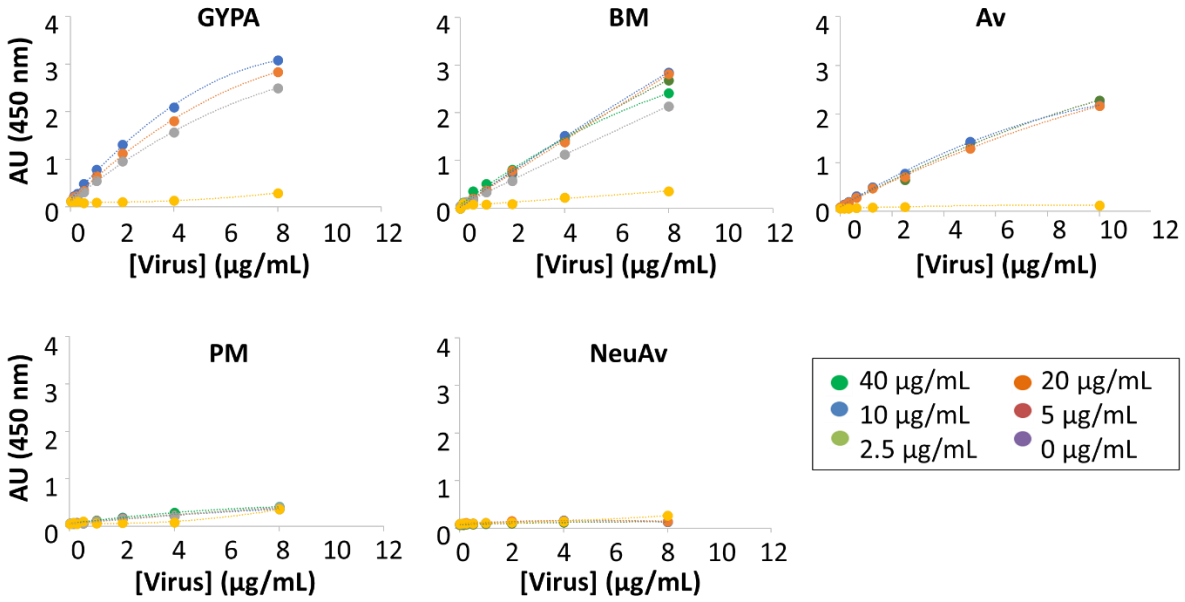

Figure 4.5 | Binding of influenza A(H1N1) A/NewCaledonia/20/99 by 4 different bioreceptor candidates and a negative control (NeuAv). Each candidate was immobilized on surface at concentration ranging 0-40 µg/mL, followed by incubation with increasing concentrations of influenza A(H1N1) and indirect immunodetection.

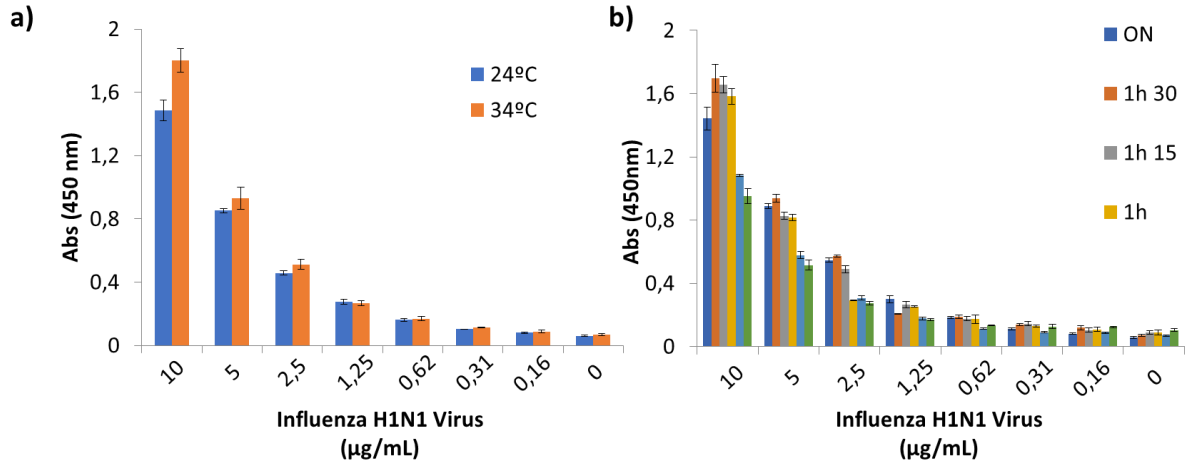

Figure 4.6 | **a**) ELISA in which the plate, modified with 20 µg/ml of BM, was alternatively incubated at 24 or 34°C with a serial dilution of influenza H1N1A/NewCaledonia/20/99. Although incubating at higher temperature provided greater signals, A(H1N1) virus could be also detected at room temperature. **b)** ELISA performed at 34°C and with different virus incubation times. Results show that the whole concentration range tested could be detected after a 30-min incubation. However, the highest signals were registered after incubating for 90 min and extending the incubation further did not improve the result.

As it can be seen in Figure 4.7, under optimal assay conditions, influenza A(H1N1) was able to bind efficiently three of these proteins, GYPA, BM and Av. The signals registered for all of them were proportional to the concentration of virus A(H1N1). The best response was observed for GYPA, which produced the highest signals with the lowest concentration of bioreceptor (10 µg/mL, equivalent to 0.5 µg/well). It is worth noting that this molecule is one of the predominant erythrocyte surface membrane proteins, and the one with the highest carbohydrate content (40-80%) compared to the other candidates tested. Furthermore, it is estimated that 75% of the total sialic acid exhibited on RBCs originates from GYPA,[176,178] which is consistent with the high recognition from influenza viruses observed here. In contrast, PM provided no significant binding, presumably due to its low sialic acid content (<2%). As anticipated, no recognition was displayed by NeuAv, which is completely deglycosylated.

As shown in Figure 4.7d, similar trends were observed for the four strains of influenza A(H1N1) tested (A/ New Caledonia/20/99; A/Solomon Islands/03/06; A/Taiwan/ 1/86; and A/Beijing/262/95). A certain degree of binding was observed for influenza B (Figure 4.7c), but none of the proteins evaluated successfully recognized influenza A(H3N2) (Figure 4.7b).

4.3. Production of sialylated beads and lectin-mediated agglutination assays (SynA)

Once the best-performing particles had been selected and receptor candidates had been characterized, they were combined to produce sialylated beads. 5 and 10 µm Sicastar-blue beads displaying amino or carboxyl groups on the surface were chemically conjugated to each bioreceptor candidate (PM, BM, GYPA and Av). In order to do so, amine beads were activated using glutaraldehyde, while carboxyl beads used EDC. The details for the full procedures are described in the Chapter 3.6.1.1. To sum up, in both cases the activation was followed by an incubation with the receptor protein for its crosslinking and a blocking step, with extensive washing after them.

Three plant lectins (WGA, SNA and MAA) were used to confirm that the sialylated proteins were correctly bounded to the particles and to carry SynA assays. Lectins are proteins with different carbohydrate-binding tropisms that could mimic the influenza virus interaction. Specifically, SNA binds preferentially to sialic acid attached to a terminal galactose in α2,6, similar to human influenza viruses, while MAA binds α2,3-linked sialic acids, as avian influenza viruses do. WGA has a broader spectrum, with high affinity for N-acetylglucosamine oligomers and sialic acid glycoconjugates.

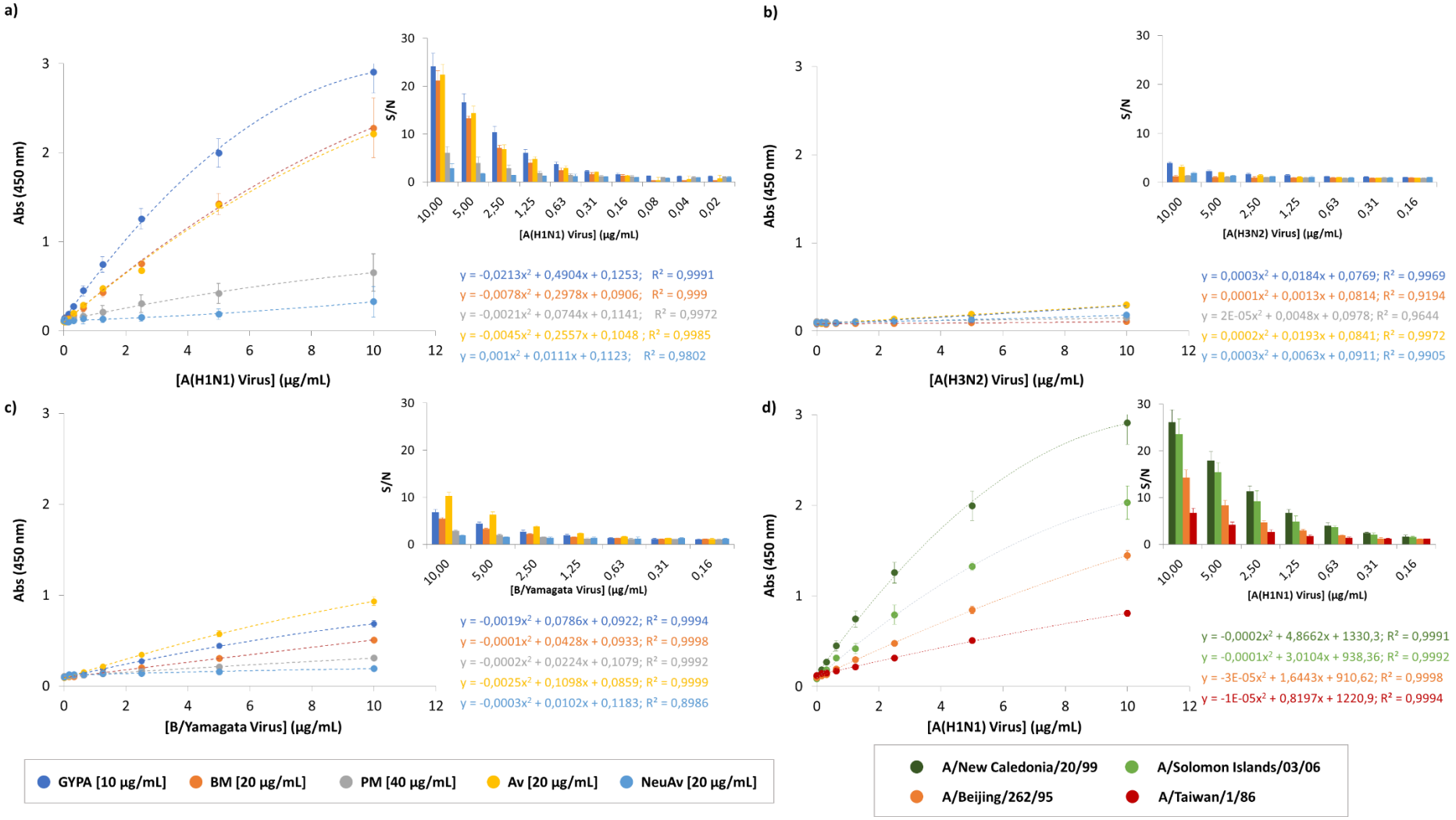

Figure 4.7 | Binding of influenza A/NewCaledonia/20/99 (H1N1) **(a),** A/Brisbane/10/07 (H3N2) **(b)** and B/Victoria/504/00 (B/Yamagata) **(c)** by 4 different bioreceptor candidates and a negative control (NeuAv). **d)** Binding of different subtypes of influenza A(H1N1) to GYPA (10 µg/mL).

Here, a fixed concentration of the modified beads was allowed to settle down for 10 min in the absence or presence of increasing concentrations of agglutinating lectins. As can be seen in Figure 4.8, agglutination was lectin-dependent. Particle sedimentation was prevented in the presence of all the lectins, although with different sensitivity for each combination. For instance, while GYPA beads detected lower concentrations of SNA, the beads modified with BM and PM were more sensitive for WGA. This indicated that GYPA had more α2,6 linked SA than mucines (BM and PM). On the other hand, MAA recognized worse GYPA and specially PM, suggesting that these proteins had little α2,3 linked SA receptors. A similar pattern was observed for 5 and 10 μm particles, but in these experiments bigger particles seemed more sensitive and detected lectin concentrations 10 times lower.

Avidin particles did not sediment clearly, neither in the absence or in the presence of the 3 tested lectins. One of the major differences between avidin and the other candidate bioreceptors was its isoelectric point (Ip), as detailed in Table 3.2. Avidin has an Ip >10, while the other proteins Ip ranges between 3 and 4 for mucins and is around 6.5 for GYPA.

In order to determine if the Ip of the exhibited protein and the pH of the medium could impact the sedimentation of the sialylated microparticles, particles were settled down in 150 mM NaCl adjusted to different pHs. As can be noted in Figure 4.9, in general, beads sedimented at pH above the Ip of the conjugated protein, when they were negatively charged. This suggested that surface charge, and more particularly negative charge, had a profound effect in microparticle sedimentation. This negative charge presumably produced repulsion between individual beads, preventing the formation of the visible sediments. This behavior resembles that described for RBCs, in which membrane sialylated proteins are negatively charged at neutral pH, producing a similar effect.[109]

It was therefore concluded that avidin-coated particles would not be useful for virus detection in SynA assays, which should be performed at neutral pH.

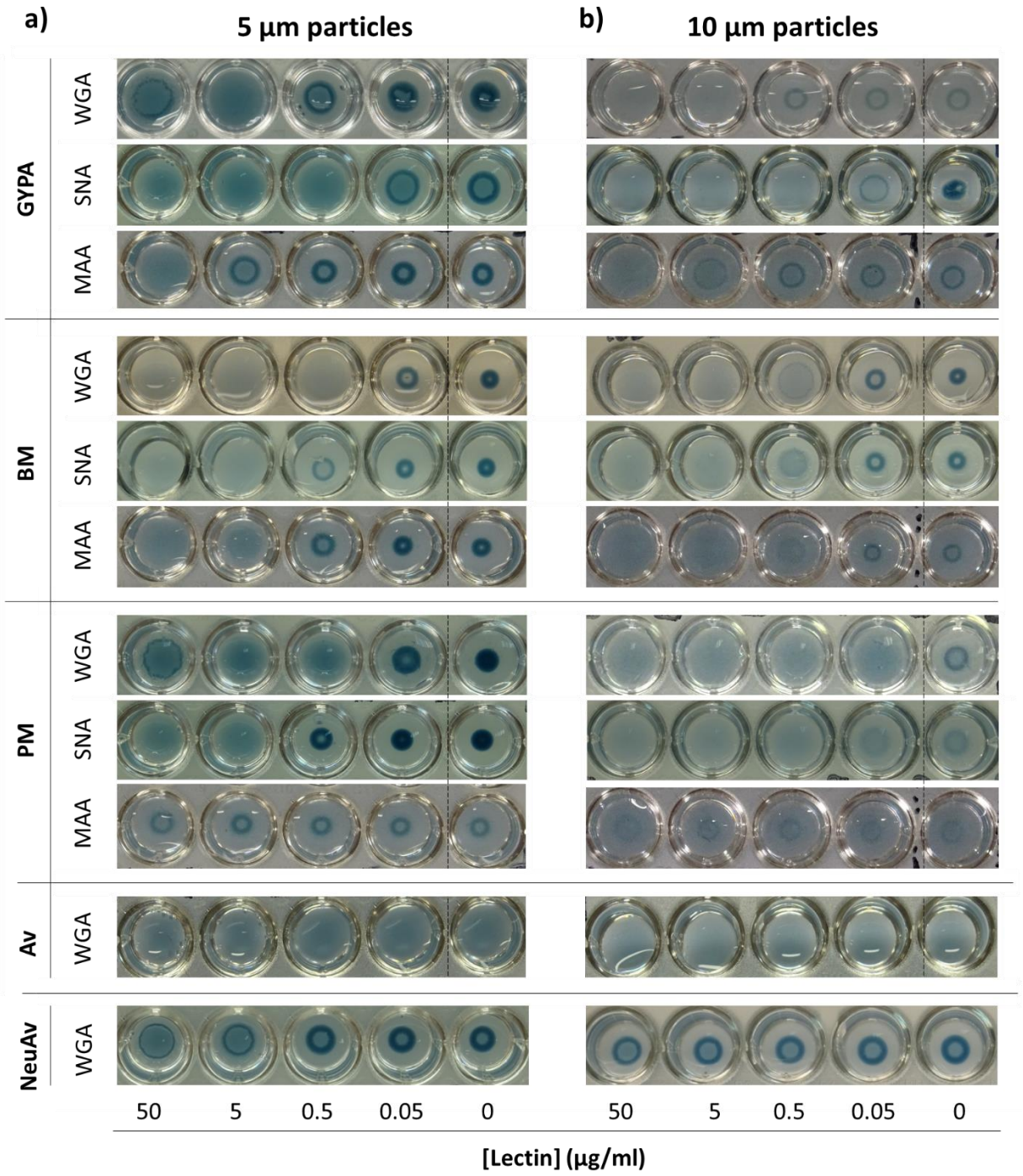

Figure 4.8 | Sedimentation of 5 **(a)** or 10 µm **(b)** beads, modified alternatively with the 4 bioreceptor candidates (GYPA, BM, PM and Av) or a negative control (NeuAv), in the absence and in the presence of increasing concentrations of three different lectins, WGA, SNA, and MAA ($7.125x10^6$ and $8.25x10^5$ beads/well, respectively). 5 and 10 µm modified beads displayed similar trends, setting down when they were incubated alone, and changing the sedimentation in the presence of increasing concentrations of agglutinating lectins. Sensitivity of the assay depended on the combination of coating protein and lectin used. GYPA particles were better recognized by SNA, while PM and BM were better recognized by WGA. In contrast, NeuAv-coated particles were not recognized by any of the lectins tested.

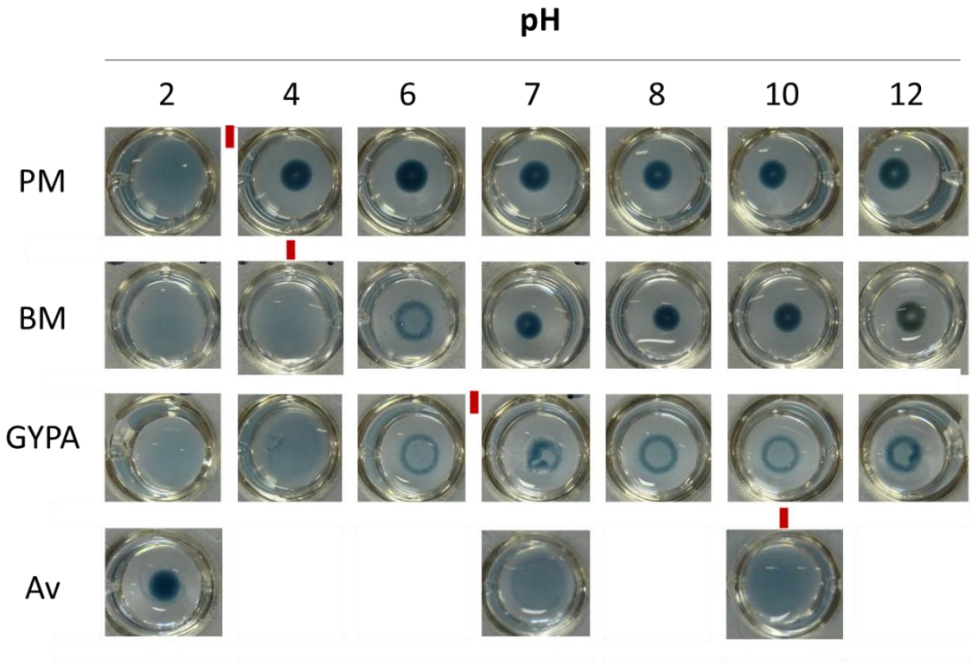

Figure 4.9 | Microparticles modified with the 4 sialylated proteins studied (GYPA, Av, BM and PM) were incubated for 10 min in 150 mM NaCl adjusted to different pHs. Red bars mark approximately the isoelectric point (Ip) for each sialylated protein. pH of the solution had a profound effect in microparticle sedimentation, which correlated with the Ip of the protein exhibited on surface.

To confirm that changes in the sedimentation were agglutination-dependent, and not random, microscopic characterization of the beads with or without lectin was done. The results showed that while the beads alone remained individualized in PBS, the presence of lectin resulted in the formation of aggregates (Figure 4.10). Moreover, the size of the aggregates increased proportionally to lectin concentration, confirming that these changes were correlated to lectin-mediated agglutination. Av-coated beads, on the contrary, did not show any agglutination in the microscopic observation. This confirmed that the lack of sedimentation observed in the microtiter plates was not due to a classic agglutination effect, but rather to repulsion between particles caused by the high surface charge.

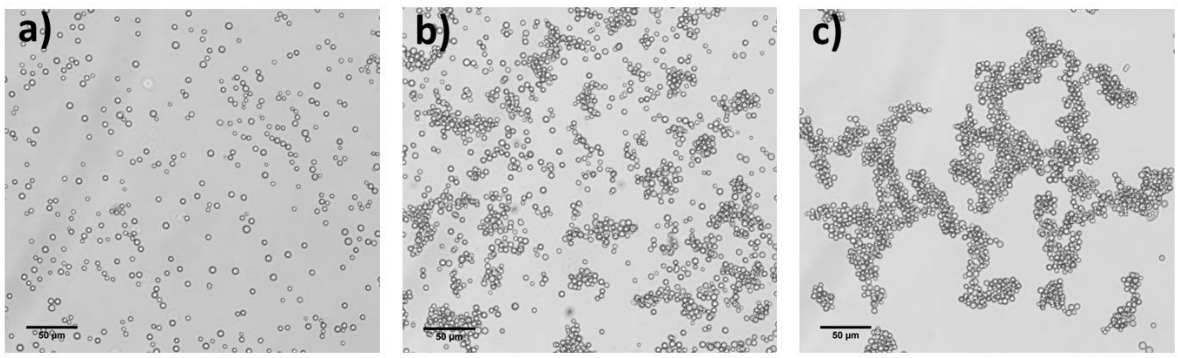

Figure 4.10 | Microscopic images of BM-conjugated 10 µm particles incubated in PBS **(a)**, or in presence of WGA at a concentration of 1 µg/ mL **(b)**, and 10 µg/mL **(c)**. Size of the aggregates increased with lectin concentration.

Diverse parameters affected the sedimentation and visualization of the particles in SynA. First, bead size had a deep impact on the sedimentation speed, with bigger beads sedimenting faster (Figure 4.11a). Particles above 15 µm, which settled down in a matter of seconds, were difficult to handle and therefore were discarded. Second, the type of conjugation influenced the final color and the width of the ring-like sediments. Carboxylated beads conjugated using EDC produced sediments of a lighter color, while amine beads conjugated with glutaraldehyde had a darker color and formed tighter pellets that were easier to interpret (Figure 4.11b). This was attributed to the unreacted COOH groups present on the surface of the carboxylated beads, which could induce repulsion between individual particles and prevent tight sedimentation. In agreement with this observation, glutaraldehyde particles were selected for subsequent experiments. Although in these experiments the best sensitivity was apparently displayed by particles modified with 50 µg of BM, which detected lectin concentrations 10 times lower than the particles modified with 100-200 µg of BM, later experiments showed that this was caused by non-specific binding.

Third, the number of beads per well also affected the performance of the agglutination assays. Higher particle loads produced darker and tighter sediments but were also less sensitive to the presence of the agglutinating lectin (Figure 4.11c). For instance, while the use of 500-750 µg of beads/well allowed detecting WGA at concentrations above 5 µg/mL, using 250-375 µg of beads/well permitted detecting WGA concentrations down to 0.5 µg/mL. However, the sediments produced by 375 µg of beads/well were more consistent across experiments, which made us select these conditions for subsequent experiments.

Two other parameters that seemed to affect the performance of the modified particles in SynA were the type of agitation imposed during conjugation (Figure 4.12a) and the volume of the conjugation reaction (Figure 4.12b). Two types of agitation, end-to-end mixing and vortexing, were studied. For this, 5 µm particles were conjugated for 2 h in continuous agitation with 300 µg of BM in Eppendorf tubes. The modified beads produced with vortex-mixing detected concentrations of lectin two-fold lower than those prepared by end-to-end mixing. Regarding the conjugation volume, when a fixed amount of particles (12.5 mg) was conjugated in Eppendorf tubes in BM volumes ranging between 250 µL and 1 mL at a fixed concentration of 300 µg/mL, best results were obtained for particles conjugated in a final volume of 0.5 mL. This allowed to also reduce the amount of sialylated protein needed, decreasing the final cost of the synthetic reagent.

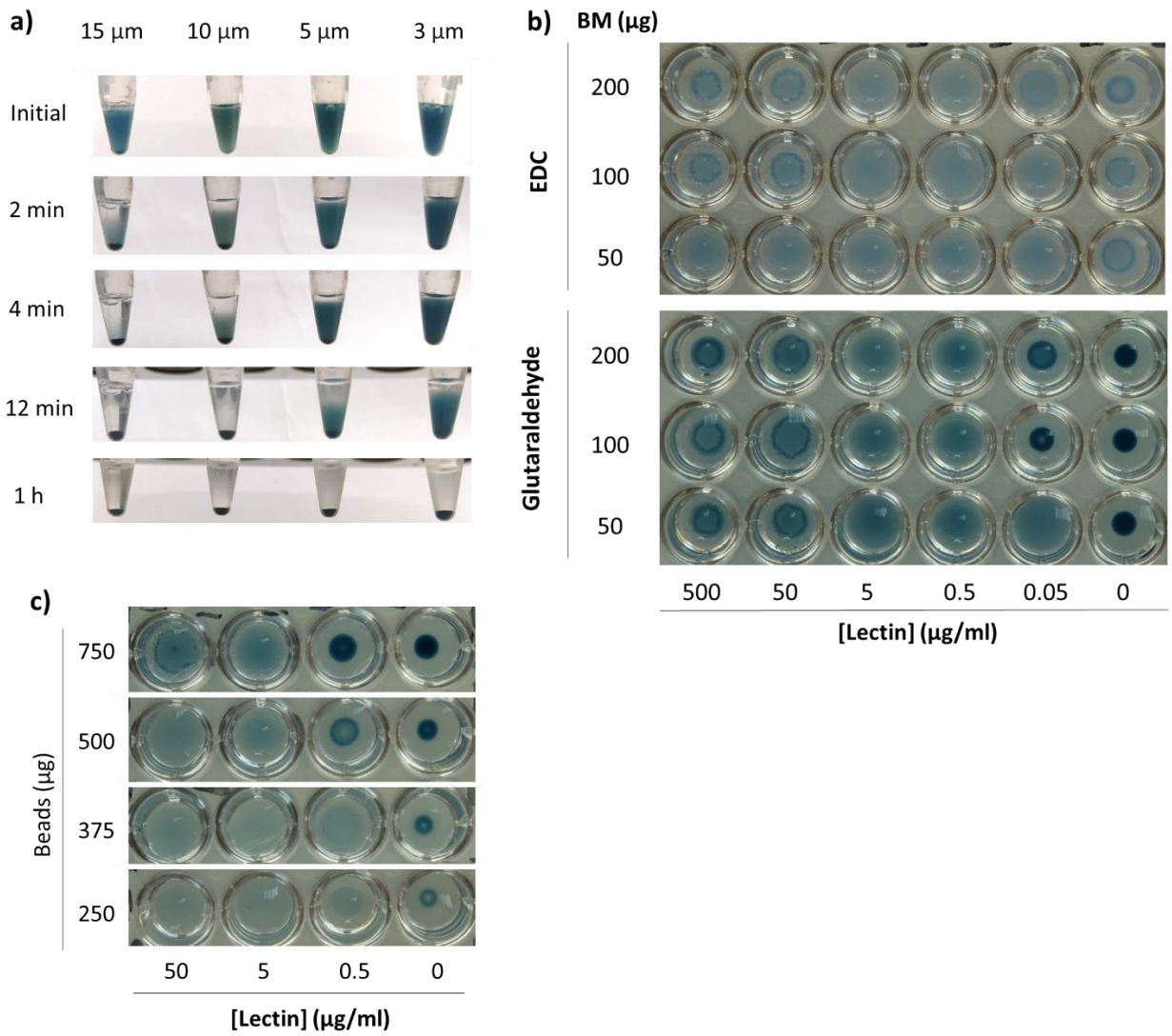

Figure 4.11 | a) 250 µL of sialylated silica beads of the same material and density but different size were allowed to sediment in a microtube with PBS for 1 h. Pictures were took at different times to show the difference in sedimentation speed between them. As it can be observed, the higher the size (and weight) of the particle, the faster the sedimentation process. **b)** 5 µm particles, displaying on surface either COOH or NH_2 reactive groups, were conjugated with 3 different concentrations of BM (200 µg/mL, 100 µg/mL and 50 µg/mL) using EDC or glutaraldehyde cross-linking, respectively. These particles were then allowed to settle down in the absence or in the presence of increasing concentrations of lectin. Glutaraldehyde-conjugated particles sedimented forming darker and tighter pellets than the particles conjugated through EDC chemistry, and therefore were selected for the next experiments. **c)** Effect of the amount of conjugated bead used per well in the performance of the agglutination assays. Different amounts of 5 µm BM-beads were incubated in the presence of increasing concentrations of WGA lectin. Best results were produced using 375 µg of beads/well.

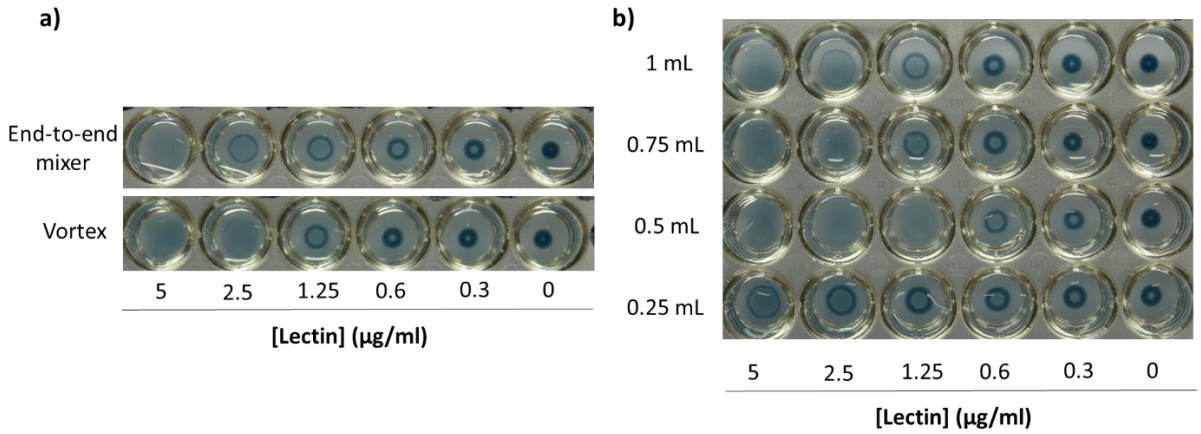

Figure 4.12 | Optimization of particle conjugation. **a)** Comparative of two types of agitation, end-to-end mixing and vortex, imposed during bead conjugation. In both cases, 12.5 mg of 5 µm particles were incubated in continuous agitation with 300 µg of BM dissolved in 1 mL of PBS. Vortex-mixing produced more sensitive beads than end-to-end mixing. **b)** Influence of the conjugation volume in the sensitivity of BM-coated particles. A fixed amount of particles (12.5 mg) was conjugated in reaction volumes ranging between 250 µL and 1 mL of BM at a fixed concentration (300 µg/mL). Particles produced in 0.5 mL showed the best sensitivity.

4.4. Behavior of sialylated beads in the presence of influenza virus and virus-mediated SynA assays

The results obtained in the ELISA and lectin-mediated agglutination experiments indicated that GYPA- and BM-coated 10 µm beads were the best candidates for influenza A(H1N1) virus detection. Recognition through ELISA was efficient for both receptors, and coated particles were able to form evident pellets and changed their sedimentation pattern when agglutinated by lectins. Additionally, 10 µm particles were, in general, more sensitive than 5 µm beads.

Therefore, GYPA- and BM-coated 10 µm particles were next allowed to settle down in the presence of increasing concentrations of A(H1N1) virus. As can be seen in Figure 4.13a, GYPA particles changed their sedimentation pattern in the presence of the virus. In contrast, BM particles did not change their behavior. The microscopy study confirmed that GYPA beads agglutinated in the presence of influenza A(H1N1) (Figure 4.13c-d), while BM beads displayed only mild virus-induced agglutination (Figure 4.13e-f). This was consistent with the lower content of sialic acids of BM and with the reports claiming that a high receptor load is required for RBCs to agglutinate in the presence of influenza virus.[188]

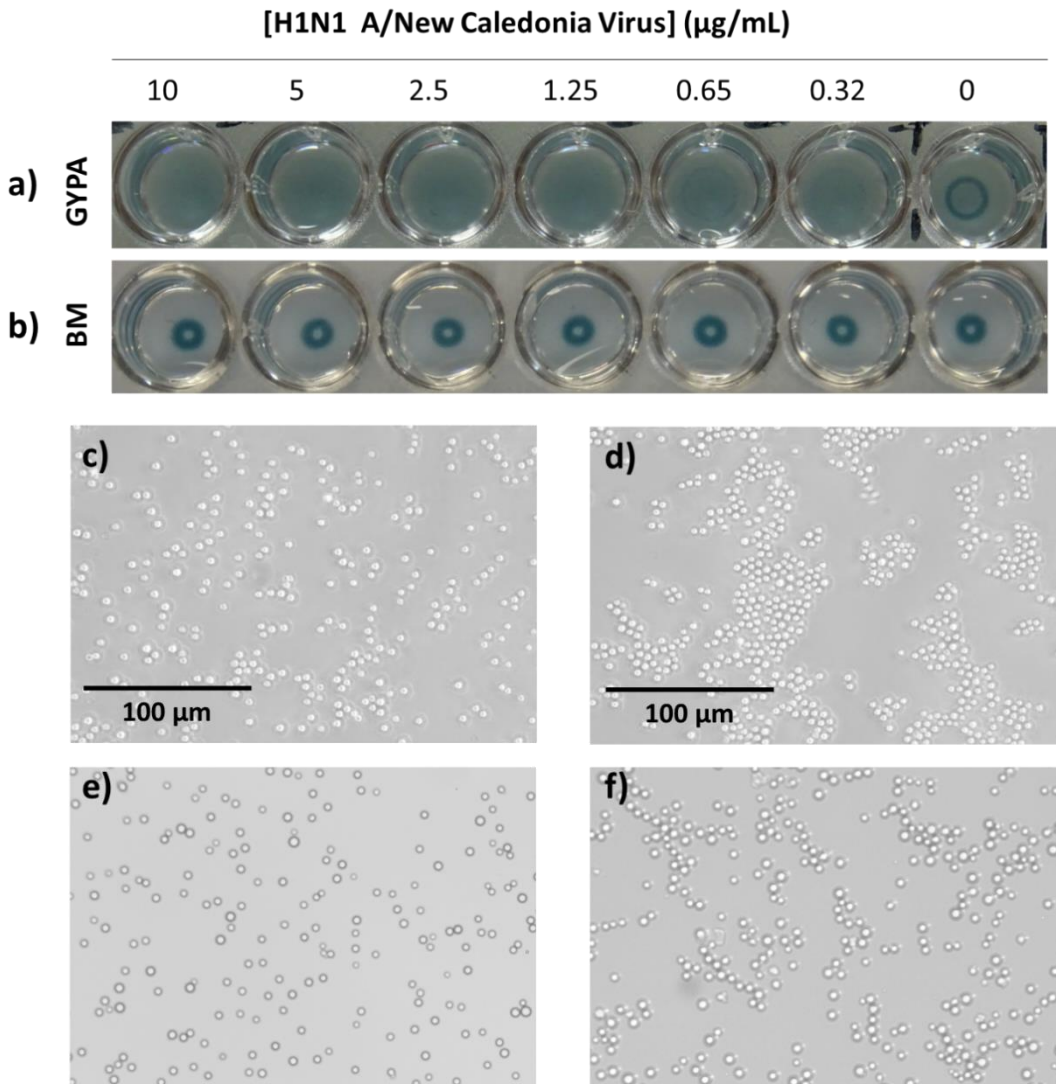

Figure 4.13 | a-b) Sedimentation of GYPA and BM particles in U-shaped wells in the presence of increasing concentrations of influenza A(H1N1). **c-d)** Microscopic images of GYPA particles incubated in PBS **(c)** or 5 µg/mL of A(H1N1) virus **(d). e-f)** Microscopic images of BM particles incubated in PBS **(e)** or 5 µg/mL of A(H1N1) virus **(f).**

Specificity of the agglutination was tested by carrying a competitive assay with soluble GYPA (Figure 4.14). The results confirmed that GYPA-beads agglutination was inhibited in the presence of high concentrations of free GYPA, because it competed for the interaction with influenza virus. Moreover, greater concentrations of virus required higher amounts of free GYPA to inhibit virus-induced agglutination efficiently, demonstrating that the virus was recognizing specifically the GYPA of the surface of the particles. In view of these results, 10 µm GYPA particles were selected to produce synthrocytes.

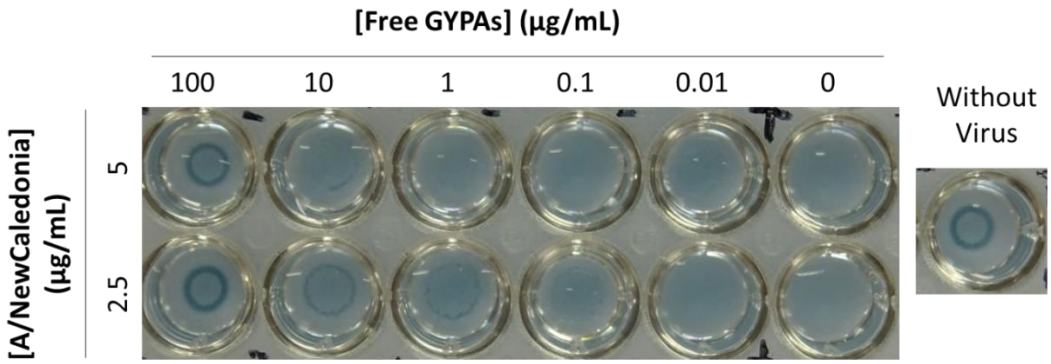

Figure 4.14 | Competition assay performed by incubating GYPA particles with 5 or 2.5 µg/mL of A(H1N1) and increasing concentrations of free GYPA in solution. Higher concentrations of GYPAs competed with GYPA-coated particles, inhibiting virus-induced agglutination.

Next, GYPA beads were incubated with different influenza A subtypes and B strains. As shown in Figure 4.14, synthrocytes recognized the different influenza A(H1N1) and B viruses tested but did not detect A(H3N2). These results were consistent with those obtained previously by ELISA (Section 4.2). Furthermore, the results were consistent with reports by other teams showing that circulating H3N2 strains do no longer agglutinate human RBCs efficiently in HA assays, which correlates with a loss of H3N2 hemagglutinin affinity for α2,6 bound SA.[189]

Interestingly, the GYPA-coated beads produced sedimentation patterns similar to those generated by animal RBCs, and were especially comparable in pellet shape to guinea pig erythrocytes. In general, synthrocytes were less sensitive than animal RBCs, requiring higher concentration of virus to produce agglutination. However, synthrocytes were significantly faster. While RBCs required between 30 and 60 min to display changes in the sedimentation pattern, synthrocytes provided results in just 5 min. These results demonstrated that synthrocytes could mimic animal RBCs in classical HA assays but providing SynA assays with a faster readout.

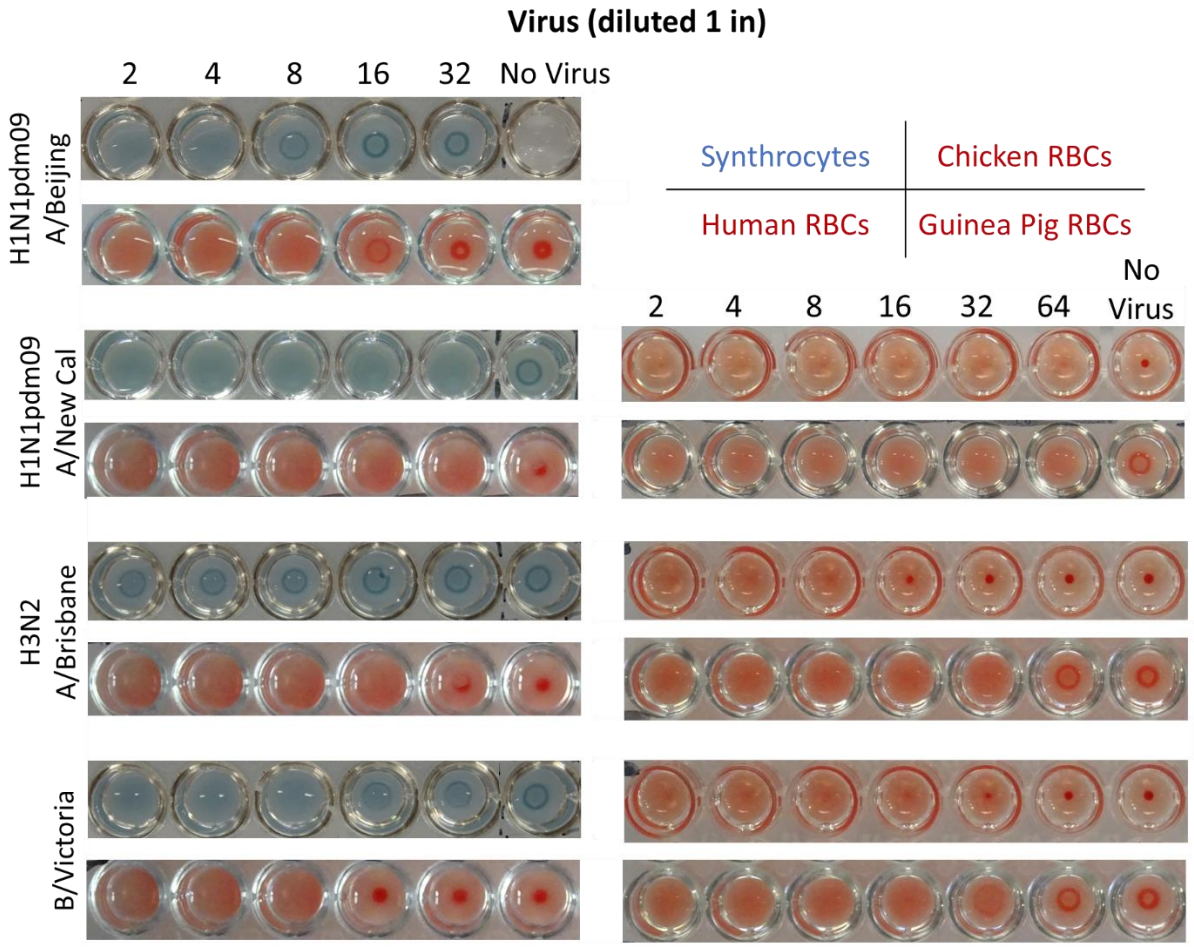

Figure 4.15 | Sedimentation of synthrocytes and RBCs from (clockwise for each virus strain) chicken, guinea pig, and human in the presence of increasing dilutions of A(H1N1). Changes were visually observable after 60 (human and guinea pig), 30 (chicken), or 5 min (synthrocytes) of incubation. Experiments carried in U-plates, except for chicken RBCs which were incubated in V-plates.

4.5. Agglutination Inhibition Assays (SynAI) Using GYPA-Synthrocytes

The next step was studying if GYPA-synthrocytes could be employed in HAI-like assays (SynAI from now on), a method that is regularly carried to study the Ab present in samples obtained from individuals after infection or vaccination, and also to characterize antigenically the viruses. In classical RBC-based HAI, sera are diluted serially, are then incubated in parallel with different influenza antigens, and are finally incubated with appropriate erythrocytes. In the presence of influenza-binding Ab, virus-induced RBC agglutination is inhibited, an effect that occurs proportionally to serum, and thus Ab, concentration. In the case of serological analysis, the sedimentation patterns registered for each sample (serum) and virus combination allow determining if a sample has Ab against one or another virus. The sample dilutions at which sedimentation inhibition occurs, provides an approximate Ab titration as well. The methodological details are explained in Chapter 3.9.

Here, two commercial neutralizing Ab (n-Ab) were used in parallel as a starting point. Both had been produced in mouse immunized with influenza A(H1N1) antigens, but Ab1 was raised specifically against influenza A/NewCaledonia/20/99, while Ab2 was produced against another A(H1N1) subtype. For this experiment, the protocol employed tried to emulate a classic HAI procedure. Briefly, a fixed amount of virus A/NewCaledonia/20/99 was incubated for 30 min in the wells of a microtiter plate with increasing concentrations of the corresponding n-Ab. Later, 50 µL of synthrocytes were added to the mixture, which were allowed to settle down for 10 min. Results showed that virus-induced synthrocyte agglutination was inhibited in the presence of high amounts (> 1 µg/mL) of n-Ab (Figure 4.16). As expected, this effect was stronger for Ab1, which had been raised specifically against the virus subtype employed in this experiment, and therefore presented a higher affinity for it.

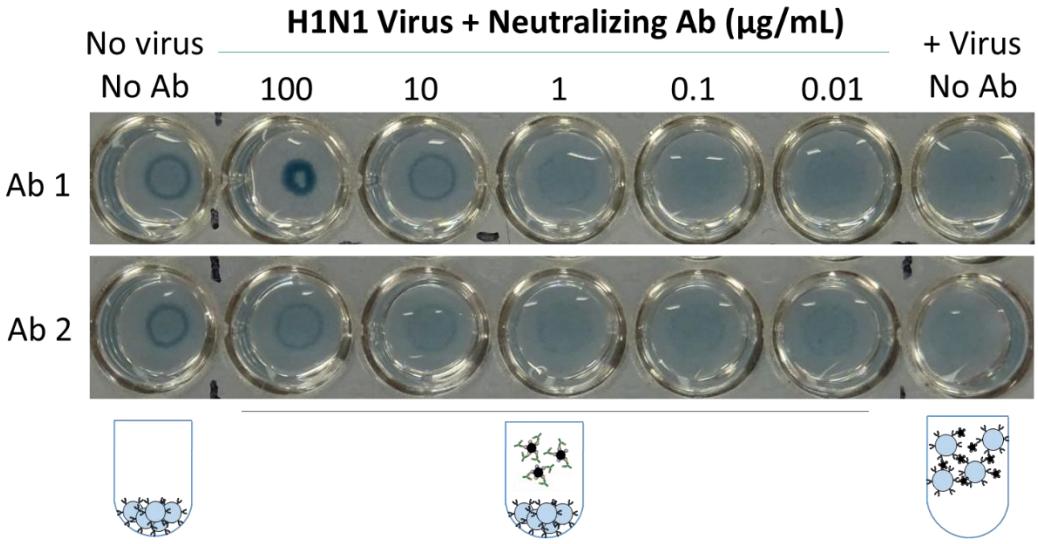

Figure 4.16 | SynAI carried in the presence of increasing concentrations of two n-Ab (Ab1 and Ab2). Each well contained 2.5 µg/mL of A(H1N1) A/New Caledonia/20/99 virus and $8.25x10^5$ synthrocytes. (Bottom) Scheme showing synthrocyte expected behavior in the different types of wells shown above. Strain-specific Ab-1 produced higher inhibition of the agglutination.

Then, SynAI was performed with the same protocol but using serum instead of n-Ab. According to the WHO guidelines, serum must be treated with Receptor Destroying Enzyme (RDE) prior to its study by classical HAI. This enzyme eliminates non-specific inhibitors potentially present in human serum that produce false positives in HAI (i.e., RBC sedimentation independently of the presence or absence of virus-binding Ab in the sample tested). It was thus first determined if RDE was also required for SynAI test performed with synthrocytes. For this, a pool of influenza-negative human sera, either RDE-treated or not, was studied by SynAI using A(H1N1) A/New Caledonia/20/99 virus. The results revealed that untreated pooled serum induced non-specific synthrocyte sedimentation at all serum dilutions tested (Figure 4.17). On the contrary, virus-induced synthrocyte agglutination occurred in RDE-treated serum diluted 1:16 – 1:128. Nevertheless, serum dilutions 1:2 – 1:8 interfered in SynAI, which suggested that synthrocytes were more sensitive to non-specific interferents than RBCs. In view of these results, it was concluded that treatment with RDE is also necessary in SynAI. Although initially disappointing, these results confirmed that synthrocytes

were mimicking RBC, promoting influenza binding and agglutination inhibition through similar molecular mechanisms.

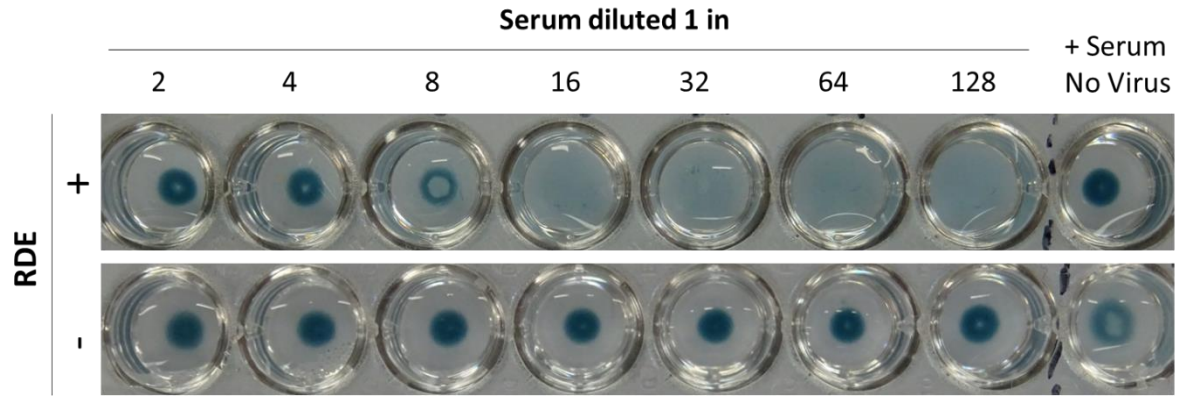

Figure 4.17 | Effect of RDE pre-treatment of serums in SynAI assays. A pool of human sera negative for influenza, treated (+) or not (-) with RDE and diluted serially, was incubated for 30 min with a fixed amount of virus, synthrocytes were added and the mixture was allowed to sediment for 10 min (A(H1N1) A/New Caledonia/20/99 virus and $8.25x10^5$ synthrocytes/well). The results show that RDE is essential to avoid non-specific inhibition of the synthrocytes agglutination, just like in classical RBC-based HAI.

Finally, synthrocytes were tested using the WHO reference reagents included in the kit for influenza surveillance (season 2018-2019). As previously explained (Section 1.3.4), these kits usually contain antigens of similar influenza virus types to the ones expected to circulate during the season. Last seasons, the kit has included four types of inactivated influenza viruses, including one A(H1N1)pdm09, one A(H3N2), and two B (Yamagata and Victoria lineages), of different strains in all cases depending on the season. They also carry five antisera, 4 against each of the influenza reference antigens and a negative control (without Ab recognizing the 4 reference antigens). The composition of the WHO kits for each season from 2018 to 2019 can be consulted in Table 3.7.

The first step to use these reagents for the identification of field strains by HAI is the titration of the control reference antigens by HA. This allows determining the minimal concentration of each viral Ag that produces RBC agglutination, which is equivalent to one hemagglutination unit (HAU), and therefore the virus dilution needed to perform HAI assays. Here, titrations were carried in parallel by HA and SynA using alternatively human RBCs and synthrocytes in order to determine the HAU-like unit applicable to synthrocytes (SynAU). As shown in Figure 4.18, synthrocytes were able to recognize all of the reference isolates except A(H3N2). This is consistent with previous results in which neither GYPA alone (in ELISA, Section 4.2) nor GYPA-synthrocytes were able to recognize commercial A(H3N2) viruses. The results also confirmed that SynA was less sensitive than HA and that synthrocytes detected the different viruses at dilutions 3-4 times lower than human RBCs (and thus at higher virus concentration).

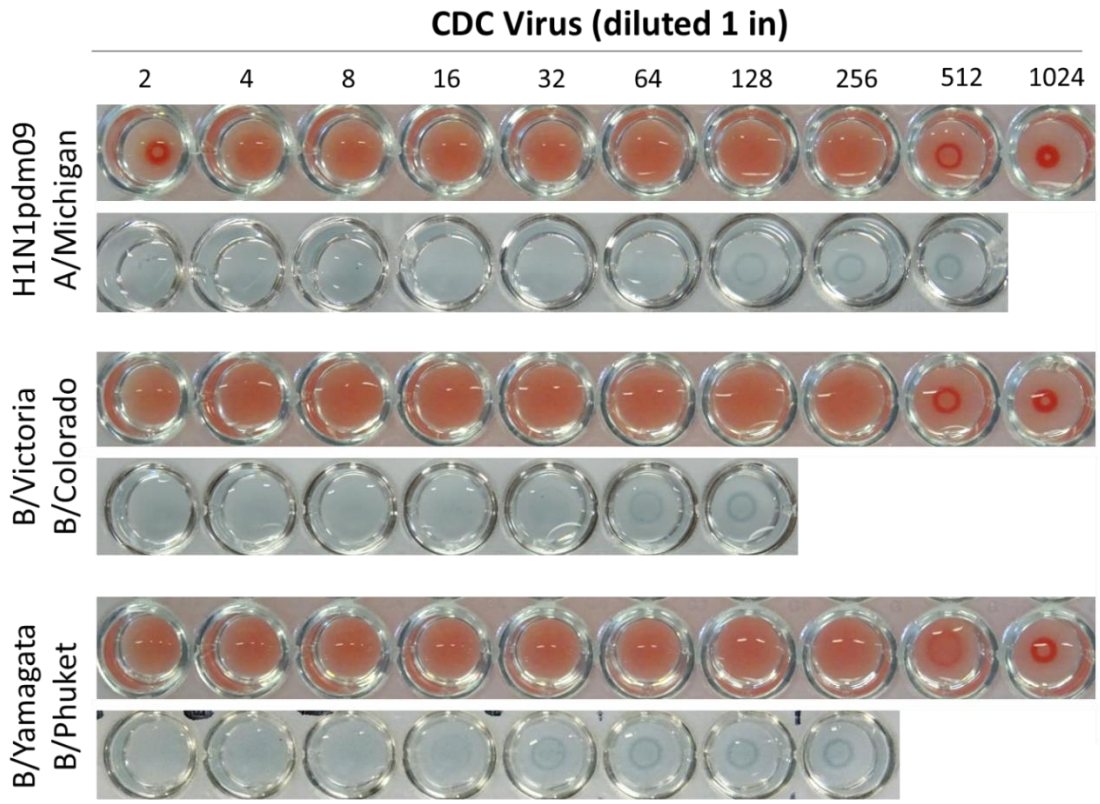

Figure 4.18 | Titrations carried to determine, for each influenza strain included in the WHO kit for influenza surveillance (season 2018-2019), the minimal virus dilution needed to produce RBC/synthrocyte agglutination. Human RBCs were washed prior to use and diluted to a final concentration of 0.75%. Two-fold serial dilutions of the antigens (50 µL/well) were mixed in the wells of a U-bottomed microtiter plate with 50 µL of RBCs (0.75%) or synthrocytes ($8.25x10^5$ beads in 50 µL of PBS) and let settle down for 1 h (RBCs) or 10 min (synthrocytes). The highest dilution of virus that caused complete (hem)agglutination was considered 1 HA/SynA unit (HAU/SynAU).

Once the reference viruses were titrated, optimization of SynAI was performed. The impact of the amount of synthrocytes employed per well for SynAI was evaluated. Two different concentrations of beads were used to perform a SynAI experiment with A(H1N1)pdm09 reference Ag and positive and negative reference sera. As can be seen in Figure 4.19, performing the assay with 375 µg of synthrocytes per well, the same quantity employed in SynA, allowed detecting tight pellets for most anti-H1N1 serum dilution tested, which could be caused by agglutination inhibition. However, pellets formed to a certain extent also in the negative control serum. These were not the expected results, because the negative control serum did not contain specific Ab against the tested virus, and therefore it should not prevent virus-induced synthrocyte agglutination. Although pellet shape was different in positive and negative serums, differences were too subtle and could be misleading. Decreasing the number of particles to 250 µg/well reduced the sedimentation in the negative serum while conserving the inhibition pattern in the positive antiserum. Albeit the pellet formed was less defined than when using more synthrocytes per well, the differences between positive and negative control sera were more evident. Even when pellets also formed for the highest concentrations of negative control sera tested, this effect was also observed in classical HAI, although at lower dilutions.

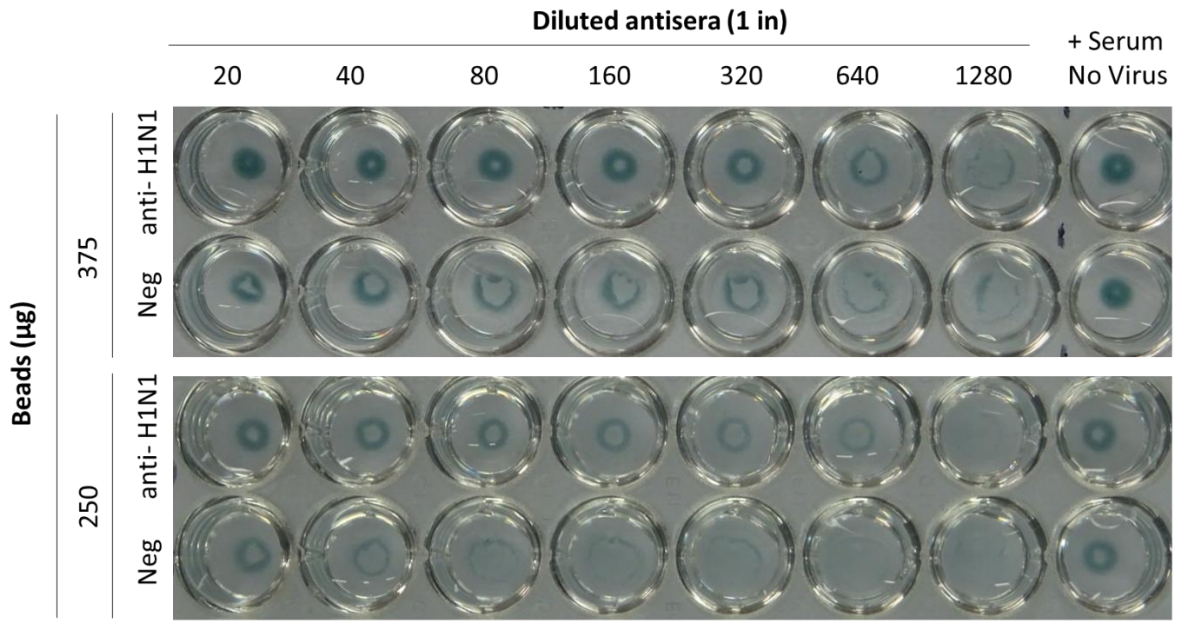

Figure 4.19 | SynAI performed with different amounts of GYPA-synthrocytes per well. In both cases SynAI was carried out using A(H1N1)pdm09 virus and either a reference negative control serum or the specific anti-H1N1 antisera. Although agglutination inhibition is clear with anti-H1N1 serum (thus synthrocyte sedimentation in the presence of virus and antiserum) when using 375 µg of particles/well, the negative serum also showed some non-specific inhibition that made the readout more difficult. Reducing the amount of particles/well to 250 µg helped to minimize this nonspecific inhibition and the sedimentation patterns displayed by positive and negative serums in SynAI were easier to distinguish.

The SynAU units required to perform SynAI were also determined. Protocols recommended using between 2 and 4 HAU/25 µL per well for classical HAI (preferably the first in order to reduce the amount of virus required). Results showed that there was no significant difference between using 2 or 4 SynAU/25 µL for WHO reference antigens in SynAI assays.

Finally, performance of synthrocytes was compared to RBCs in agglutination inhibition assays. These experiments were carried out using all the WHO reference antigens and antiserums recognized by synthrocytes. Therefore, A(H3N2) virus and its antisera were not evaluated. As shown in Figure 4.20, synthrocytes were able to mimic RBCs behavior in SynAI for A(H1N1) and B viruses. As before, synthrocytes were less sensitive than RBCs, but still displayed differential sedimentation in the presence of positive and negative antisera. Disappointingly, synthrocytes exhibited also more nonspecific inhibition at high concentrations of the negative control serum, which was also observable in RBC-based HAI, but only at the highest concentrations of serum tested.

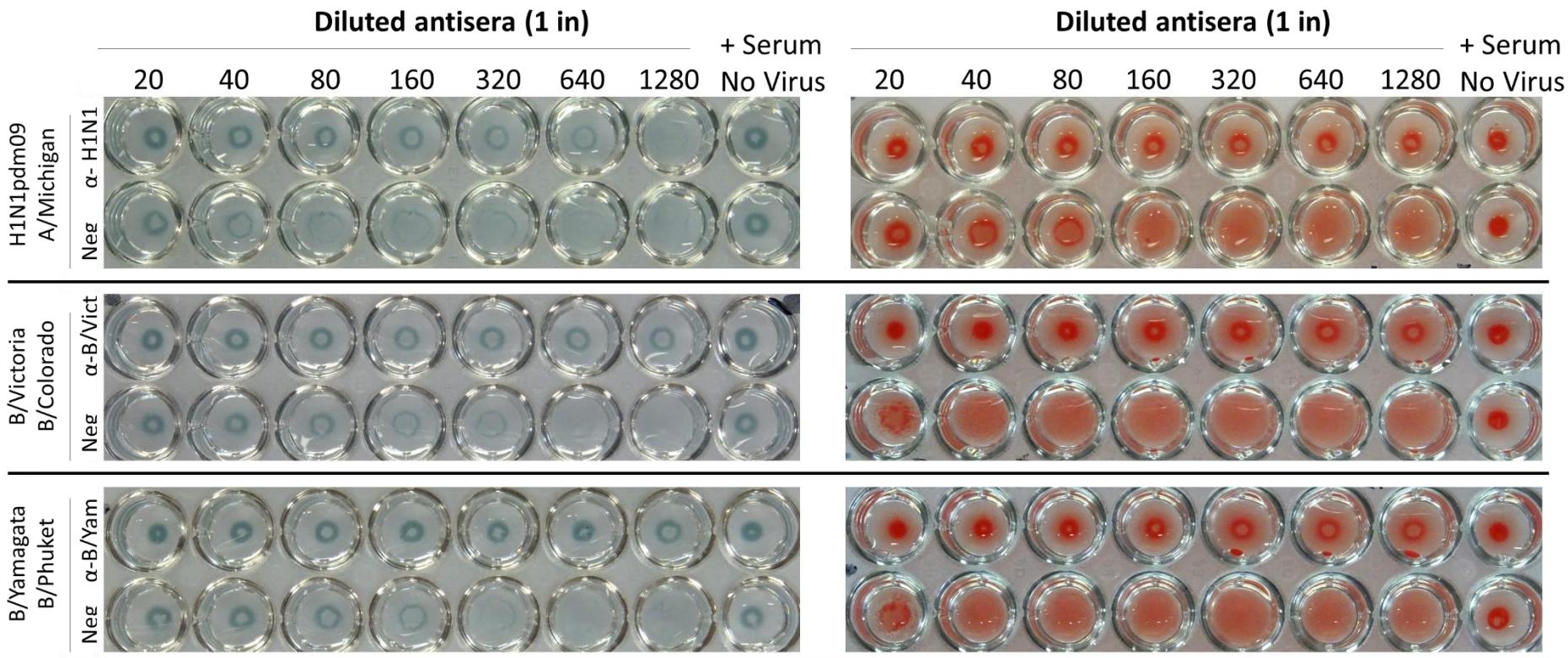

Figure 4.20 | Agglutination inhibition assays performed with synthrocytes (up, 5 min) or human RBCs (bottom, 60 min), using WHO reference viruses and antisera from season 2018-2019.

This issue was subsequently studied. Antiserum against A(H1N1) and negative control serum were analyzed in search of Ab that could react against the different components of the synthrocytes and cause this non-specific inhibition. Another concern was that the blocking step carried with BSA during particle conjugation could be insufficient to prevent subsequent non-specific binding of non-target sample components. Thus, different commercially available blocking solutions were studied. This study was carried by ELISA, which allowed testing several blocking conditions per plate. Wells were coated alternatively with GYPA, BSA or the new blockings. Then, the plate was blocked with either BSA or the different blocking solutions tested, and both positive and negative WHO reference serums (all produced in goat) were incubated. Next, an HRP-labelled anti-goat IgG was used to detect any Ab present in the goat serums that reacted against the synthrocytes components.

Results displayed in Figure 4.21 showed than both serums, but specially the negative control one, produced signals that were proportional to serum concentration when tested against most of the candidate blockings studied. Since background noise (without serum) kept low in these ELISAs, these results evidenced that the two sera tested contained Ab with affinity for components of the blocking solutions. The exception was BSA, which displayed the lowest recognition and was confirmed as the best blocking for synthrocytes. Even though negative serum generated 30-40% more signal than anti-H1N1 antiserum in general, for GYPA it presented an increase of more than 400% (Figure 4.21c). This indicated that negative serum contained Ab that reacted specifically against GYPA, which explained the agglutination nonspecific inhibition observed for GYPA-synthrocytes in this sample. Although anti-GYPA Ab were not found consistently in all the control sera provided by the WHO, this also suggested that this version of synthrocytes was not ideal.

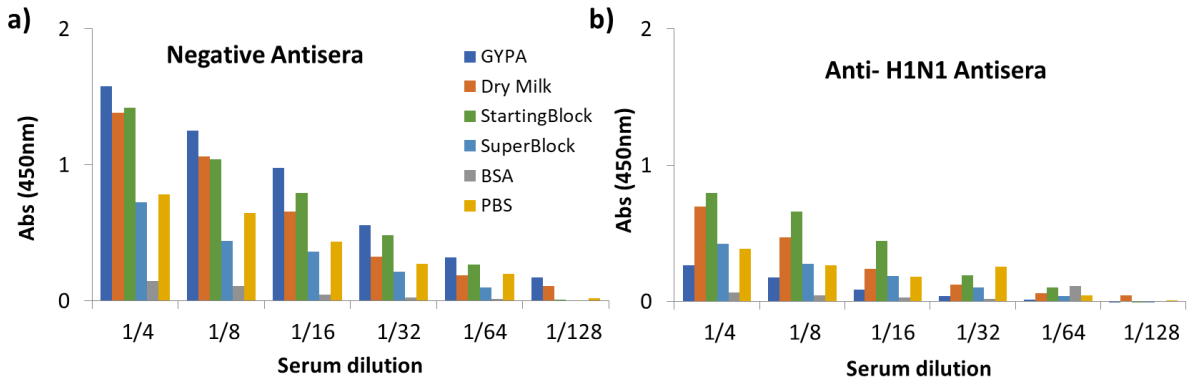

Figure 4.21 | Presence of Ab against synthrocyte-components in WHO reference antiserums, either negative **(a)** or positive **(b)** for anti-H1N1 influenza virus. The graphs show the absorbance signals (after blank subtraction) obtained by ELISA for detection of goat IgG with affinity for the different components coated on the plate surface. Signals obtained with negative serum were significantly higher, especially for GYPA recognition.

Nevertheless, this first proof of concept showed that it was possible to substitute RBCs in HA and HAI-like SynA/SynAI assays for influenza surveillance. As it has been discussed above, GYPA-synthrocytes were able to bind to influenza A(H1N1) and B viruses, triggering synthrocyte agglutination. This process produced changes in the sedimentation pattern that could be observed by naked eye in less than 10 min, compared to the 30-60 min that required animal RBCs. Furthermore, the interaction between synthrocytes and influenza could be inhibited by specific n-Ab, which allowed performing HAI-like SynAI assays for antigenic characterization and serological studies.

However, sensitivity and selectivity still needed improvement. A(H3N2) viruses remained undetectable, and some of the reference antisera displayed recognition of the synthrocytes components hindering SynAI results readout. Moreover, GYPA price was elevated, increasing significantly the cost of synthrocytes production. Therefore, the need for new receptors able to overcome these problems was compulsory.

4.6. New sialylated proteins as receptor candidates

Due to the aforementioned limitations, a search for new receptors for influenza binding was performed. Two new sialylated proteins were identified, fetuin and transferrin, which according to previous reports were recognized by influenza.[190–192] Both proteins had a similar molecular weight (Mw of 64 KDa and 78 KDa, respectively; compared to 50-80 KDa for GYPA), but their sialic acid composition was different.[193,194] Fetuin contained α2-3–linked and α2-6–linked sialiosides (α2-3–linked in higher proportion[194]) while transferrin contained only α2-6–linked.[195] Detailed description of each protein can be found in Chapter 3.1.2.

To begin with, we evaluated the ability of both proteins to bind different influenza viruses (A(H1N1), A(H3N2) and B). In order to do so, both proteins were studied using the sandwich ELISA described in Chapter 3.3 and used in Section 4.2 to assess previous receptors. Here, fetuin or transferrin were immobilized in the plate, followed by blocking, virus incubation and indirect detection through Ab-HRP. Fetuin and transferrin plate coating concentration had been previously optimized using A/New Caledonia/20/99 virus.

As can be seen in Figure 4.22, for A/H1N1/New Caledonia/20/99 and B/Victoria/504/00, signals were proportional to the concentration of virus. This showed that both viruses bound the two proteins studied, although fetuin generated higher signals for all the viruses tested. Moreover, fetuin was able to recognize more A(H1N1) subtypes compared to transferrin, including Solomon Islands/03/06, A/Taiwan/1/86 and Beijing/262/95 subtypes, which was attributed to the α2-3–linked sialic acids it contained. Neither fetuin nor transferrin were able to recognize H3N2 viruses efficiently. This could indicate that the amount of α2-6–linked SA displayed by these proteins was insufficient for H3N2 virus binding.

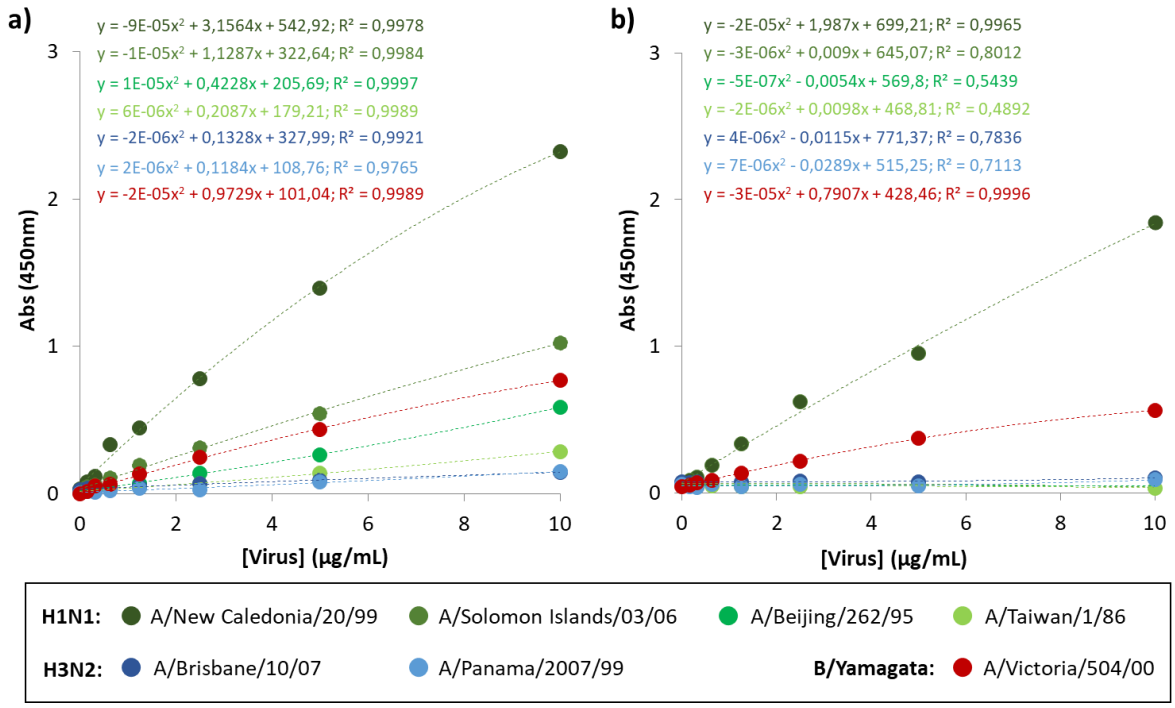

Figure 4.22 | Binding of different subtypes of influenza A(H1N1), A(H3N2) and B/Victoria by fetuin **(a)** or transferrin **(b)**, both coated on plate at a concentration of 20 µg/mL Fetuin was recognized by all the H1N1 viruses tested except A/Taiwan/1/86, which had worse recognition. Transferrin, on the other side, only recognized A/New Caledonia/20/99 virus and B/Victoria/504/00. None of them was able to bind any of the H3N2 viruses tested.

Even though transferrin performance was inferior, both proteins were conjugated to 10 µm Sicastar aminated particles using the same protocol described in Section 3.6.1. Then, particles were allowed to settle down for 10 min in the presence or absence of A/New Caledonia/20/99 virus and the sedimentation pattern was assessed. Figure 4.23 shows that virus recognition through fetuin-synthrocytes was successful down to 0.94 µg/mL, while transferrin-synthrocytes only suffered agglutination at concentrations of virus above 3.75 µg/mL. These results agree with the ones obtained previously by ELISA. Sensitivity of fetuin-synthrocytes was slightly lower compared to GYPA-coated synthrocytes (detection down to 0.94 µg/mL vs 0.32 µg/mL of H1N1, respectively), but the protein cost was noticeably lower. GYPA had a price approximately 215 times higher than fetuin.

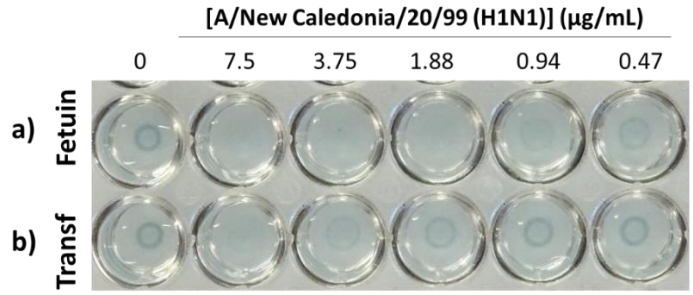

Figure 4.23 | Sedimentation in U-shaped wells of fetuin and transferrin coated particles in the presence of increasing concentrations of influenza A/New Caledonia/20/99 (H1N1). Fetuin showed higher sensitivity than transferrin (4-fold).

4.7. Production of fetuin-synthrocytes

Thanks to the decrease in the bioreceptor price, it was possible to try new surface engineering strategies in an attempt to incorporate a higher amount of fetuin on synthrocyte surface to improve assay sensitivity.

The first approach consisted in directly increasing the amount of protein during the conjugation process from 75 to 300 µg/reaction. Then, the different coated particles were sedimented in PBS in the absence or presence of increasing concentrations of A/New Caledonia/20/99 virus. As can be seen in Figure 4.24, the best results were obtained for the conjugation with 150 µg/reaction of fetuin. Carrying the conjugation with more fetuin did not entail higher sensitivity. This could be due to the limited amount of amine or glutaraldehyde-activated amine reactive groups available in the surface. On the other hand, when the fetuin concentration was decreased in the conjugation, a subtle halo developed in SynA at 1.87 µg/mL of virus indicating that sensitivity was dependent on fetuin incorporation.

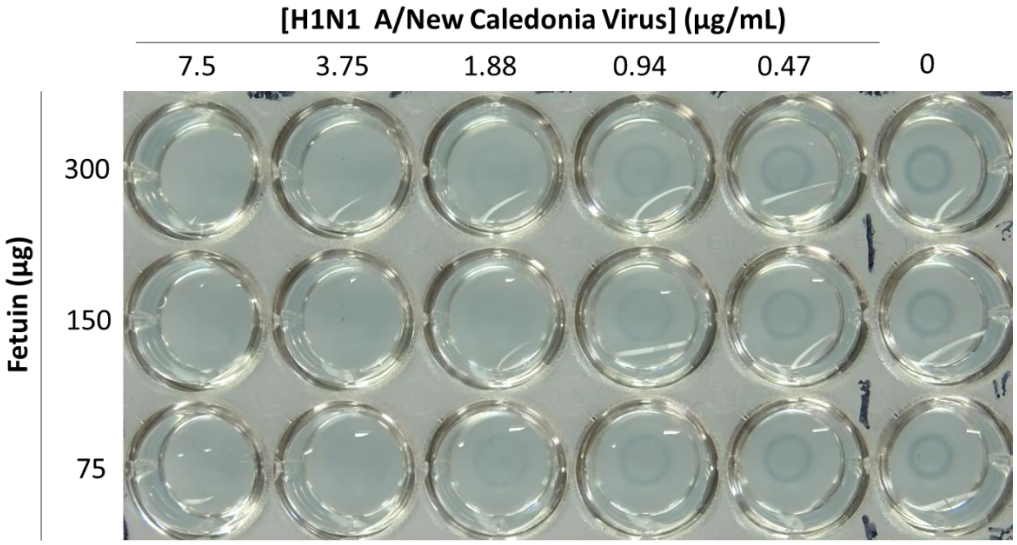

Figure 4.24 | SynA assay performed with particles conjugated with increasing amounts of fetuin. 375 µg/well of 10 µm fetuin coated-beads were incubated with increasing concentrations of A/New Caledonia/20/99. Increasing the amount of fetuin in the conjugation above 150 µg/reaction did not improve sensitivity.

The following step was trying to increase the number of reactive groups on the particles' surface. Fetuin was being incorporated to the particles using a two-step conjugation protocol, in which the amine groups in the particles were first activated with glutaraldehyde, followed by particle washing and fetuin incorporation. Fetuin-synthrocyte performance improved if the concentration of glutaraldehyde in the activation step increased from 4 to 8%, to keep unchanged for higher concentrations (Figure 4.25a). Some studies showed that more intense crosslinking can be achieved when proteins are firstly adsorbed on the surface and then treated with glutaraldehyde. Under these circumstances, glutaraldehyde molecules bound to the protein can react covalently with glutaraldehyde molecules bound to the amino groups of the support, establishing multi-point connections between them.[196] Here, integration of activation and conjugation in a single step was performed in an attempt to increase these

available attachments. However, as can be seen in Figure 4.25b, this single-step conjugation protocol did not provide any improvement compared to the classical two-step protocol. This confirmed that the limiting issue was not the activation of the surface amine groups, but the number of available binding points on the beads.

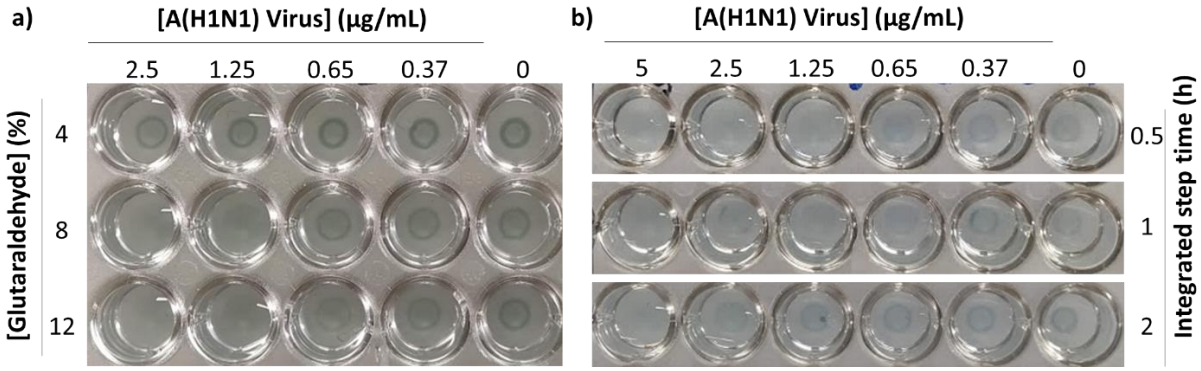

Figure 4.25 | SynA assay performed with fetuin-synthrocytes produced **(a)** using increasing concentrations of glutaraldehyde to crosslink fetuin in a two-step conjugation protocol, or **(b)** carrying a single-step conjugation of different legnths. In both cases, the images show the sedimentation pattern in presence of increasing concentrations of A/New Caledonia/20/99.

Therefore, a new approach was assessed, this time using NeuAv-biotin amplification. Initially, particles were coated with NeuAv as in Section 4.3 and 3.6.2.1. Then, NeuAv-modified beads were coated with biotinylated fetuin. The process to produce this biotinylated fetuin is described in Section 3.6.2.2. NeuAv contains four identical biotin-binding subunits, which should allow the incorporation of between 1 and 4 biotinylated fetuin molecules per NeuAv, although the process is not 100% efficient (Figure 4.26a).

Once conjugated, neutravidin particles, modified or not with biotinylated fetuin, were settled down in PBS. As can be seen in Figure 4.26c, particles coated with NeuAv were able to form a visible pellet. In contrast, sedimentation was inhibited when biotinylated fetuin was bound, both in V and U-shaped wells. This effect did not occur when fetuin was bound directly to the particle surface (previous section and Figure 4.26b), and no agglutination was observed in the NeuAv-fetuin particles by microscopy evaluation. Employing different molecular ratios of fetuin:NeuAv during particle modification did not improve the sedimentation. As did not the use of biotinylation reagents displaying spacers of different length to produce biotinylated fetuin.

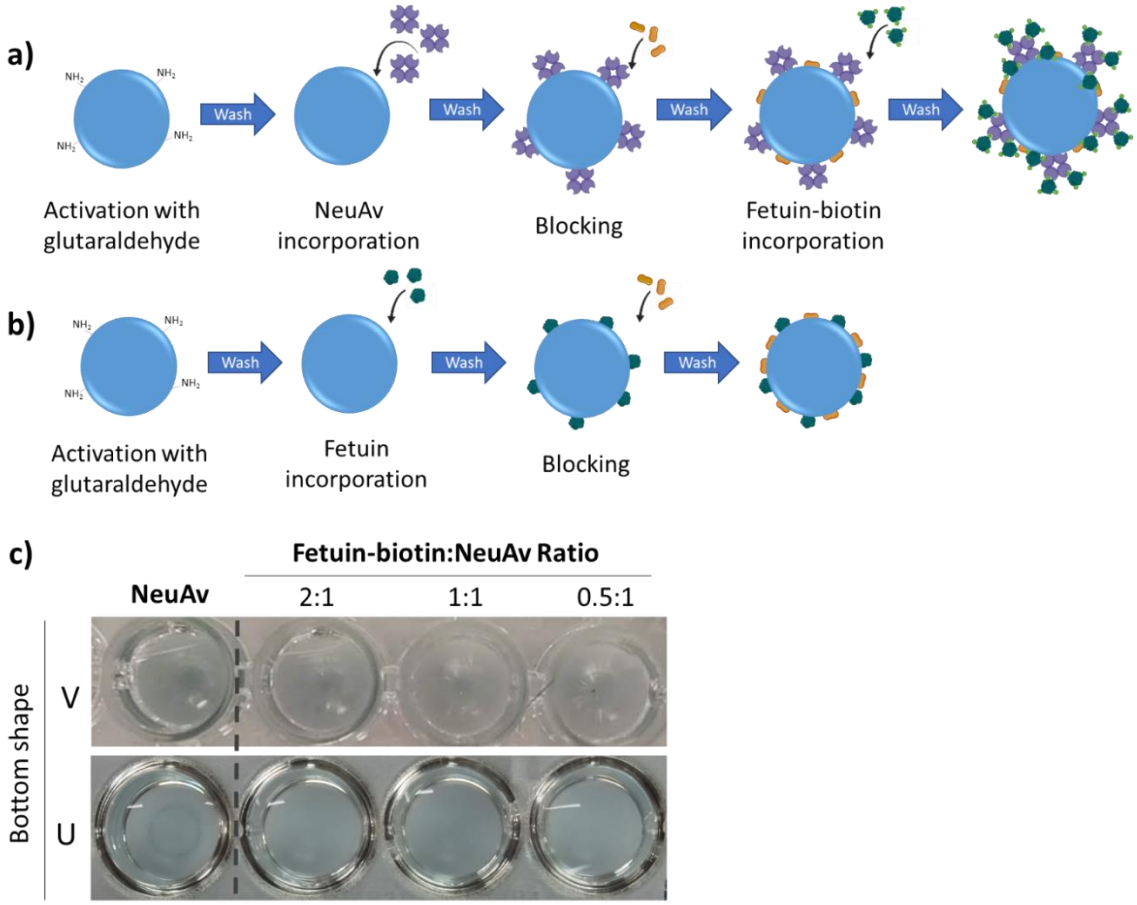

Figure 4.26 | Scheme of indirect **(a)** or direct **(b)** incorporation of fetuin. Indirect incorporation required a first conjugation with NeuAv followed by incorporation of biotinylated fetuin. Direct conjugation followed the same protocol described in Section 3.6.1 and allowed incorporation directly through amine surface groups crosslinked to fetuin amine groups. **(c)** NeuAv particles were incubated with different molar ratios of biotinylated fetuin (2:1, 1:1 and 0.5:1). Then, 375 µg of 10 µm of indirectly conjugated particles were sedimented in PBS for 15 min in V- or U-shaped wells. In all cases, sedimentation of the particles was inhibited. Same NeuAv particles without biotynylated fetuin were able to sediment (left well).

In order to confirm if the biotinylated protein contained enough biotin to bind NeuAv without impairing the recognition of fetuin by influenza virus, it was tested by ELISA. In order to do so, fetuin was biotinylated using different biotin-fetuin molar ratios (5, 10 and 18). Then, the biotinylated fetuin was coated on plate either directly or through NeuAv-biotin affinity binding. For this, NeuAv was immobilized on the plate, followed by a BSA-blocking. Then, biotinylated fetuin was incubated for 30 min at different NeuAv-fetuin molar ratios. After washing, plates were incubated with a dilution series of H1N1 virus and indirect detection through HRP-Ab and colorimetry was performed. Results are shown in Figure 4.27.

Decreasing the amount of biotin used to modify fetuin did not decrease the signal obtained (Figure 4.27a). This indicated that a 5:1 biotin-fetuin ratio was enough to guarantee efficient binding to NeuAv, while keeping the virus recognition intact. Still, results showed that NeuAv binding decreased the signal obtained by 20% compared to the use of biotinylated fetuin coated directly on surface, independently of the number of biotins per fetuin molecule used for

biotinylation. This could be due to a worse adsorption of NeuAv in the plate or to steric effects, which reduced the space available for incorporation of biotinylated fetuin molecules.

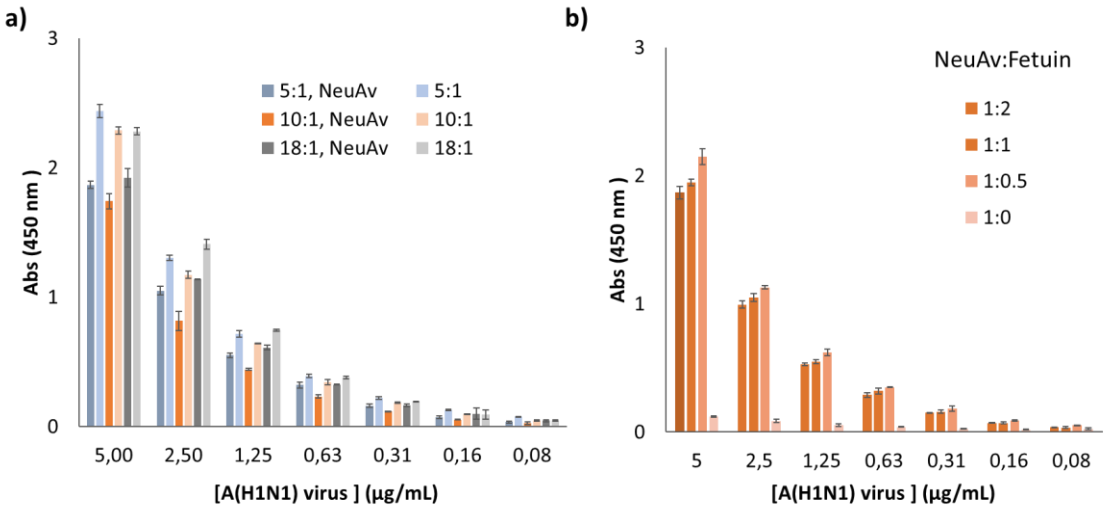

Figure 4.27 | ELISA for detection of A(H1N1) using for capture biotynylated fetuin. **(a)** Comparison of A(H1N1) recognition using biotynylated fetuin produced with different biotin:fetuin ratios, coated on surface either directly or through NeuAv affinity binding. Decreasing the amount of biotins per molecule did not improve the recognition capacity of the virus. On the other hand, increasing biotin number did not improve the binding to NeuAv. **(b)** Comparison between incubations with different molar ratios of NeuAv:fetuin during its binding.

On the other side, different ratios of NeuAv:Biotinylated fetuin had a small impact in virus recognition (Figure 4.27b). Results suggested that lower ratios could produce higher signals (6% higher), but the increase was not significant. In absence of biotinylated fetuin, signal was strongly suppressed, which confirms that virus recognition was specific and fetuin directed.

The lack of sedimentation of the particles modified with neutravidin and biotinylated fetuin may be explained by changes in surface charges. Fetuin is a highly glycosylated protein that has a high content of SA. This can be observed in its low Ip, partially due to its SA content.[197] Consequently, a considerable amount of these SA (with their negative charge) should be externally exposed. Biotinylation and NeuAv-biotin binding could alter the exposition of these SA on the molecule surface, changing the total surface charge of the particle and preventing sedimentation.

4.8. Conclusions

To sum up, the first proof of concept of synthrocytes conjugated with naturally sialylated glycoproteins showed that this reagent could substitute RBCs in HA- and HAI-like SynA/SynAI assays for influenza surveillance. More specifically, GYPA-synthrocytes were able to bind to influenza A(H1N1)pdm09 and B viruses (but no A(H3N2) viruses), triggering synthrocyte agglutination and a change in the sedimentation pattern visible by naked eye in less than 10 min, compared to the 30-60 min that require avian or mammal animals, respectively. Furthermore, the interaction between synthrocytes and influenza could be inhibited by specific

n-Ab, which allowed performing HAI-like SynAI assays for antigenic characterization and serological studies.

More receptors were evaluated to improve the sensitivity and selectivity of synthrocytes, achieve A(H3N2) recognition, and decrease the cost of synthrocyte production, which was elevated due to GYPA cost. The fact that some reference antisera displayed recognition of the GYPA-synthrocytes components, hindering SynAI result readout, highlighted also the need for finding new receptors.

Fetuin was chosen as a promising candidate because of its recognition of A(H1N1) and B viruses and its significantly reduced price. However, although different strategies were attempted to increase the sensitivity of fetuin-synthrocytes to at least GYPA-synthrocyte level, none of them was successful. Increasing the amount of fetuin during particle modification, optimizing glutaraldehyde conjugation to increase the number of active surface groups in the particles, or amplifying the number of possible binding spots through biotin-NeuAv linking did not improve the performance of the fetuin-synthrocytes produced. Moreover, H3N2 viruses still remained undetectable by fetuin. These results were attributed to the fact that native sialylated proteins contained an unpredictable variety of SA, and only some of them were recognized by influenza viruses. For this reason, we decided to explore the use of synthetic receptors instead of naturally sialylated proteins. Using synthetic SA should allow us to incorporate on the synthrocyte surface only selected receptors for targeted virus binding.

Chapter 5

Synthrocyte development using synthetic SA

Chapter 5. Synthrocyte development using synthetic SA

Protein-conjugated particles have been used for a long time for pathogen detection. However, most of these particles used Ab as bioreceptors for pathogen capture due to their specificity and easy conjugation chemistry.[166,198,199] Ab present high affinity for their targets, and therefore their interactions are stronger that the ones mediated by SA. Nevertheless, Ab tend to be highly specific, which hampers the use of a single Ab for the detection of the full variety of strains of influenza viruses.

In this Thesis project, we considered that employing batteries of Ab for bead modification, in order to achieve multiplexed influenza detection, would be too expensive and complex (in terms of assay optimization). Thus, as described in Chapter 3, approaches based on the recognition of SA by influenza viruses were explored instead. The use of sialylated native proteins, such as the GYPA or fetuin employed in the previous chapter, provided promising results but exhibited diverse drawbacks. All the sialylated proteins tested as bioreceptor candidates in this Thesis were obtained commercially. All of them had been directly obtained from their biological sources and none was a recombinant protein produced *in vitro*. This led to a complete lack of control of the composition of their SA. For most of the sialylated proteins we obtained, their exact SA content and composition was not facilitated by the provider. Moreover, not only the SA content was not always quantified; it was also inconsistent between production lots. This certainly affected reproducibility between batches of synthrocytes fabricated with these proteins, and therefore produced variations in influenza virus recognition. For that reason, synthetic SA of different molecular structure were explored here as influenza-binders.

SA have been exploited for therapeutic purposes, especially as inhibitors of influenza H. For example, Matrosovich and colleagues were among the first to demonstrate that synthetic polymeric compounds that contained SA could inhibit influenza virus receptor-binding activity.[200] They later observed that monovalent SA, although able to interact with the virus, had limited success due to its low binding strength.[201] On this basis, polyvalent neoglycoconjugates were created to improve the recognition. Two different strategies were used in order to produce compounds with multiple SA residues.[202,203] The first was using as carriers biomolecules like proteins[202,204] or glycopeptides.[205] The second approach entailed using synthetic backbones such as polymers (e.g., poly(acrylamide),[206,207] poly(glutamic acid)[208] and poly(phenylacetylene),[209] dendrimers,[210–212] or liposomes.[213,214]

Nowadays, the production of new glyconanomaterials is expanding.[215] The need for novel SA-containing structures that allow their use in virus-detection biosensors or as antiviral drugs is rapidly increasing. Even so, most of the systems reported for influenza binding involve tailor-made oligosaccharides (as the ones described above) or immobilized sialylated proteins (such as fetuin) that contain the carbohydrate pattern recognized by the virus.

This chapter describes the diverse alternatives that were tested along this Thesis to incorporate synthetic SA to the surface of the particles. These included affinity binding of biotinylated SA residues displaying spacers of different length and type, chemical conjugation

of SA modified with amino groups, and cross-binding of SA-BSA glycoconjugates. The characteristics of the different SA used have been summarized in Table 3.4. With these approaches we intended to reduce non-specific interactions and improve the control of the SA composition, while increasing the number of SA of interest on the surface of the beads.

5.1. Incorporation of biotinylated SA by affinity binding

Although in the previous chapter we had sedimentation problems when using biotin-NeuAv linkers for bead conjugation, we decided to try this approach again mostly because of three reasons. First, avidin-biotin affinity binding is a simple and efficient method that is widely used for surface bioengineering, and that is compatible with extensive surface blocking to prevent non-specific adsorption of non-target components. Second, biotinylated SAs that displayed spacers of different length and composition were commercially available. Third, the presence of different spacers could change the surface charge of the particle and modify the sedimentation pattern compared to that observed previously with biotinylated-fetuin particles.

For these studies, we obtained biotinylated SA from two different providers. Dextra was one of these identified companies, which could supply 6'-SL SA that displayed a terminal biotin through a 3-carbon spacer (6'-SL-b). This SA had been previously used to study influenza H and N interactions with their host cells.[216]

The second group of biotinylated glycan probes was purchased from Glycotech. In this case, the union between the carbohydrate probes and the biotin molecules was through a polyacrylamide (PAA) polymer with a molecular weight of approximately 30 kDa. These synthetic SA were multivalent, meaning that each probe contained a trisaccharide, three residues of the selected SL bound together ($[SA]_3$-PAA-b). Glycotech could provide three different SA of this type ($[6'\text{-SL}]_3$-PAA-b, $[6'\text{-SLN}]_3$-PAA-b, and $[3'\text{-SL}]_3$-PAA-b). A more detailed description of these receptors can be found in Section 3.1.2.2.

5.1.1. Biotinylated SA characterization by ELISA

The first step for substituting native sialylated proteins by synthetic SA in synthrocytes was to assure the ability of influenza viruses to recognize SA alone. In order to do so, a new ELISA was optimized to evaluate the different types of biotinylated SA.

To begin with, we studied which biotin-binding protein could capture and expose better the SA to the influenza viruses. Briefly, NeuAv, Av or streptavidin (StrpAv) were immobilized by adsorption in a microtiter plate, followed by blocking with BSA. Then, incubation with 6'-SL biotinylated glycan probes (either 6'-SL-b or $[6'\text{-SL}]_3$-PAA-b) was performed as a model for all the available SA. After the reagent excess was washed away, incubation with different concentrations of influenza virus A/New Caledonia/20/99 (H1N1) was carried out. The procedure continued as in the ELISA described in Chapter 3.3, with three serial incubations with primary Ab, HRP-labelled secondary Ab, and TMB as chromogenic enzymatic substrate. Finally, absorbance was measured using a spectrophotometer.

As can be seen in Figure 5.1, [6'-SL]$_3$-PAA-b immobilization trough NeuAv and StrpAv produced comparable trends, which slightly higher signals for NeuAv, while plate modification using Av generated significantly lower signals. This contrasts the fact that the expected affinity for biotin of these 3 proteins is similar, and even lower for StrpAv than for the other two (Kd of $1.3x10^{-15}$ for Av and NeuAv, and $0.04x10^{-15}$ for StrpAv according to the supplier's data sheets). The differences observed in these signals could be explained because Av is a highly glycosylated protein that also presents other carbohydrate moieties and SA, which could impact the recognition of the A(H1N1) virus or even repel electrostatically the synthetic [6'-SL]$_3$-PAA-b that were being linked to it. As shown in Figure 5.1a, a concentration of 333 ng/mL of [6'-SL]$_3$-PAA-b was enough to maximize virus recognition, and therefore it was selected for the subsequent experiments. This concentration equaled to approximately 1 pmol/well and was 16 times lower than the NeuAv molar concentration used (16 pmols/well). The unexpected low incorporation of the SA could be explained by an excess of NeuAv unable to bind to the well during plate modification, decreasing the amount of available NeuAv far from the theoretical 16 pmol/well, or to steric effects (NeuAv local overcrowding, NeuAv partial denaturation, or repulsion between [6'-SL]$_3$-PAA-b molecules). On the other hand, each [6'-SL]$_3$-PAA-b contains diverse residues of biotin that could bind to more than one NeuAv molecule simultaneously. Thus, each [6'-SL]$_3$-PAA-b. molecule could block/occupy several biotin-binding sites. Because in particle conjugation it was also necessary to incorporate an excess of the capture protein, this issue was not further optimized.

In contrast, as can be seen in Figure 5.2a, the signal obtained when using 6'-SL-b was very low, almost indistinguishable from the negative control. This could be partly explained because the amount of SA was markedly lower in SA-b oligosaccharides compared to [SA]$_3$-PAA-b, and partly because individual 6'-SL-b moieties were incorporated on surface farther from each other. It is worth stressing that, while in 6'-SL-b probes each SA was linked directly to a biotin in a 1:1 ratio, in the case of [SA]$_3$-PAA-b they were paired in trios and linked several times along the PAA polymer. The later was expected to perform better, because the interactions between the hemagglutinin and individual SA moieties are rather weak (*Kd* ~1 mM),[217] which is compensated by multivalent binding. Thus, H has a trimeric structure, which contains three recognition sites that can bind to multiple SA moieties simultaneously. The type of multivalent glycan probes employed in this section should enhance the stability of the SA-receptor union, compared to the monovalent probes from Dextra.[218]

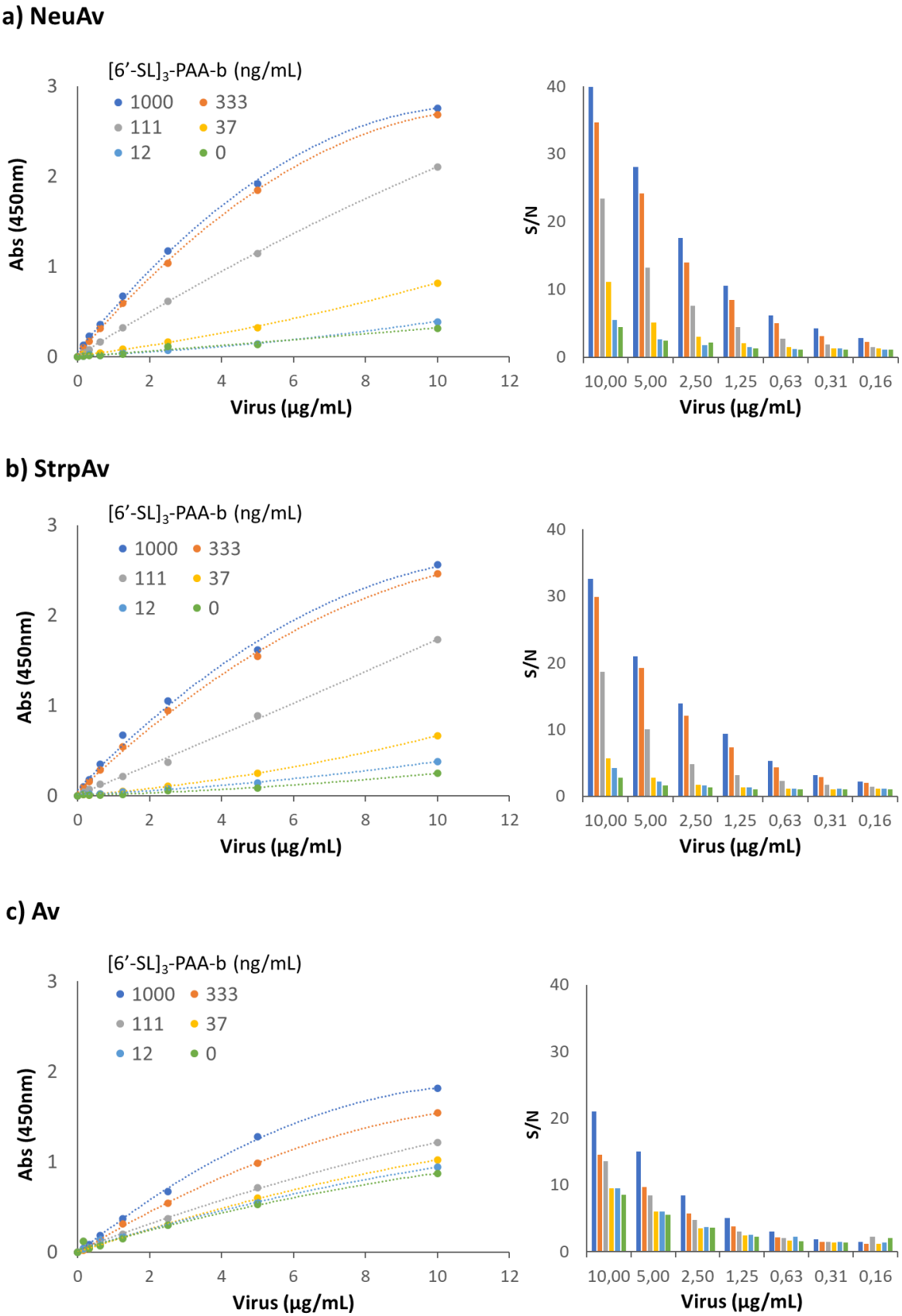

Figure 5.1 | Comparison of signals obtained by immobilization of the [6'-SL]$_3$-PAA-b on microtiter plates through NeuAv **(a),** StrpAv **(b)** and Av **(c).** Left, signals obtained for each [6'-SL]$_3$-PAA-b concentration tested after blank subtraction. Right, signal to noise for each of them.

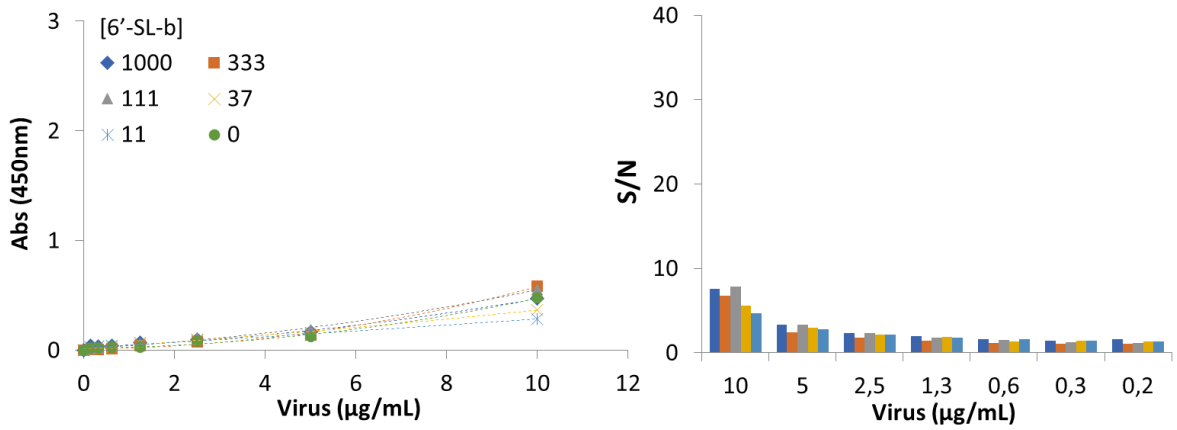

Figure 5.2 | Signals obtained when using NeuAv to immobilize 6'-SL-b on microtiter plates, followed by incubation with increasing concentrations of virus A/New Caledonia/20/99 (H1N1). Left, signals with the blank subtracted, right, signal to noise.

Next, we studied the recognition of three different $[SA]_3$-PAA-b ($[6'\text{-SL}]_3$-PAA-b, $[6'\text{-SLN}]_3$-PAA-b, and $[3'\text{-SL}]_3$-PAA-b) by a battery of influenza viruses (obtained from Hytest). This recognition was evaluated using the same ELISA settings previously described, using NeuAv for $[SA]_3$-PAA-b immobilization and incubating with increasing virus concentrations. Figure 5.3 shows that A(H1N1) viruses were able to recognize the three SA probes although with different affinity. A/Taiwan/1/86 and A/Beijing/262/95 recognized better $[3'\text{-SL}]_3$-PAA-b, they detected to a certain extent $[6'\text{-SLN}]_3$-PAA-b and they displayed minimal affinity for $[6'\text{-SL}]_3$-PAA-b. In contrast, A/New Caledonia/20/99 subtype produced higher signals with $[6'\text{-SLN}]_3$-PAA-b and $[6'\text{-SL}]_3$-PAA-b, although its recognition level of $[3'\text{-SL}]_3$-PAA-b was comparable to the other A(H1N1) viruses. According to the provider, all of these viruses had been isolated from human hosts and grown in embryonated eggs, and should bind α2,6-linked SA preferentially. However, it is well demonstrated that propagation of human influenza viruses in eggs usually alters their binding preferences.[43] Generally, egg-adaptation results in (artificially) increased affinity of human-derived viruses for α2,3-linked SA, and decreased binding to the α2,6-linked SA, which could explain the results obtained here.

On the other hand, A(H3) and B viruses preferred 6'-SLN and 6'-SL ends, although the signals obtained for H3 viruses were lower than those observed for B viruses.

5.1.2. Microparticle modification with biotinylated SA

Once the recognition of biotinylated SA by diverse influenza viruses had been assessed, indirect incorporation to the particles was performed. The used protocol was similar to the one described in Section 3.6.2. In accordance with the results shown in Figure 5.1, NeuAv was selected as the binder on the particles. Then, NeuAv-particles were modified with different concentrations of $[SA]_3$-PAA-b, using different molar ratios of $[SA]_3$-PAA-b:NeuAv. These ratios were based on the optimal theoretical ratio defined in the previous ELISA (0.063:1), but slightly increased to ensure an excess of SA even if the NeuAv incorporation was more efficient than in the plate wells.

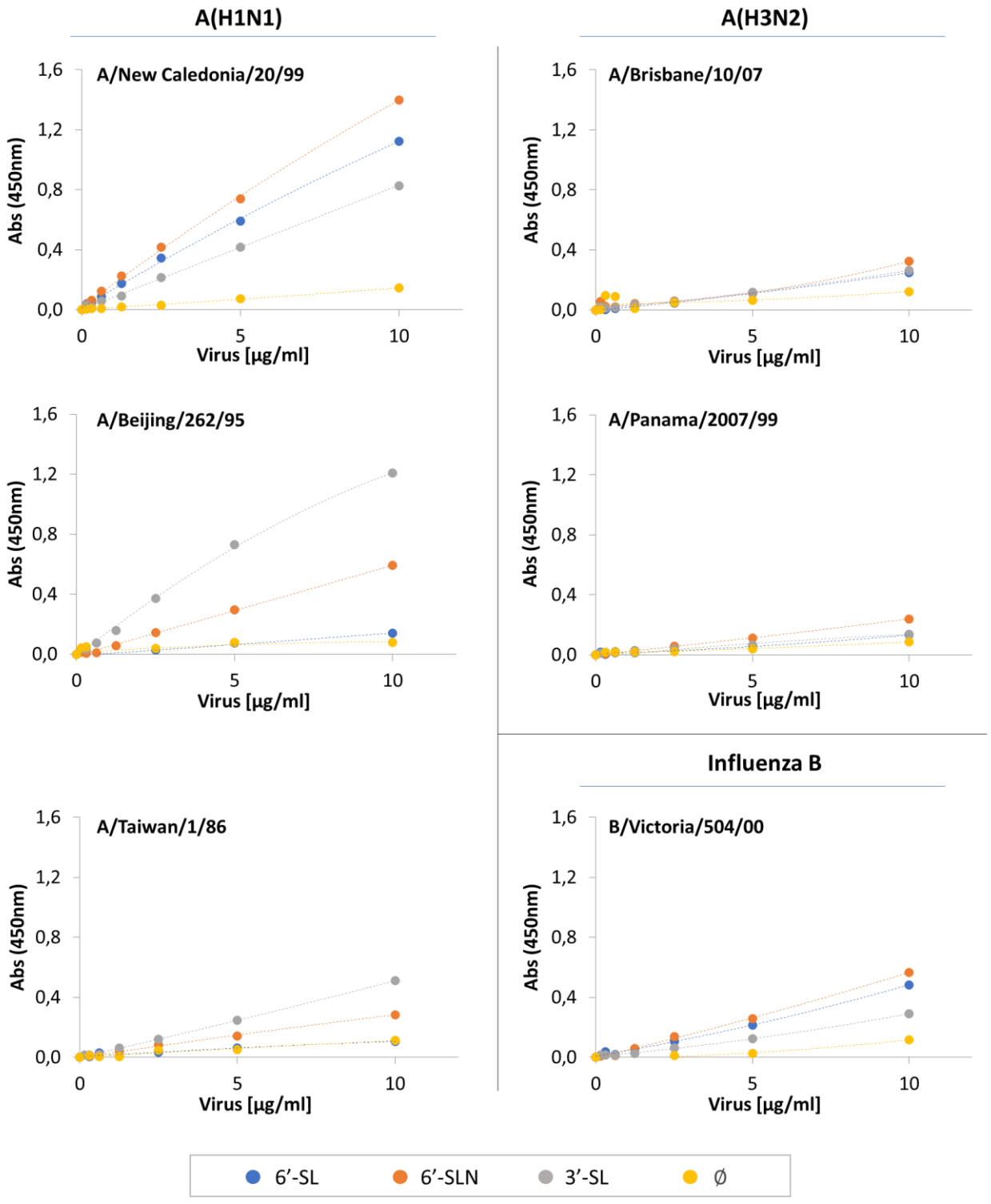

Figure 5.3 | Binding of different influenza viruses (A(H1N1), A(H3N2) and B) by different types of $[SA]_3$-PAA-b captured through NeuAv on microtiter plates (6'-SL, 6'-SLN and 3'-SL).

The different conjugated beads obtained were then allowed to sediment in the presence or absence of influenza A/New Caledonia/20/99 (H1N1) virus. Their behavior, which can be observed in Figure 5.4, was similar to that displayed by particles produced by indirect incorporation of biotinylated fetuin in Section 4.7. This is, particles conjugated with [6'-SL]$_3$-PAA-b did not sediment, even when the number of particles per well or the sedimentation time increased (Figure 5.4.a-b). Augmenting or decreasing the amount of [SA]$_3$-PAA-b did not improve the sedimentation either. This contrasts with the performance of NeuAv-conjugated particles alone, which were able to form a pellet. This suggested that the problem was the [SA]$_3$-PAA-b addition step and not the initial NeuAv conjugation.

Finally, no difference in sedimentation pattern was observed when exposing the beads to the virus (Figure 5.4a-b, bottom).

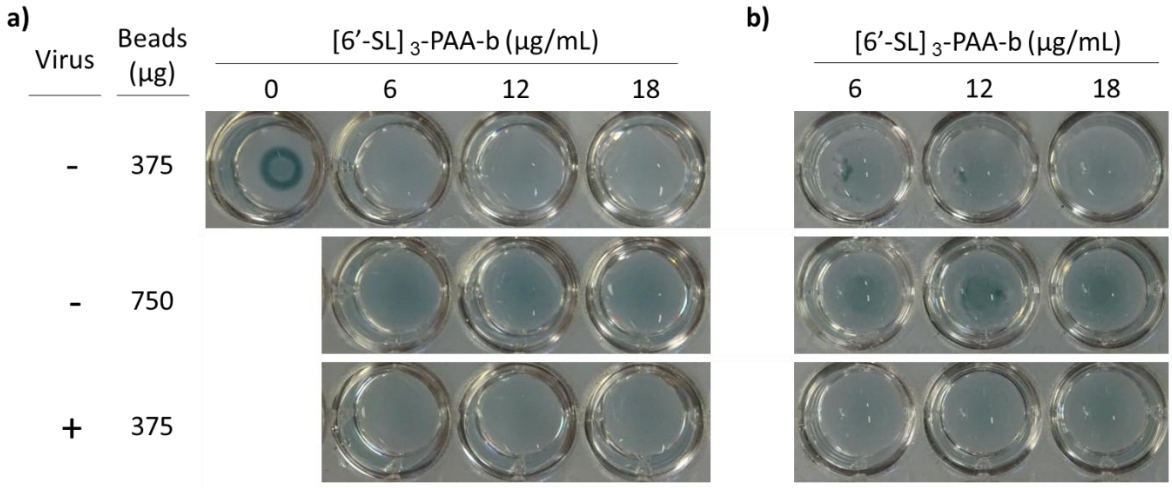

Figure 5.4 | a) Sedimentation of NeuAv coupled particles modified without or with increasing concentrations of [6'-SL]$_3$-PAA-b, equivalent to theoretical [6'-SL]$_3$-PAA-b:NeuAv molar ratios 0:1, 0.08:1, 0.16:1 and 0.25:1, respectively. Two different amounts of particles were tested (375 and 750 µg/well) with equal results. The sedimentation pattern did not change after incubation with 5 µg/mL of A(H1N1) virus. **b)** Same sedimentation patterns than in **(a),** after allowing particles to settle down for 48 h.

The buffer used in the assay was modified in an attempt to improve the sedimentation of [6'-SL]$_3$-PAA-b-NeuAv particles. Performing the assay in buffers of different pH did not produce any effect (Figure 5.5a). On the other hand, surfactants were added to increase medium viscosity, disperse better the particles, and force their sedimentation compared to performance in just PBS. As can be seen in Figure 5.5b, diverse concentrations of Tween20 and Triton X-100 were tested. Sedimentation was achieved only in the presence of Tween20, which had this effect at concentrations as low as 0.001%. However, particles also sedimented in the presence of influenza virus for most concentrations of Tween20 tested. Although some changes in sedimentation attributed to virus-induced agglutination could be observed at low Tween20 concentrations (such as 0.0025%), these results were not reproducible. Therefore, we also discarded this option.

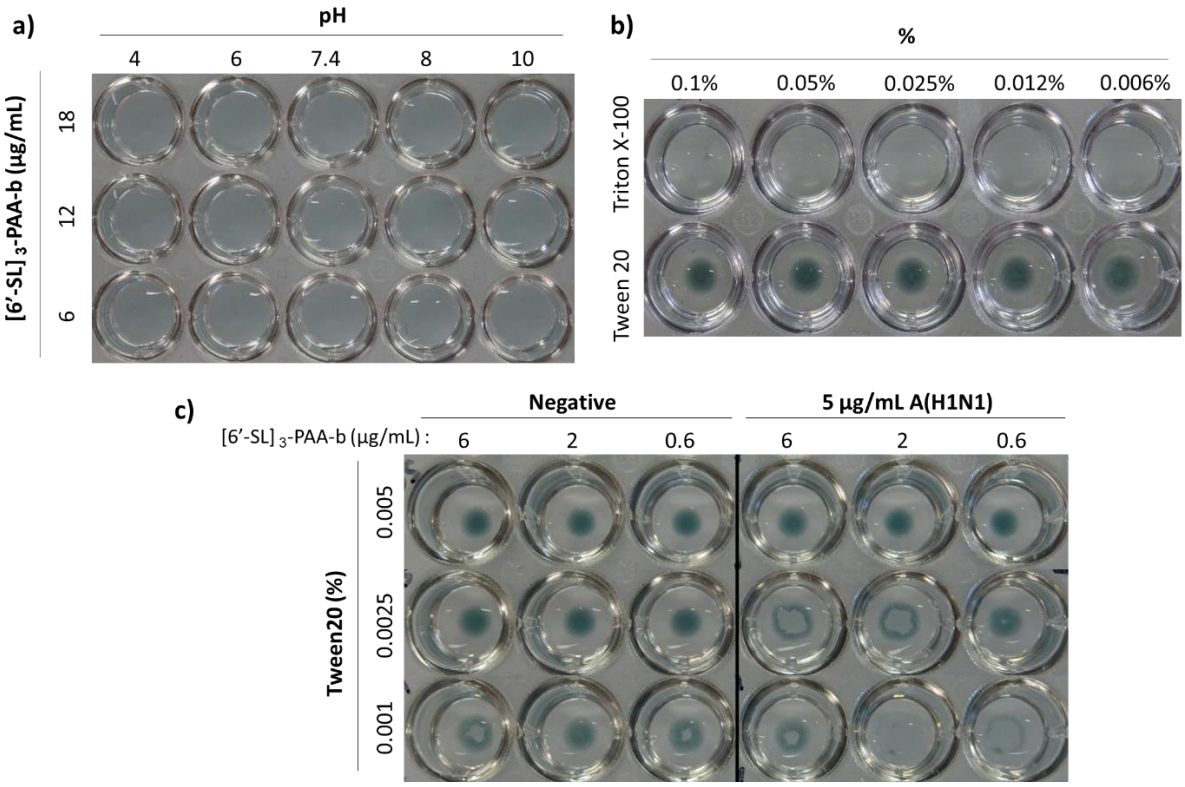

Figure 5.5 | Sedimentation of synthrocytes modified with different concentrations of [6'-SL]$_3$-PAA-b. Effect of pH **(a)** and detergents **(b)** in the sedimentation. **c)** Effect of different concentrations of Tween20 in particle sedimentation in the absence (left) and in the presence of virus (right).

The results obtained when using [SA]$_3$-PAA-b in ELISA confirmed that viruses were able to recognize these synthetic SA by themselves, but when these biotinylated polymers were coupled to the beads, they prevented particle sedimentation. This was consistent with the results obtained when conjugating biotinylated fetuin and corroborate that receptor incorporation through biotin affinity binding was not an appropriate approach for synthrocyte production. Therefore, new strategies to incorporate the sialic acids were necessary.

5.2. Chemical incorporation of aminated SA

Chemical coupling of SA was next explored using a SA bound to a molecule of glycine in a 1:1 proportion with a NH_2 terminal available for conjugation (SA-NH_2). In this case, the SA-NH_2 were not evaluated by ELISA and were tested directly on the surface of the particles.

SA-NH_2 were bound to the particles by glutaraldehyde conjugation using the protocol described in Section 3.6.1, which derives from the one employed in Chapter 4.1 for production of GYPA-synthrocytes.

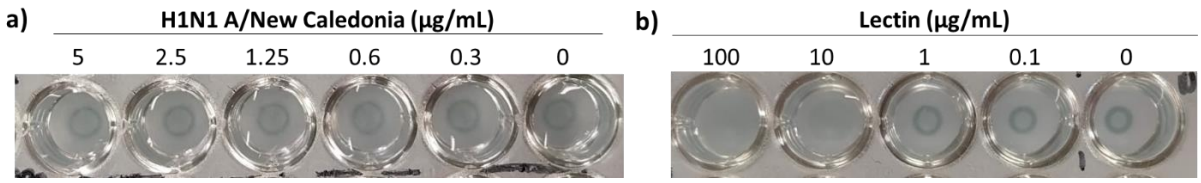

Figure 5.6 | Sedimentation pattern of particles conjugated with 6'-SL-NH_2 in the presence of different concentrations of A(H1N1) virus **(a)** or SNA lectin **(b).**

As can be seen in Figure 5.6, particles conjugated with 6'-SL-NH_2 were able to sediment in the absence of influenza viruses. This confirmed that the lack of sedimentation identified in the previous section for particles modified with $[SA]_3$-PAA-b was due to the biotin linker and not caused by the SA itself. Unexpectedly, 6'-SL-NH_2 coated particles did not recognize influenza. Independently of the concentration of 6'-SL-NH_2 used in the conjugation, these particles did not change their sedimentation pattern in the presence influenza virus A/New Caledonia/20/99 (H1N1), and they did not agglutinate when observed under the microscope. To discard conjugation issues, we confirmed the incorporation of the SA to the particles through SNA-lectin recognition. The particles modified with 6'-SL-NH_2 agglutinated and changed their sedimentation in the presence of SNA-lectin, but at concentrations higher than those detected by particles modified with native sialylated proteins (Figure 5.6b vs 4.8). In these oligosaccharides, each SA displayed a single glycine moiety, which equals the 1 to 1 link to biotin showed for 6'-SL-b in Figure 5.2. Therefore, the behavior of these two molecules was similar. Accordingly, the null recognition of influenza could be explained by reduced incorporation and uneven distribution of the SA on the surface of the particles, where they were probably too far from each other to promote virus binding. In view of the high price and bad performance of SA-NH_2, this strategy was no longer pursued.

5.3. SA incorporation trough BSA-carriers

Another accessible option was modifying the particles with a synthetic glycoconjugate displaying a known amount of selected SA. Here, we used conjugates obtained from Dextra, which consisted of a molecule of BSA that contained between 7 and 13 molecules of the selected SA attached to it through a 3-atom spacer (SA-BSA). We started by testing a conjugate that displayed 6'-SL (6'-SL-BSA).

The first step to test 6'-SL-BSA was to perform an ELISA to evaluate the level of recognition by the virus and to define conjugate optimal concentration. For this, we adsorbed increasing concentrations of 6'-SL-BSA directly in the plate. The rest of the assay proceeded as before, including blocking with BSA, capture of serially diluted influenza, and serial incubations with primary Ab, HRP-labelled secondary Ab and TMB substrate before spectrophotometric detection.

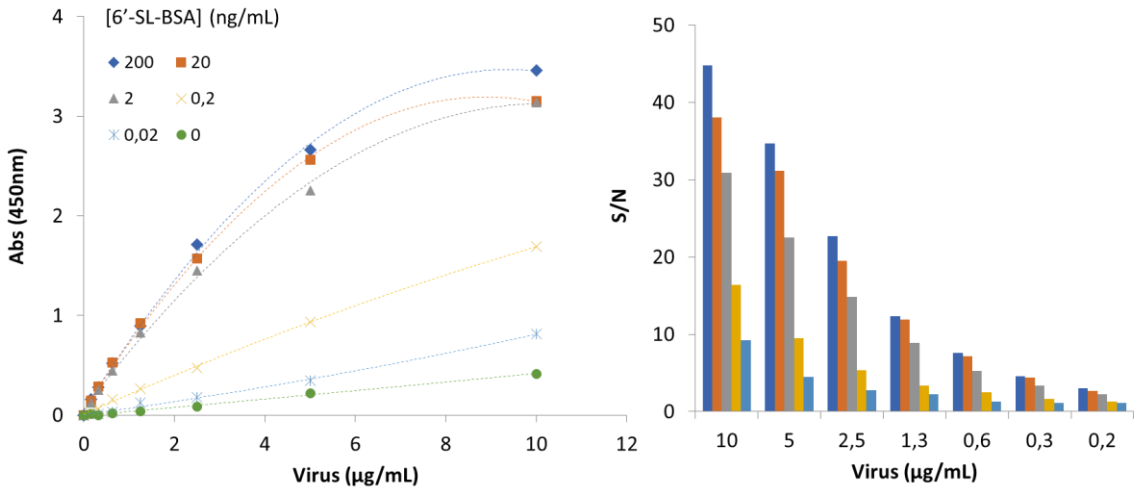

Figure 5.7 | Detection of influenza A/New Caledonia/20/99 (H1N1) by ELISA using as surface-bound receptor different concentrations of 6'-SL-BSA. Left, signals after blank subtraction, right, signal to noise (S/N).

Influenza virus recognized SA better when they were coupled to BSA than to a biotinylated linker, and 2 ng/mL of 6'-SL-BSA were enough to produce completely functional surfaces (compared to 333 ng/mL needed for $[6'\text{-SL}]_3$-PAA-b) (Figure 5.7). This could be explained because each molecule of BSA carried a relatively large number of SA, specifically 7 in the case of 6'-SL-BSA, which allowed further SA molecules to be exposed closer to each other than when SA-b or $[SA]_3$-PAA-b were incorporated on surface. However, this result could also indicate that the PAA spacer in $[SA]_3$-PAA-b affected particle surface charge, hydrophilicity or NeuAv biotin affinity binding. In any case, employing 6'-SL-BSA improved the recognition by the viral HA, similarly to when using multivalent polymers.[201]

On the other hand, when chemically conjugated to particles, 6'-SL-BSA displayed better recognition of the A/New Caledonia/20/99 (H1N1) virus than the other counterparts tested above. These results were consistent with the signals obtained from the previous ELISA. As shown in Figure 5.8a, 6'-SL-BSA coated particles sedimented in the absence of virus and did not in its presence. Moreover, the agglutination titer was dependent on the amount of 6'SL-BSA incorporated on the surface during the conjugation. This is, particles conjugated with more 6'-SL-BSA detected the virus at lower concentrations. In contrast, particles conjugated with just BSA (without SA) sedimented always, independently of the amount of virus they were incubated with. This confirmed that the virus-SA recognition was specific.

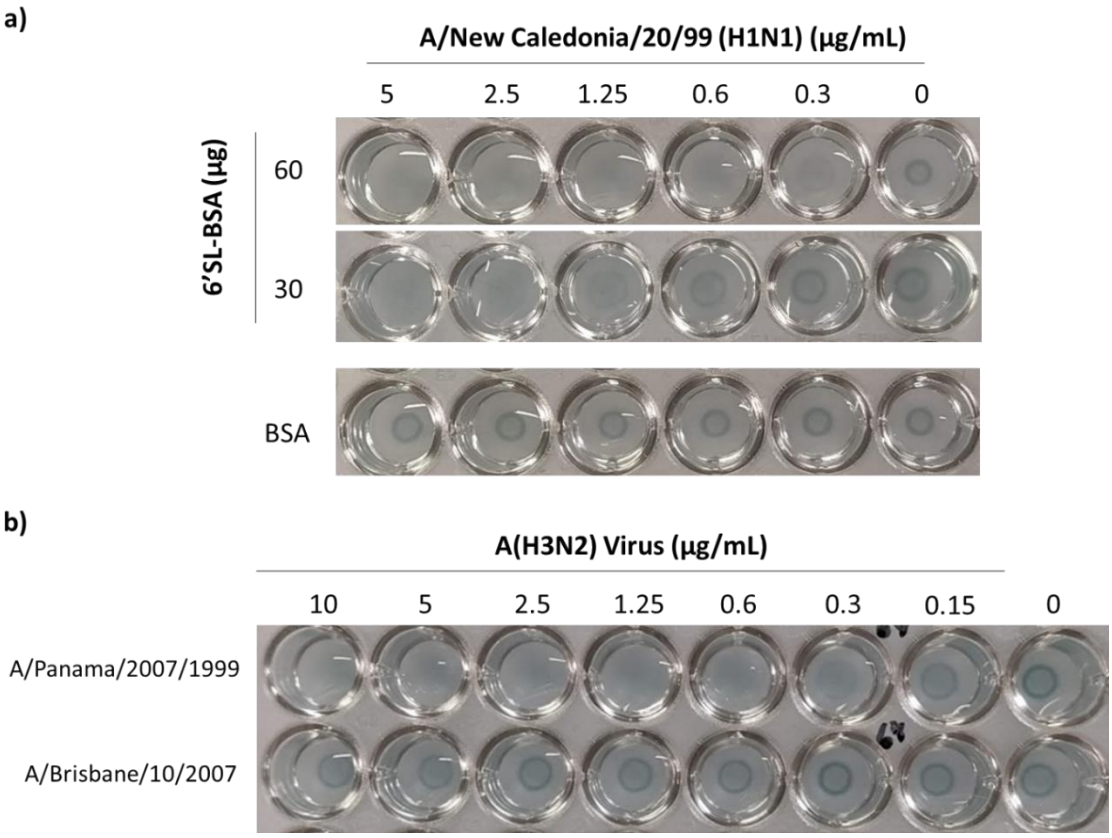

Figure 5.8 | a) Sedimentation pattern of particles conjugated with different concentrations of 6'-SL-BSA or BSA alone, in the absence or in the presence of different concentrations of A/New Caledonia/20/99 (H1N1) virus. **b)** SynA pattern obtained for 6'-SL-Synthrocytes with different concentrations of A(H3N2) A/Panama/2007/1999 and A/Brisbane/10/2007.

Next, we evaluated the recognition of these particles by viruses of the A(H3N2) subtypes. This group of viruses was not recognized by any of the native proteins previously tested. Moreover, recognition of these viruses is critical because their culture and assessment are one of the most problematic for the WHO.[117,219] In fact, HA of some H3 viruses must be done in the presence of Oseltamivir, an inhibitor of the neuraminidase that increases the agglutination capacity of the cells.

Of the two A(H3N2) viruses analyzed, we were able to recognize one with considerable sensitivity (Figure 5.8b). Although this certainly left room for improvement, this result was encouraging and a noticeable improvement compared to the outcome of all the previous particles.

At this point, discontinuation in the virus supply chain forced a change of the virus source and only the virus antigens included in the 2018-2019 WHO Influenza reagent kit were employed in subsequent experiments (described in Section 3.1.4). As can be seen in Figure 5.9, neither A(H1N1) nor A(H3N2) recognized this version of 6'-SL-synthrocytes, which was attributed to the presence of large aggregates in the virus preparations. However, both B/Yamagata and B/Victoria reference Ag were detected down to 1:128 and 1:256 dilutions, respectively.

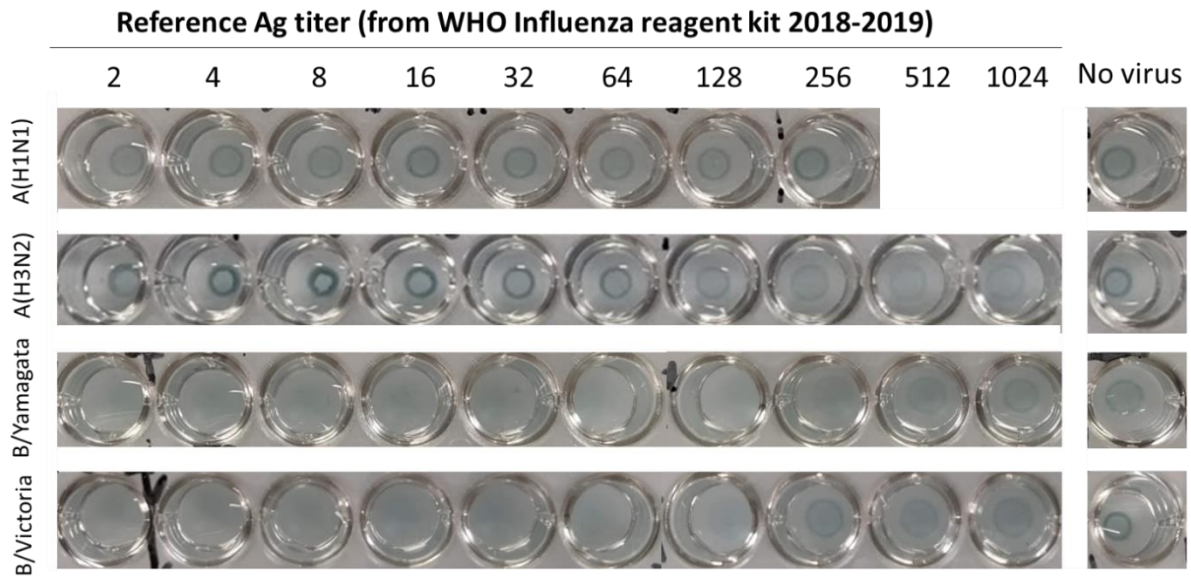

Figure 5.9 | SynA performed with 6'-SL-Synthrocytes and all the reference antigens of the 2018-2019 WHO Influenza reagent kit. It included the following 4 reference Ag, which were egg-grown viruses inactivated with BPL: A/Michigan/45/2015 NYMC X-275 (H1N1), A/Singapore/INFIMH-16-0019/2016 (H3N2), B/Phuket/3073/2013 (Yamagata) and B/Colorado/2017/06/2017 (Victoria).

After these results, we selected the WHO B/Yamagata B/Phuket/3037/2013 reference Ag as a model for subsequent 6'-SL-Synthrocyte re-optimization. This virus has been part of the kit and the annual vaccine recommendations since 2013 and has been consistently available from the IRR-WHO since then.

Then, particles were re-optimized, starting with the amount of 6'-SL-BSA used in their production. For this, particles were conjugated in parallel with increasing amounts of 6'SL-BSA before being blocked with BSA 0.5%. Decreasing the amount of SA-BSA under 40 µg/conjugation had a considerable negative impact in virus recognition, probably because the particles were not completely coated (Figure 5.10a). On the other hand, increasing the amount of 6'SL-BSA above 40 µg/conjugation did not produce better-performing synthrocytes, raising their fabrication cost unnecessarily. This concentration was thus selected as the optimal.

Under these conditions, the number of molecules of 6'-SL-BSA per particle was small compared to the amount used for native sialylated proteins in the previous chapter. As a result, blocking with BSA 0.5% was insufficient and the coated particles displayed non-specific agglutination in the presence of virus-free serum (Figure 5.10b). Because of this, the blocking was also re-optimized, testing BSA concentrations spanning between 0.5 and 4%. As discussed above, at the lowest concentration tested, the blocking was not efficient, and we observed some non-specific agglutination in the presence of virus-free serum. Blocking with BSA 1% was enough to counteract this effect, although the pellets formed in the presence of serum were still wider than those obtained in PBS. Problems in virus recognition aroused at the highest blocking concentration tested, producing a slight but observable sediment in the presence of it. Therefore, we increased the blocking from 0.5% to 2% BSA before continuing with the next SynA and SynAI experiments. Particles modified with 40 µg/conjugation of 6'-

SL-BSA and blocked with 2% of BSA produced similar pellets in PBS and virus-free serum, and generated agglutination patterns in the presence of virus.

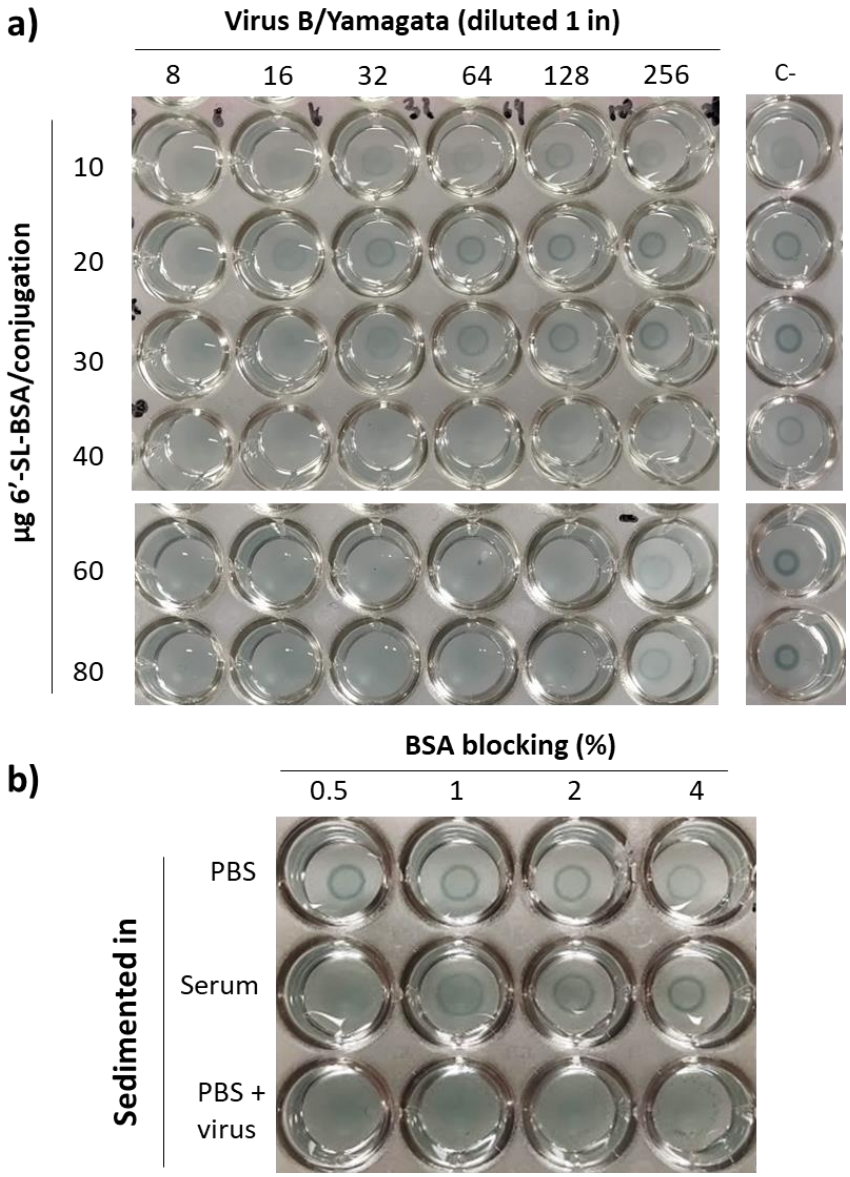

Figure 5.10 | a) Optimization of the amount of 6'-SL-BSA required for particle modification (particles blocked with BSA 0.5%). With 6'-SL-BSA concentrations under 20 µg/conjugation, particles were not coated enough and the pellets obtained in SynA tests were not consistent. **b)** Particle sedimentation in PBS (top), human serum (mid) and 5 µg/mL of B/Yamagata virus in PBS, after modification with 40 µg/conjugation of 6'-SL-BSA and blocking with BSA 0.5-2% (bottom). Particles blocked with BSA 0.5% displayed non-specific agglutination in the presence of serum. Particles blocked with BSA 4% produced a diffuse pellet in the presence of virus instead of a clear agglutination pattern.

5.4. Improvement of particle staining

At this point of development, it became clear that the commercial Sicastar blue particles had color reproducibility issues. As can be seen comparing figures from Chapter 4 and Chapter 5 (for example the sediments in Figure 4.11 and Figure 5.8), the intensity of the halos observed varied importantly between production batches. This impacted negatively the visual

observation of the sedimented pellets, forcing to use more beads per well, and thus making the assay more expensive and less sensitive.

Initially, these changes were attributed to the differences in the handling and variability during the conjugation process. But once the optimization of the different parameters was finished and the protocol was stablished, we realized that the problem came mainly from the commercial beads. As can be seen in Figure 5.11, the level of particle staining in the different batches provided by the supplier was clearly different. Moreover, color was not related to the aging of the particles or to the concentration of particles present in each batch, but to the staining intensity of each one.

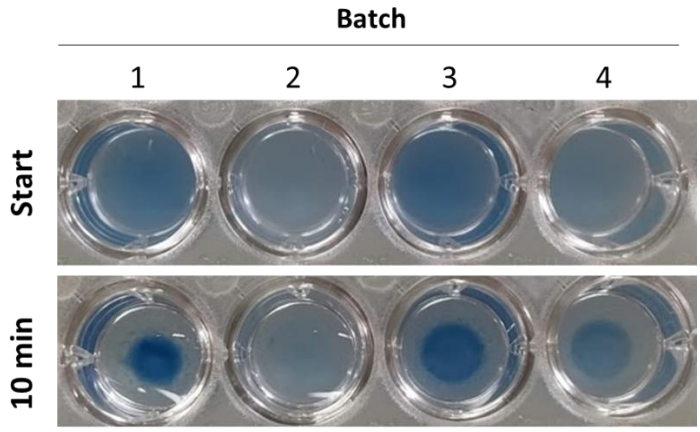

Figure 5.11 | Sedimentation of as-received commercial 10-µm bare Sicastar blue beads of different production batches. 7.5 µL were pipetted in 92.5 µL of PBS and were observed either immediately (top) of after 10 min of sedimentation (bottom). In all the cases, the number of particles per µL ranged between 135.000 and 150.000 and did not correlate with the color.

In an attempt to standardize bead color intensity, a customized dying protocol was developed and optimized by another member of the team (Section 3.5). This protocol allowed producing particles of reproducible color intensity. Furthermore, because the custom-dyed beads were more intense than the commercial ones, it was possible to decrease the number of particles/well necessary to perform the assays. As can be seen in Figure 5.12, the reduction was from 375 µg/well necessary for the commercial blue beads, to 250 µg/well of the custom-dyed ones. Sediments could be observed even with 200 µg/well of dyed beads in the negative controls (without virus), but the results were less reproducible than when using 250 µg/well. The 30% reduction of the particle numbers cheapened the assay considerably, because the extra cost of dying the particles was very low (of the order of 0.77 €/10 mL). This decrease in bead working unit also improved the sensitivity of the assay. As shown in Figure 5.12b, particles were more sensitive the fewer they were.

From then on, all the particles used in SynA and SynAI were custom-dyed and quality checked using particle count and spectrophotometry absorption as described in Section 3.5.

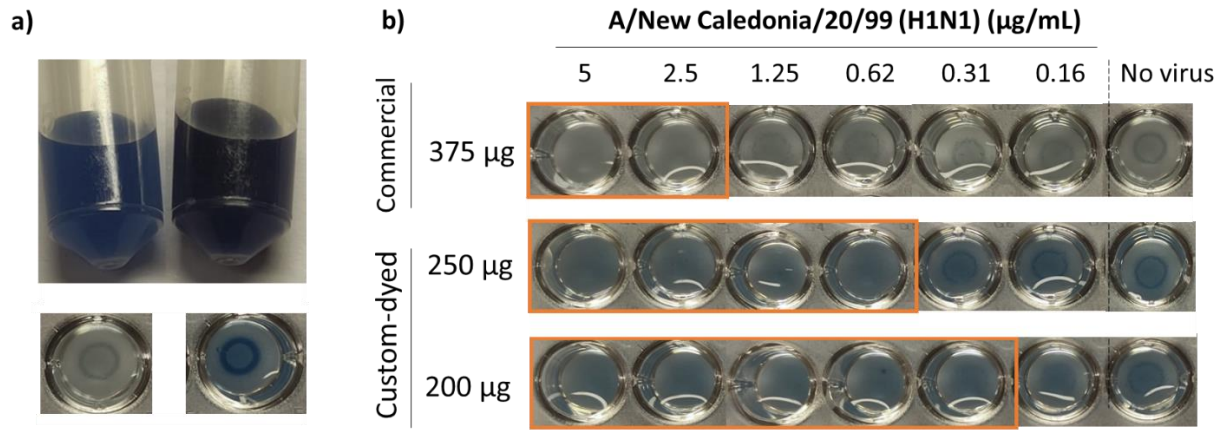

Figure 5.12 | a) Bare beads in solution (top) and conjugated with fetuin and sedimented (bottom). While the images on the left correspond to commercial Sicastar blue particles, the images on the right display custom-dyed particles, which were more intense in color. **b)** SynA using fetuin-conjugated particles. On top, using commercial blue particles, middle and bottom using custom-dyed beads with two different amounts of particles per well. The rectangles label the wells with agglutination patterns, showing that custom-died particles provided more sensitive synthrocytes that could be used at lower concentration.

5.5. Sedimentation pattern of particles conjugated with different SA-BSA

Once the particles were successfully dyed, they were conjugated with different SA-BSA. We used the 3 SA-BSA neoglycoproteins that were available commercially from Dextra, which included 3'-SL, 3'-SLN and 6'-SL as terminal sialic acid residues coupled to the BSA. Furthermore, we employed N-Acetyllactosamine-BSA (N-Ac-BSA) as a negative control. This molecule contains the same structure than SA-BSA, but lacks the α2,6- or α2,3- terminal residue, which is crucial for influenza virus recognition.[220]

Finally, we performed a SynA using the diverse SA-BSA conjugated particles and the 4 reference Ag included in the 2018-19 WHO kit for influenza surveillance (Figure 5.13). As expected, each of the viruses displayed different affinity for each of the SA tested. For example, A(H1N1)pdm09 virus recognized better 3'-SL and 3'-SLN SA than 6'-SL, which exhibited almost no recognition. Although influenza human viruses should present a higher recognition of α2,6-SA, this virus has its origin in Swine influenza and is propagated in eggs, which increases α2,3-SA affinity. Moreover, no clear consensus exists on the recognition of α2,3-SA by A(H1N1)pdm09, with some results suggesting the dual recognition of α2,3 and α2,6,[150,221,222] while others detecting very limited binding to α2,3-SA.[36,223,224] Nevertheless, HA protocols recommend using turkey RBCs to perform A(H1N1) virus HA, which should express higher α2,3-linked SA.[225]

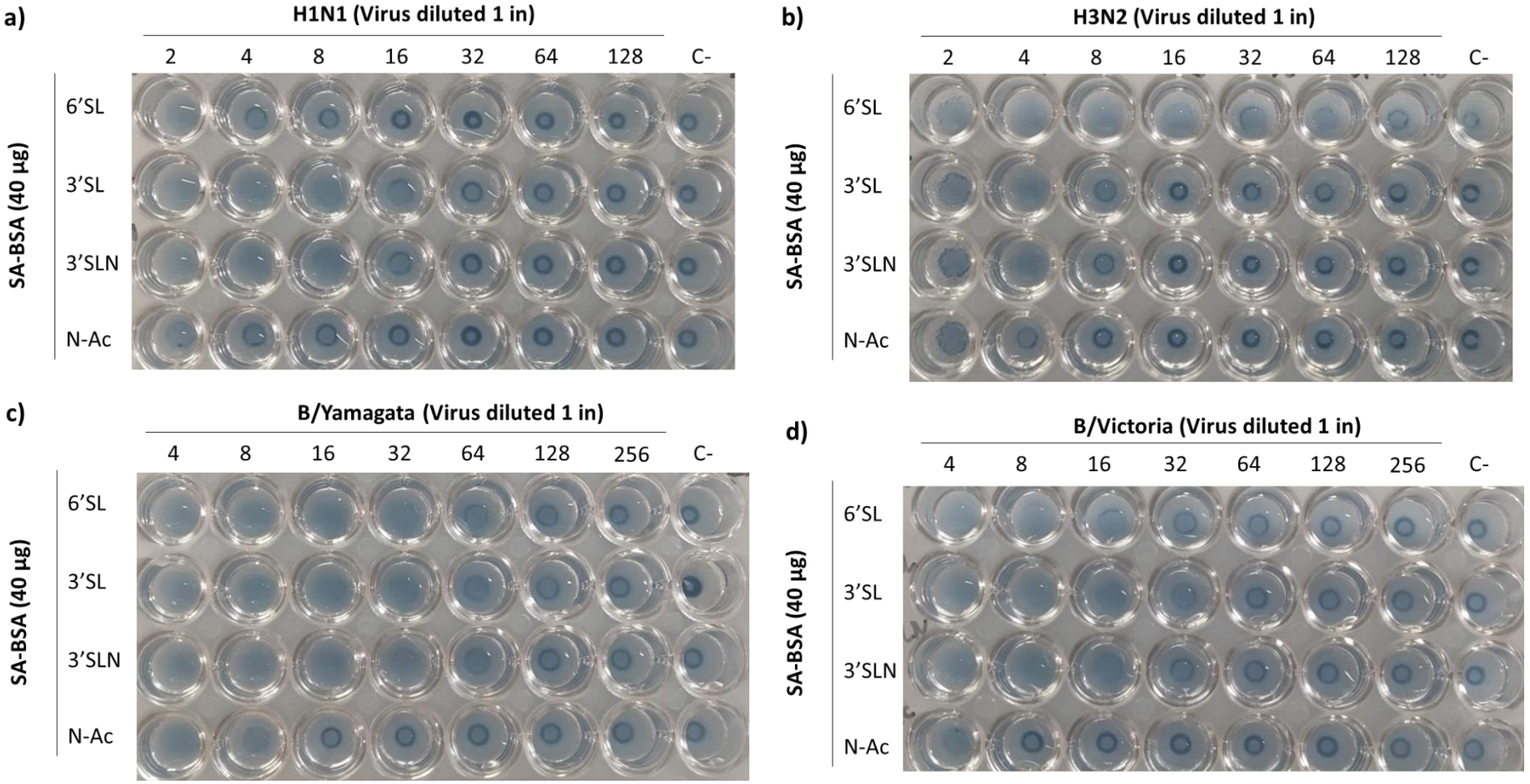

Figure 5.13 | SynA performed with 250 µg/well of custom-dyed beads conjugated with 6'SL-BSA, 3'SL-BSA, 3'SLN-BSA and N-Ac-BSA from top to bottom row in each experiment. The tested viruses were those provided in the WHO Influenza Surveillance Kit (2018-2019), detailed in Section 3.1.6. In the top images virus dilution started 1 in 2, while for Influenza B (bottom images) it started 1 in 4. Each virus had different binding affinities for each of the tested SA. N-Ac-BSA acted as a negative control.

A(H3N2) virus, on the contrary, exhibited higher agglutination titers when exposed to 6'SL-BSA beads and had almost no recognition of α2,3-linked SA. On the other side, influenza B viruses showed a similar recognition for all the SA-BSA tested. We also used N-Ac-BSA coupled beads to assess the level of non-specific interaction of the virus with the BSA and its linker to the SA. As can be seen in Figure 5.13, N-Ac-BSA-particles sedimented even at high concentrations of the WHO reference Ag, proving that the agglutination obtained in SA-BSA SynA assays was specific. Only B viruses exhibited non-specific interactions at the highest viral concentrations assessed (to a titer of 4).

These results indicated that using a single SA for bead coating would not grant binding of all influenza A viruses. Furthermore, as reported in the literature, A(H1N1) and A(H3N2) recognition required different SA. This is similar to what currently happens with RBCs, since erythrocytes from different species must be used in order to detect the different influenza viruses. Therefore, producing synthrocytes for simultaneous binding of A(H1N1), A(H3N2) and B influenza viruses demands for an equilibrium between α2,3- and α2,6-linked SA present on the surface. Accordingly, particles were next modified with batteries of receptors instead of individual ones.

5.6. Particle modification with batteries of influenza-binding receptors

At this point, the team dedicated to synthrocyte development grew. Therefore, it is worth mentioning that all the data shown in this section is the result of combined efforts between diverse group members to achieve a common objective: define the best combination of influenza receptors to detect the maximum number of virus types and subtypes.

5.6.1. Performance of GYPA/6'-SL-BSA-synthrocytes

We started this process using combinations of GYPA and 6'-SL-BSA receptors. We chose GYPA because, despite its higher cost, its performance in the recognition of some A(H1N1) viruses was better than with 3'-SL synthetic receptors. As shown in Chapter 4, GYPA-synthrocytes did not agglutinate in the presence of A(H3N2) virus. Therefore, 6'-SL-BSA was added to the particle coating in order to promote the simultaneous recognition of A(H3N2) and A(H1N1) viruses.

The protocol used for conjugation was the same previously employed (Chapter 3.6.1), but protein crossbinding was performed simultaneously with 6'SL-BSA and GYPA, mixed in different proportions. The battery of GYPA/6'-SL-synthrocytes obtained in this way was then evaluated by SynA in the presence or absence of A(H1N1), A(H3N2) and B/Yamagata virus dilutions. A summary of the results is presented in Table 5.1.

Table 5.1 | Summary of the GYPA/6'-SL-BSA combinations studied. Diverse ratios of 6'-SL:GYPA were used to produce synthrocytes, which were evaluated by SynA using A/Brisbane/02/2018 (H1N1), A/Kansas/14/2017 and B/Phuket/3073/2013 (Yamagata)

Receptor (µg/conjugation)		Molar ratio (6'-SL:GYPA)	Influenza virus titer		
6'-SL (µg)	GYPA (µg)		A(H1N1)	A(H3N2)	B/Yamagata
40	0	1:0	2	32-	128-
36	15	2.2:1	32-	32-	128-
34	22.5	1.4:1	32	32-	128-
32	30	1:1	32	16	128-
28	45	0.6:1	32	16-	128
0	150	0:1	64	8	128

All the combinations produced recognition of the 3 influenza viruses tested. In these experiments, GYPA-synthrocytes showed recognition of A(H3N2) virus down to a 1:8 dilution. This contrasts with the results obtained in Chapter 4, in which A(H3N2) virus was not bound by GYPA-synthrocytes. This was attributed to the use of custom-dyed particles here, which reduced the amount of beads required per well and enhanced sensitivity, as previously stated. The recognition of both A viruses was more dependent of the coating combination than that of B/Yamagata viruses, which remained almost unchanged for all the combinations tested. Furthermore, recognition of A(H1N1) and A(H3N2) viruses was inversely related to each other, meaning that when A(H1N1) titer increased (together with GYPA proportion in the mix), A(H3N2) titer diminished due to a reduction in the total 6'-SL content. As can be seen, best performance was achieved with 34 µg of 6'-SL and 22.5 µg of GYPA per conjugation, which equals a molar ratio of 1.4:1 (6'-SL:GYPA). With this combination, recognition of both A(H1N1) and A(H3N2) reached a titer of 32, while B/Yamagata arrived to a titer of 128. SynA results for the selected condition are shown in Figure 5.14a.

Then, SynAI was performed using GYPA/6'-SL-synthrocytes with WHO reference antisera and their corresponding B/Yamagata virus. As can be seen in Figure 5.14b, these synthrocytes showed considerable interference when employed in SynAI. The specific antisera produced inhibition up to a 640 titer, while the negative antisera reached a titer of 320, far exceeding the WHO recommendations for negative controls. These results are accordant with the ones obtained in the previous chapter (Section 4.7), which demonstrated that some serums cross-reacted against GYPA. This made impossible the use of these GYPA/6'-SL-synthrocytes in HAI-like SynAI assays. This synthrocyte version was thus abandoned.

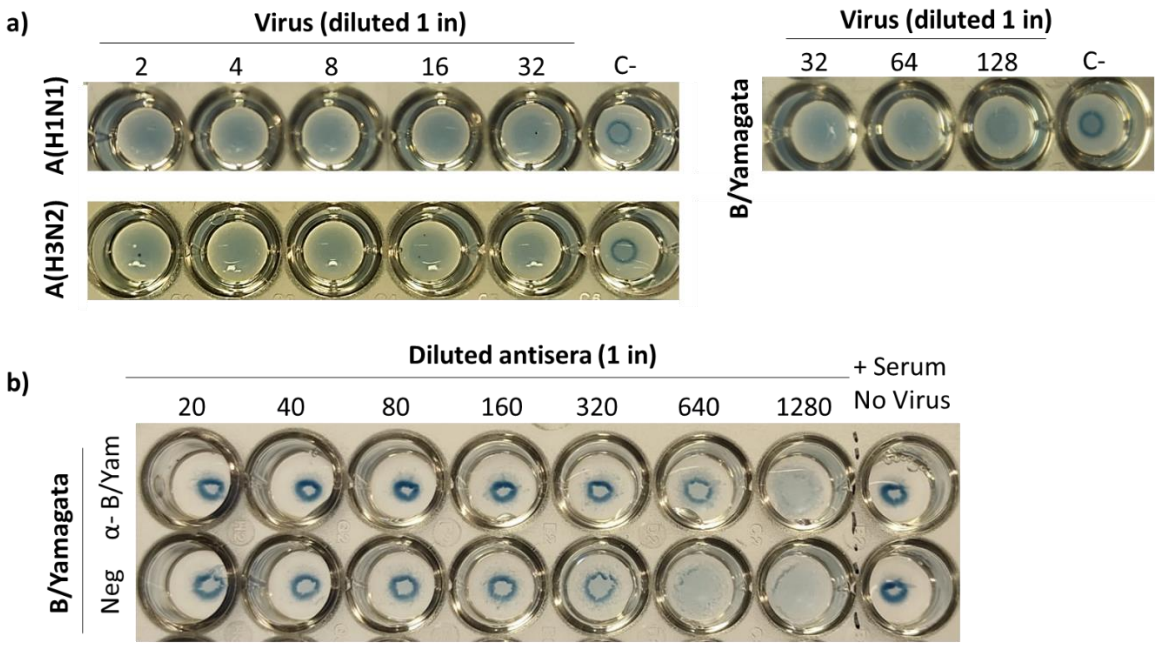

Figure 5.14 | Performance of GYPA/6'-SL-synthrocytes. **a)** Results of SynA performed with the best 6'-SL:GYPA combination (1.4:1 ratio) for each virus. **b)** SynAI performed with anti-B/Yamagata antiserum and negative antiserum with their corresponding B/Yamagata virus.

5.6.2. Evaluation of SA-BSA combinations

Although with GYPA/6'-SL-BSA-synthocytes we recognized A(H1N1) and A(H3N2) viruses simultaneously, in general sensitivity was lower than expected. Increasing the µg of receptors used during the conjugation step of the 10 µm particles did not improve the sensitivity, indicating that the surface of these particles was already saturated and unable to bind more protein. We decided to decrease beads size and use 3 µm beads to increase the total surface available (sizes studied in the range between 1 and 10 µm). Although these particles had been initially discarded due to their low reproducibility (Chapter 4.1), once they were custom-dyed and quality controlled by us, they gained enough robustness to proceed with the next experiments.

Moreover, we discarded GYPA as a potential receptor for synthrocytes due to its significant interference during the SynAI and its elevated cost, and instead focused on batteries of combinations of SA-BSA. Figure 5.15 shows a summary of the diverse combinations examined. Particles were conjugated as usual, with the incubation step performed with a mix of SA-BSA instead of just one of them. The total amount of SA-BSA used was kept constant in all the conditions (120 µg/conjugation). Then, SynA was carried out to evaluate synthrocyte performance. Previous results using GYPA/6'-SL-synthrocytes had showed that the recognition of A(H1N1) and A(H3N2) subtypes of viruses inversely correlated, meaning that higher A(H1N1) recognition leaded to lower A(H3N2) recognition and vice versa. In contrast, as Figure 5.13 already demonstrated, B viruses produced the same titer regardless the SA-BSA employed. Therefore, these SynA were evaluated using only A(H1N1) and A(H3N2) viruses.

As can be seen in Table 5.2, different SA-BSA combinations displayed different affinity for each virus. Binding of A(H3N2) viruses was heavily dependent on the 6'-SL-BSA content. In the absence of 6'-SL receptors, the tested A(H3N2) displayed null recognition of the synthrocytes. A(H1N1) viruses, on the contrary, relayed more in α2,3 links exposed on the surface, with slightly better recognition of 3'-SL than 3'-SLN for the virus tested. Combining the two types of receptors made possible to recognize both influenza A subtypes.

We enhanced assay sensitivity by using the 3-µm synthrocytes. Although it depended on the virus strain and the receptor combination attempted, generally we improved the recognition at least one titer when compared to 10-µm synthrocytes with the same surface composition. Furthermore, we reached a sensitivity even better than when using GYPA (specially for A(H3N2) viruses), but with a 7-fold reduction in the receptor cost.

SA-BSA (µg/conjugation)			Influenza virus titer	
6'-SL	3'-SL	3'-SLN	A(H1N1)	A(H3N2)
60	60		16	64/128
60		60	8	64/128
	60	60	32	0
40	40	40	32	64/128

Table 5.2 | Summary of SA-BSA combinations tested. Titer obtained by SynA for A/Brisbane/02/2018 (H1N1) and A/Kansas/14/2017 (H3N2) for each combination.

After optimizing the process, we determined that the best combination was using 40 µg of each SA-BSA per conjugation (6'-SL/3'-SL/3'-SLN-BSA-synthrocytes). Decreasing more the 6'-SL-BSA content produced a decay in the ability to recognize A(H3N2) viruses. On the other hand, using both 3'-SL- and 3'-SLN residues simultaneously allowed for a broader recognition of different influenza strains.

Influenza viruses were titrated using these mixed 6'-SL/3'-SL/3'-SLN-BSA-synthrocytes and with human RBCs in parallel. We tested different strains of A(H1N1) and A(H3N2) viruses that had been included over time in the WHO Influenza Surveillance kit, an also one strain of each influenza B lineage. Results obtained in these SynA tests are shown in Figure 5.15. As can be seen, these 3-µm SA-BSA-synthrocytes were able to recognize the 4 subtypes/lineages of currently circulating seasonal influenza viruses. In general, the overall sensitivity of the SA-BSA-synthrocytes was similar to that of the human RBCs, obtaining the same titer (or a 1-titer difference) for most of the tested viruses. A notable exception was the A/Tasmania/503/2020 (H3N2), for which the recognition was 3-titer better with synthrocytes than with RBCs.

On the other side, A/California/07/2009 NYMC X-179A (H1N1) showed null recognition of synthrocytes, but RBCs recognition was also lower than expected (reaching a titer of 4, while this should be around a titer of 128 according to the WHO specifications). A/California/07/2009 NYMC X-179A was the oldest A(H1N1) of the virus preparations tested, and previous bibliography highlighted a significant decrease in its stability compared to other A(H1N1)

strains, or even compared to other isolates derived from the same A/California/07/2009 original strain,[226] which could explain these results.

Finally, 6'-SL/3'-SL/3'-SLN-synthrocytes were used in a SynAI assay employing one A(H1N1), one A(H3N2) strain, one B/Yamagata virus and their corresponding antiserums. In all the cases, a negative reference antiserum was employed in parallel to monitor interferences. As can be seen in Figure 5.16, interferences considerably decreased compared to employing 10-µm GYPA-6'-SL-synthrocytes (Figure 5.14b). This improvement could be explained by diverse factors. First, the total amount of functional receptors available increased due to the larger curvature and total surface of the smaller particles, allowing more interactions between synthrocytes and virus particles (thus making their binding more stable). Second, although the µg of synthrocytes remained the same, the number of particles raised from $2.65x10^5$ to $1x10^7$ per well. This reduced the impact of nonspecific interactions because their inhibitor capacity (for example, by covering the particles and preventing them to interact with the virus) was distributed among more particles, diluting their effect.

Even then, nonspecific agglutination inhibition could still be observed in some of the SynAI tests. For example, the negative control serum diluted from 20 to 320 produced a faint sedimentation halo for 6'-SL/3'-SL/3'-SLN-synthrocytes in the presence of A(H1N1) virus, albeit it was easily distinguished from the specific inhibition produced by the anti-A(H1N1) serum. The same effect was noted in the A(H3N2) SynAI, although between 20 and 160 titers. Nevertheless, in all cases, when the inhibition was induced by the specific Ab of the corresponding antiserums, a tight sedimentation pattern was observed, similar to the one obtained in the control well in the absence of virus.

In the light of these results, we concluded that 3-µm 6'-SL/3'-SL/3'-SLN-synthrocytes displayed the best performance for SynA and SynAI assays. In SynA, these synthrocytes were recognized by the 4 main seasonal influenza viruses, and even by diverse viral strains in the case of A(H1N1) and A(H3N2) viruses. Furthermore, with these particles, the agglutination titer obtained generally was the same than with human RBCs (±1 titer).

Although SynAI performed with the WHO reference antiserums still exhibited some interferences, they were greatly reduced compared to the previous GYPA-6'-SL-synthrocytes. Moreover, all these results were achieved with incubations of 20-25 min (instead of the 5-10 min needed for 10 µm synthrocytes), which were comparable to the 30-min incubation required for avian RBCs and half the time required for mammalian RBCs.

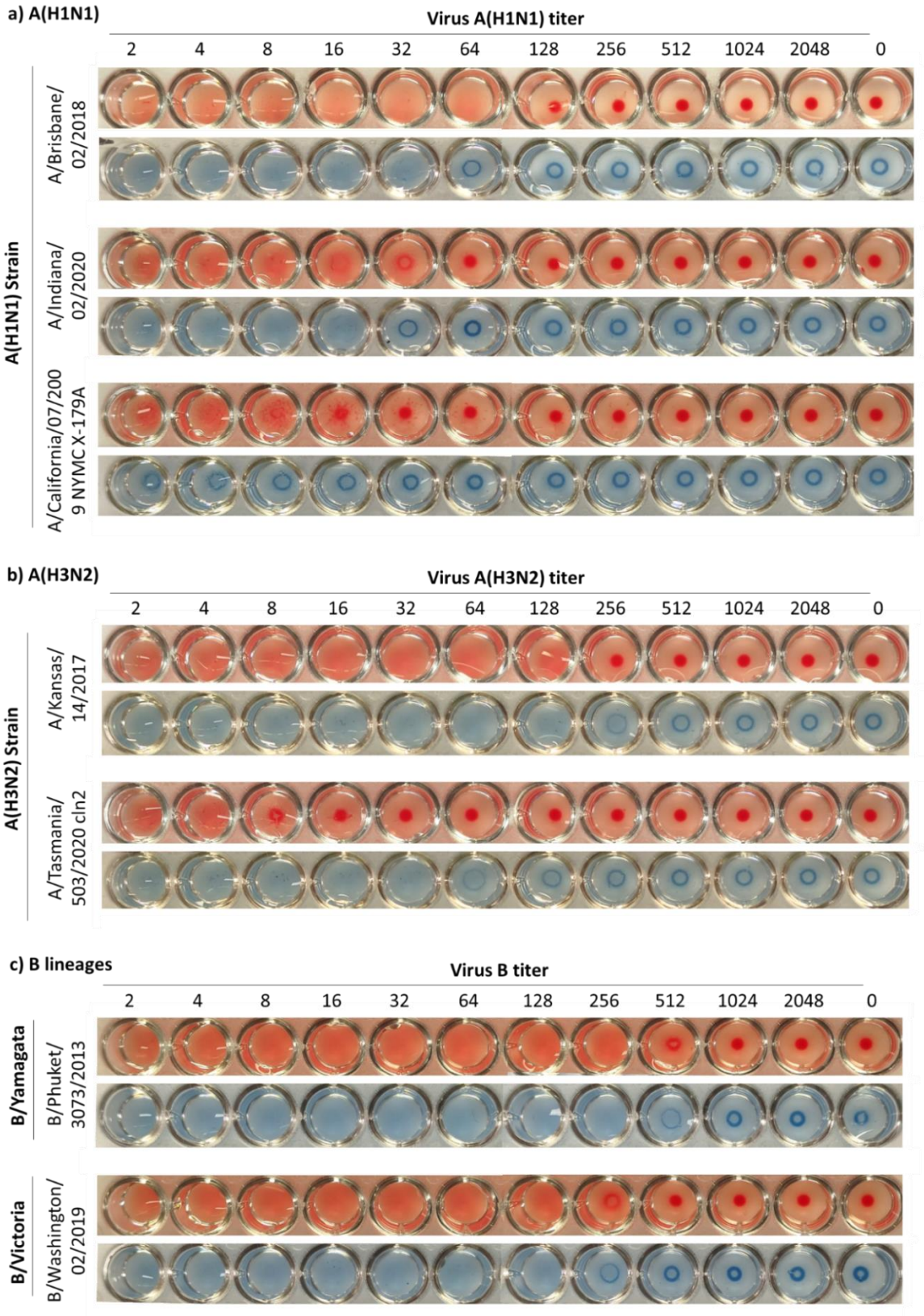

Figure 5.15 | Comparison of HA performed with 0.75% human RBCs and SynA carried with 250 µg/well of 6'-SL/3'-SL/3'-SLN-synthrocytes (3 µm) using different A(H1N1) and A(H3N2) strains, and one virus from each B lineage. All viruses were obtained from different WHO Surveillance Reagent Kits.

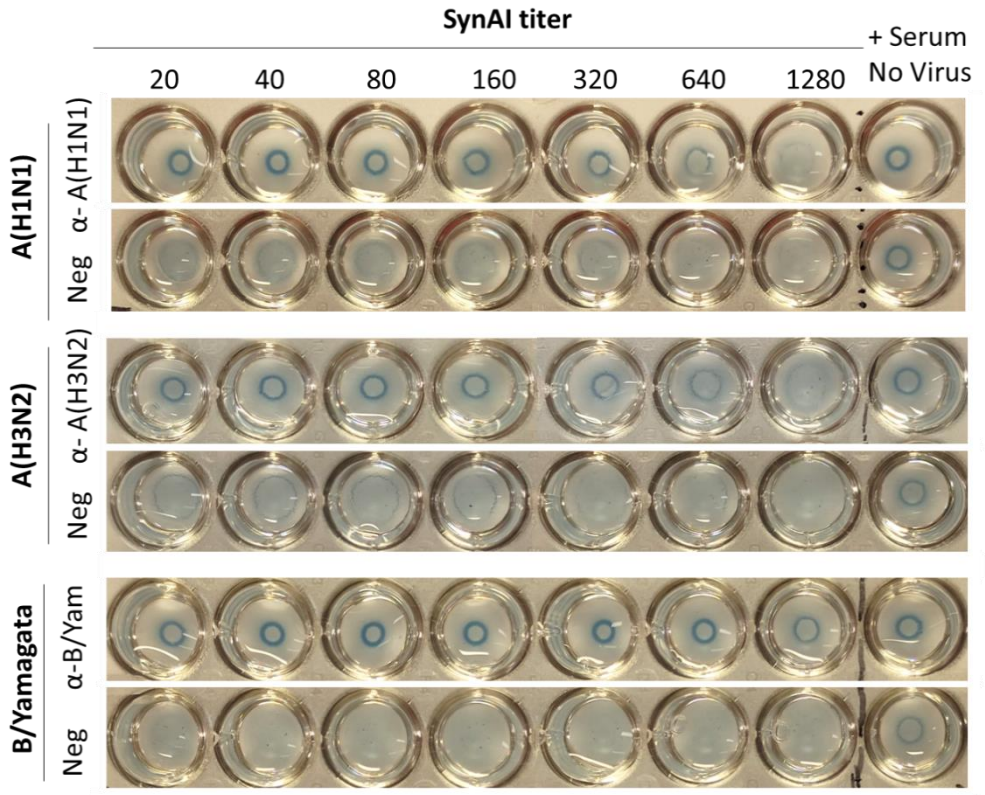

Figure 5.16 | SynAI performed using 250 µg/well of 6'-SL/3'-SL/3'-SLN-synthrocytes (3 µm) and A/Brisbane/02/2018 (H1N1), A/Kansas/14/2017 (H3N2) or B/Phuket/3073/2013 viruses and their corresponding antiserums (from WHO Influenza Surveillance Reagent Kit).

5.6.3. Performance of 6'-SL/3'SL/3'-SLN-synthrocytes with non-seasonal influenza viruses

We proved that the new combined 6'-SL/3'-SL/3'-SLN-synthrocytes recognized diverse A(H1N1), A(H3N2) and influenza B strains. The importance of these viruses lies in their routine circulation among people, being responsible for flu seasons each year. These subtypes and lineages of influenza virus are constantly monitored by the GISRS and constitute the 4 types of influenza viruses present in the quadrivalent flu vaccine. Nevertheless, other subtypes of influenza A viruses are also monitored to detect new emerging zoonotic viruses that could produce pandemics, with special attention to swine and avian influenza viruses.

Almost all the known subtypes of influenza A viruses can infect birds. Among them, H5, H7 and H9 subtypes of avian influenza viruses have caused the majority of the reported infections in humans. More specifically, some A(H5N1) and A(H7N9) viruses were considered highly pathogenic avian viruses responsible for more severe symptoms and higher mortality.[227]. In order to antigenically characterize them using HA and HAI, it is recommended to use mostly chicken RBCs, although turkey or guinea pig could also be useful in these assays. Horse RBCs are also suggested to identify human Ab against avian strains, because their content of α2,3-Gal linked residues is higher than the other types of RBCs.[114] Furthermore, previous results indicate that the titers obtained for human Ab using avian or guinea pig RBCs was not satisfactory.[112,228]

We explored if our synthrocytes would be useful for the surveillance of other influenza viruses than the current circulating human seasonal influenza viruses. We started by analyzing 3 different strains of A(H5N1) influenza virus, including one isolated from chicken (A/chicken/Vietnam/NCVD-016/2008). As can be seen in Figure 5.17, synthrocytes were able to recognize the three A(H5N1) virus studied. Two of them, A/Vietnam/1203/2004 and A/chicken/Vietnam/NCVD-016/2008, were recognized with a sensitivity comparable to human RBCs, but turkey RBCs were 2-3 titers more sensitive.

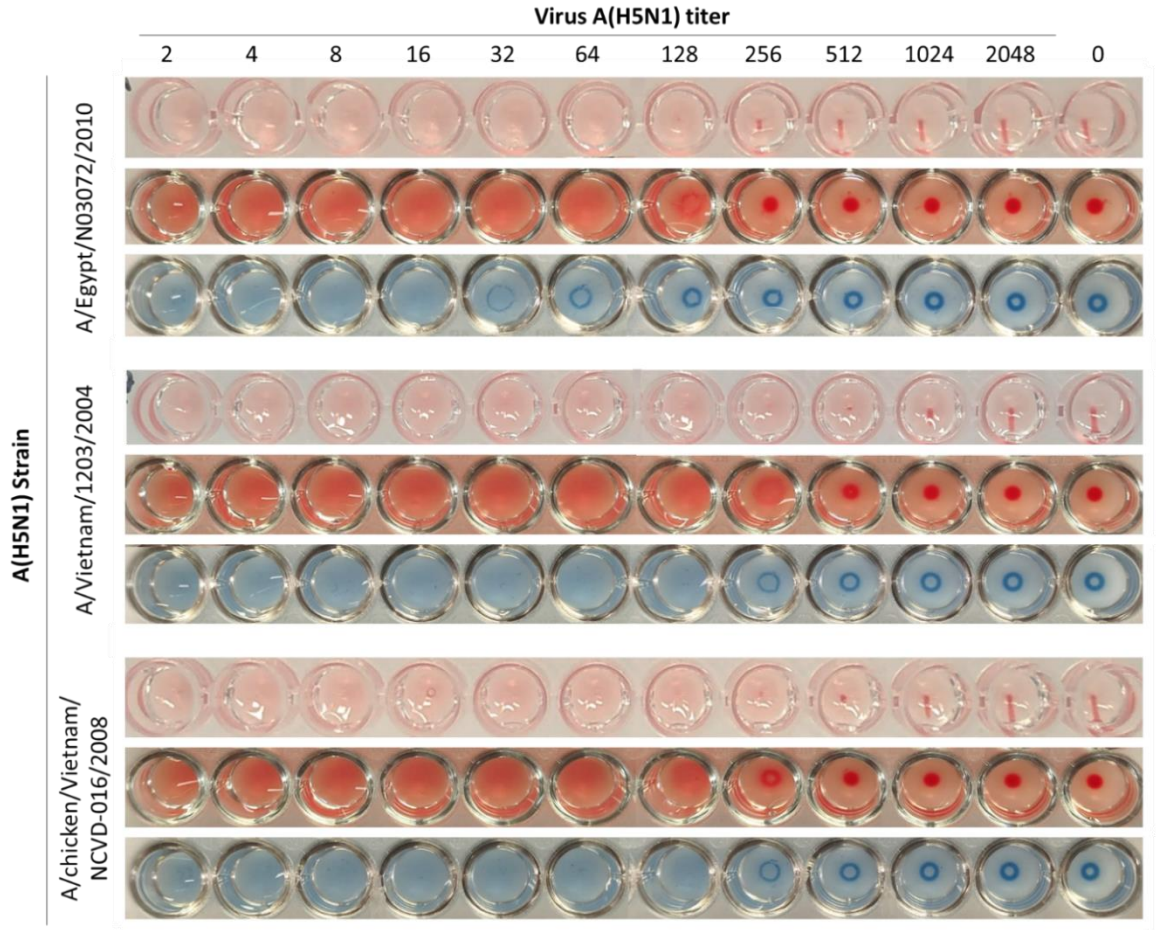

Figure 5.17 | HA and SynA performed with 3 different strains of A(H5N1). 0.5% of turkey RBCs (top), 0.75% of human RBCs (middle) or 6'-SL/3'-SL/3'-SLN-synthrocytes (bottom) were employed for the assays.

Next, a strain of A(H7N9) and another of A(H9N2) were also titrated using RBCs and 3-μm 6'-SL/3'-SL/3'-SLN-synthrocytes. These results are shown in Figure 5.18. A(H7N9) virus was recognized with synthrocytes with a titer 2-fold lower than any of the tested RBCs. A(H9N2), on the other side, presented a considerably lower titer when tested with RBCs, and was not correctly recognize by this version of synthrocytes.

Overall, the lower titers obtained for non-seasonal influenza viruses with synthrocytes compared to turkey RBCs could be explained by the proportions of α2,3- and α2,6-residues in the surface of the synthrocytes. Turkey RBCs express a mixture of α2,3- and α2,6-Gal linkages, with some studies yielding a ratio of 1:1 between them,[229] while others find their α2,6-

Gal content higher than α2,3-Gal.[114] Human RBCs also express both linkages in similar proportions. Most avian influenza viruses bind preferentially to α2,3- residues, and therefore we expected an increase in the recognition because the theoretical proportion of α2,3-Gal residues in synthrocytes should be higher, more similar to the composition of chicken RBCs. Unexpectedly, the titers obtained with synthrocytes were lower than in turkey RBCs. Although the total amount of 3'-SL and 3'-SLN-BSA employed in the conjugation of the synthrocytes was higher than that of 6'-SL-BSA, we did not know if the incorporation of the receptors to the surface maintained this proportion.

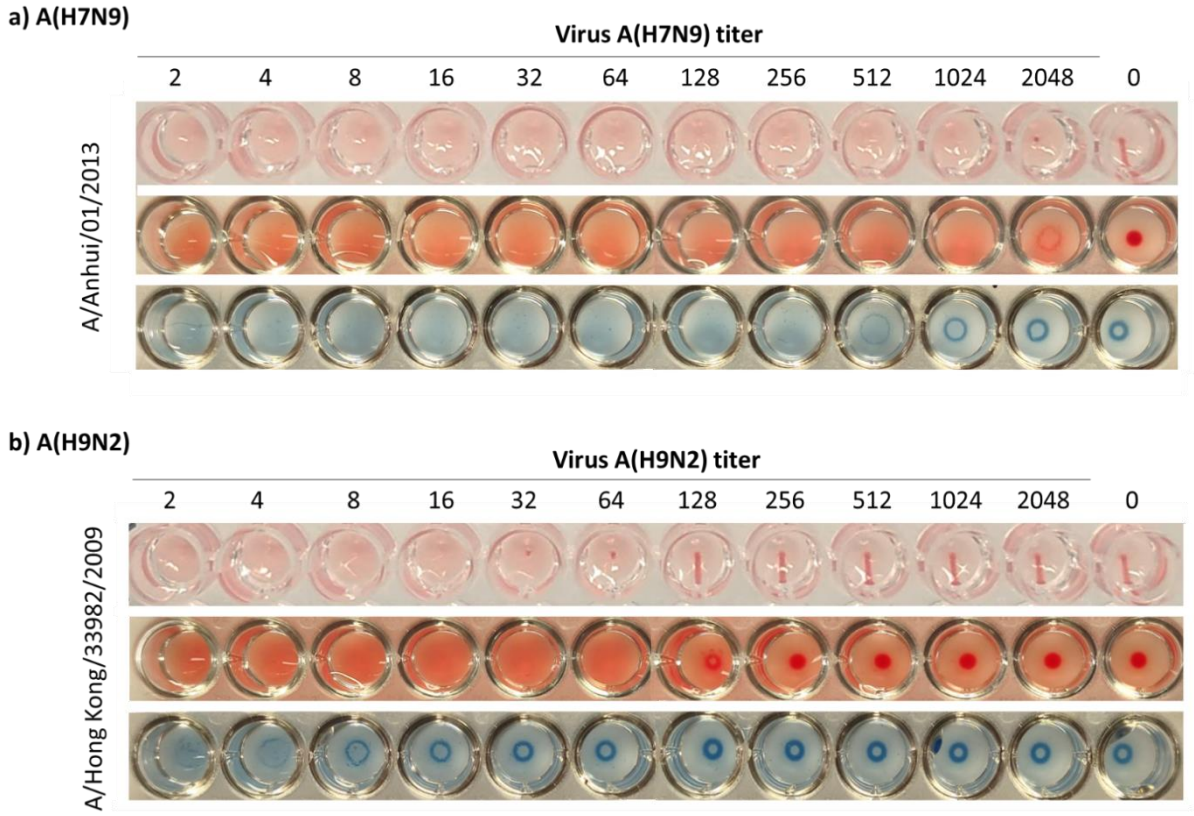

Figure 5.18 | HA and SynA performed with A(H7N9) and A(H9N2) virus. 0.5% of turkey RBCs (top), 0.75% of human RBCs (middle) or 250 μg/well of 6'-SL/3'-SL/3'-SLN-synthrocytes (bottom) were employed for the assays.

More analysis will be required to confirm that synthrocytes could be useful for surveillance of zoonotic influenza viruses. Sensitivity needs to be increased for this application, which may be achieved by increasing even more the proportion of 3'-SL/3'-SLN residues in the synthrocytes, due to avian virus preference for α2,3-linked SA. One option would be employing α2,3-only synthrocytes, mimicking the horse RBC usually used in HAI for avian viruses.[112,113]

Moreover, SynAI still needs to be performed to confirm its usefulness for antigenic characterization. Nevertheless, detecting 3 strains of A(H5N1) and one A(H7N9) tested are the first steps towards the development of synthrocytes potentially helpful for non-seasonal influenza surveillance.

5.7. Conclusions

The results in this chapter demonstrate that 3-µm synthrocytes coated with a combination of 6'-SL/3'-SL/3'-SLN-BSA bind diverse A(H1N1), A(H3N2) and influenza B strains. These viruses circulate constantly and are responsible for seasonal flu epidemics each year, therefore they are constantly monitored by GISRS. To help with it, these subtypes are the main antigenic components in the WHO Influenza Reagent Kit and are also present in the annual flu vaccine.

6'-SL/3'-SL/3'-SLN-synthrocytes displayed the best performance for SynA and SynAI assays, achieving an agglutination titer equal to the human RBCs (±1 titer) in just 20-25 min, compared to the 60 min incubation required for human RBCs. Although SynAI performed with the WHO reference antiserums still exhibited some interferences, they were greatly reduced compared to the previous GYPA-synthrocytes. Furthermore, when the inhibition was induced by the specific antiserums, a tight sedimentation pattern was observed, similar to the one obtained in the control well in the absence of virus.

These version of synthrocytes were also able to recognize some influenza viruses from zoonotic origin, such as A(H5N1) and A(H7N9), which are also monitored to detect new emerging zoonotic viruses that could produce pandemic. Although more experiments and specific optimization will need to be done before confirming their usefulness (including SynAI assays for non-seasonal viruses), this indicates a promising application for 6'-SL/3'-SL/3'-SLN-synthrocytes in pandemic prevention.

Chapter 6

Synthrocyte stabilization and production scaling up

Chapter 6. Synthrocyte stabilization and production scaling up

One of the main drawbacks of using biological reagents is their limited stability. Methods to extend the shelf-life of some bioreagents, such as Ab, are well known. For example, using stabilizer buffers, lyophilizing, or even drying the Ab directly in paper in the presence of certain sugars can extend their shelf-life to weeks or months.[230] Nevertheless, few of these strategies are applicable to whole cells, including erythrocytes.

RBCs have a lifespan of around 120 days in the bloodstream.[231] In the case of blood transfusion bags, this lifespan is shortened to 42 days maximum, albeit it is advised to consume the RBCs before 21 days. When RBCs age, they suffer different changes in their surface, apart from hemolysis and loss of their stiffness. One of these alterations is a decrease in the amount of SA exposed on the RBCs membrane, which can impact its morphology and surface charge, often leading to the generation of aggregates.[232,233] In fact, in older RBCs (>21 days), the load of SA is approximately 35% lower than in younger cells.[231] This effect is even greater in stored blood compared to circulating RBCs.

This characteristic is especially critical when using erythrocytes for influenza HA assays, because influenza viruses recognize specifically these SA. For this application, it is recommended to discard the RBCs just a week after the extraction to avoid hemolysis and RBCs changes that could lead to false results. In order to solve this, diverse strategies have been tested to increase the shelf-life of these cells. For example, once extracted, RBCs were treated with glutaraldehyde to fix them and preserve their structure. Unfortunately, erythrocytes treated with different concentrations of glutaraldehyde displayed slight differences in the titer obtained when HA was performed, which even differed depending on the RBCs species origin.[234] Moreover, it has been shown that when glutaraldehyde-treated erythrocytes were employed in HA assays for blood typing, the strength of agglutination was reduced when using RBCs treated with increasing concentrations of glutaraldehyde.[235]

An alternative approach entails lyophilizing the erythrocytes. Diverse attempts of performing RBCs lyophilization have been made, with limited success.[236,237] In all the cases, lyophilizing RBCs involved using complex mediums to minimize the damage of the cell membrane during the freezing-drying process and during rehydration. Some of these buffers included the use of high concentrations of polymers such as dextran-40 and polyvinylpyrrolidone,[238] sugars such as trehalose and glucose, antioxidants, proteins such as human serum albumin, or even viscous solvents such as DMSO.[236] Even when using all these protective agents, which must be washed away before performing further analysis, hemolysis was still a challenging setback and recovery of RBCs rarely surpassed 85%.

RBC instability is one of the main issues for HA standardization. Thus, one of the objectives of this Thesis work was producing a more stable synthetic alternative that could be mass-produced. It seemed clear that producing synthrocytes of longer shelf-life than RBCs would be a key point for synthrocytes to have any chance to replace RBCs. Along this Thesis we have shown different versions of synthrocytes, with coatings ranging from native proteins naturally containing SA to modified BSA coupled with synthetic SA. In this chapter, we will

analyze the stability of the different synthrocyte versions and the strategies tested to extend their shelf-life. Specifically, we will show the optimization of a lyophilization process that allowed extending synthrocyte stability to months, obtaining a ready-to-use product that was extremely easy to distribute, resuspend and handle. The last section includes also the first attempts to scale-up synthrocyte production, demonstrating that the bead staining and conjugation protocols developed for volumes of hundreds of microliters could be scaled-up to tens of milliliters. These characteristics would be essential to distribute the synthrocytes among the GISRS laboratories and across the globe, facilitating standardization of the methods used for influenza surveillance.

Although all lyophilizing-related experiments have been clustered in this chapter to facilitate their understanding, most of these results were obtained in parallel with the results of Chapter 4 and 5 and over a 12-month stage in the company BioSystems. This explains why lyophilization was not optimized directly with the final synthrocyte prototype and why this chapter refers to different synthrocyte versions.

This work has been possible thanks to the contribution of Biosystems R&D Team, which kindly provided the industrial lyophilizer, the materials needed to use it (vials, caps and reagents necessary for the process) and their know-how. The continuation of this collaboration has allowed extending this work, which is still in process.

6.1. Stability of synthrocyte suspensions and optimization of the storage buffer

Once synthrocytes had been successfully conjugated and recognition of influenza viruses had been assessed, we needed to test their stability. We started by studying the stability of synthrocytes in solution, when they had been resuspended in different storage solutions.

6.1.1. Stability of GYPA-synthrocytes in solution

The first version of synthrocytes, produced with GYPA-coated 10-µm particles, was initially evaluated. As a reminder, at that point particles were still not custom-dyed, and thus the sediments were lighter and it was required to use 375 µg of the conjugated particles per well.

SynA was performed after 2 weeks of synthrocyte storage at 4°C in different storage solutions, which included PBS supplemented with different concentrations of BSA with or without NaN_3. Results demonstrated that using BSA concentrations higher than 0.1% did not increase GYPA-Synthrocytes stability (Figure 6.1). Using NaN_3, on the contrary, increased the durability of Synthrocytes and even their performance. Both preserving agents combined produced the best results, granting detection of lower virus titers than the other storage solutions tested. Therefore, PBS-BSA(0.1%)-NaN_3(0.1%) was selected for long-term storing of synthrocytes.

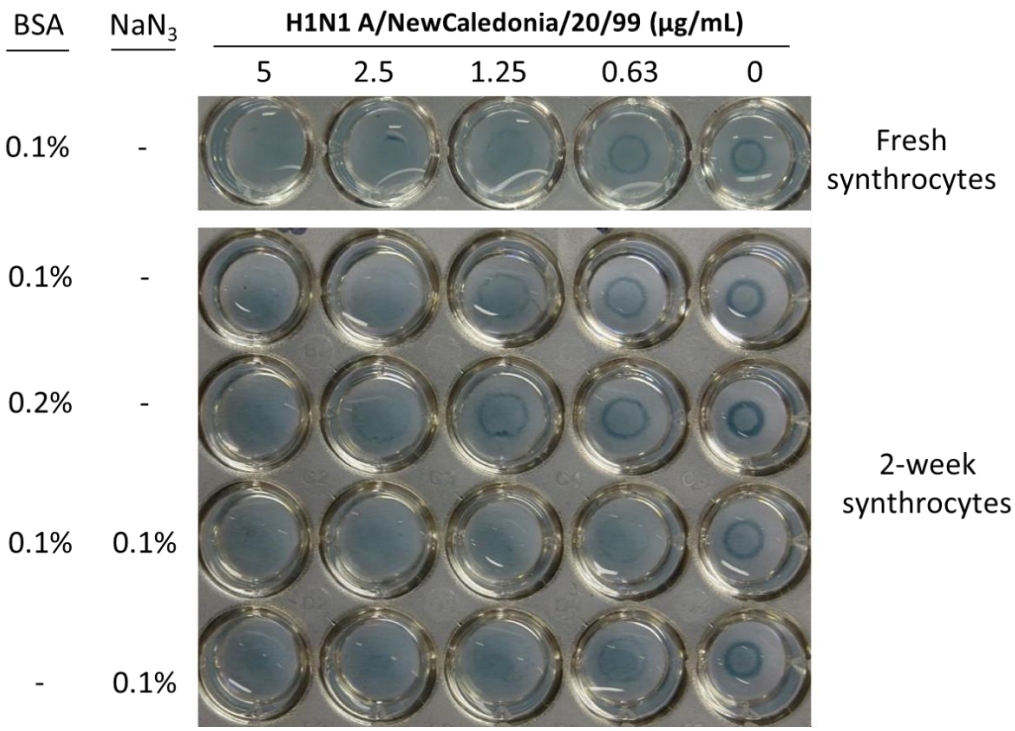

Figure 6.1 | SynA carried in parallel with GYPA-Synthrocytes of the same production batch, but that had been stored for 2 weeks at 4°C in PBS supplemented with different concentrations of BSA and NaN_3. Increasing the amount of BSA in the storage buffer decreased the sensitivity of the assay, which displayed a faint halo for 2.5 ug/mL of A(H1N1) virus. Adding NaN_3, on the other side, increased the sensitivity and stability of synthrocytes, reducing the lowest virus agglutinating concentration to at least 0.63 µg/mL.

Once determined the best storage buffer, synthrocyte stability was compared to that of RBCs. In order to do so, SynA was performed weekly using GYPA-Synthrocytes that had been produced following the usual protocol, but had been aliquoted and stored at 4°C in PBS-BSA(0.1%)-NaN_3(0.1%). Guinea pig erythrocytes were used as a reference, which were obtained commercially and stored at 4°C in the same solution they were received in. Results employing H1N1 A/New Caledonia/20/99 virus are shown in Figure 6.2.

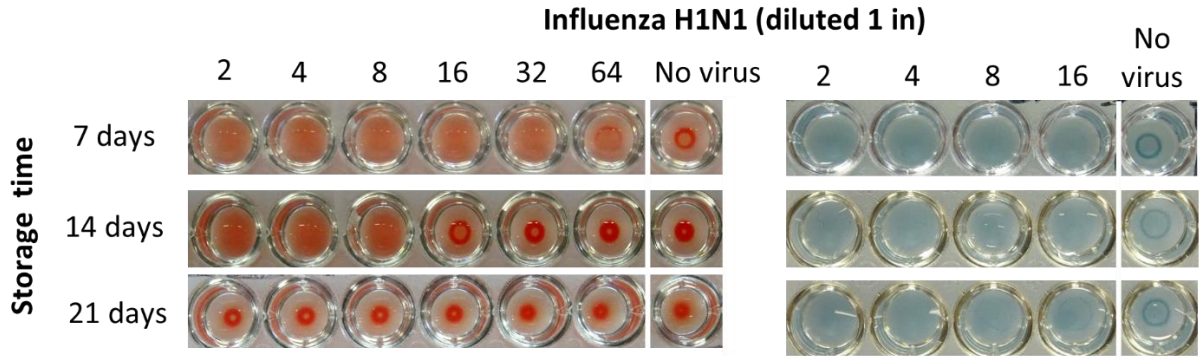

Figure 6.2 | Performance of guinea pig RBCs (left) and GYPA-synthrocytes (right) after storage at 4°C. RBC were stored in the buffer they were received in (Alsever's solution); GYPA-synthrocytes were stored in PBS-BSA(0.1%)-NaN_3(0.1%). Synthrocytes were more stable and could be used after 3 weeks of storage at 4°C, while erythrocytes had lost performance after 2 weeks at 4°C and did not recognize the virus 1 week later.

As can be seen, erythrocytes decreased their performance at least 8-fold each week, and after 3 weeks they did not recognize the virus at all. This was critical for erythrocytes acquired commercially. For example, the guinea pig RBCs displayed in Figure 6.2 were imported from the USA because no local supplier was found. For this reason, at least 7 days had passed between their extraction (including RBCs separation, washing and resuspension in Alsever's solution with preservatives) and their delivery to the laboratory, when we could perform the first HA. By then, they could not be used for longer than 2 weeks, which left a very small window period to perform HA. This correlates with the general recommendations of using RBCs for no more than 6-7 days to carry HA/HAI and demonstrated that, at least for this application, the 28-day shelf-life claimed by the supplier was overoptimistic. Moreover, due to the fast degradation of the RBCs, a HA had to be done daily prior to HAI to confirm the RBCs ability to agglutinate and readjust the amount of virus needed, and RBCs had to be washed before their use if they displayed signs of hemolysis.

GYPA-Synthrocytes, on the other hand, were initially less sensitive, but could be used after 3 weeks of storage and did not lose their performance at the same speed as RBCs. Only after 4 weeks of storage, GYPA-Synthrocytes started losing performance, which was attributed initially to the limited stability of GYPA itself. In addition, synthrocyte suspensions could be used straightforward, without needing centrifugation or washing steps.

6.1.2. Stability of 6'-SL-BSA-syntrocytes in solution

Although the results indicated that the shelf-life of GYPA-synthrocytes was superior to that of RBCs, it was still insufficient for a synthetic RBC mimetic. To solve this and other issues previously stated, a new generation of synthrocytes was developed, this time using synthetic SA-BSA as the virus binder (6'-SL-BSA-synthrocytes) as described in Chapter 5. The stability of these synthrocytes was evaluated and results can be seen in Figure 6.3.

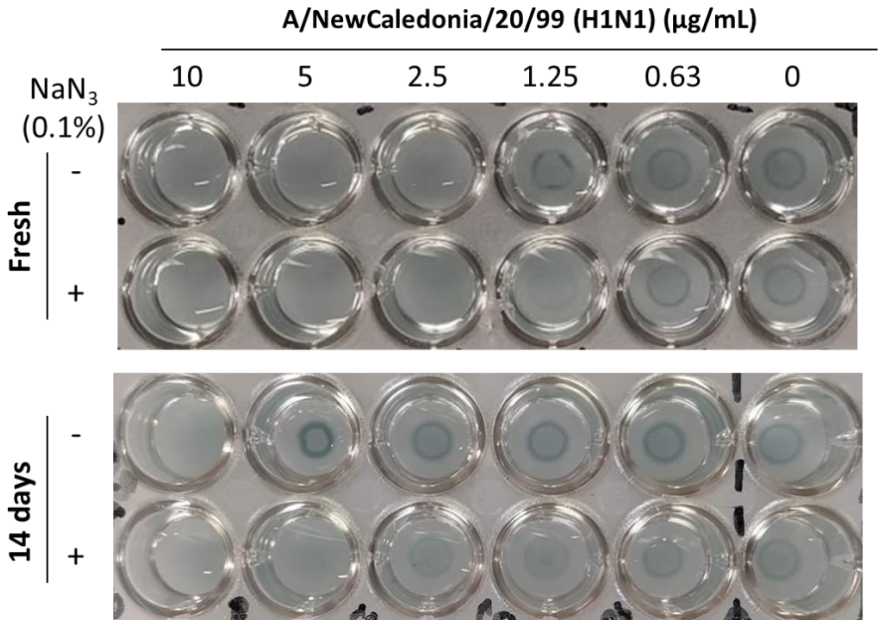

Figure 6.3 | 6'-SL-BSA-Synthrocytes performance in SynA after 14 days stored at 4°C in PBS-BSA(0.1%) with (+) or without (-) 0.1% of NaN_3.

As can be seen, while freshly produced 6'-SL-BSA-synthrocytes detected this A(H1N1) virus down to 1.25 µg/mL, the virus produced agglutination of 14-days old synthrocytes only at concentrations above 5 µg/mL. Hence, using 6'-SL-BSA on surface did not improve synthrocyte stability compared to GYPA coating. Although using NaN_3 improved the performance of 6'-SL-BSA-synthrocytes, they were less stable than GYPA-synthrocytes. These results were unexpected due to the highest stability described in the bibliography for SA, which could reportedly last up to 817 days at 25°C and pH 7.[239]

Our results could be produced by the detachment of the 6'-SL-BSA from the particles, by decomposition of the 6'-SL-BSA itself, or by a combination of both. Therefore, we decided to test the stability of the 6'-SL-BSA molecules in different storage buffers. In order to do it, we adsorbed a fixed amount of 6'SL-BSA (0.2 µg/well) in a 96-well plate, then blocked the wells with BSA(1%) and filled them with different storage buffers which included trehalose, mannitol and lactose, among others. After up to 2 months at 4°C, these wells were washed with PBS and were used in an ELISA to detect H1N1 A/New Caledonia/20/99 virus (5 µg/mL) as described in Chapter 3.3. Results are shown in Figure 6.4.

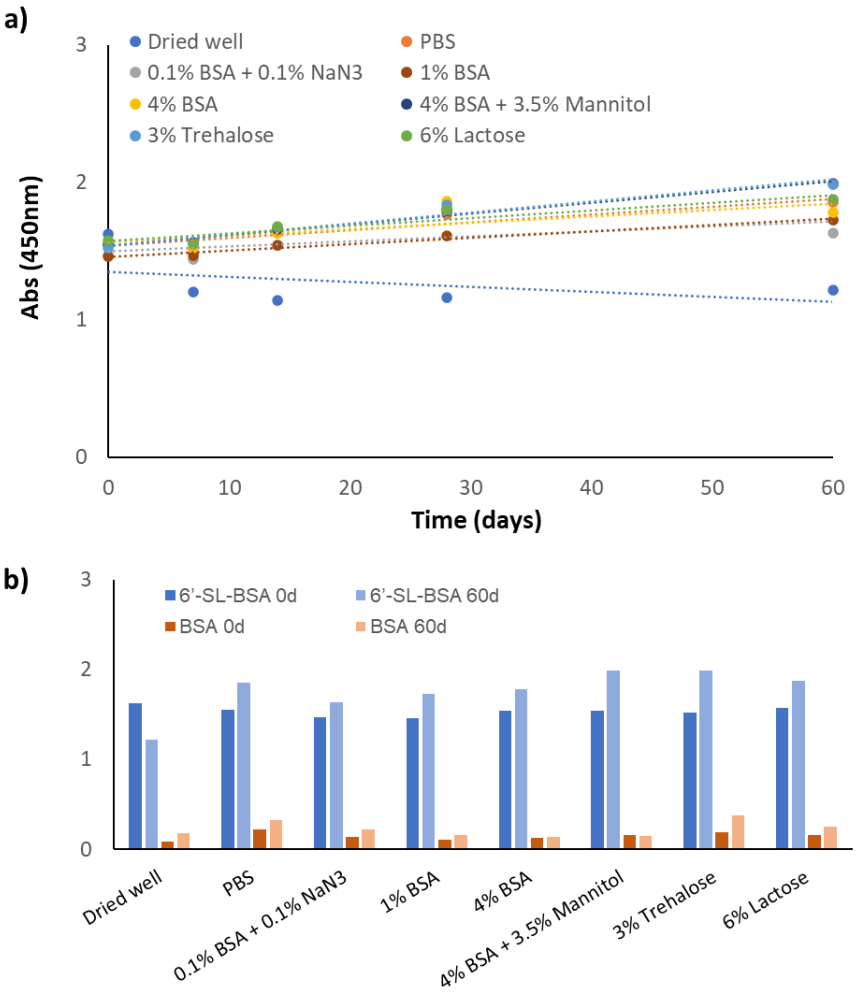

Figure 6.4 | a) Signals obtained by ELISA using 6'-SL-BSA for virus capture, immobilized on the well surface and stored for up to 2 months in different storage buffers. Wells were kept stored at 4°C in a humid chamber during all the process. **b)** Comparison of signals at the starting point (0d) and after 2 months at 4°C (60d), for the wells with or without 6'-SL-BSA (BSA, negative control).

As can be noted in Figure 6.4, the signals obtained by ELISA barely changed over storage time, confirming that the 6'-SL-BSA layer was stable. Furthermore, the virus attached to the wells coated with 6'-SL-BSA, but not to the negative control ones (without 6'-SL-BSA). This ensured that virus recognition was specific for 6'-SL-BSA and not due to SA-BSA detachment from the surface (which could allow the virus to adsorb directly to the well and produce false signals). These results suggest that the low stability of the 6'-SL-BSA-synthrocytes was not due to the SA-BSA itself, because the recognition by influenza virus persisted over the duration of the ELISA-based experiment. If the SA split from the 6'-SL-BSA adsorbed on the plate, and consequently was washed away in the first washes, we should have observed a decrease in the signals obtained, something that did not happen in this experiment.

Signals obtained showed little differences between storage buffers, but they were not significant and could be attributed to the variability of the assay. Results showed that storing the 6'-SL-BSA dried, without any buffer, reduced virus recognition. This impact could be explained because the drying of the wells was performed in just PBS, without any preserving agent, which could have impacted the viability of the SA-BSA.

Therefore, we concluded that the low stability of SA-BSA synthrocytes was not caused by the SA-BSA molecule itself, but probably by the conjugation to the NH_2-particles or by the stability of the particle coating after the process, a phenomenon that could not be controlled at that point of the development. Moreover, adding preservatives as the diverse sugars tested did not significantly improve the stability of the SA-BSA molecule.

6.2. Synthrocyte lyophilization for long-term storage

Even if synthrocyte suspension shelf-life was slightly extended using the storage buffer containing NaN_3 (one month for GYPA-synthrocytes or 2 weeks for SA-BSA-synthrocytes), the stability was far from optimal for a synthetic reagent conceived to be mass produced and worldwide distributed.

Ideally, the shelf-life of this reagent should be long enough to allow its shipment from the manufacturer facilities to the International Reagent Resource (IRR, the WHO distribution center in charge of the delivery of other official Influenza Surveillance Kit reagents), its distribution to the different GISRS laboratories, and its utilization to carry SynAI in each center. This means that synthrocytes should be stable for months to be accepted by end-users.

The results of Section 6.1. indicated that synthrocyte suspensions were not appropriate for distribution. Although it could increase synthrocyte stability, plain freezing was also discarded because it would have complicated the transport of the reagent, requiring -20°C containers and consequently increasing the shipping cost. Moreover, freeze-thaw cycles, which are frequent during shipping and handling processes, could negatively impact the stability of the reagent.

Therefore, we decided to evaluate lyophilization of synthrocytes as a strategy for long-term storage.

6.2.1. Short introduction to lyophilization

Lyophilization is a water removal process that generally involves 3 different stages: freezing, primary drying (sublimation) and secondary drying (adsorption).[240] A schematic depiction of the process is shown in Figure 6.5.

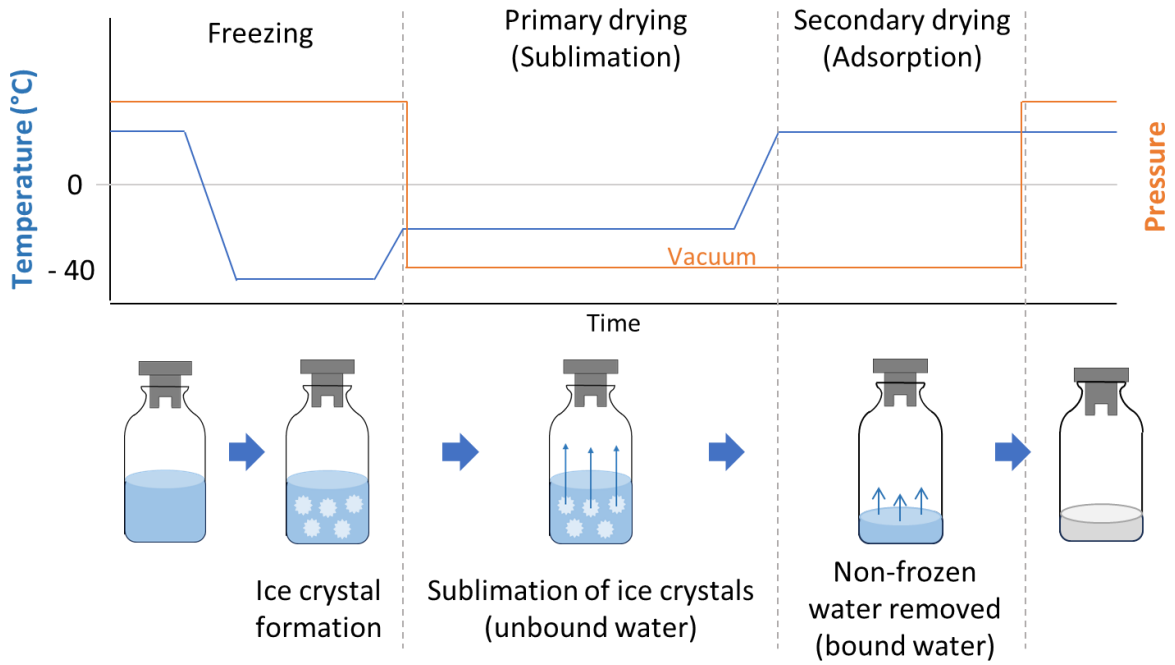

Figure 6.5 | Scheme of lyophilization process adapted from [240].The procedure consists of three different phases (freezing, primary drying and secondary drying), distinguishable by the different temperature and pressure applied in each of them. The combination of these phases allows for the removal of most of the water content in the lyophilized product.

During the freezing phase, the reagent is cooled down (usually to around -40°C) at atmospheric pressure until the water turns into ice crystals.

At the primary drying stage, the chamber pressure is reduced below the triple point of water, a combination of pressure and temperature at which water exists in all solid, liquid and gas states. Heat is then provided, which results in sublimation of the ice crystals present in the vials. This step requires the longest incubation of the lyophilization process. The temperature and time required to achieve this state must be optimized for each reagent and excipient formulation.

Finally, in the secondary drying step the temperature of the product is raised. The aim of this step is to remove any non-frozen water molecules that remain ionically-bound to the product. This allows reducing the final residual water content to an acceptable limit in the range of 1-4%. When the lyophilization process is complete, vacuum can be broken using an inert gas such as nitrogen before the material is sealed.

In order to successfully lyophilize synthrocytes, we needed to optimize their formulation (including amount of synthrocytes per flask, buffer composition, the excipients needed, and total volume) and the lyophilization “recipe”, which included the design of the temperature and

pressure cycles. The choice of the excipients added to the formulation can impact the thermal characteristics of the reagent and hence affect its ability to lyophilize. Therefore, depending on the excipients and the characteristics of the product itself, the requirements for the cycles could change substantially.

For this optimization, we based our excipient selection and cycle recipe in the established processes at Biosystems, with the aim to facilitate a future recipe transfer and to ensure that the use of industrial equipment was feasible. Part of this information, especially the diverse lyophilization recipes tested, are confidential and will not be disclosed here.

6.2.2. Optimization of the lyophilization excipients.

Lyophilization was optimized initially for 10-µm 6'SL-BSA-synthrocytes. Performance of the optimized lyophilization protocol was confirmed later on by lyophilizing 10-µm GYPA-synthrocytes and a smaller version of the 6'SL-BSA-synthrocytes produced with 3-µm particles.

For the first trials, we used in parallel equal volumes and concentrations of 4 types of excipients that are frequently used in lyophilization processes, which included BSA, lactose, saccharose, and trehalose. Because these experiments were done simultaneously to the development of the final synthrocyte version, the particles used to test lyophilization were the custom-dyed 10 µm SA-BSA coated ones, and unless otherwise stated, the 6'-SL-BSA-coated. Hence, 6.25 mg of 10-µm 6'-SL-BSA-synthrocytes were mixed with PBS supplemented with 40 g/L of the corresponding excipient up to a final volume of 0.5 mL and were lyophilized.

As can be seen in Figure 6.6, the dried sediment (named cake) obtained with each excipient (using the same recipe and initial reagent volume) differed considerably. In all the cases, two different layers could be observed. The bottom blue layer was common to all of them and tended to locate in the edges of the vial. This layer was formed by the 10 µm particles themselves, which sedimented to the bottom of the vial during the long lyophilization process, and thus separated from the liquid phase. The top layer was made mainly by the excipient and was clearly diverse between them. For example, BSA formed a thick compact white cake that could be detached from the vial walls. Saccharose and trehalose formed a small and irregular white cake, which was not large enough to cover all the bottom of the vial. Lactose, on the other side, formed a faint crystalline structure instead of the desirable cake. Changes on the employed recipe did not improve the formation of the lactose cake.

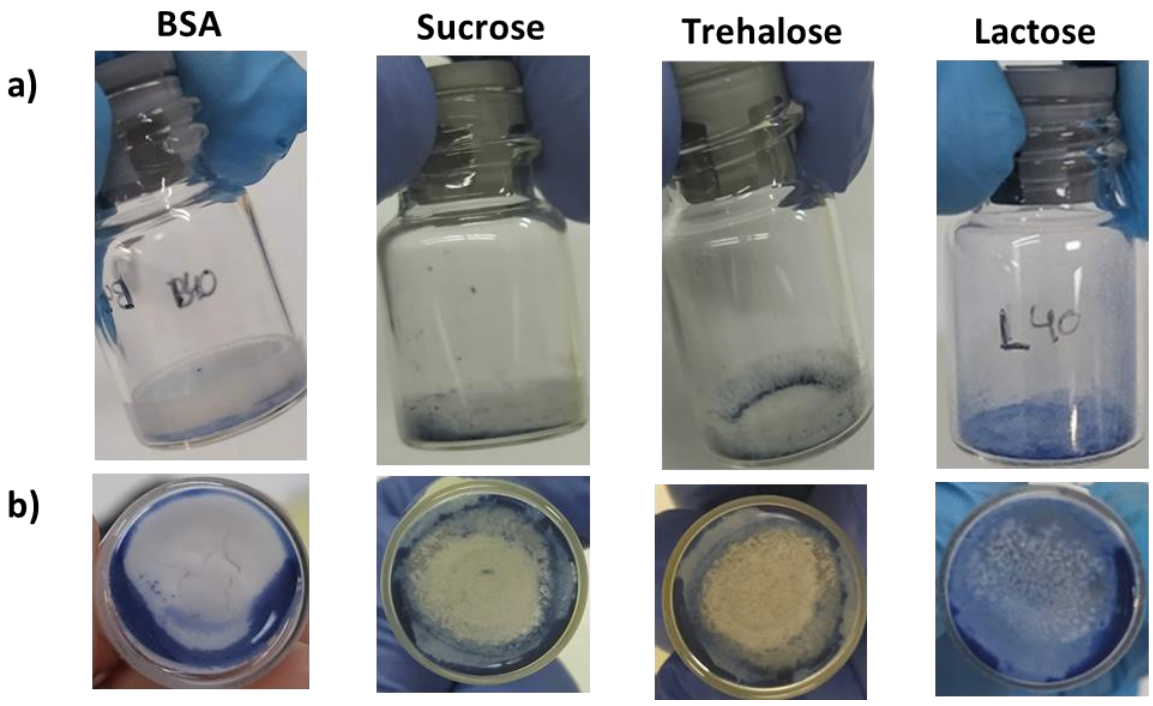

Figure 6.6 | Vials of 10-µm 6'-SL-BSA-synthrocytes lyophilized with different excipients. **(a)** Side or **(b)** bottom view of each vial. Two phases can be discerned, a white cake on the top (mainly excipient) and a blue layer on the bottom (the particles).

Although only BSA produced a compact cake, all the vials were reconstituted with 2 mL of PBS for 20 min in agitation and were homogenized by pipetting (final concentration of 7.2 g/L of excipient). After that, the sedimentation pattern of the particles was assessed, using the same number of beads per well considered optimal for the non-lyophilized 6'-SL-BSA-synthrocytes (250 µg/well). All the synthrocytes sedimented, except the ones containing lactose that were discarded (Figure 6.7a, right). The pellets obtained with the other excipients were tighter and more visible than those observed for freshly produced particles. This was especially evident for particles lyophilized with BSA, for which the halo-like pellet was substituted by a button similar to the pattern displayed by avian erythrocytes.

In view of these results, SynA was performed using B/Phuket/3073/2013 (Yamagata lineage) to evaluate its ability to agglutinate and alter the sedimentation of the different synthrocyte preparations. As can be seen in Figure 6.7a, the synthrocytes were able to recognize the virus even after lyophilization, albeit with less sensitivity than before the treatment. BSA was the excipient that better preserved the particles, although it reduced the SynA titer 3-fold and generated some non-specific sedimentation in some wells (e.g. at titer 16). Trehalose and saccharose reduced the SynA titer at least 4-fold.

Because the pellets formed after lyophilization were more defined than in freshly prepared synthrocytes, we decided to lower the amount of particles per well, which was expected to increase the sensitivity of SynA, as previously observed in Figure 6.7b for fresh synthrocytes. Diminishing the particles to 150 µg/well (a 40% reduction) improved the sensitivity of the assay. For saccharose and trehalose we obtained a SynA titer 2-times higher than before, but still one titer below that of fresh particles. On the other hand, the pellet produced in absence

of virus was fainter and more similar to the halo observed for fresh synthrocytes in the negative controls. For BSA-lyophilized synthrocytes the titer remained unchanged, but non-specific sedimentation was not observed and the pellets formed in absence of the virus were still more defined than those generated by synthrocytes lyophilized with the sugar excipients.

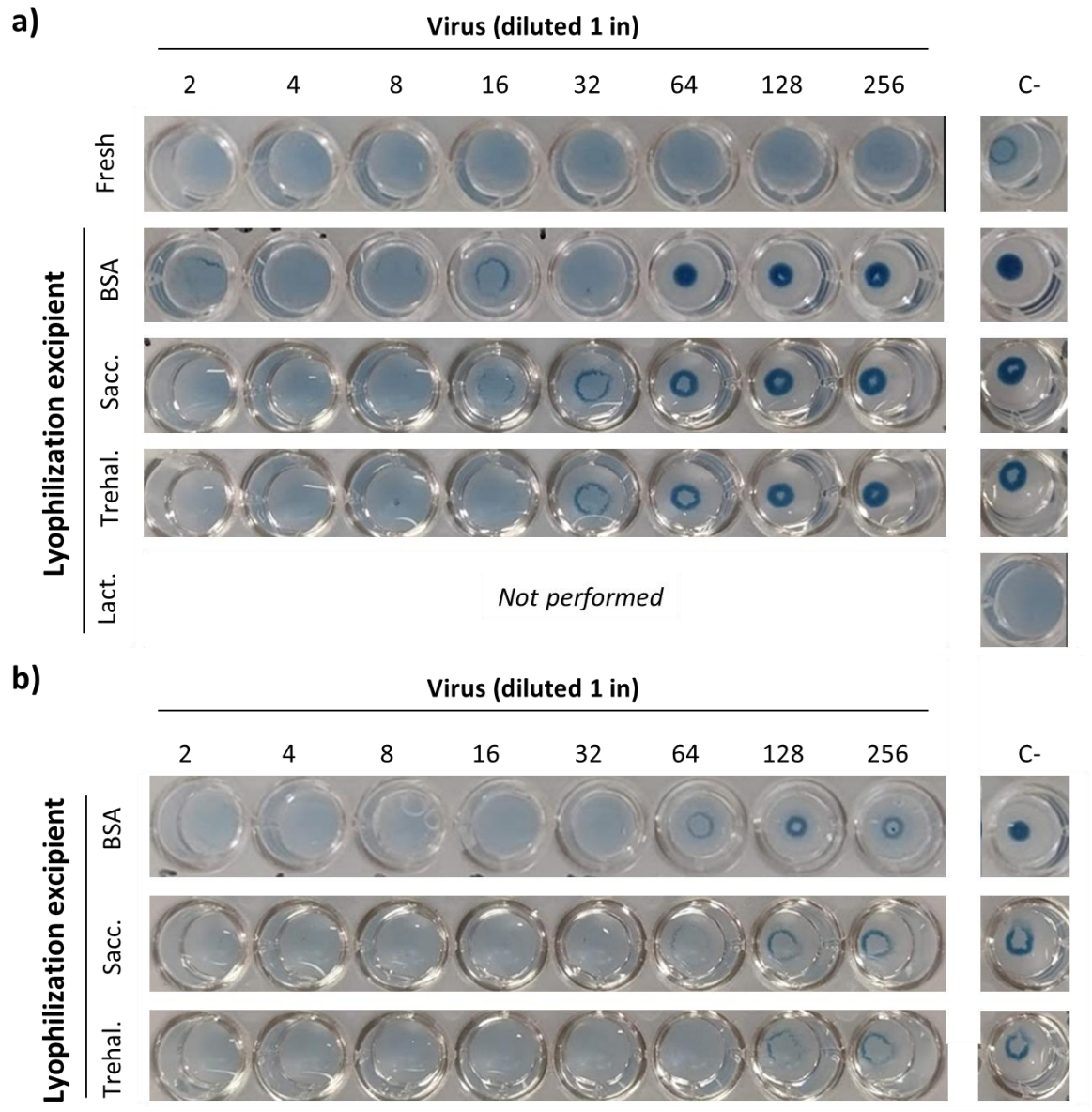

Figure 6.7 | SynA performed with 6'-SL-BSA-synthrocytes either freshly made (top row) or lyophilized using different excipients (40 g/L) in the absence (C-) or the presence of serial dilutions of influenza B/Phuket/3073/2013. Lyophilized synthrocytes were resuspended using PBS to a final concentration of 250 µg/well **(a)** or 150 µg/well **(b).**

As has been seen before, carrying SynA in a complex medium, such as serum, affected the sedimentation of the beads. This was the case for the lyophilized particles that, after reconstitution, where resuspended in a medium supplemented with a high concentration of the BSA or sugars used for the lyophilization. These molecules could shield the surface charges of the synthrocytes, promoting their sedimentation through a "snowball effect", where rolling particles pushed each other down the well bottom and produced a tighter pellet. As

shown in Figure 6.8, decreasing the BSA concentration used as lyophilization excipient increased the sensitivity of the SynA assay. Nevertheless, at concentrations of 10 g/L the pellet formed in the negative controls started to dim, likely due to a reduction of the "snowball effect". The agglutination titer obtained with 6'-SL-BSA-synthrocytes lyophilized with 15 g/L of BSA was comparable to the titers obtained using saccharides instead, but with the negative control pellets being more defined and reproducible. We decided to prioritize this reproducibility and 15 g/L of BSA was selected as the optimal excipient for lyophilization. Once particles were reconstituted, the final concentration of BSA in the synthrocytes "ready-to-use" was 2.7 g/L.

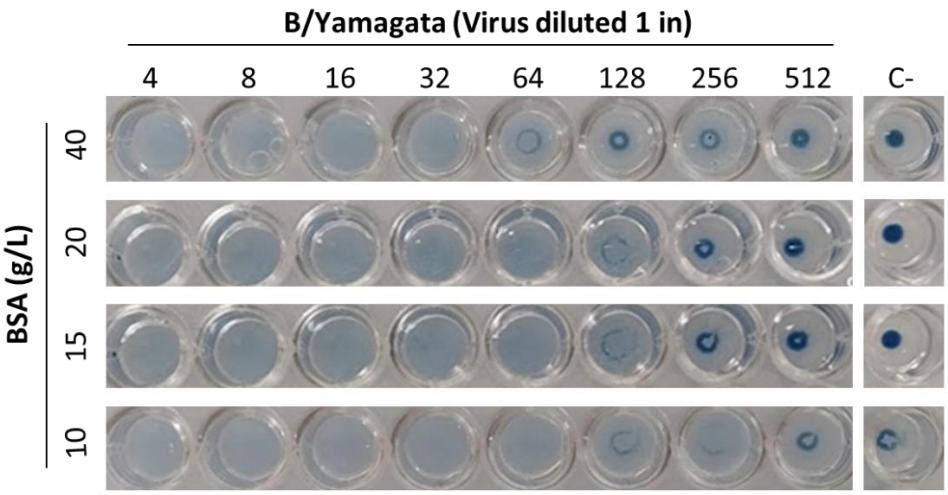

Figure 6.8 | Impact of BSA concentration used as lyophilization excipient in synthrocyte SynA performance. In all cases, 6.25 mg of 6'-SL-BSA-synthrocytes were lyophilized in 0.5 mL of PBS supplemented with 10-40 g/L of BSA. Upon reconstitution with 2 mL of PBS, the final BSA concentration was of 7.2, 3.6, 2.7 and 1.8 g/L, respectively. Synthrocyte concentration in SynA was 150 µg/well.

In order to confirm the robustness of the protocol defined for the lyophilization of the 10 µm, it was next employed to lyophilize a battery of synthrocytes. These were produced using alternatively different receptors (GYPA, 6'-SL-BSA, or mixtures of both), which were conjugated to particles of either 10 or 3 µm of diameter. Lyophilization was carried using always 15 g/L of BSA as an excipient at a fixed volume. All the synthrocytes were lyophilized successfully and all of them recovered SynA performance upon reconstitution with PBS. Figure 6.9a shows the results obtained for the 3-µm 6'SL-BSA-synthrocytes. After lyophilization, these smaller synthrocytes formed a cake very similar to that obtained for 10 µm particles, which also contained two distinguishable phases. The blue phase stayed more distributed around the vial base compared to the 10 µm particles. Once reconstituted, the color of the solution was darker than with the bigger particles, a phenomenon that was consistent with the more intense blue color of the particles before lyophilization. When 3 µm synthrocytes were tested in a SynA assay, they were more sensitive (SynA titer of 64 compared to 32 for 10 µm synthrocytes). Furthermore, the amount of particles could also be reduced by 40% to 150 µg/well, increasing the SynA titer obtained to 128-256 depending on the production batch (compared to 64 for 10 µm beads), although the pellet became wider in the negative control wells (Figure 6.9b).

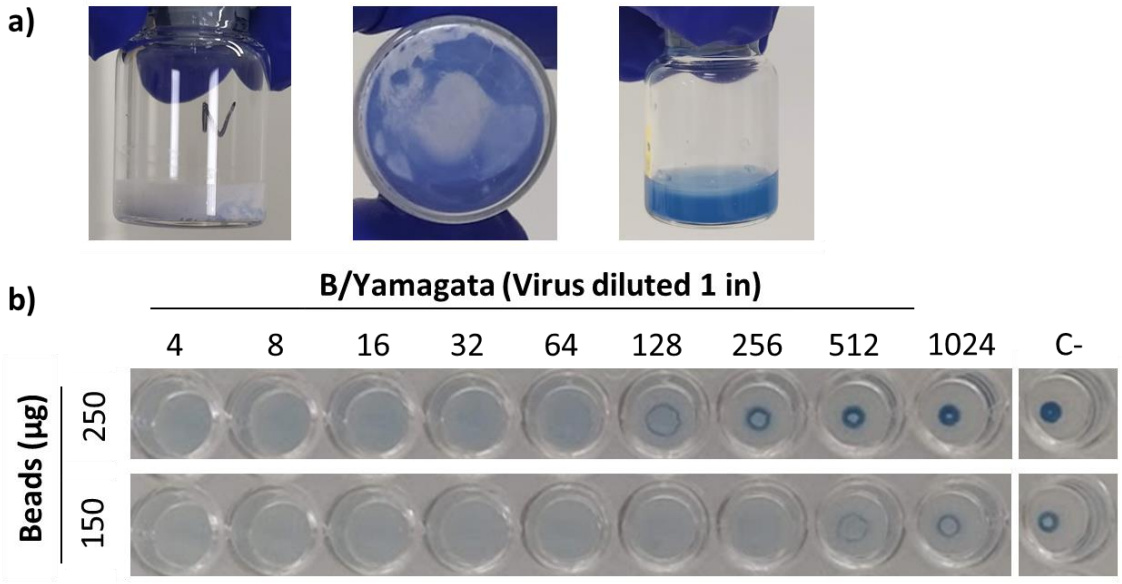

Figure 6.9 | Behavior of lyophilized 3 µm 6-SL'-BSA-synthrocytes before and after reconstitution. **a)** From left to right, vial after lyophilization (side and bottom view) and subsequent resuspension. **b)** SynA performed using B/Phuket/3073/2013 as a model for B/Yamagata, with two different amounts of synthrocytes per well (250 and 150 µg/well).

These results confirmed that synthrocytes could be lyophilized and that after reconstitution they retained the ability to bind influenza virus and be used in SynA assays. Nevertheless, the SynA titers observed for lyophilized synthrocytes worsened between 1 and 3 titers compared to freshly produced particles.

6.2.3. Optimization of synthrocyte dosification

One of the objectives of developing synthrocytes was to provide users a method as similar as possible to classical HA using animal RBCs. Therefore, to carry SynA, 50 µL of resuspended synthrocytes should be added to each well (which corresponded to 150 µg of solid synthrocytes per well), to be mixed with 50 µL of virus-containing sample. In this way, around 5 mL of the ready-to-use synthrocytes were needed to carry SynA in a whole plate (plus some reagent excess to ease the handling), which was equivalent to approximately 15 mg of particles. To this point, all the lyophilization tests had been performed using 6.25 mg of synthrocytes per vial in a volume of 0.5 mL, which entailed a 1:3 proportion between the volumes of particles and excipient. It was thus decided to increase the amount of particles per vial, in order to produce lyophilized units with enough synthrocytes for one full 96-well plate.

To achieve the required increment, we explored two different strategies: to increase the final pre-lyophilization volume (from 0.5 mL to ~1.2 mL, keeping the concentration of particles constant) or to increase just the ratio of particles to excipient volume (from 1:3 to 1:1, maintaining the pre-lyophilization volume constant). These two different approaches could impact the lyophilization process in a different way. Changing the lyophilization volume often requires re-optimization of the recipe, usually expanding the time of the cycles. Modifying the

ratio, on the other hand, could impact the ability to form a cake and the stability of the particles afterwards.

Results showed that the best option was to increase the pre-lyophilization volume, which did not impact the sensitivity of the SynA assay (Figure 6.10). Furthermore, this option opens the door to increase in future the size of the vials further. This would be crucial to produce vials large enough to contain enough synthrocytes to carry SynA in more than one plate, easing distribution, storage, and waste management. Increasing the ratio, on the other side, affected the sedimentation of the particles to the point where the negative controls were not well defined. Moreover, the reproducibility between vials for this condition was not satisfactory.

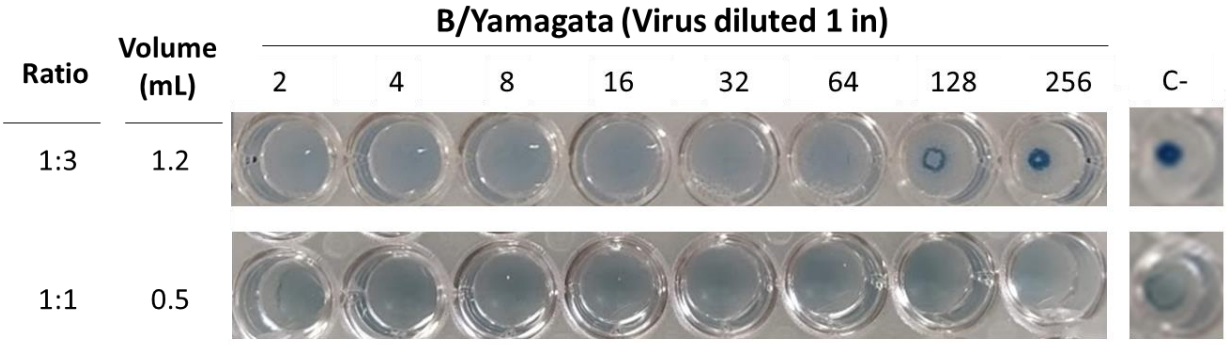

Figure 6.10 | SynA performed with 6'-SL-BSA-synthrocytes lyophilized through two different strategies to increase the amount of particles in each vial (from 6.25 mg to 15 mg). In this experiment, volume refers to the volume buffer (PBS supplemented with 15 g/L of BSA) pre-lyophilization. On top, particles lyophilized doubling the volume of particles and lyophilization buffer, maintaining a particle:excipient v:v ratio of 1:3. At the bottom, particles lyophilized by increasing the particle:excipient v:v ratio to 1:1 (i.e., doubling the amount of particles but keeping constant the volume of the BSA excipient).

6.2.4. Stress and stability studies of lyophilized synthrocytes

After determining the optimal concentration, ratio and recipe for synthrocyte lyophilization, lyophilized vials were subjected to an accelerated stability test through thermal stress in order to evaluate their stability. Accelerated aging is based in the fact that reactions occur faster at higher temperatures. Accordingly, exposing a reagent for short periods of time to relatively high temperature, at which it is still stable, allows simulating how the reagent will behave at lower temperatures over a longer time.[241] These experiments allow to explore, for example, the viability of a reagent during the transport process, compare alternative formulations and packaging, and predict its shelf-life.

In order to do so, we maintained the lyophilized vials of 10 µm 6'-SL-BSA-synthrocytes at either 45°C (stressed) or 4°C (control) for 5 days. After this time, stressed and control synthrocytes were reconstituted and used in a SynA test with B/Yamagata as a model virus. Two concentrations of BSA were analyzed, 40 and 15 g/L. As can be seen in Figure 6.11a, the thermal treatment did not significantly impact synthrocyte ability to recognize the virus and agglutinate. Although the sedimented pellet became more irregular and broader for stressed particles, it was still possible to differentiate clearly between positive and negative wells.

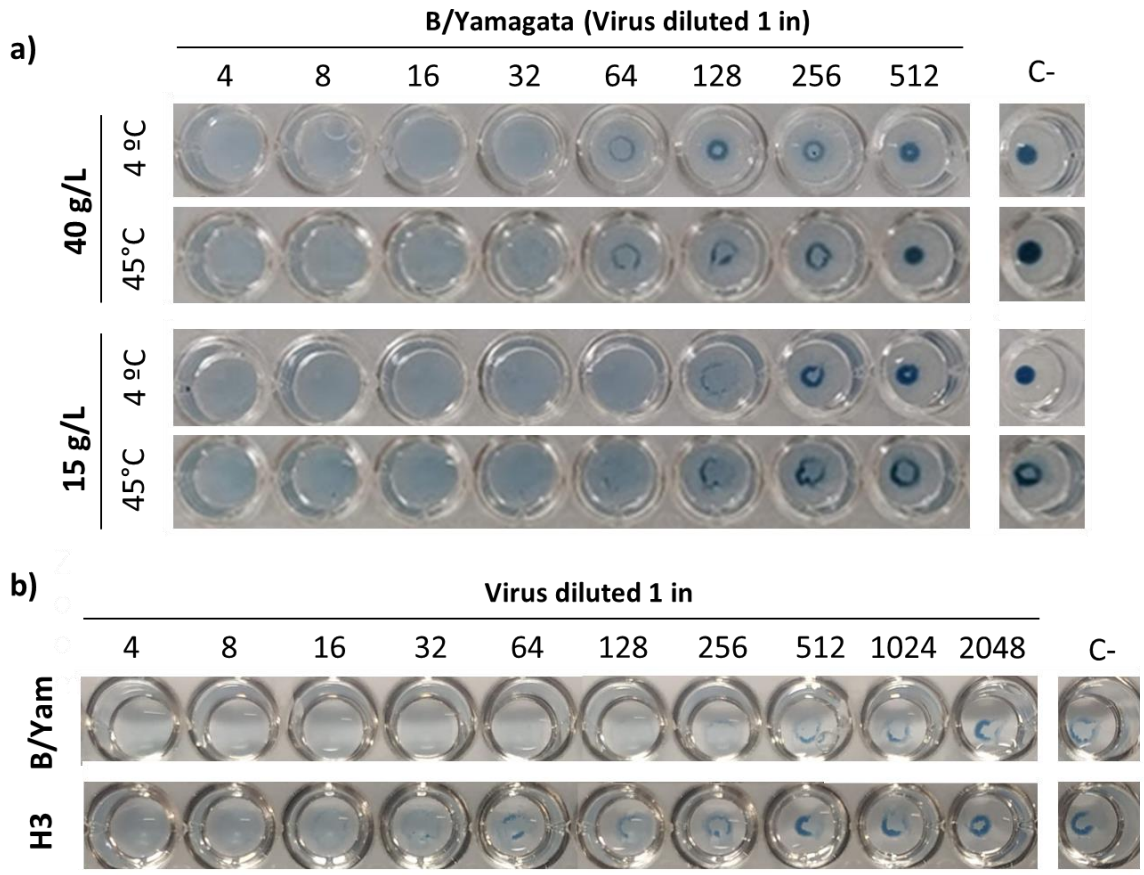

Figure 6.11 | a) Effect of thermal stress in the performance of lyophilized 10 µm 6'-SL-BSA-synthrocytes in SynA. The different vials were prepared from the same stock of synthrocytes, lyophilized simultaneously, and then stressed (45°C) or stored at 4°C for 5 days. **b)** SynA performed for B/Phuket/3073/2013 and A/Kansas/14/2017 using 10 µm 6'-SL-BSA-synthrocytes lyophilized and stored at 4°C for 9 months. It should be pointed out that the vials employed in this assay were remnants of the ones prepared for Chapter 7, and therefore they had been transported without temperature control multiple times, which could negatively impact the stability.

Lyophilized synthrocytes are intended to be stored at 4°C, like the rest of the WHO Surveillance Kit Reagents. It is worth noting that aging for 5 days at 45°C is equivalent to aging for 90 days at 4°C or 20 days at 24°C (calculated with a standard Q10 value of 2.0). Therefore, we confirmed that lyophilized synthrocytes were stable for at least 3 months at 4°C after lyophilization and could withstand relatively high temperatures, which suggests that they could be transported at room temperature without special temperature conditions. A real-time stability experiment was next performed by maintaining the lyophilized vials for 9 months of storage at 4°C. Results showed that synthrocytes were able to recognize the virus for at least this period, although the pellets in the negative controls were more similar to the stressed ones, and even fainter (Figure 6.11b). Although these results seemed promising (increasing the shelf-life at least 39-fold compared to RBCs), better pellet formation should be achieved after synthrocyte lyophilization and reconstitution. Thus, future work should include testing alternative methods of storage of the lyophilized vials (such as freezing) and assessing the stability of the final versions of synthrocytes over time.

The accelerating aging test (5 days at 45°C) was carried also for 3 µm 6'-SL-BSA-synthrocytes. As can be seen in Figure 6.12a, the pellet formed in the absence of virus was also wider and less tight in stressed than in control 3 µm 6'-SL-BSA-synthrocytes, but it was clearly distinguishable from agglutinated wells. Unexpectedly, SynA sensitivity seemed to improve after synthrocyte aging. This could be explained because, as seen previously for 10 µm synthrocytes, the pellet became fainter for particles exposed to the thermal stress.

Finally, because the product had to be reconstituted before being used in SynA or SynAI assays, we also analyzed its stability once reconstituted with PBS (i.e., in solution). Moreover, the final BSA concentration in the reconstituted buffer was higher than the one used in the storage buffer used for freshly made particles (0.02% of BSA, equivalent to 0.2 g/L) and thus we needed to assess the impact of this BSA excess in the storage of such reconstituted synthrocytes. For this, the lyophilized 3 µm 6'-SL-BSA-synthrocytes were reconstituted and stored at 4°C to study their evolution for a month. As can be seen in Figure 6.12b, particles were not stable after 2 weeks. They produced inconsistent patterns, which could be caused by bacterial contamination. We repeated the same experiment after supplementing the lyophilization buffer with NaN_3, which did not affect the performance of fresh 3 µm synthrocytes, nor affected the formation of a proper cake after lyophilization with BSA. Figure 6.12c shows how with NaN_3, reconstituted synthrocytes were stable for at least 4 weeks without losing much of their functionality.

Currently, the NIC laboratories employ fresh RBCs over a full week. Therefore, reconstituted synthrocytes displayed stability 3 times longer. This suggested that producing larger vials of lyophilized synthrocytes (for example vials containing enough synthrocytes to carry SynA/SynAI in 5-10 microtiter plates), easier to distribute and store than many small vials, was feasible. In this way, large vials could be reconstituted and stored at 4°C, to be used over time. In addition, with their long stability in the lyophilized state, we demonstrated that synthrocytes can improve the handling and preservation compared to using RBCs.

Having a reagent almost "ready-to-use", which only requires adding a determined PBS volume and mix, makes the handling much more comfortable for the final user compared to obtaining the blood, separating the RBCs and doing the multiple washes to prepare them, a cumbersome process that usually takes hours. Moreover, synthrocyte production can be standardized, making sure that the amount of particles is consistent between batches. This avoids the need for cell counting or hematocrit correction, reducing the time required to prepare the reagents before performing the assay.

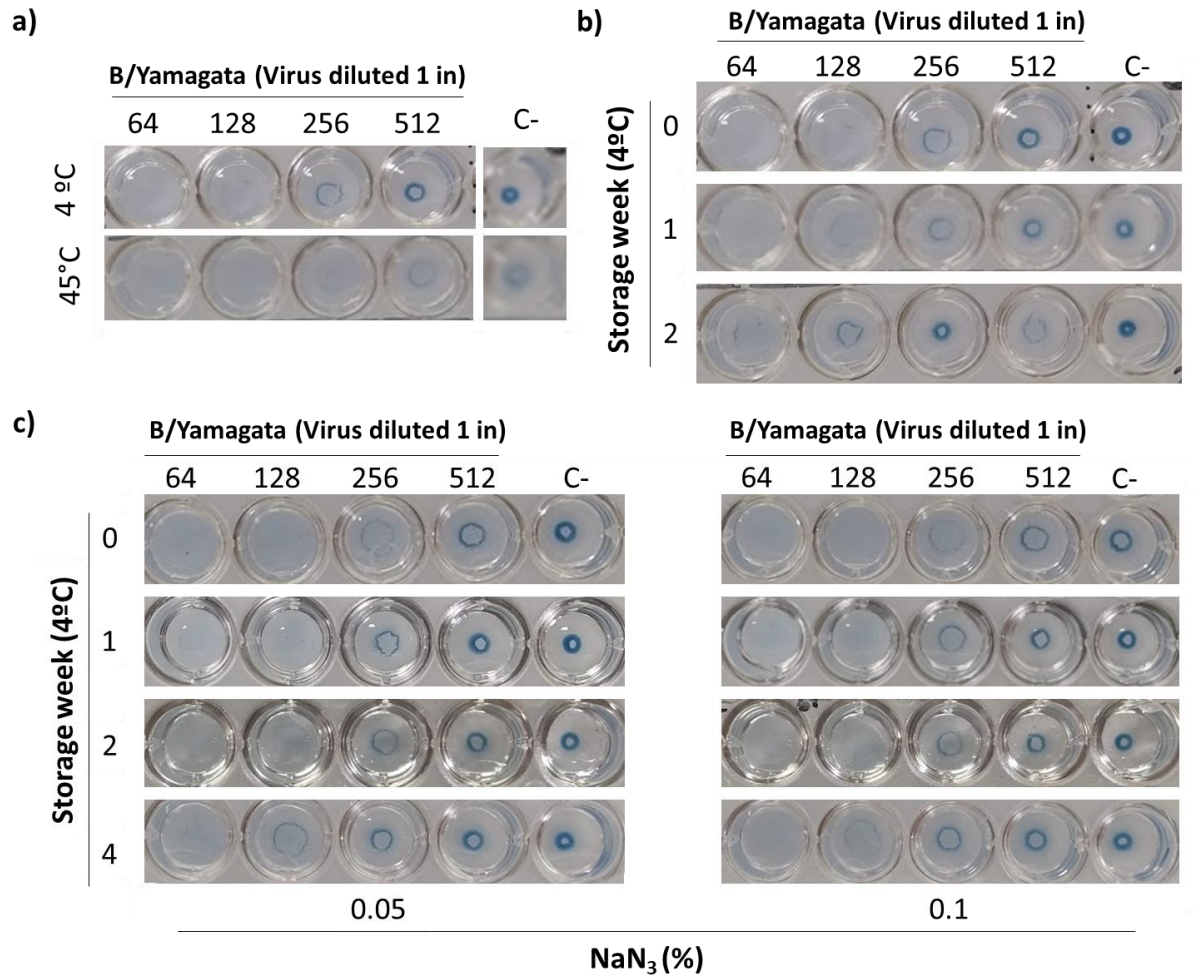

Figure 6.12 | a) Accelerated aging on 3 µm 6'-SL-BSA-synthrocytes. Synthrocytes were lyophilized, were submitted to thermal stress for 5 days at 45°C or stored at 4°C, and then used in SynA with B/Phuket/3073/2013 virus. **b)** Stability of synthrocytes after reconstitution with PBS. c) Stability of reconstituted synthrocytes that contained different amounts of NaN_3 in their lyophilization buffer, besides 15 g/L of BSA.

6.2.5. SynAI using lyophilized synthrocytes

After having demonstrated that synthrocytes could be lyophilized for long-term storage and be reconstituted for SynA, we tested if lyophilized synthrocytes could be used in SynAI, which is carried in the presence of sera samples of variable and complex composition. Specifically, we wanted to check if lyophilization contributed to counteract part of the non-specific interactions observed for fresh RBCs and fresh synthrocytes, or multiplied them.

These experiments were carried with three types of lyophilized synthrocytes, 10 µm 6'-SL-BSA-synthocytes, 10 µm GYPA-6'-SL-BSA-synthocytes (a version that displayed on surface a mixture of GYPA and 6'-SL-BSA), and 3 µm 6'-SL-BSA-synthocytes, in all cases using WHO Reference materials in SynAI (i.e., inactivated virus antigen, negative control serum without Ab against the virus tested, and positive control serum with Ab against the virus). As can be seen in Figure 6.13, the two 10 µm versions generated well defined pellets in the presence of serum without virus (labelled "+Serum No virus" in the figure). However, 10 µm GYPA-6'-SL-

BSA-synthocytes produced also pellets in the presence of virus in both negative and positive sera down to 1:640 dilutions. This suggested that some serum components bound the particles, inhibiting virus-driven agglutination. These interferences were reduced when using 10 μm 6'-SL-BSA-synthocytes, which evidenced virus-driven agglutination in the presence of negative serum diluted 1:160 or more, but sedimentation, and thus agglutination inhibition, in the presence of Ab-containing positive serum diluted between 1:160 and 1:1280. This is consistent with results in Chapters 4 showing that negative serums contained some Ab against GYPA. Lyophilization did not seem to decrease this type of non-specific interferences, further confirming the need to employ synthrocytes coated just with combinations of SA-BSA as the bioreceptor.

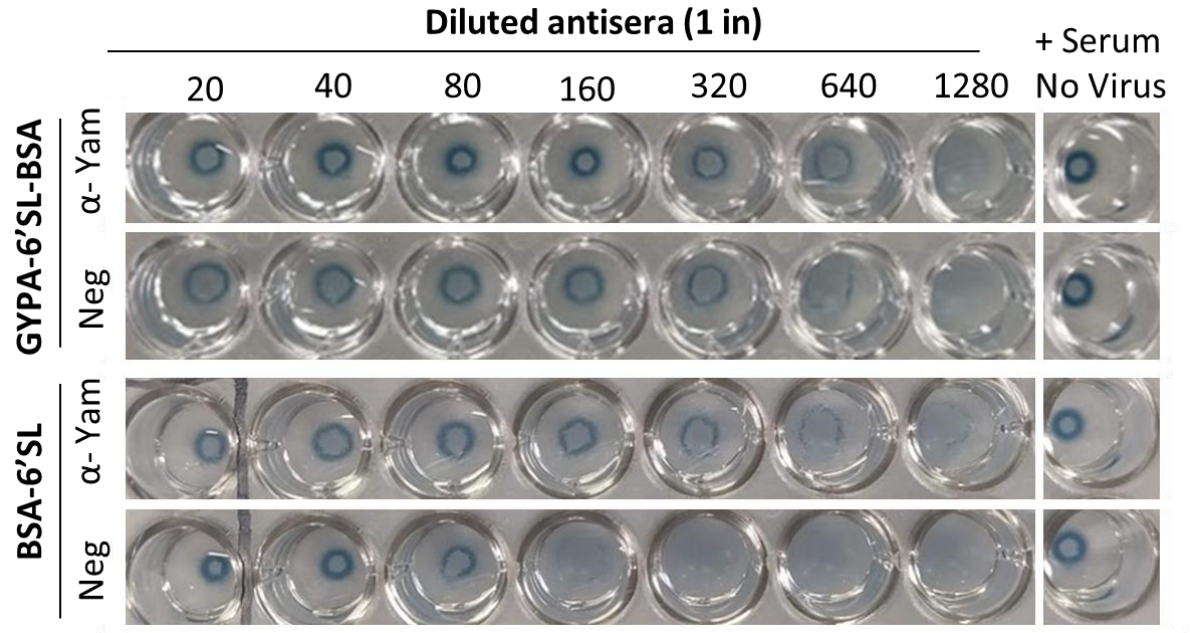

Figure 6.13 | Performance of lyophilized synthrocytes in SynAI. Dilutions of negative serum or antiserum against B/Yamagata were incubated with B/Phuket/3073/2013 virus. Then, 150 μg particles/well of 10 μm GYPA-6'-SL-BSA-synthocytes or 6'-SL-BSA-synthocytes, lyophilized and reconstituted in PBS, were added to the wells. Negative controls (well on the right) were carried by incubating the synthrocytes with the corresponding serum and no virus.

As an additional confirmation, 3 μm lyophilized synthrocytes coated with 6'-SL-BSA were lyophilized, reconstituted, and tested in SynAI using WHO Reference materials. More specifically, we used B/Yamagata and A(H3N2) viruses and their corresponding antiserums (plus the negative serum). The same experiment was repeated in parallel using RBCs as a reference. As can be seen in Figure 6.14, 3 μm lyophilized 6'-SL-BSA-synthrocytes exhibited clear agglutination inhibition (thus sedimentation) in the presence of virus and its corresponding antiserum (diluted between 1:20 and 1:1280), while they agglutinated in the presence of virus and the negative control serum. This behavior resembled that observed for fresh RBCs. Moreover, SynAI was more sensitive and was less prone to non-specific interference than when using 10 μm 6'-SL-BSA-synthrocytes. Nevertheless, the negative controls obtained for 3 μm lyophilized 6-'SL-BSA-synthrocytes in the presence of antiserum, but without virus, still showed a certain degree of nonspecific agglutination, appreciable

because the pellet was wider and more subtle than the ones observed in absence of serum (Figure 6.9b). This phenomenon was also observed with the freshly produced particles (without lyophilization; Chapter 5), but in fact it improved with the lyophilization and the effect of the increased BSA content in the buffer after reconstitution.

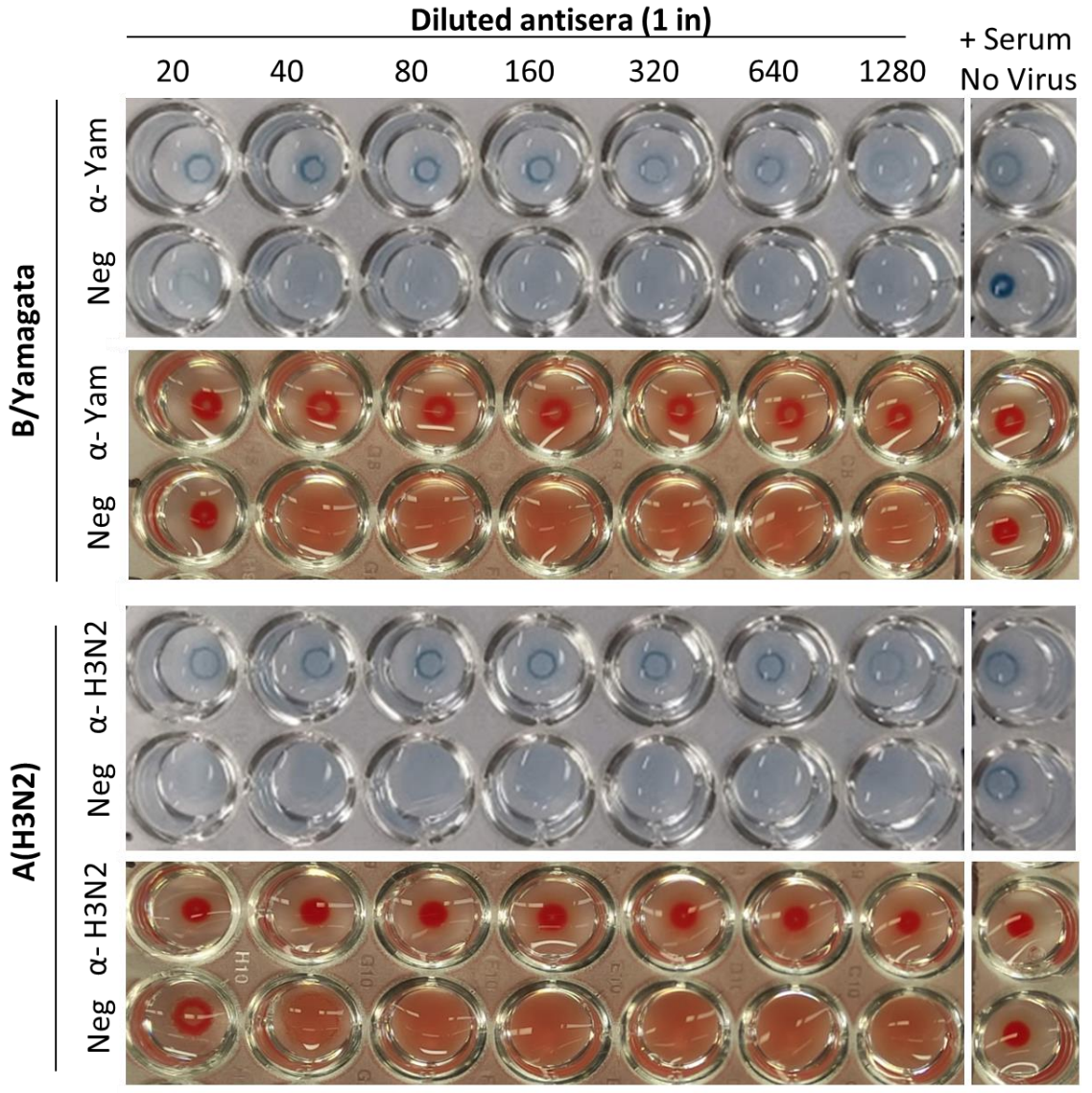

Figure 6.14 | SynAI performed with 3 µm 6'-SL-BSA-synthrocytes, B/Phuket/3073/2013 or A(H3N2) A/Kansas/14/2017 virus, and their corresponding antiserums and negative control serum (150 µg beads per well). Each SynAI is compared with its corresponding HAI performed in parallel using human RBCs.

In conclusion, lyophilized synthrocytes could be used to carry HAI-like SynAI assays, requiring less particles per well than freshly made synthrocytes, which decreased the cost of the assay and improved its sensitivity. Furthermore, 3 µm synthrocytes were more sensitive than their 10-µm counterpart and were also less sensitive to nonspecific interactions by serum sample components.

6.3. Production scale-up

In parallel to stability improvement, it was necessary to confirm the potential scalability of the synthrocyte production process. Usually, taking a technology from the benchtop to the commercial scale presents some significant challenges. It entails the adjustment of protocols for larger scale fabrication, sometimes implying the reformulation of the product, changes in the temperature or mixing, or even modification of the time required to perform the different procedures. Moreover, technical aspects such as cleaning needs and waste management should also be considered.

As previously stated, the procedure to produce synthrocytes entails different consecutive steps: particle custom-dying, conjugation of the selected receptors, surface blocking, and lyophilization. To begin with, we decided to scale-up the dying process. This was a simple but very robust protocol that provided reproducible and stable custom-dyed particles that could be easily quality-controlled. Moreover, although the chemical reactions for the dying and the conjugation phases were different, their methodological procedure was similar, involving incubation steps under end-to-end mixing using a rotator (Figure 6.15a) and centrifuge washing. Thus, another advantage was the potential transferability of the materials and procedures selected initially to scale up particle staining to the conjugation process later on.

End-to-end mixing through a horizontal axis (also called rotation) is technically feasible at the level of laboratory production (1-2 mL, Figure 6.15a), but challenging when the process needs to be escalated to liters because there are not many industrial “end-to-end lab rotators” available. The know-how of Biosystem’s R&D Team was crucial in the selection of an alternative type of mixing since, although our objective for this thesis was to escalate the production from µL to mL, the final expected volume for the annual synthrocyte production should reach 10-20 L in future.

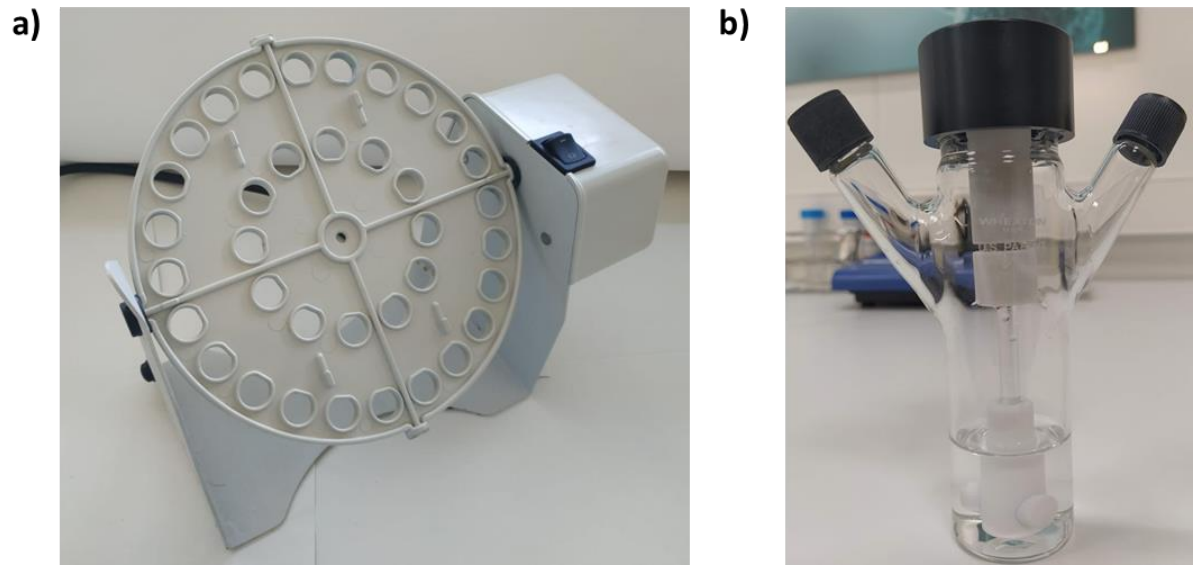

Figure 6.15 | a) Labnet rotator employed in laboratory production. **b)** Spinner-flask system used for the proof of concept of production scale-up. We chose the 50 mL system because it was the smallest available and improved production volume up to 40-fold.

Among the marketed technologies, we decided to use a glass spinner flask for agitation (Figure 6.15b). These types of flasks are frequently employed for cultivating cells and are available in a wide range of volumes, ranging from 50 mL to 15 L. They include a glass flask with a wide upper mouth and two smaller lateral arms that can be opened and closed independently. One feature of these flasks is the conservation of height-to-width aspect ratio along the different sizes, which eases scalability. Usually, this system has an internal paddle with an integrated magnet that is designed to provide an even rotation at different speeds when placed on a standard magnetic agitator. The two sidearms facilitate the access via pipes or pipettes without interrupting the mixing. Bell's work demonstrated that the initial speed required to lift the particles could be different (and higher) than the speed required to maintain them in suspension.[242] Therefore, the possibility of not stopping the process to introduce or remove buffers could avoid unnecessary changes in stirring speed during the procedure that could affect the process outcome. Moreover, the access through sidearms is of special importance for the addition of hazardous buffers and reagents, such as THF for the dying and glutaraldehyde for the conjugation, which must be manipulated inside a fume hood.

When used in cell culture, these flasks often stir at a controlled low speed preventing cell shearing stress. Here, stirring had to be slow enough to prevent the breakage of particles, but high enough to avoid their sedimentation while minimizing impact on their integrity. Therefore, already custom-dyed 10 µm particles (to facilitate their observation) were subject to different speeds of agitation for 10 min, ranging from 25 to 150 rpm. Immediately after halting the stirrer, particle sedimentation was visually assessed. The optimal speed was defined as the minimal stirring speed for which the particles remained completely suspended in solution. As shown in Figure 6.16, below 125 rpm particles sedimented, notably around the magnet spinner. Therefore, 125 rpm was selected as the optimal agitation speed for 10 µm particles.

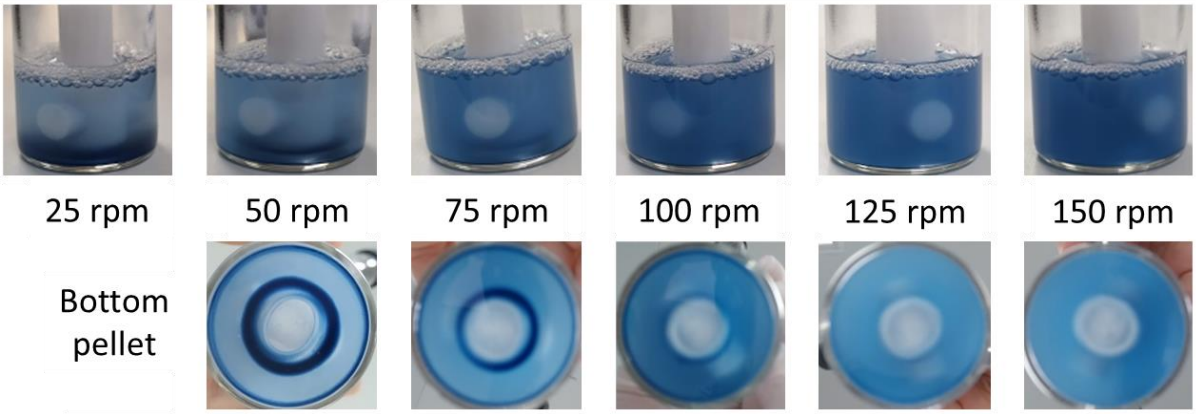

Figure 6.16 | Sedimentation of 10 mL of custom-died 10 µm particles in the spinner flask viewed from the side (top row) and from below (bottom row) after 10 min of agitation at different stirring speeds. Sedimented particles are clearly visible at the bottom for stirring speeds up to 100 rpm.

Once stirring speed was defined, the staining process was scaled-up. We started with 10 mL of 10 µm particles, which was a volume 20 times larger than the usual amount produced in the laboratory. All the buffers were scaled accordingly. Briefly, the non-stained particles were placed inside the spinner flask with 125 rpm agitation to ensure their complete suspension before starting the dying process. Dye was prepared as usual (Section 3.5), and once

completely dissolved, it was added through a tube placed at one of the sidearms on top of the suspended particles. After 1 h of agitation, the flask was opened and particles were transferred to a centrifuge tube, where they underwent the regular water washes.

Washed particles were subject to the usual quality control, including counting their number and absorption spectra analysis. After further optimization of the handling along the process, we achieved beads with a color intensity equal to the benchtop-stained ones. However, while at the laboratory scale we recovered in average ~ 75% of the initial particles, with this process recovery increased to 98%. As a result, carrying particle staining with larger volumes contributed to decrease synthrocyte production cost, presumably by minimizing particle lost by nonspecific adsorption to the material.

Next, we studied if a similar procedure could be employed for particle conjugation scale-up. For this, 10 µm custom-died particles were conjugated in parallel using the laboratory or the scaled-up process. Fetuin was selected for these optimizations due to its availability and lower cost compared to SA-BSA.

The conjugation procedure was similar to bead dying. Stirring was maintained at 125 rpm and incubation times and reagent final concentrations (particles, glutaraldehyde, fetuin, blocking BSA) were those optimized previously for the benchtop process, although total reagent volume increased proportionally to the scale. In this case, 7.5 mL of particles were conjugated using the scale-up process (a volume 30 times higher than the regular laboratory procedure). Since the protocol included different incubations under stirring conditions, particles were transferred after each one to a centrifuge-adapted vessel for washing and resuspension. The procedure finished with particle characterization by counting and spectrophotometric study.

Once counted, the recovery for these particles was of around 92%, compared to the 85% in the laboratory process. This increase was not as significant as during the dying process, which could be explained by the particle loss during the multiple manual washing steps. Although a recovery above 90% was considered acceptable from an economical point of view, automation of the washing steps in future should ameliorate this numbers additionally.

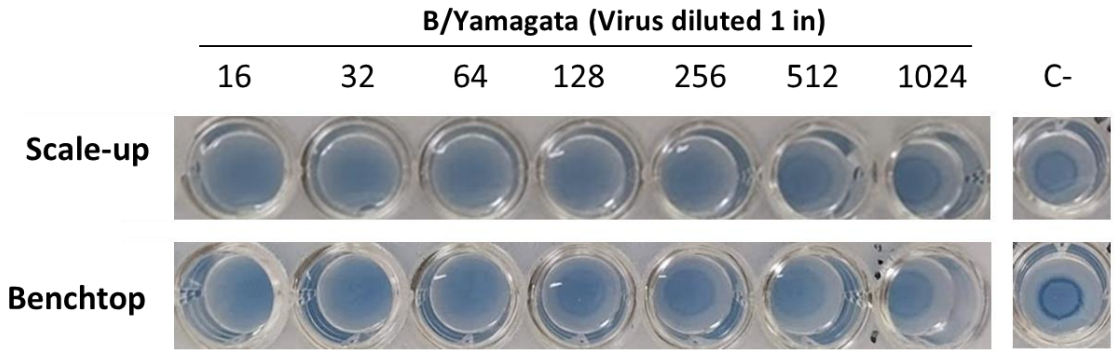

Figure 6.17 | SynA performed with B/Phuket/3073/2013 with 10 µm fetuin-synthrocytes produced in parallel using the scale-up process (top) or the classic benchtop protocol (bottom). All the solutions (such as glutaraldehyde or blocking solutions) were common between these two conditions.

Figure 6.17 shows how 10 µm fetuin-synthrocytes produced with the scaled-up protocol recognized the B/Yamagata virus with better sensitivity than when they were laboratory-produced, but generating lighter pellets in the negative controls. This effect was partly attributed to aggregation of the particles during conjugation, because these particles displayed under the microscope more clusters of 2-3 particles than the benchtop particles. This could explain the fainter pellet in the sedimented wells without virus but did not justify the difference in 3-titers observed in SynA when compared with the benchtop-produced.

6.4. Conclusions

To sum up, synthrocytes lyophilized using BSA as the main excipient could be used in SynA and SynAI assays, reducing the number of particles per well compared to fresh synthrocytes. This decreased the cost of the assay and improved its sensitivity, especially in the case of 3 µm synthrocytes, that were also less sensitive to nonspecific interactions by serum sample components than their 10-µm counterpart.

These results showed that scale-up of the microparticle dyeing and conjugation processes was also possible, although the removal of the manual washing steps should be the next priority. It is worth noting that this proof-of-concept was performed with 10 µm particles and fetuin (instead of SA-BSA because of its lower cost), and therefore should still be transferred and adapted to the 3 µm SA-BSA-synthrocytes in future. We have already confirmed that these smaller synthrocytes are more sensitive in SynA/SynAI assays and equally lyophilizable, but produce less non-specific interactions than the 10 µm in the presence of serum samples. Based on the results at laboratory level, once the agitation speed is re-optimized, it should be feasible to scale-up the fabrication process for this size of synthrocytes as well.

Chapter 7

Validation in a National Influenza Center

Chapter 7. Validation in a National Influenza Center

National Influenza Centers (NICs) are an essential part of the GISRS network. Usually, NICs collect virus specimens from patient samples and perform preliminary analysis of them. These analyses include typing and subtyping by PCR, often followed by cell or egg culture of a representative selection of these viruses. Some of the NICs also perform HA and HAI to titer and/or to characterize antigenically the viruses isolated and grown, while others perform neutralization assays, IF or genetic sequencing of the viral samples, or even neither of them. After that, some of these viral isolates are shipped to WHO CCs for advanced antigenic and genetic analysis.

A few of the NICs participate more closely in influenza vaccine monitoring, such as Valladolid's NIC in Spain. In addition to culturing the virus samples and pre-analyzing them, they also collect sera from vaccinated patients (both before vaccination and 14-21 days after immunization) and test by HAI their immunological response against the viruses included in that season's vaccine. This center kindly provided us the opportunity to test our synthrocytes and carry out a first field validation with them. Testing our reagent in a NIC boosted the technology to achieve Technology Readiness Level 5 (TRL 5 – technology validated in relevant environment),[243] an important milestone in the development of our synthrocytes. Moreover, it provided invaluable information about their standard working procedures and feedback from the final users on the handling and performance of the synthrocytes.

This chapter will describe the validation performed in their facilities, the feedback obtained by end users, and the measures taken to improve synthrocyte performance in accordance to this feedback. It is important to state that, when this validation was performed, the final version of synthrocytes was still under development. This is, lyophilization of 3 µm synthrocytes and particle modification with combinations of different SA-BSA had not been optimized yet. For this reason, we tested lyophilized 10 µm 6'-SL-BSA-synthrocytes and GYPA-6'-SL-BSA-synthrocytes, plus fresh 3 µm 6'-SL-BSA-synthrocytes. Hence, these are results of the performance of a prototype version of synthrocytes, which were later improved based on this feedback to obtain the updated version shown in this Thesis.

7.1. SynA with WHO reference antigens and egg-grown viruses

The first step to validate the synthrocytes was to evaluate if they recognized viruses that had been directly isolated from patients and later grown in eggs. In order to assess that, we performed in parallel a SynA assay using synthrocytes and U-bottomed wells and a HA assay using chicken RBCs and V-bottomed wells. The protocol followed by Valladolid NIC members for HA started with the addition of the virus directly to the first wells, instead of using a 2-fold dilution with PBS as recommended.[115] We adapted our protocol to fit theirs. All the experiments using RBCs were performed by Valladolid NIC members, while SynA were carried out by us.

Because the goal of this experiment was to test the maximum number of different viruses, we used 10 µm lyophilized GYPA-6-'SL-BSA-synthrocytes. As has been stated in Chapter 5

(section 5.6.1), these synthrocytes were able to recognize A(H1N1), A(H3N2) and both lineages of B influenza viruses. We studied the recognition of 3 series of viruses:

- 5 reference antigens of the WHO Surveillance Kit (2021 and 2020 B/Victoria) already tested in our laboratory, in order to give us a picture of the reproducibility of the assay between laboratories and confirm that synthrocytes were operational after transportation;

- 3 WHO reference antigens from B lineages that were ether-extracted, in which virus cleavage increases the hemagglutinin availability facilitating HA detection;

- and 5 viruses obtained from patients and grown in eggs by the Valladolid NIC members, including one A(H1N1), two A(H3N2) and two B/Yamagata, to determine if synthrocytes detected them.

Figure 7.1a. shows as an example the results obtained for the WHO reference Ag B/Yamagata, while Figure 7.1b depicts the same Ag but ether-extracted. A detailed comparison of the results obtained previously in our laboratory versus those generated in the NIC validation using synthrocytes and chicken RBCs is shown in Figure 7.1c. For the classical WHO antigens, sensitivity was considerably lower for synthrocytes compared to fresh chicken RBCs, with differences in SynA titer that spanned between 1-2 titers for B/Victoria, to up to 3-4 titers for A(H1N1) viruses. Part of these differences were attributed to the lyophilization, which reduced slightly the titer obtained in the SynA (~ 1 titer). Comparison between these results and performance of fresh synthrocytes processed at our laboratory previously sustained this, confirming that synthrocytes worked as expected even after their transport to the NIC (Figure 7.1c). On the other side, and as NIC responsible confirmed, RBCs worked better than usual. The reference HA titer provided by the WHO for each of these viruses when using chicken RBCs was 128, which contrasts with the 512 titer obtained for most of them. This could be due to the use of a fresher RBCs preparation or to a higher dilution of the RBCs than ordinary.

a)

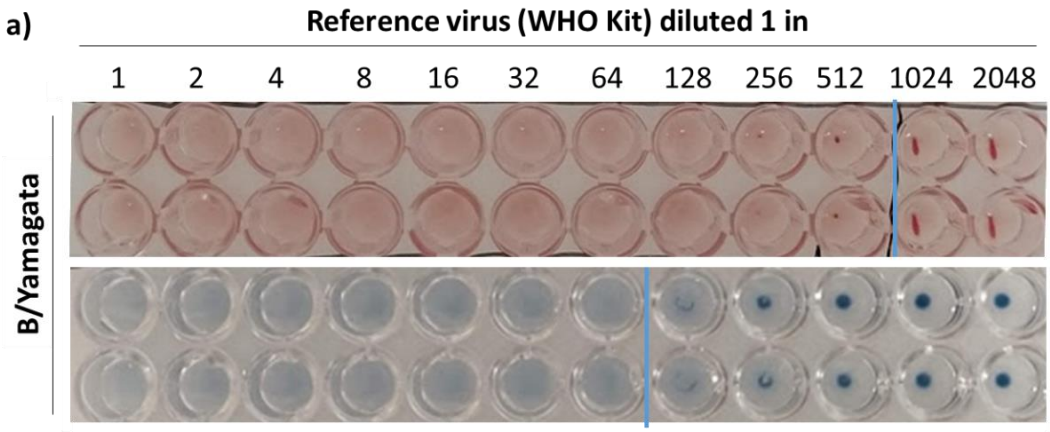

b)

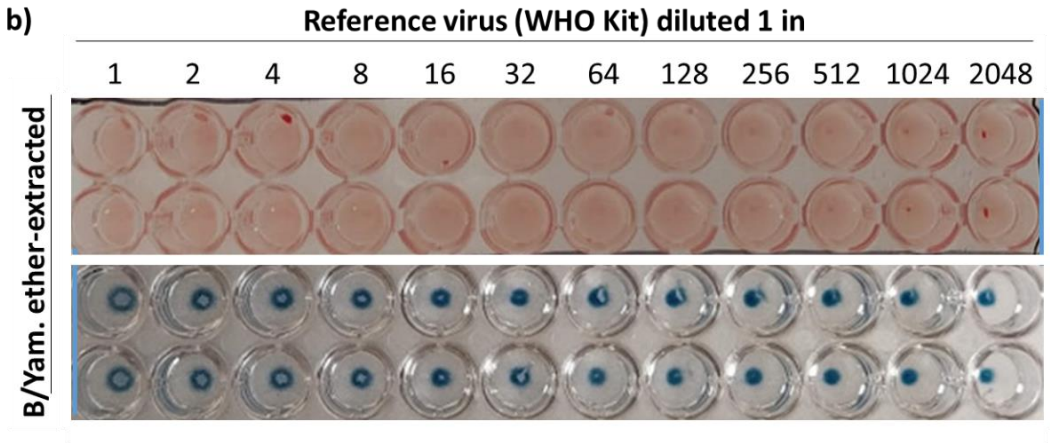

c)

Virus	Laboratory	NIC	Chicken RBCs
A/Brisbane/02/2018 (H1N1)	32	32	512
A/Kansas/14/2017 (H3N2)	32-	32-	128
B/Phuket/3073/2013 (Yamagata)	128-	64	512
B/Washington/02/2019 (Victoria)	*nd*	32	256
B/Colorado/06/2017 (Victoria)	*nd*	32	512

Figure 7.1 | Results obtained for some of the WHO reference antigens, which were evaluated in parallel by HA with fresh chicken RBCs and by SynA with 10 µm lyophilized GYPA-6'-SL-BSA-synthrocytes during validation at the Valladolid NIC. Chicken RBCs were freshly obtained, washed and prepared, and HA was performed and evaluated following NIC protocol by their members. SynA was performed in parallel by us. **a-b)** HA and SynA for B/Phuket/3073/2013 **(a)** classical and **(b)** ether-extracted WHO reference antigen. Blue marks signal the agglutination titer determined by NIC experts. **c)** Comparison of agglutination titer obtained for the same antigens in our laboratory using fresh synthrocytes (Laboratory), at the NIC using lyophilized synthrocytes (NIC) and with chicken RBCs. *nd: not determined*.

None of the ether-extracted B-antigens were recognized by synthrocytes. In fact, their sedimentation was faster than usual, which indicates that residues of ether present in these antigens may interfere with synthrocytes performance, promote their sedimentation, and/or inhibit virus-driven agglutination.

On the other side, all five egg-grown viruses were recognized by synthrocytes, which formed the expected agglutination pattern (Figure 7.2).

a)

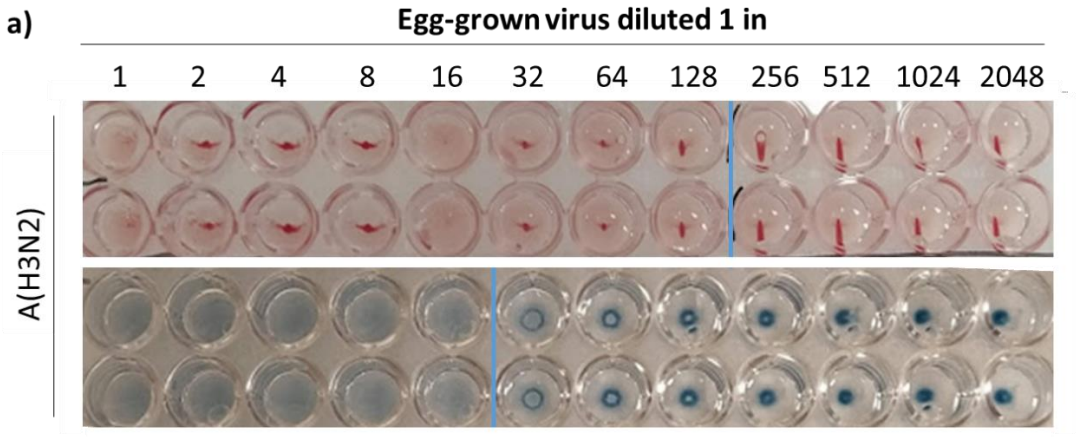

b)

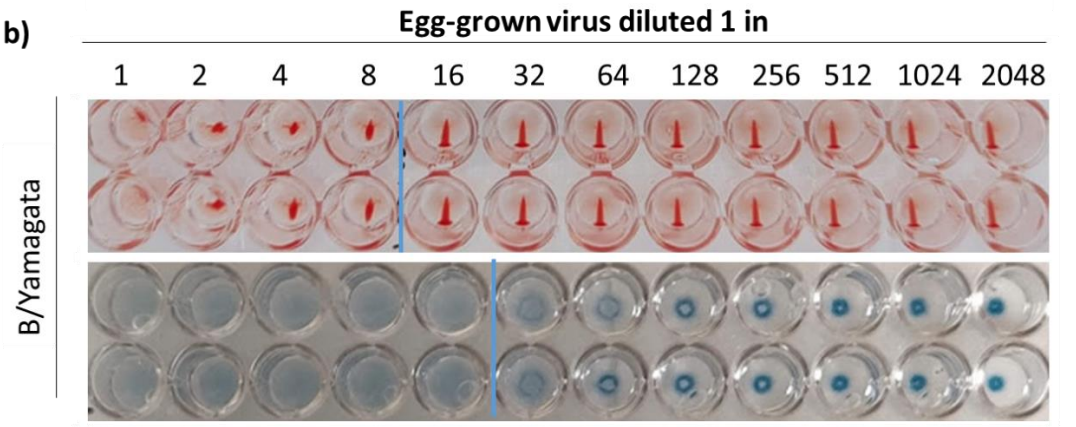

c)

Virus (similar to)	Expected	SynA	HA
A/Victoria/504/2005 (H1N1)	128	16	256
A/Texas/50/2012 (H3N2)	256	32	128
A/Texas/50/2012 (H3N2)	32	16	128
B/Massachusetts/2/2012 (Yamagata)	64	64-	64
B/Massachusetts/2/2012 (Yamagata)	64	32	8

Figure 7.2 | Summary of the results obtained for egg-grown antigens evaluated in parallel by HA using fresh chicken RBCs and SynA using 10 µm lyophilized GYPA-6'-SL-BSA-synthrocytes during validation at the Valladolid NIC. HA was performed and evaluated following NIC protocol by their members, simultaneously with SynA performed by us. **a-b)** HA and SynA for A/Texas/50/2012 **(a)** and B/Massachusetts/2/2012 **(b)** -like viruses. Blue marks signal the agglutination titer determined by NIC experts. **c)** Summary and comparison of agglutination titer obtained for the same viruses using SynA and HA compared to the expected titer determined retrospectively by NIC members (Expected).

For influenza A viruses, the SynA titer was also 3 to 5 times worse for synthrocytes than for RBCs (for A(H3N2) and A(H1N1) respectively), a result similar to that obtained with the WHO reference antigens. Nevertheless, the titers obtained by HA and SynA correlated well. For instance, when two batches of the same H3N2 virus were compared, both RBC-based HA

and synthrocyte-based SynA revealed a difference of one agglutination titer between them. This confirmed that, albeit less sensitive, synthrocytes could also detect changes in the virus concentration. Unexpectedly, synthrocytes displayed equal to higher sensitivity (of 1-2 titers) for B influenza viruses than RBCs. B viruses have a limited host range and are usually restricted to humans. Therefore, their growth in eggs and analysis with chicken RBCs are usually more difficult compared to other influenza viruses.[117,219,244] According to these results, synthrocytes were a competitive candidate for the study of influenza B viruses, which could avoid the need for ether-extracted antigens that are usually used for serologic diagnosis because of their higher sensitivity.

Finally, we studied the reproducibility of SynA between users and gathered user's feedback on synthrocyte handling. In order to do so, SynA was performed for A(H3N2) and B/Yamagata viruses by a NIC technician, who used automatic multichannel pipettes and reagent plastic reservoirs as he used to do for RBC-based HA (Figure 7.3). He was given a flask of lyophilized synthrocytes, information of the volume of PBS needed for reconstitution and volume of reconstituted synthrocytes needed per well, and advice to shake reconstituted synthrocytes regularly to prevent their sedimentation. Due to their higher availability and lower cost, the lyophilized 6'-SL-BSA-synthrocytes were used here instead of the GYPA-6'SL-BSA ones.

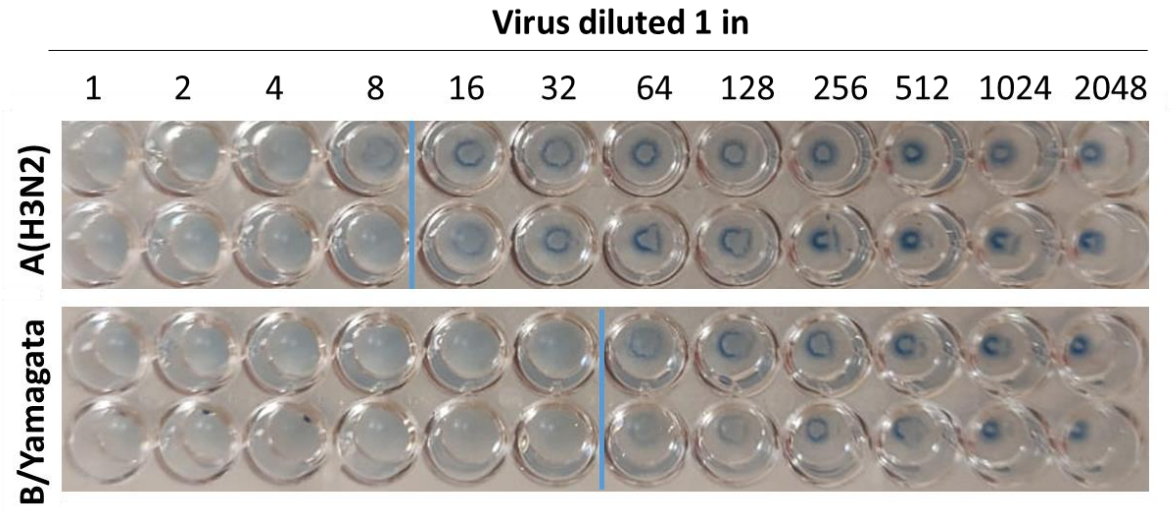

Figure 7.3 | SynA performed by NIC members for two different viruses using lyophilized 6'-SL-BSA-synthrocytes and automatic multichannel pipettes, without further training. Blue marks signal the SynA titer determined by NIC experts.

Results were very similar to the ones previously obtained in our laboratory, confirming that synthrocyte handling could be achieved by personnel familiar with HA/HAI without further training and using their own equipment. Nevertheless, users reported that synthrocytes sedimented too fast compared to RBCs. Although this made it possible to obtain the results faster, it also hindered handling when high volumes of synthrocytes had to be used. Usually, for performing multiple HA/HAI assays, RBCs are placed in a reservoir designed for multichannel pipettes and then distributed into the plate wells. Because their sedimentation takes between 30 min and 1 h, it is not necessary to agitate or mix them during the procedure. 10 µm synthrocytes in the reservoir sedimented faster, which could produce differences in the

number of particles dispensed in each well if not correctly resuspended, potentially producing false results. While feasible, the handling was more uncomfortable because it required faster dispensation or more mixing during the process.

In short, these experiments show that synthrocytes could recognize the four main types and lineages of influenza viruses, which is essential for influenza surveillance. Moreover, they could recognize patient sample viruses isolated and grown in eggs, as is regularly performed at NICs. In addition, synthrocytes proved to be reproducible when handled by different personnel and similar enough in their handling to RBCs not to require further training. Despite this, improving the sensitivity of the particles and decreasing their sedimentation speed would be key to compete satisfactorily with chicken RBCs.

7.2. SynAI for vaccine response evaluation

Once the usability of synthrocytes for SynA was demonstrated, we analyzed their performance in HAI-like SynAI assays. As previously stated, Valladolid NIC is one of the centers that also cooperates in evaluating vaccine response, participating in the iMOVE network (Influenza - Monitoring Vaccine Effectiveness in Europe). This means that they also use HAI assays to evaluate the serums of vaccinated people to assess the level of Ab against the vaccine strains, and not only to subtype the viruses isolated from patient samples.

As a suggestion from Valladolid NIC members, we tested 15 serums from vaccinated people plus two reference antiserums from the WHO Surveillance Kit. For this application we used fresh 3 µm 6'-SL-BSA-synthrocytes, for which lyophilization had not been optimized yet, instead of 10 µm GYPA-6'-SL-BSA-synthrocytes. The reason was that the last experiments performed before the validation on-site revealed that particles containing GYPA produced more interferences in SynAI, despite improving detection and allowing the recognition of the 4 types of reference influenza viruses. In addition, 3 µm particles exhibited better surface blocking than the 10 µm, contributing to decrease nonspecific interferences caused by serum samples. Therefore, for these SynAI experiments we used 6'SL-BSA coated particles instead of the mixed ones, even though the virus recognition was limited to A(H3N2) and B viruses. Consequently, HAI/SynAI assays were performed only with WHO reference A(H3N2) and B/Yamagata viruses.

Figure 7.4 shows the HA and SynA done before the HAI/SynAI to establish the agglutination titer for both viruses. As expected, 3 µm 6'-SL-BSA-synthrocytes were more sensitive than 10 µm, but still displayed agglutination titers 1-2 lower than chicken RBCs.

Once the corresponding titer was defined, viruses were diluted to 4 HAU-SynAU/25 µL (twice the amount usually used in our group) and HAI/SynAI were performed in parallel. For this, all the serums were previously treated with RDE and adsorbed using RBCs as the protocol recommends. Dilution series were next prepared for each serum, were dispensed in the wells of a microtiter plate (V-bottomed for RBCs and U-bottomed for synthrocytes) and were incubated for 30 min with 4 HAU/SynAU of the virus (either A(H3N2) or B/Yamagata). RBCs or synthrocytes were finally added and sedimentation was allowed to proceed (for 60 min in the case of RBCs; for 20 min in the case of synthrocytes). The inhibition titer for the RBCs

was determined by NIC members, while for the synthrocytes it was determined jointly. Samples inducing agglutination inhibition, and thus RBC/synthrocyte sedimentation, had Ab against the virus tested. The comparison of sample inhibition titer before and after vaccination allowed determining if that individual had produced Ab against each virus.

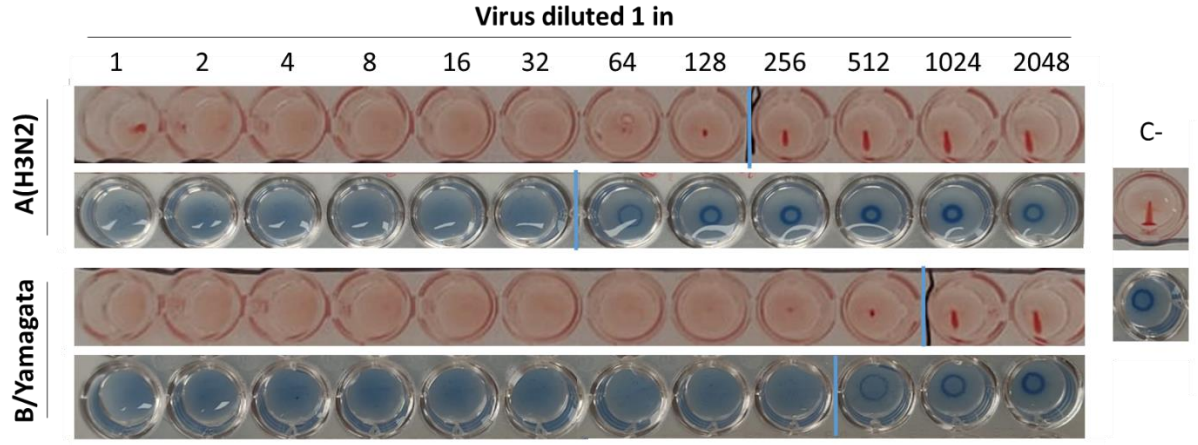

Figure 7.4 | Comparison between HA and SynA using 3 μm 6'-SL-BSA-synthrocytes. This experiment was performed prior to HAI/SynAI in order to establish each virus agglutination titer.

Figure 7.5a,b shows an example of the results obtained for some of the serums evaluated by HAI and SynAI ((a) for H3N2 and (b) for B/Yamagata virus), and Figure 7.5c summarizes all the results obtained. For WHO reference antiserums, the inhibition titer was higher in the presence of their corresponding virus, as expected, but they showed some crossed reaction (in both RBCs and synthrocytes) with the other virus tested as well. For instance, the cross-reaction of anti-B/Yamagata serum for A(H3N2) virus reached in HAI an inhibition titer of 40, while the cross-reaction of anti-A(H3N2) serum for B/Yamagata virus reached even 80. According to the WHO standards,[115] these results were slightly worse than recommended. In synthrocytes this effect was also present and even increased because synthrocytes were less sensitive. Albeit cross-reaction of anti-B/Yamagata serum for A(H3N2) virus produced also a SynAI titer of 40 (as for HAI), this was only 1 titer below that produced by the corresponding anti-A(H3N2) antiserum for A(H3N2) virus (a SynAI titer of 80, compared to a HAI titer 320). In contrast, the SynAI titer of anti-A(H3N2) serum for B/Yamagata virus shifted to 160 in SynAI, compared to 80 in HAI.

The study of the serums obtained from patients was in general also less sensitive by SynAI than by HAI. This was especially critical for A(H3N2) virus, for which the inhibitions generally produced a SynAI titer 2-3-fold lower than for RBCs. Moreover, titer reduction was not always constant, and samples with lower SynAI titers did not always correlate with low HAI titers (Figure 7.5c). For example, sample 3 (which had a relatively low SynAI titer) had a difference of one titer when assessed by SynAI and by HAI (40 and 80, respectively), while sample 1 had a difference of three titers (increasing from 20 with synthrocytes to 160 with RBCs).

The SynAI results correlated better with those obtained in HAI in the case of B/Yamagata. This could be explained because of the high concentration of B/Yamagata-binding Ab present in almost all the tested samples (Figure 7.5d). Further dilutions of the serum samples

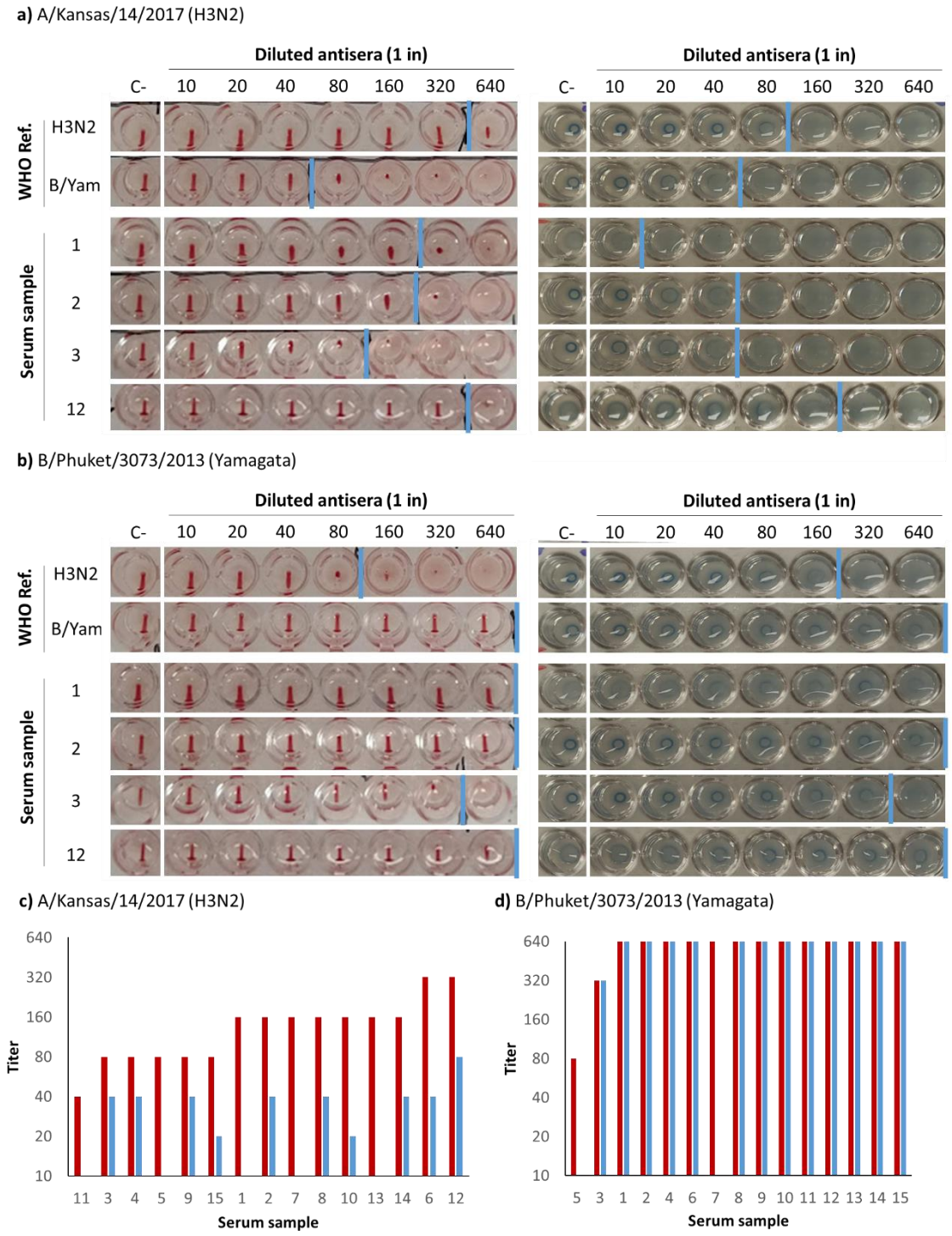

Figure 7.5 | Study of serum samples from patients by HAI and SynAI. **a-b)** HAI and SynAI results for the two reference antiserums tested plus 4 serum samples from vaccinated donors as examples, using A/Kansas/14/2017 **(a)** or B/Phuket/3073/2013 virus **(b)**. Blue marks signal the titer determined by NIC experts. Negative controls refer to the corresponding serum diluted (1/10) without the presence of virus. **c-d)** Summary of all the serum samples analyzed for A/Kansas/14/2017 **(c)** or B/Phuket/3073/2013 **(d)** viruses. Red bars correspond to HAI titers, while blue lines correspond to SynAI titers for each sample. All the donor samples were sorted based on the HAI titer and exhibited from lower to higher titers, arranged for each virus independently. This explains the differences in the placement of each donor between c and d figures. Samples without blue bars correspond to the ones with non-specific agglutination that ruled out SynAI titer determination.

would be required in order to establish differences between SynAI and HAI. Despite this, one of the two samples that showed a lower titer in HAI, sample 3, presented a similar titer in SynAI (320 in both cases); the other one, sample 5, could not be analyzed by SynAI due to agglutination interferences.

It is important to note that some serums (such as sample 1 in Figure 7.5a,b) interfered in synthrocyte sedimentation, which made impossible to determine an accurate SynAI titer. Among them, samples 5 and 7 (13% of the samples) prevented synthrocyte sedimentation in all the SynAI assays carried, and samples 1, 11 and 13 displayed interference only in SynAI carried for A(H3N2) (for which 33% of the samples failed). These serums showed a fainter or non-existent halo in the negative control (left column in the Figures 7.5a and b, which are wells with the corresponding antiserum but without virus). Because synthrocytes displayed an agglutination pattern in the presence of these serums, inhibition of virus-driven agglutination was masked and was barely distinguishable even at high serum concentrations (when more Ab are present).

Despite this interference, inhibition was produced. For example, in Figure 7.5b, while sample 1 produced synthrocyte agglutination patterns at high serum concentrations (1:10 to 1:20), synthrocytes sedimented for more diluted serum, contrary to what was expected. This indicated that B/Yamagata-binding Ab were present in this sample and that inhibition of the agglutination occurred along all the row. However, it was not appreciable in the first wells because some serum interferent produced non-specific synthrocyte agglutination and masked the inhibition. The effect of this interferent was compensated when diluting the serum, allowing the particles to show sedimentation again when inhibition occurred.

To sum up, this experiment showed that synthrocytes still displayed interferences in the presence of some human sera that impacted negatively in SynAI performance. Although these interferences were less relevant in WHO reference antiserums, they had a huge impact in the study of human serums. These interferences were attributed to the fact that, compared to RBCs, synthrocytes displayed a simpler and more homogeneous surface coating. Hence, either synthrocytes required additional surface blocking and/or engineering reoptimization to prevent non-specific binding, or the standard serum pre-adsorption using RBCs removed synthrocyte-binding interferents inefficiently and should be substituted by pre-adsorption using synthrocytes instead. Therefore, more development was needed before being able to use synthrocytes in SynAI assays for vaccine response evaluation.

7.3. General feedback for synthrocytes

After carrying out the different assays in Valladolid and evaluating their results, feedback from the final users was requested to survey synthrocytes usability and improve their performance.

In their opinion, the main strength of synthrocytes was their almost ready-to-use format, obtained thanks to the lyophilization. Reconstitution only took ~30 min with light mixing to ensure the complete rehydration of the particles, compared to the handling required to obtain animal RBCs, including displacement to extract blood from caged animals, refrigerated and biosecurity transport to the NIC facilities, and the subsequent washes to isolate RBCs, which

could take half-day. Synthrocytes were even easier to use than commercially purchased RBCs, which also require having the number of cells standardized. In order to do so, RBCs had to be counted and/or have their hematocrit analyzed and normalized before performing any HA/HAI. Synthrocytes, on the other hand, were standardized before lyophilization and thus did not require any extra step besides adding 5 mL of PBS per vial.

Synthrocytes also had increased stability compared to RBCs, both in the lyophilized state, when the particles could potentially be stored for more than 9 months at 4°C, or once resuspended, when they remained stable for around a month, 4-times more than RBCs. Moreover, being able to guarantee the stability of synthrocytes for at least a couple of weeks could decrease the number of SynA required to perform SynAI. For example, users could carry out a single SynA per vial just after synthrocyte reconstitution and then perform only small back-titrations to confirm the correct virus dilution prior to the successive SynAI, instead of performing a full HA daily prior to each HAI as now. This could be especially useful if large synthrocyte vials were available, which could reduce the waste of virus and synthrocytes.

Other interesting aspects were result reproducibility between users and the fact that SynA/SynAI handling and pattern readout were very similar to those of classical HA/HAI, which spared further training for the technicians. Synthrocytes could be even used with automatic multichannel pipettes, which eased the dispensation in the wells. Furthermore, time of the assay was decreased from 30-60 min to 20 min for 3 µm synthrocytes (or 10 min for 10 µm synthrocytes).

Although the feedback was in general positive, some concerns aroused about the sensitivity of synthrocytes. With 10 µm beads, the recognition was 3 to 4 titers lower than with RBCs, a difference too high to be acceptable. As a reference, WHO criteria allow a maximum difference of 1 titer between different assays and users performed with the same conditions.[115] Sensitivity of 3 µm particles, in contrast, was within this range for some of the viruses, such as for B/Yamagata. Another issue was the speed of sedimentation, which provided fast results, but also hampered the handling of the particles due to their fast sedimentation in the reservoir during pipetting. NIC members agreed that having to mix synthrocytes continuously to prevent their sedimentation was “stressful” and produce user discomfort. Moreover, fast synthrocyte sedimentation could create concentration gradients in the reservoirs, increasing result variability between wells. This could be crucial for eventual SynA/SynAI automation.

Lastly, interferences were detected when SynAI was performed using human serums from vaccinated donors. In HAI assays, serums must be treated systematically to avoid interferences. On one side, RDE is used to eliminate non-specific agglutination inhibitors. All the WHO reference antiserums employed in SynAI along this Thesis were treated with RDE as a part of the standard protocol (Chapter 3.9.2.1). However, the main interference detected in these SynAI was non-specific agglutination. In HAI, serums are also pre-adsorbed with RBCs (in a ratio 1:20 v:v) to remove non-specific agglutinins, a pre-treatment that seemed not efficient enough to remove synthrocyte-binding interferents.

Donor serums tested at the NIC were also pre-adsorbed with RBCs following the WHO protocol. Results obtained during this validation confirmed that our synthrocytes also required

pre-treatment of the serums, and doing it with RBCs was not enough. Usually, these RBCs capture non-specific agglutinins present in the serum that could interact with RBCs during HAI assay. Synthrocytes exhibit different molecules on surface compared to erythrocytes, and therefore serums presumably needed to be pre-adsorbed using synthrocytes instead of RBCs to remove all the non-specific agglutinins.

As shown in Chapter 5 and 6, when synthrocytes were employed in SynAI using WHO reference antiserums (which are produced in goat or sheep), interferences were also present, albeit lighter. None of these reference antiserums were previously pre-adsorbed. As a result of this validation, we identified the need to include this step in our protocols, which highlights the need for cheaper synthrocytes production costs to be able to use them in pre-adsorption.

7.4. Synthrocyte upgrading

Some of the improvements that resulted from the feedback provided by Valladolid NIC members have been already disclosed during this Thesis, especially in Chapter 5. This mostly included the substitution of 10 µm beads by 3 µm particles. As was proved on-site and in our laboratory, this replacement increased the sensitivity of synthrocytes to almost the range required for satisfactory SynA. In addition, the time required for sedimentation of 3 µm beads doubled that of 10 µm particles (~20-25 min vs 10 min), which improved user handling following NIC recommendations but without compromising the total incubation time of the assay (20-25 min).

It is worth highlighting that the protocol used for HAI in Valladolid NIC differed from the one we used at Vall d'Hebron, and both were slightly different to the one described in the WHO Manual for the laboratory diagnosis and virological surveillance of influenza.[115] Moreover, in parallel they were testing a new protocol provided by FLUCOP. This brings forward the need for a standardization of the HA and HAI protocols, an objective that could be achieved by substituting the RBCs by a synthetic reagent coupled with specific instructions for its use.

The requirement for a combination of receptors to recognize all the 4 main subtypes and lineages of influenza viruses became evident during this validation. The development of synthrocytes moved forward to approach a fully synthetic RBC-mimetic reagent, by substituting sialylated native proteins such as GYPA by a battery of SA-BSA receptors. As it has been shown in Chapter 5, this contributed to reduce nonspecific interferences, facilitate surface tuning, and reduce the production cost.

Finally, we confirmed the need for serum pre-adsorption to remove non-specific agglutinins, especially important for human serum pre-treatment. Different methods for pre-adsorption were assessed in our group to try to mimic the removal of nonspecific agglutinins with RBCs. The method selected due to its performance and similar procedure to RBCs was pre-adsorbing the serums with a large volume of colorless SA-BSA-synthrocytes (Figure 7.6). Particles for pre-adsorption did not require color because they were removed by centrifugation (imitating RBCs procedure), thus the cost of dying could be reduced.

The synthrocyte:serum proportion used for this preabsorption was slightly higher than that required for RBCs, probably because the number of receptors in the surface was insufficient

to correctly treat the high volumes of serums. Increasing the number of receptors in the surface (if the cost of SA-BSA could be reduced) or reducing the size of the particles to allow for more receptors would improve the pre-treatment of the serums.

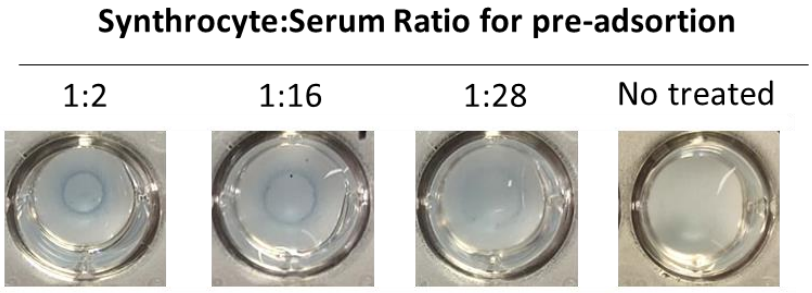

Figure 7.6 | Sedimentation of synthrocytes in serum, either untreated or pre-treated with different conditions. Serum without pre-treatment (right) produce non-specific agglutination of synthrocytes. To remove these agglutinants, serum was pre-treated with different amounts of synthrocytes and then centrifuged to eliminate those synthrocytes. These serums were then dispensed in the wells of a plate and synthrocytes were added and allowed to settle down. Only pre-treatment with synthrocyte:serum ratios of 1:2 depleted efficiently the nonspecific agglutinant from the serum. For higher ratios (thus lower amount of depleting synthrocytes), the sediments obtained were fainter and broader, and even disappeared.

7.5. Conclusions

In conclusion, synthrocytes were able to improve user experience and reproducibility of the assay compared to RBCs and obtained the positive feedback from Valladolid' NIC members. These experiments showed that synthrocytes were able to bind egg-grown viruses isolated from patients, even with the preliminary 6'-SL-GYPA version tested here. Based on results from Chapter 5, it is expected that the subsequent versions of synthrocytes will recognize at least the same combination of viruses, probably with better sensitivity.

Nevertheless, synthrocytes still displayed interferences in the presence of some human sera, which made them of limited usefulness in SynAI assays for vaccine response evaluation. Part of these interferences were attributed to the simpler surface coating of synthrocytes compared to RBCs, and to the lack of pre-adsorption of the serums using synthrocytes. Firsts steps to reoptimize serum adsorption are already under development.

Chapter 8

Assay automatization

Chapter 8. Assay automatization

HA and HAI are worldwide extended methods, which are used for a broad range of applications and not just influenza surveillance. For example, HA is used routinely as a screening assay in blood banks to detect Ab against blood group antigens before blood transfusions, and to titer such Ab as well.[245] HA is also a method to monitor virus growth *in vitro* for the manufacturing of vaccines and viral antigens. Moreover, due to its wide range of applications, HA and HAI possess the flexibility to be used from single sample testing to scale-up analysis using automated platforms in clinical laboratories.

As discussed before in this Thesis dissertation, one of the main limitations of HA/HAI assays is the high variability of the results produced. Some of this variability can be attributed to the compulsory use of RBCs, but subjective outcome interpretation also plays a role in it. Many factors contribute to this variability, including human bias, cognitive impaired performance after the repetitive task, operator level of expertise, or differences in training between laboratories. Moreover, the procedure for titer determination can also differ, with some laboratories relaying in just one expert judgment, while others gather multiple interpretations for every plate and establish a consensus result.

In an attempt to solve these problems, various solutions have been proposed. One of them was the development of robotic equipment to remove the subjectivity from the result readout, as proposed by Warren's group.[246] These instruments improve the reproducibility of the assay interpretation thanks to the automatic recording and analysis of the HA wells. Moreover, they provide traceability of the data thanks to its digitalization. Nevertheless, when using this equipment to interpret the results, some HA steps still have to be carried out manually. This type of equipment does not provide a quantitative readout either. Instead, serial sample dilutions have to be tested to estimate the minimal agglutinating dilution, which consumes time and resources.

Another approach to solve the subjectivity of the reads consisted in employing devices that facilitate the quantification of the agglutination. Some of these devices were based on microfluidics, which allowed carrying faster assays in lower sample and reagents volumes. In general, microfluidic devices designed to work with HA (mainly for blood typing) entail accurate micropumps and flow control.[245,247,248] Capillary-driven systems are an alternative to powered pump-based microfluidics, enabling fast and accurate flow control with a low production cost and no energy consumption.[249] Within this group, laminated designs, based on stacking multiple layers of pre-cut paper or polyester films to form microchannels,[250,251] are increasing their relevance. This strategy allows the use of non-porous materials, such as polyester films, which can improve particle and sample transport with minimal nonspecific adsorption, an essential feature for agglutination assays.

In this chapter, we will explore two different schemes for the quantification and automation of SynA. For the first approach, SynA assays were read using a spectrophotometer able to scan the well surface and produce a color matrix with the absorbance of the different well areas.

This was useful to imitate the process of the automated equipment used in some WHO CCs laboratories.

For the second strategy, we designed a semi-automatic low-cost device that delivered a quantitative result for SynA after image analysis. Then, we produced calibration curves and demonstrated that the amount of influenza A(H1N1) virus in spiked culture medium samples could be successfully quantified. This device was developed thanks to the contribution of Dr. Henry's group, from Colorado State University (USA), during a 5-month internship carried out during this Thesis.

8.1. Spectrophotometric scan readings of SynA

The use of the HA and HAI techniques is not uniform among the GISRS laboratories. WHO-CCs conduct the majority of these assays because they centralize the reception of the samples collected in their regions and carry most of their antigenic characterization. To facilitate the analysis of these hundreds of plates, the biggest GISRS centers usually employ one of the few automatic equipment available to perform HA/HAI and/or to interpret the results.

For example, SciRobotics, in collaboration with Tecan, developed an instrument that enabled partial automation of the liquid handling steps in HAI.[252] To carry the assay with this platform, the user has to check and dilute manually the viruses and RBCs and prepare the serial dilutions of the antisera prior to their loading in the workstation. Then, the instrument carries out the dispensation, incubation and even the tilting of the HAI assay plates when necessary (i.e., when using avian RBCs in V-plates). Finally, it photographs the plates and analyzes images for each individual well using an algorithm to recognize changes in shape and size in the settling patterns. This intelligent software is trained on user plates, for example using the results obtained from virus controls for each assay.[252] Other devices, such as the InDevR's Cypher One Automated Hemagglutination Analyzer, are unable to tilt the plates or perform reagent dispensation, but can image and analyze the plate using an algorithm designed specifically to avoid this tilting.[253]

The use of this type of equipment increases the number of plates that can be processed in a day, improving the consistency of well interpretation and, in some cases, offering some handling standardization. Furthermore, they facilitate data analysis and provide a traceable record for each plate through automated digital record keeping.[253,254]

In this project, after the first on-field synthrocyte validation at Valladolid NIC, we decided to test the performance of our synthrocytes in instruments of this type based in the suggestion of the NIC collaborators. However, only a few GISRS laboratories currently use these automated analyzers due to their high acquisition cost, and none of them could be contacted to perform these tests during this Thesis. We thus explored readily available alternatives for HA/HAI objective interpretation.

For this, we employed a microplate reader with an area scanning function (FLUOstar Omega, BMG Labtech). This approach was also used by Zhao *et al* to perform galectin-3-induced HAI using chicken RBCs, reporting objective and robust data interpretation of the HAI assays.[255] In our case, the instrument measures individual absorbance unit (AU) values in multiple points

of each well (60 points, from a 9x9 matrix), displays each scanned point (or groups of them) graphically, and creates a color map for each well. Although not the same, this approach also uses characteristics employed by the automatic analyzer algorithm (mostly size, density and shape of the sedimented pattern) to interpret each well.

To evaluate the usefulness of this instrument, a SynA was performed using 6'-SL/3'-SL/3'-SLN-Synthrocytes (3 µm custom-dyed particles) and a reference virus (B/Yamagata) in a U-bottomed plate (Figure 8.1a). Then, the plate was analyzed using the matrix scan function of the microplate reader. The wavelength used for these measurements was the same employed for the quality control of the custom-dyed particles (604 nm). The AU values obtained for each point were finally represented in either a 2D (Figure 8.1b-c) or a 3D gradient color scheme (Figure 8.1d).

Synthrocytes, as well as RBCs, are not evenly distributed across the whole well when sedimented. Therefore, determining the number and distribution of the points useful for the analysis was necessary. The instrument software allowed scanning from 60 points that comprised an area of 6 mm of diameter (ø) in the well, down to a minimum of 2 mm ø (12 points), which corresponded to the center of the well (Figure 8.1c). Figure 8.1e summarizes the average signals registered for each well after blank subtraction (this is, after subtracting the signals registered in just PBS, without synthrocytes, under similar measurement conditions). As can be seen, the diameter and thus area scanned significantly impacted the average AU values obtained for each well. The highest differences between agglutinated and non-agglutinated synthrocytes were obtained when the analysis took into account only the central area (2 to 3 mm ø, or 12 to 16 points respectively). When analyzing a 4 to 5 mm ø well area, differences could still be observed, but they were reduced because the average included points outside the sedimented pattern.

In the 6 mm ø area, signals were remarkably lower for both agglutinated and sedimented wells. This could be explained because the analysis included points in the perimeter of the wells, which were U-bottomed and thus displayed different solution deepness across the well bottom. As it can be easily seen in Figure 8.1f, which shows the distribution and the average of the signals registered in a blank well (containing just PBS without synthrocytes) for each diameter analyzed. When using the 6 mm ø area, the blank value increased 10-fold, a raise that was not constant in all the wells, which affected background subtraction. On the other hand, the well periphery displayed no synthrocytes in SynA well, which also contributed to decrease the average signals registered for 6 mm ø areas. Altogether, this made it impossible to quantify the agglutination or define an agglutination titer.

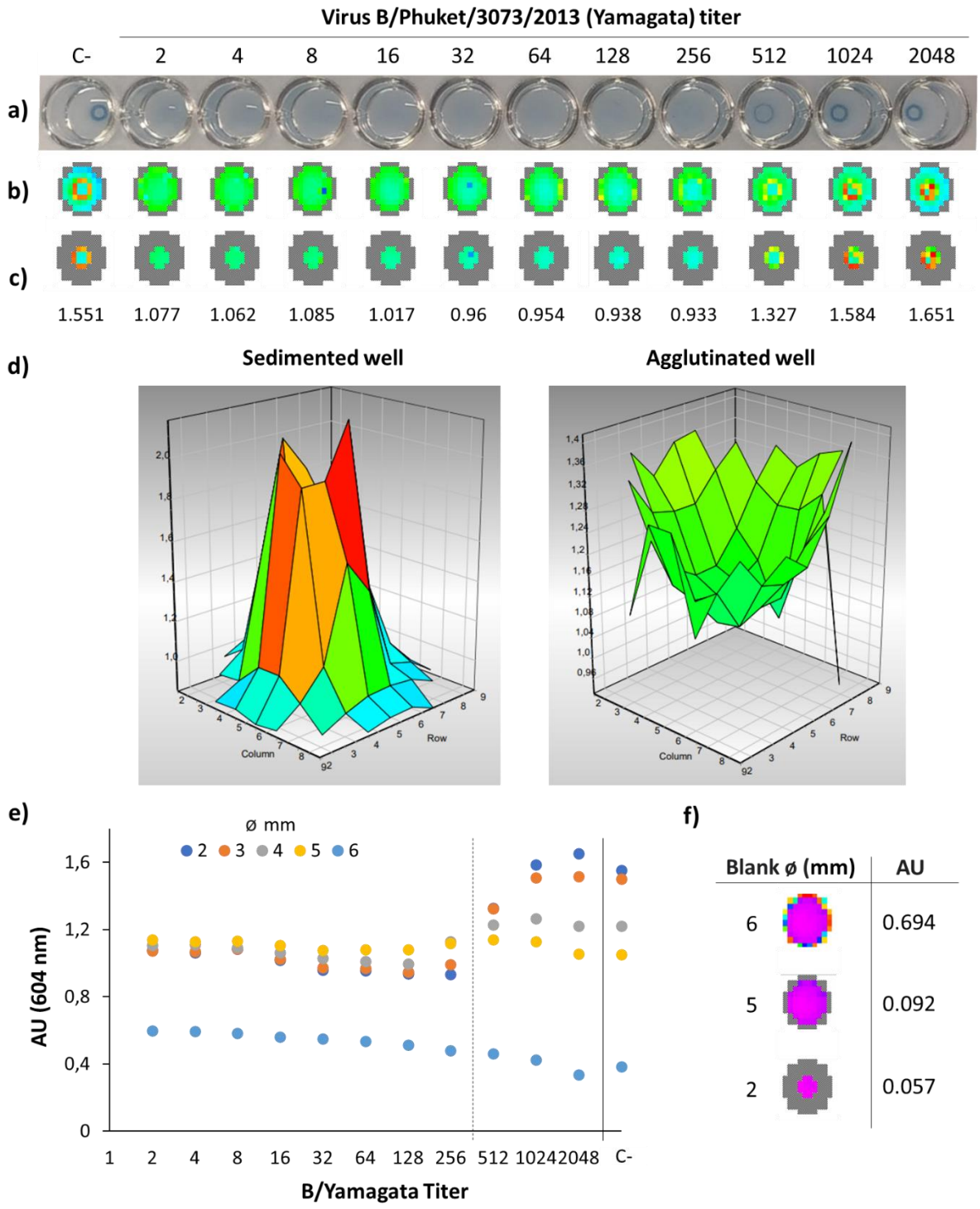

Figure 8.1 | SynA performed using 250 µg of synthrocytes/well and B/Phuket/3073/2013 as a reference virus. **a)** Image of the SynA pattern directly observed compared to the scan obtained by spectrophotometry for each well and an analyzed well ø area of either 5 mm **(b)** or 2 mm **(c)** to obtain the average absorbance for each well (values shown below in AU for 2 mm). **d)** 3D chart representation of the absorbance obtained for a sedimented well (negative control without virus) and an agglutinated well (2-fold virus dilution). **e)** Plot of the signals obtained for each well of the SynA and different well ø areas. The dashed line represents the agglutination titer determined visually (256). The filled line separates the negative control (synthrocytes without virus). **f)** Graphic representation of a scanned blank well (just PBS without synthrocytes) when the software analyses different well ø areas, with the average AU value obtained depending on the area analyzed.

The comparison between the image taken by the camera (Figure 8.1a) and the representation of the scanned values for each well revealed that 5 mm ø signals provided a full view of the usable scanned surface (Figure 8.1b). However, as previously discussed, a 2 mm ø was more useful to calculate the average values for each well (Figure 8.1c,e). Results show that the differences between agglutinated and non-agglutinated wells were registered correctly by the instrument and the circular synthrocyte sediments were noticeable even when the 2 mm ø was used to calculate the average absorbance values. Under these conditions, and even if all the wells produced significant signals due to the blue color of the synthrocytes, the average signal registered increased around 44% in the sedimented wells compared to the agglutinated ones. On the other hand, the virus agglutination titer obtained by visual interpretation (256) correlated with the one obtained using the automated plate reader. Moreover, similar to the naked eye assessment, we could observe that the sediment appeared gradually for decreasing virus concentrations, generating increasing average signals.

One of the problems when using the scan function was that the equipment bulb was in a fixed position and the plate was moved step-by-step to obtain the images of the different wells one-by-one. This resulted in agitation of the wells' content. Although the patterns produced by 3 µm synthrocytes were stable when resting on a surface, we did not know how the agitation would impact them, which was crucial to read a full plate. If the agglutination was not stable enough, particles would sediment and patterns would disappear before the final well was reached, producing false results depending on the well position in the plate.

When the plate of Figure 8.1 was read a second time, the agglutinated patterns were slightly affected, producing faint and wide halos in wells that did not display synthrocyte sedimentation in the first reading (Figure 8.2a and b). The truly sedimented wells also produced a tighter pellet at the bottom. This made more difficult to determine the agglutination titer with the naked eye. However, because the quantification in the second reading was also performed in the central area of each well, the average signal obtained was not affected. Figure 8.2c shows a comparison between the first and the second signals read, which were almost equal in the agglutinated wells. The sedimented wells were still detected, and the difference in signal between sedimented and agglutinated particles even increased up to 71%.

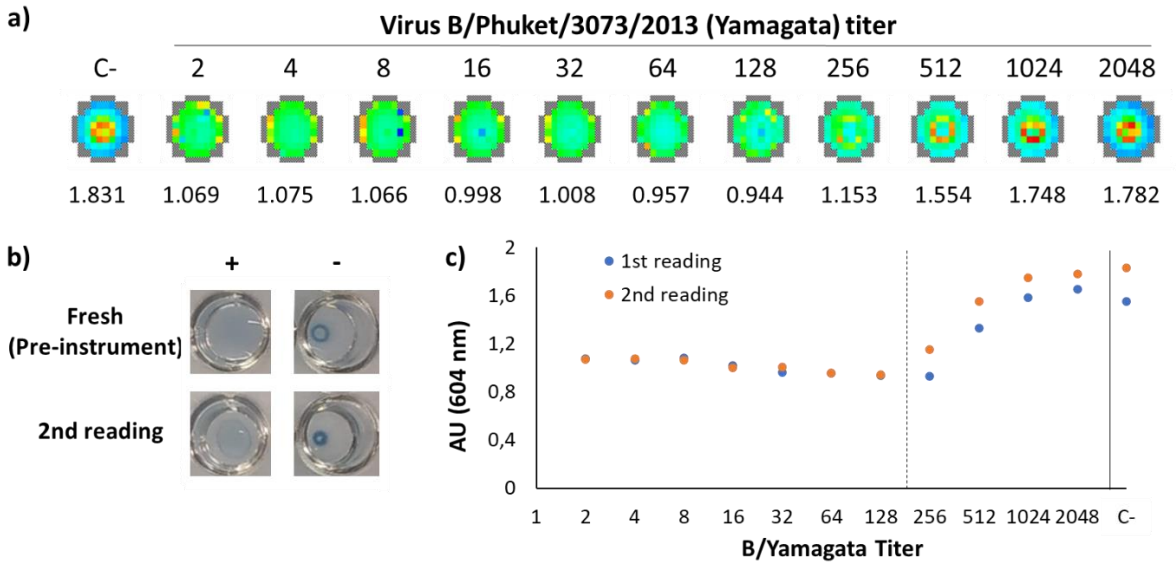

Figure 8.2 | a) Second scanning with a 5 mm ø of the SynA shown in Figure 8.1, after a previous full reading of the plate that produced agitation. Average absorbance values for each well were obtained using the 2 mm ø area previously defined and are shown under the wells scan. **b)** Image of an agglutinated and a sedimented well, fresh (before the first reading on the instrument) and after the second reading. **c)** Comparison of the signals obtained for each well in the first and the second read.

It is worth to note that when using 10 µm particles, the agitation produced by the automatic plate movement to take the images forced the sedimentation in all the wells, making them unsuitable for use in these types of automated settings. Nonetheless, the results obtained with 3 µm synthrocytes suggest that these patterns are stable enough to be read by automatic readers such as the ones used in the WHO CCs. Moreover, this feature could be useful in other applications that require a quantitative outcome, because agglutination patterns produced absorbances that increased proportionally to the concentration of the agglutinating agent. This should allow quantification of blind samples by interpolation in a calibration plot after the analysis of a single or few sample dilutions, compared to classical HA that requires the analysis of a whole dilution series.

8.2. Capillary-flow device for SynA quantification and objective reading

Even if RBCs could be substituted by synthrocytes in classical HA-like SynA assays, the method still entailed some drawbacks. Both HA and SynA depended on subjective outcome interpretation, which could cause some variability in the results reported by different users. Although introducing automatic readout instruments and software to analyze the plates would decrease this variability, it was still subject to the formation of an interpretable pattern. Moreover, HA and SynA did not provide a quantitative readout *per se*. Instead, a series of sample dilutions were tested to identify the minimum virus titer that resulted in RBC/synthrocyte agglutination. This increased the amount of sample and reagents necessary to perform the assay, as well as the analysis time. For these reasons, we decided to develop a microfluidic device able to perform SynA semi-automatically, producing a more objective pattern that could be easily quantified.

This work was performed in the context of a 5-month stay in Dr. Henry's laboratory, in Colorado State University (Colorado, USA). At that point, the hosting group was developing a technique based on microfluidic laminated devices made of low-cost materials.[249] These devices consisted of alternating layers of transparent polyester film (100 µm thickness) and double-sided adhesive (50 µm). Each layer displayed unique laser-cut features that, upon device assembly, formed microfluidic channels and chambers.[249,256,257] In this way, if a buffer/solution was injected in the device inlet, it flowed along the channels by capillarity, without any external pump or power source being needed. Furthermore, the pre-cut layers were manually and quickly assembled without any external equipment, which was suitable for fast prototyping and allowed for an easy scale-up of the technology as well.

For the development described in this section we used 10 µm synthrocytes coated with fetuin, due to our deep knowledge of this type of particles at that time and their cheap cost.

8.2.1. Device design optimization

We started the development of these devices based on the previous results of the hosting group, and therefore we decided to use the same materials for our device. The first step was to ensure that the capillary flow generated in this type of devices was strong enough to transport the microparticles along a microfluidic channel. For this, we designed a simple device comprising 2 layers of polyester film and a double-sided adhesive layer with the channel cut on it (Figure 8.3a and b). The device had an inlet at one end to allow the particles to enter the channel. At the other channel end, a fan-shaped filter paper acted as a passive pump to drive the flow and compensated for the decay in the flow rate observed in its absence in previous works.[258]

To test this device, a mixture of synthrocytes with PBS (250 µg of particles plus 10 µL of PBS) was pipetted in the inlet and the flow was monitored for 5 min. As can be seen in Figure 8.3c, most of the synthrocytes flowed to the end of the device, where they were retained by the paper filter. Even so, some synthrocytes still remained in the edges of the inlet, unable to enter the channel. This occurred because the sedimentation rate was higher than the speed at which synthrocytes were absorbed by the channel, which produced a considerable variation between devices. To solve this, the height of the channel was increased by substituting the 50-µm thick double-sided adhesive for another of 100 µm thickness. This improved the absorption capacity of the channel and made the particle mixture enter directly inside when dropped in the inlet. Once there, the capillarity force exerted on the buffer was enough to drag the particles along the channel. This simple design allowed us to optimize the diameter of the inlet required to hold all the liquid (5 mm ø), and the height (100 µm) and maximum length (25 mm) of the channel that sustained the flow successfully to its end.

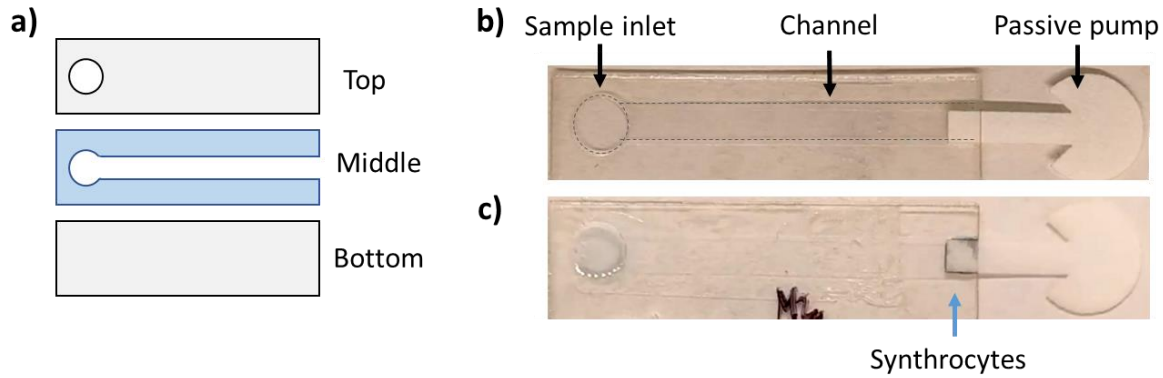

Figure 8.3 | a) Scheme of the different layers used for assembling the device. In grey, polyester film layers; in blue, double-sided adhesive layer. **b)** Image of the device with the channel indicated with dashed lines. **c)** Device after adding the particles in the inlet and letting them flow for 3 min. Most synthrocytes reached the end of the device, where the passive pump retained them. No visible particles remained in the channel, although some could be observed in the inlet.

In an attempt to distinguish between agglutinated and non-agglutinated flowing particles, we introduced a second fragment of filter paper (Whatman grade 4), this time inside the channel, that acted as a filtration unit (Figure 8.4a). In this case, synthrocytes were mixed with or without MAA lectin in a tube and were incubated for 5 min to induce agglutination. We decided to use lectin instead of the influenza viruses because the clumps obtained with lectin were bigger than with influenza viruses (Chapter 4.3), which could ease result interpretation during the development of this device. Once incubated, the mixture was transferred to the device inlet and was let to flow for 3 min. Figure 8.4b shows the difference in behavior between agglutinated and non-agglutinated particles. Non-agglutinated synthrocytes were able to flow through the paper to the end of the channel. Agglutinated particles, on the contrary, formed clumps bigger than the paper average pore size (~20-25 µm ø) that were retained at the start of the filtration unit, forming a colored line distinguishable by naked eyes.

The size and material of the filtration unit was optimized. We tested fiberglass paper, Fusion 5 and Whatman grade 1 and 4, with sizes between 1.25- and 5-mm in length. The best differentiation between agglutinated and non-agglutinated synthrocytes were obtained using a piece of Whatman grade 4, 2.5 mm in length, and therefore it was selected for subsequent experiments.

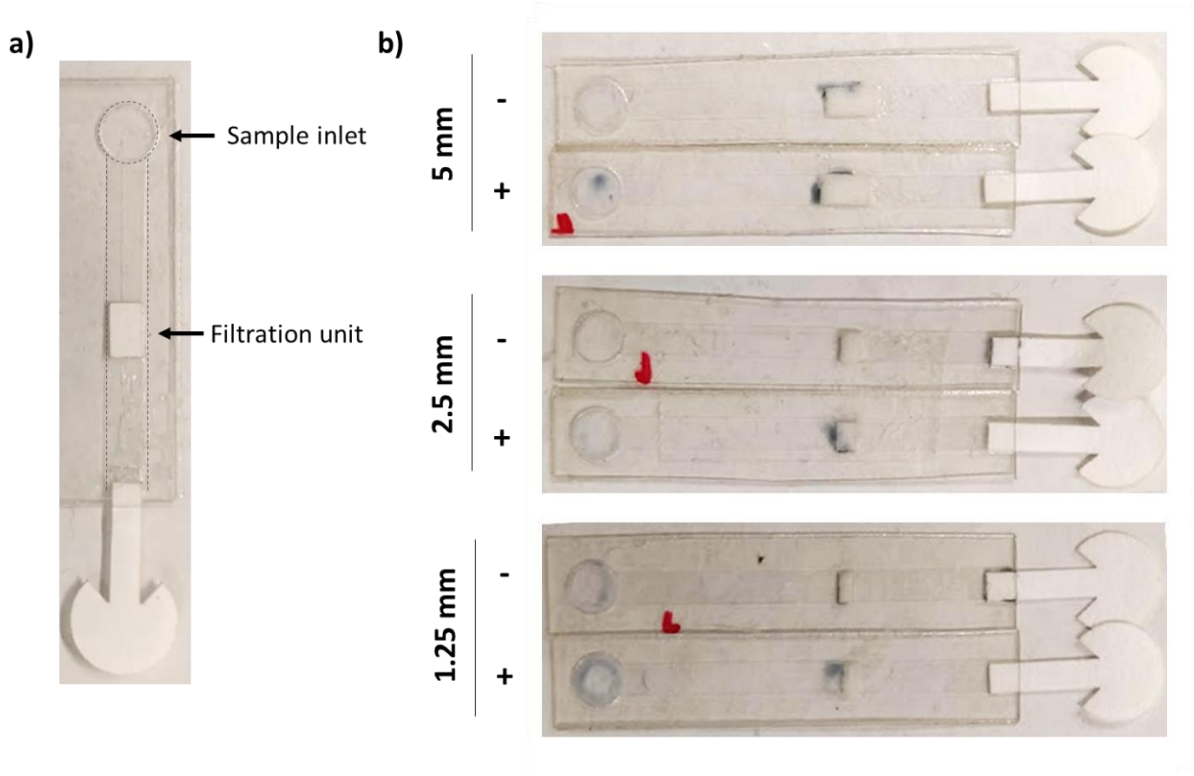

Figure 8.4 | a) Image of the device containing a filtration unit within the microfluidic channel, prior to its use. **b)** Optimization of the size of the filtration unit. A mixture of synthrocytes without (-) or with (+) 10 µg/mL of MAA lectin was added to the device after the 5-min incubation outside. Each pair of devices contained filtration units of different lengths (1,25, 2.5 and 5 mm). The biggest difference between agglutinated and non-agglutinated particles was observed when using the 2.5 mm pad.

8.2.2. Integration of synthrocyte-lectin incubation

Although the differences between agglutinated and non-agglutinated synthrocytes were always visible, the thickness of the line presented a high variability between experiments. This could be explained because the incubation of the particles with lectin was produced outside the device, in a microtube. When transferring this mixture to the device, some of the agglutinates were broken due to the pipetting, introducing variability in the results. The next step was to adjust the device design in order to carry the incubation on-chip.

In order to achieve this, we incorporated 2 symmetric curved channels that were placed at different levels of the device (L2 and L6 in Figure 8.5a). They displayed two inlets placed side-by-side in the assembled device and overlapped in their final section. Here, the two channels connected to a higher chamber that worked as a valve to control the flow (L3-L5 in Figure 8.5a). This valve was a modification of one previously designed by Jang.[249] The height of both channels was of 100 µm, and the chamber was approximately 300 µm high. After the chamber, both paths united in a single exiting channel (100 µm height) located in the bottom level, where the paper pump was connected.

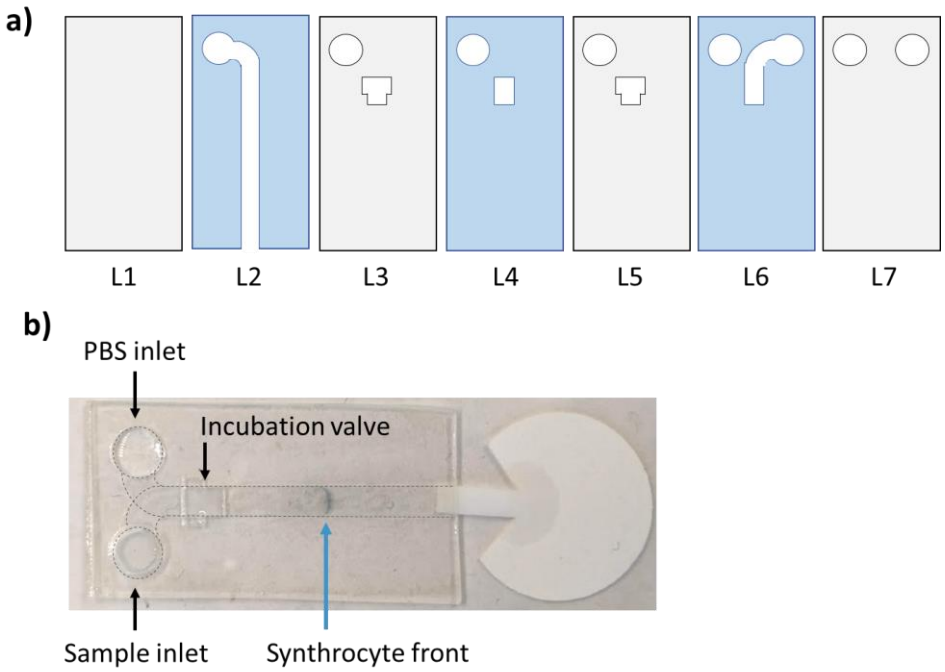

Figure 8.5 | a) Scheme of the different layers used for assembling the device. In grey, polyester film layers; in blue, double-sided adhesive layers. The bottom layer corresponds to L1, the top layer to L7. From L3 to L5 form the valve chamber, where combine the two symmetric curved channels (L2 and L6). Synthrocytes were added to the sample inlet, they flowed along the curved section of the channel in L2 until they reached the valve. Here, the sudden increase in height (from 100 to 300 µm) interrupted the capillary flow. After PBS addition to the PBS inlet (L6), this filled the valve chamber and the mixture resumed flow along the exiting channel (L2) to the end of the device. **b)** Image of the device after the PBS addition. The synthrocytes (and liquid) front moved along the exiting channel to the passive pump, which absorbed the buffer.

For the assay, fetuin-synthrocytes were mixed with MAA lectin and 10 µL were directly transferred to the sample inlet. The mixture moved forward due to capillarity until it reached the chamber, where the abrupt change in height stopped the buffer. After 5 min of incubation, 30 µL of PBS were added to the PBS inlet. When the new buffer reached the chamber, it filled the gap completely and allowed the flow to continue forward to the single exiting channel. This ended in the fan-shaped paper pump that provided enough suction to keep the flow constant. Results showed that the valve chamber was able to stop the flow for at least the 5 minutes required to perform an incubation. After PBS addition, the particles flowed across the chamber and were able to continue along the exiting channel to the end of the device (Figure 8.5b).

8.2.3. Laminated device final design

Once we confirmed that the incubation step could be performed inside the device by exploiting a valve chamber and that a paper-based filtration unit was enough to separate agglutinated and non-agglutinated synthrocytes, we fused both features in a single device of enhanced design. This design included 2 inlets, one exit and 3 channels (Figure 8.6a and b). The top and bottom channels connected with the PBS inlet, while the middle channel was attached to the sample inlet. The three channels joined at the valve chamber, which was approximately

550 µm in height. The bottom PBS channel was added to increase the total height of the valve chamber and reduce potential leakages during incubation. Moreover, it prevented backflow of the particles and facilitated driving them to the exiting channel and to the detection zone.

This detection zone was located in the exiting channel, which ran in the bottom layer of the device (L2, height of 100 µm). It contained a paper filtration unit (Whatman grade 4, 2.5 mm long) where agglutinated and non-agglutinated particles were separated. At the end, as in the previous designs, there was a passive paper pump fan-shaped.

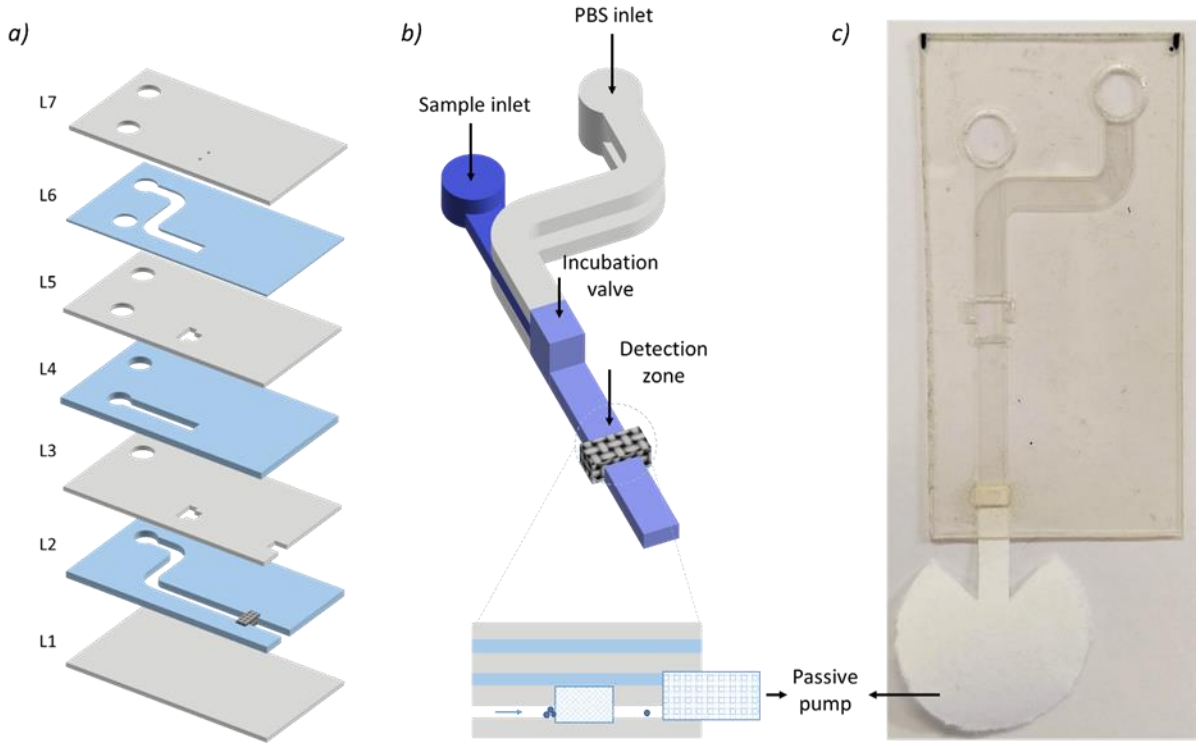

Figure 8.6 | a) Exploded view of the device, which was produced by laminating 4 polyester film layers (grey) and 3 double-sided adhesive layers (blue) previously cut, creating the 3D microfluidic network represented in **(b).** A paper filter in the exiting channel (L2) acted as the filtration unit and detection zone (dark grey square) and a paper passive pump connected at its end maintained the flow during the whole assay. (Insert) Cross-section of the detection zone. **c)** Front image of the fully assembled capillary-driven device.

During the development of this design, we optimized the distance between the valve chamber and the detection zone (20 mm) in the exiting channel and the length of the PBS channels to keep the assay time under 10 min. Moreover, two small holes (0.05 mm ø) were added at the top layer (L7) of the valve chamber. These holes allowed the air to exit the device (when it was pushed by the solution front), which created a more homogeneous flow and produced a uniform synthrocyte front across the whole detection zone, improving the colored line visualization.

8.2.4 Differentiation of lectin-agglutinated synthrocytes in the device

In the final device architecture, the assay was initiated when a lectin and synthrocytes mixture was pipetted into the device (10 µL) through the sample inlet. The mixed solution flowed along the middle channel and stopped at the incubation valve entrance due to the difference in the channel height. Thus, the lectin-synthrocytes mixture was incubated for 5 min in the middle channel, which acted as an incubation chamber just upstream from the valve entrance, to promote particle agglutination in case of the presence of MAA lectin. Then, PBS was added (60 µL) to the PBS inlet and the flow was resumed across the valve chamber and along the exiting channel. Here, the paper filter at the detection zone separated agglutinated from non-agglutinated particles. Free particles flowed through the paper pores, while agglutinated synthrocytes were retained, forming a colored band that was detectable with the naked eye (Figure 8.7a). The full workflow of the device took 10 min until the buffer flowed completely to the paper pump and the synthrocytes band appeared. Finally, a picture of the detection zone was taken and analyzed through image analysis using an open source software (ImageJ).

One of the parameters that had to be optimized to guarantee optimal performance was the number of particles required to obtain a clear line for the agglutinated beads. We tested a range comprising from 100 µg to 375 µg of synthrocytes per sample. Using 175 µg produced well defined bands in agglutinated synthrocytes without impacting the negative control. Under these experimental conditions, although part of the single/non-agglutinated beads remained in the incubation channel, those reaching the detection zone flowed efficiently through it and reached the passive pump. Compared to the amount of particles required to perform SynA in a microtiter plate, this entailed a 53% reduction. We also optimized the amount of PBS required to fill the channels and the valve chamber, testing a range between 50 and 100 µL. We established that 60 µL was the ideal volume to fill both cavities simultaneously.

Once the device and experimental conditions had been optimized, we studied if the system could provide quantitative results. In order to do this, we employed serial dilutions of lectin (ranging from 1 to 100 µg/mL) and mixed them with 175 µg of fetuin-synthrocytes (3.5 µL from the stock solution), to obtain a final volume of 30 µL. 10 µL of each mixture were then transferred to the device and the workflow was started as described above. Figure 8.7b shows how agglutinated synthrocytes formed clumps that could be visually observed in the incubation channel. As expected, the size of these clumps was proportional to the lectin concentration used for the agglutination. The flow produced by the subsequent addition of PBS was enough to push those agglutinates to the detection zone.

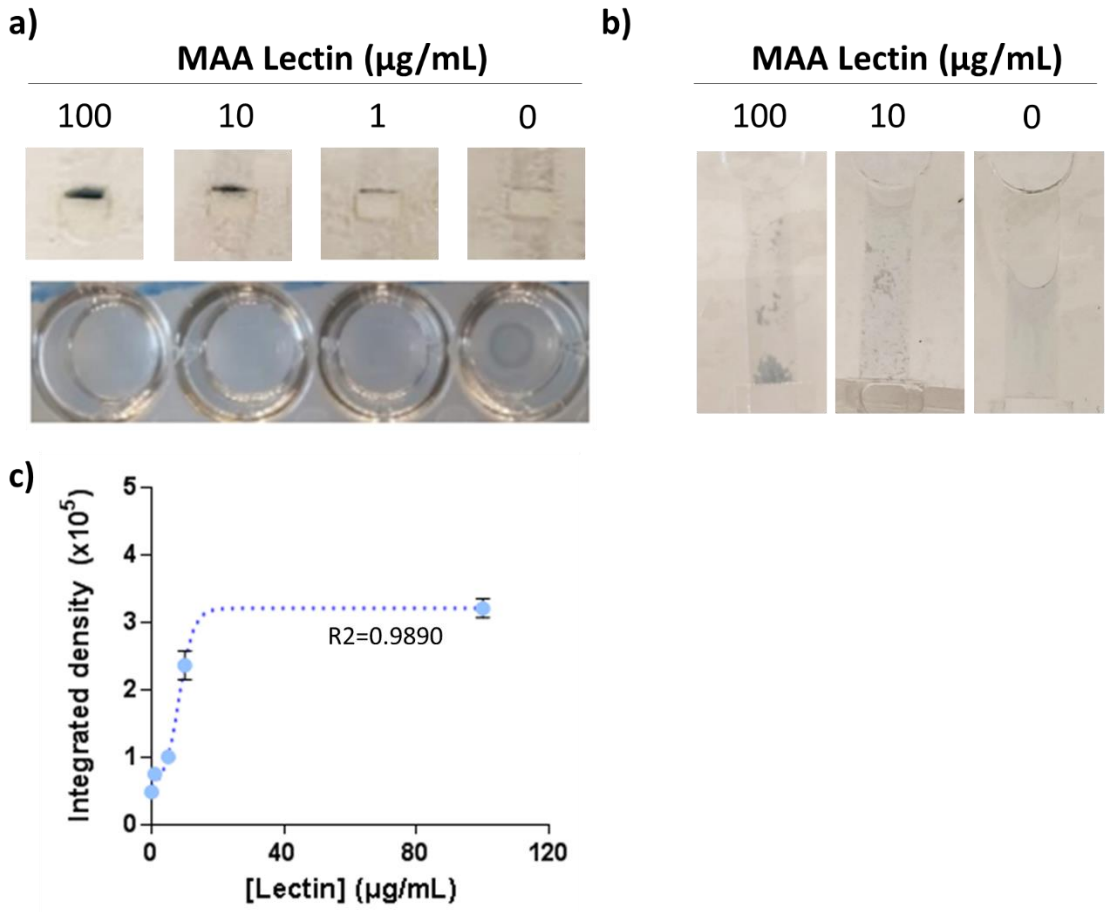

Figure 8.7 | a) Comparison between the patterns formed by fetuin-synthrocytes in the presence of different concentrations of an agglutinating lectin either in the device (top) or in a 96-well plate (bottom). The device displayed a sensitivity similar to the original technique, but provided a semi-quantitative readout. **b**). Incubation channel just after addition of PBS in the PBS outlet, when the front resumes the flow. Clumps formed by agglutination of particles during the incubation in the presence of lectin can be observed. **c**) Quantitative interpretation of the agglutination bands obtained for increasing concentrations of lectin after their image analysis (n=2). Calibration curve plotting band color density versus lectin concentration (integrated density = grey mean value x area). Data fitted with a 4PL regression.

After using the device, images of each detection zone were obtained and analyzed using ImageJ software. The intensity of each image was analyzed following the protocol described in Section 3.11.4 As can be seen in Figure 8.7a, the intensity and width of the band was proportional to the lectin concentration in the initial mixture, and it could be observed even in concentrations of 1 µg/mL. This sensitivity was similar to that obtained performing the classical SynA assay in a 96-well plate. Figure 8.7c represents the data obtained after quantification of band color intensity. The device presented signal saturation at the highest concentration of lectin tested. This was attributed to the limited amount of particles in the device. This is, if a certain concentration of lectin produced agglutination of most of the particles, higher lectin concentrations did not increase bead accumulation in the paper filter. Furthermore, since the filter pores had a diameter of approximately 20-25 µm, once the clumps had a size of 3-4 particles/clump they were already unable to pass through them and larger clumps produced similar patterns.

8.2.5. Quantification of virus-agglutinated synthrocytes

After confirming the performance of the capillary device to detect lectin-driven synthrocyte agglutination, quantification of virus A(H1N1) was attempted. Fetuin-synthrocytes were mixed with increasing concentrations of virus A/New Caledonia/20/99 and were directly transferred to the device, where the process continued as described in the previous section. Here, particles agglutinated in the presence of high concentrations of virus did not form clumps as large as the lectin-induced ones. This was consistent with the observations by microscopy, which evidenced that virus-agglutinated synthrocytes clustered in small groups (2-3 particles each) but were not clumped.

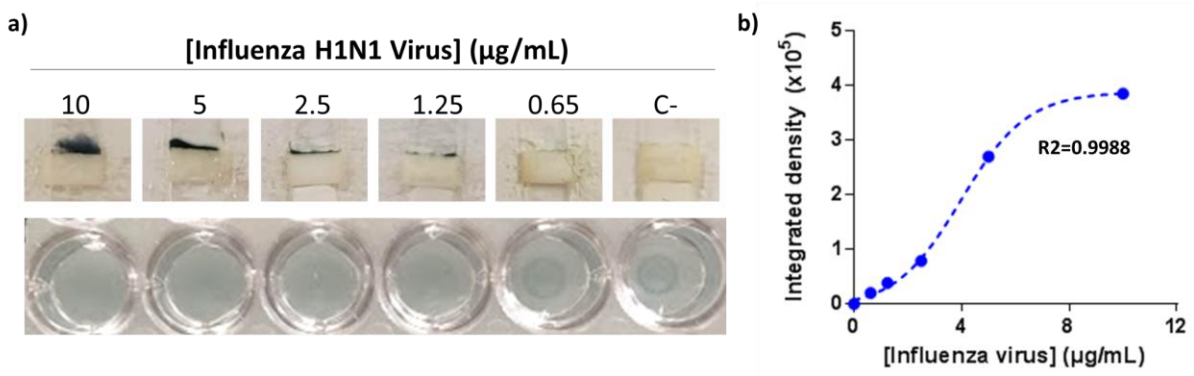

Figure 8.8 | a) Comparison of the patterns formed by synthrocytes in the presence of different concentrations of virus either in the device (top) or in a 96-well plate (bottom). The color and thickness of the colored bands formed by agglutinated synthrocytes in the device (top) are proportional to the concentration of influenza A(H1N1) present in the sample. The device displays currently a sensitivity similar to that of the original plate-based technique (bottom) but requires less reagent and entails little manipulation by the user. **b)** Quantification of the agglutination bands obtained in (a) after image analysis. The calibration curve plots band color density versus A(H1N1) concentration (integrated density = grey mean value x area) fitted with a 4PL regression.

Influenza-induced bands could be detected by the naked eye at virus concentrations down to 1.25 µg/mL, which was similar to the lowest concentration that could be observed in the plate-based assay (Figure 8.8a). However, the volume of sample required to obtain the results in the chip was approximately 6 times lower. Therefore, the virus could be detected down to 10 ng/device by visual inspection, while in the plate this limit was of 31.25 ng/well.

When color density of the bands was analyzed using the ImageJ software, the LOQ improved to 5.68 ng/device (0.71 µg/mL). Moreover, quantification of the bands was proportional to the concentration of influenza virus A(H1N1) present in the sample, which allowed producing a calibration curve (Figure 8.8b).

8.2.6 Virus quantification in spiked culture samples

Finally, device performance was evaluated in culture medium spiked with known concentrations of A(H1N1). This medium was RPMI supplemented with 0.5% of fetal bovine serum (FBS), which was traditionally used in our center to culture influenza viruses in MDCK-

SIAT1 cells. The aim of this experiment was to assess if the device could be used to quantify influenza virus in cultures directly, without using a serial dilution.

For these experiments, synthrocytes were custom-dyed as described in Section 3.5 to increase the color and improve the visualization of the particles in the device. We continued using 10 µm beads coated with fetuin for this proof-of-concept.

We first obtained a calibration curve in culture medium, which was a significantly more complex matrix than the PBS employed in previous experiments, to evaluate the matrix effect. Figure 8.9a shows the calibration curve obtained in medium compared to the previous one in PBS. As can be seen, the integrated density registered increased in average 19% for all the points evaluated except the negative control, which increased 40% ($0.03x10^5$ integrated density for PBS vs $0.048x10^5$ for the medium). This was attributed to the use of the custom-dyed particles, which had more color intensity and made the colored bands more visible. This suggested that the channels of the device and the time required to carry the assay could be shortened when using custom-dyed particles (because less PBS was enough to push sufficient synthrocytes to be visualized in the detection zone), or that the number of particles could be decreased, potentially reducing the cost of the assay. Nevertheless, more optimization was required before changing the defined parameters or the geometry of the device, which could not be afforded at this time of the development.

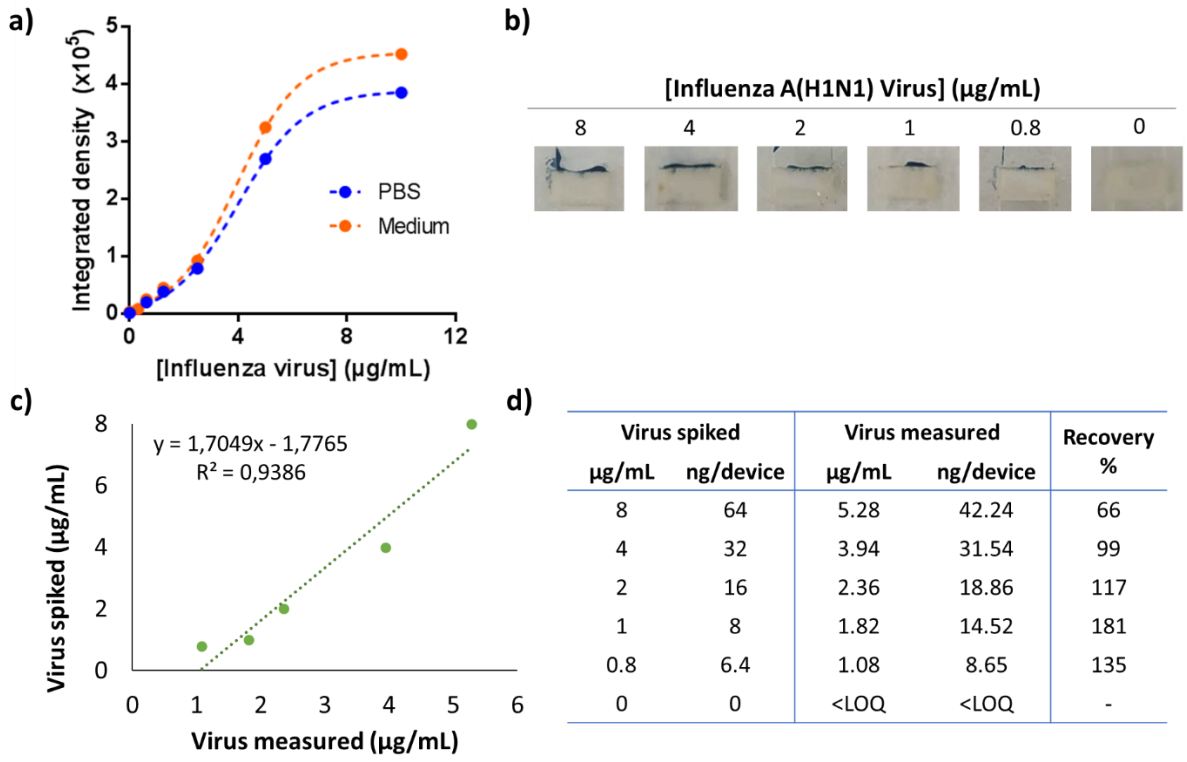

d)

Virus spiked		Virus measured		Recovery
µg/mL	ng/device	µg/mL	ng/device	%
8	64	5.28	42.24	66
4	32	3.94	31.54	99
2	16	2.36	18.86	117
1	8	1.82	14.52	181
0.8	6.4	1.08	8.65	135
0	0	<LOQ	<LOQ	-

Figure 8.9 | a) Comparison of the calibration curves obtained in virus-spiked medium using custom-dyed particles (in orange) and in PBS using commercially-dyed beads (in blue). **b)** Images of the bands generated in the detection zone for 5 spiked blind samples. **c)** Correlation between the concentration of virus spiked and that measured with the device. **d)** Summary of the quantification obtained for all the spiked samples compared to the expected values, with the concentration and the total amount of ng quantified in each device.

Besides this, using the culture medium did not affect significantly the device LOQ. Visual interpretation remained similar to that obtained with PBS (LOQ 1.25 µg/mL), as was the LOQ when analyzed using the ImageJ software (0.75 µg/mL, equal to 5.96 ng/device).

Next, we processed 5 different spiked blind samples displaying concentrations of viruses ranging between 0.8 and 8 µg/mL. The bands obtained for each sample can be seen in Figure 8.9b. These bands were analyzed with ImageJ as before and the values obtained were interpolated in the calibration curve previously obtained in culture medium. The concentration of virus spiked and measured in each sample was then compared, as shown in Figure 8.9c and d. Results showed correlation between the expected and the obtained values, except for the sample of 1 µg/mL for which virus recovery reached 180%. This difference could be explained because in this specific device the synthrocytes did not flow homogeneously through the whole channel width, producing a wider band in the center of the channel, which resulted in signals unusually high. Nevertheless, the correlation in the remaining samples was acceptable, showing that this device could be used to directly quantify influenza A(H1N1) virus through SynA assays.

8.3. Conclusions

Chapter 8 has shown two strategies to facilitate SynA performance and interpretation.

On the one hand, results obtained when reading 3 µm synthrocyte patterns using a microtiter plate reader suggest that these patterns are stable enough to be read by the automatic readers currently used in WHO CCS. Furthermore, we demonstrated that synthrocyte patterns produced absorbance proportional to the concentration of the agglutinating agent, and therefore they could be analyzed in a quantitative way after studying just one or few sample dilutions followed by calibrate interpolation.

On the other hand, we achieved SynA automation using a low-cost laminated device. One of the advantages of using this device was that the amount of sample and synthrocytes needed was considerably decreased compared to carrying SynA in a microtiter plate. With this low-cost device, SynA could be performed in <10 min, with little user handling. Moreover, it reached an LOD of 5.68 ng/device and enabled straightforward virus quantification based on interpolation in a pre-existing calibration curve.

One of the possible applications for this device could be to monitor the growth of influenza viruses in *in vitro* cultures, for example during production and characterization of vaccine candidate viruses or manufacturing of virus-based vaccines. Nevertheless, further research will be required to develop completely functional devices. For example, future development should include incorporating pre-loaded reagents to the device to facilitate handling further. This includes the particles, which could be stored inside the device lyophilized, and PBS, so that the user would only require to add the sample, easing the handling of the device.

Chapter 9

Alternative applications

Chapter 9. Alternative applications

Although synthrocytes were initially developed with the sole purpose of substituting RBCs for influenza virus surveillance, the results obtained during their development opened the door to other potential applications, especially taking into account their possible quantitative read out using spectrophotometers (Chapter 8).

One of the main advantages of synthrocytes is their tuneability. In other words, synthrocytes' coating can be modified to display selected receptors on the surface. Albeit these receptors need to meet certain characteristics concerning their molecular weight, charge, and chemical structure, which have to be similar to the ones described in the previous chapters, this means that we could potentially link on the surface receptors for any other target.

Agglutination techniques are well-known assays used in many settings. In all cases, they involve the agglutination of particles, such as bacteria, RBCs or latex particles. Some of these assays are designed to detect antigens from diverse pathogens and contribute to disease diagnosis. For example, Ab-coated particles agglutinate in the presence of their target antigen, which can be visualized employing glass slides to detect leishmania or malaria.[259,260]

Other agglutination assays are designed to determine the presence of specific Ab in patients' sera (for example after infection). These serological assays are faster and cheaper than ELISA or CLIA, and are suitable for point-of-care testing due to their portability and reagent stability. Most of them use latex particles coated with selected antigens to elicit the specific binding of targeted Ab. However, some efforts have been made to substitute them by cheaper particles or yeast-displayed ligands.[261]

In this chapter we will discuss two alternative applications that we explored to demonstrate the versatility of SynA assays. In the first one, we will prove that synthrocytes can be coated with Ab to recognize biomarkers distinctive of infectious diseases, such as malaria, and will compare them to other particle-based methods developed in the laboratory.

In the next section, we will show a proof-of-concept of a fast and semi-quantitative SynA assay to detect anti-SARS-CoV-2 Ab using spike-coated synthrocytes. As it will be shown, the assay allowed the classification of clinical samples depending on their Ab titer using a small volume of patient diluted serum. This system was developed in collaboration with Biosystems and was optimized and evaluated using real COVID-19 samples kindly provided by them.

9.1 Malaria Ag detection using Ab-coated synthrocytes

There are many bead-based agglutination assays currently used for diagnosis.[262] Most of them make use of latex particles which are coated with Ab against an Ag of the target microorganism. In the presence of the antigen, and generally with some agitation required, particles agglutinate. The agglutination of colored particles is often determined in tubes, on glass slides or on white cards, either by the naked eye or under an optical microscope. When the particles are white or of a clear color, the assay may have to be performed in a colored card to facilitate its reading. In all cases, particle agglutination impels changes in the optical

properties of the solution, which can be also evaluated spectrophotometrically (for instance by measuring the change in turbidity). The main limitation of agglutination tests is their susceptibility to produce false-negative results in the presence of high concentration of target Ag in the samples, in which is known as the prozone phenomenon.

Malaria is a disease caused by parasites of the genus *Plasmodium*, which are transmitted by the bite of infected female *Anopheles* mosquitoes. The gold standard for confirming malaria infections is microscopic examination of blood smears, although it requires an experienced microscopist and is a time-consuming process.[263] Rapid diagnostic tests (RDTs) were developed to solve these issues and ease the diagnosis in the field. For example, immunochromatographic-based RDTs detect *Plasmodium* antigens in whole blood with very little handling for the user, generating results in <30 min. Nevertheless, RDTs display limitations as well, such as high variability between production batches and producers, insufficient detection limits, qualitative yes/no response, and subjective result interpretation.

In an attempt to give response to these drawbacks, Polpanich and colleagues developed an agglutination assay for malaria detection using polystyrene particles coated with *Plasmodium* Ag and monoclonal or polyclonal Ab to *Plasmodium falciparum* heat shock protein 70[259]. Patient plasma was mixed with the modified particles on a glass slide, agitated for 2 min and agglutination was microscopically analyzed. The authors claimed a sensitivity of 90% and a specificity of 80%, although the number of samples analyzed was limited. Moreover, the degree of agglutination observed did not correlate with sample parasitemia.

Here, we decided to test a likewise alternative application for synthrocytes, in which they were used similarly to the traditional agglutination assays available for diagnosis. In order to do so, we targeted the *Plasmodium* lactate dehydrogenase (pLDH), an enzyme secreted by all the human-infecting *Plasmodium* species. pLDH is being increasingly employed as a malaria diagnostic biomarker in commercially available tests, which used to target only *Plasmodium falciparum* histidine rich protein (HRP2). pLDH has also been proposed as a potential biomarker to monitor patient response to treatment, in order to prevent the selection of treatment-resistant parasites. Although developing an agglutination assay was not innovative, this new synthrocyte application was interesting because the agglutination was produced through the interaction of the Ab-coated particles with multimeric protein antigens (instead of a full viral particle with multiple receptors on the surface).

For this assay, we coated the particles with an Ab to pLDH, which had been selected for a previous work in our group to detect malaria in blood samples.[264] Specifically, the team had developed an immunoassay for pLDH detection using MP coated with these Ab,[265,266] which could be used as the reference method to evaluate the sensitivity of the Ab coated-synthrocytes.

We decided to use commercial 10 µm Sicastar blue particles, which were the ones employed for influenza detection at that time (the custom-dying protocol had not been developed yet). The protocol employed for the conjugation was equal to the one used for influenza bioreceptors, through glutaraldehyde amino homo-cross linking reaction, but using 25 µg of Ab per conjugation, the same amount used in MP protocols (Figure 9.1a). It is important to

mention that the batch of commercial particles used in these experiments (shared with Section 4.7) was particularly faint and the halos were more difficult to observe.

Then, SynA was performed with the Ab-conjugated particles (Ab-synthrocytes) in the presence of increasing concentrations of recombinant *Plasmodium falciparum* LDH (PfLDH). Even if pLDH is a tetramer in the nature, the recombinant PfLDH used in these experiments was a dimer according to the provider's technical information. Again, the protocol employed was the same as for influenza agglutination assays. To sum up, pLDH serial dilutions were prepared in PBS, starting at 500 ng/mL, and were incubated in the U-shaped wells of a plate (50 µL/well) for 10 min with Ab-synthrocytes (375 µg particles/well).

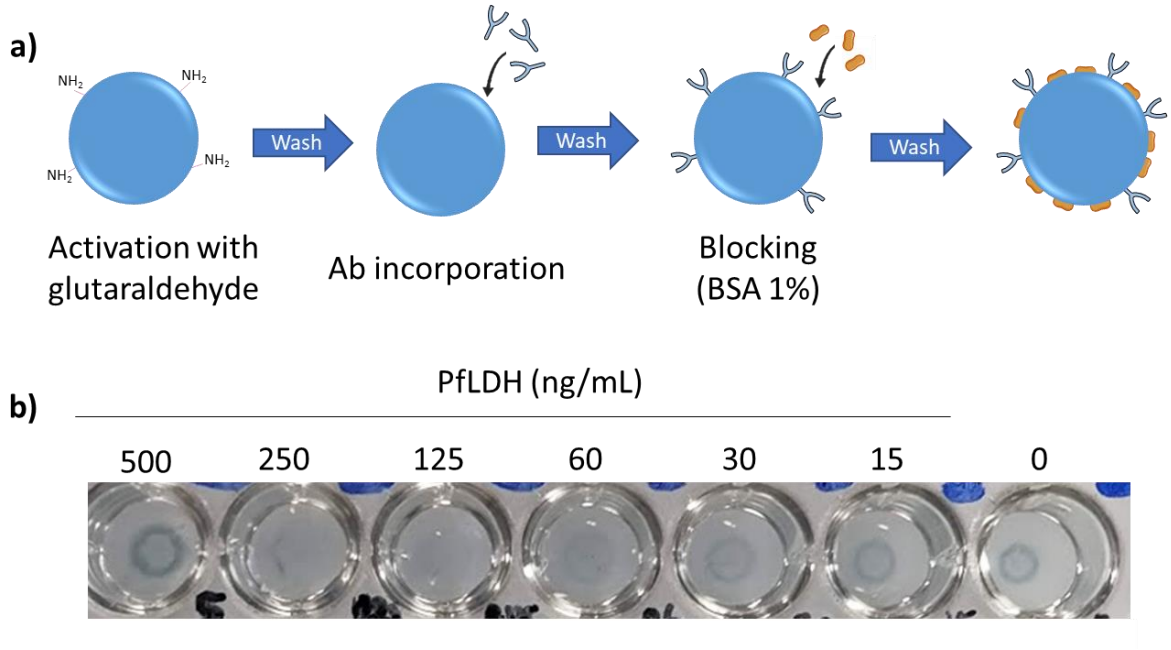

Figure 9.1 | a) Scheme of direct incorporation of anti-pLDH Ab (25 µg) on the surface of the commercial 10 µm amino-beads through amino-homocrosslinking. **b)** Sedimentation of Ab-synthrocytes in U-shaped wells in the presence of increasing concentrations of PfLDH.

As can be seen in Figure 9.1b, in this first attempt, Ab-synthrocytes detected PfLDH at concentrations down to 125 ng/mL. It is important to note that at high Ag concentrations (such as 500 ng/mL), sedimentation reappeared forming a halo susceptible to be interpreted as a false negative result. This could be explained by the prozone effect mentioned earlier. Here, the excess of Ag in the sample presumably capped all the receptors exposed on the surface of the particles, preventing the formation of the Ag-Ab lattice necessary to produce visible agglutination.

The narrow range of PfLDH concentrations that could be detected suggested that the amount of Ab on surface was insufficient. To confirm that the change in sedimentation was induced by Ag-Ab interaction and to increase the assay sensitivity, we modified the quantity of Ab present in the surface of the particles. For this, synthrocytes were conjugated with different amounts of Ab and then evaluated by SynA (Figure 9.2a). When the Ab concentration was doubled, agglutination occurred even at concentrations of 15 ng/mL of PfLDH, showing almost a 10-fold increase in sensitivity. This confirmed that the initial 25 µg of Ab employed were not

enough to completely coat the large surface area of synthrocytes. On the other side, when the quantity of Ab was diminished, PfLDH was not detected below 250 ng/mL, confirming that the agglutination was specifically induced by the Ag-Ab interaction.

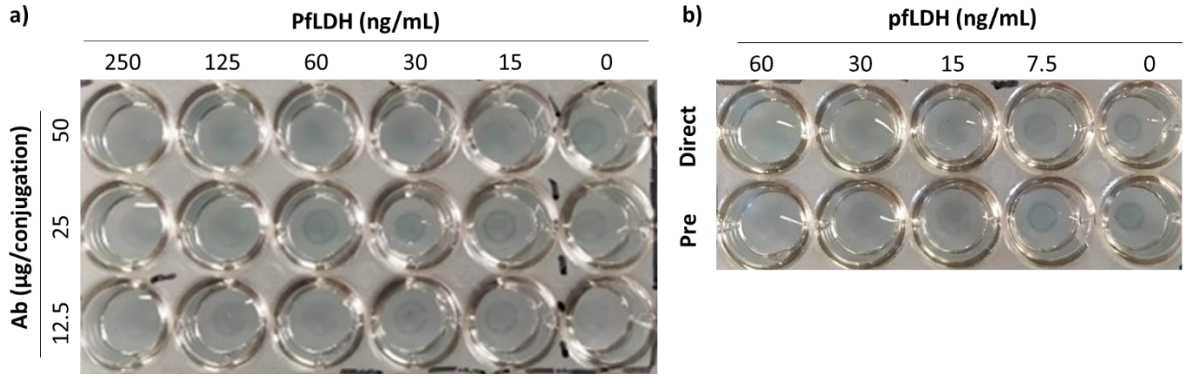

Figure 9.2 | a) SynA performed in U-shaped wells with serial dilutions of PfLDH and synthrocytes conjugated with different amounts of Ab. Ab-synthrocytes improved their performance when the concentration of Ab was increased. **b)** Sedimentation of Ab-synthrocytes directly incubated in the wells with different concentrations of PfLDH (top) or after a 15-min pre-incubation step carried in agitation in tubes (bottom).

Because the interaction Ag-Ab is more stable than that produced between influenza and SA, and in case it required also more time to take place, we studied if pre-incubation of Ab-synthrocytes with PfLDH-containing samples could amplify agglutination and enhance detection. Performing a pre-incubation step, in which synthrocytes were kept in agitation for 15 min in tubes with PfLDH prior to their transfer to the plates, did not improve synthrocyte performance (Figure 9.2b). This suggested that PfLDH recognition occurred fast, which is consistent with our previous observations.[264]

Compared to the performance of the same Ab in the MP-based sandwich immunoassay reported previously by our group, which reached LODs of 0.12 ng/mL for colorimetric detection or even 0.02 ng/mL for chemiluminescence detection using an enzymatic signal amplifier,[266] the obtained results fell short. Despite their different size (i.e., 1 µm and 10 µm diameter for Ab-MP and Ab-synthrocytes, respectively), the total surface exposed for each type of particle was larger in synthrocytes, considering the number of beads used per sample (75.4 mm^2 of surface/sample for MP vs 124.9 mm^2 of surface/sample for synthrocytes). The amount of Ab needed to produce the conjugate was also higher (and costlier) in the case of synthrocytes. Therefore, we concluded that the limited performance of synthrocytes was not related to the theoretical maximum number of Ab potentially exposed at the surface. Nonetheless, particle surface properties and Ab chemical incorporation path differed in the two cases, which was not studied additionally. Taking into consideration the differences between the two methods, we expected a decrease in the sensitivity when using synthrocytes due to a considerable reduction in the assay time, from 40 min (plus washes) with MP to just 10 min with Ab-synthrocytes. Moreover, SynA results were obtained directly by the naked eye in a single 10-min step, instead of using a spectrophotometer to measure absorbance readouts produced in the multi-step MP-assay employing enzymatic signal amplification.

On the other hand, these experiments were carried in PBS, instead of in diluted blood or serum that could interfere to a larger extend in result interpretation, and assay sensitivity was insufficient to diagnose malaria in patients with low parasite titers. Nevertheless, the results obtained showed that production of Ab-coated synthrocytes was feasible and that Ab-synthrocytes agglutinated and changed their sedimentation in the presence of multimeric protein targets. This effect was possible even when the Ag was just a dimeric protein and not a complex structure such as a complete pathogen. Consequently, and even if this application was not developed additionally at that time, the results confirmed that synthrocytes could be helpful as a fast diagnostic tool.

9.2 Detection of anti-SARS-CoV-2 Ab through spike-coated synthrocytes

Serology testing is often employed for infectious disease diagnosis and surveillance. Detecting Ab against specific pathogens can be used to assess disease prevalence in epidemiological surveys, for screening donors suitable for plasma donation, and to study the changes in individual immunological response over time,[267] among others.

Serology tests are carried regularly to evaluate the efficacy of the annual flu vaccine to elicit the appropriate immunological response and have been used extensively for SARS-CoV-2 surveillance. Since the emergence of the SARS-CoV-2 virus in 2019, serological tests have played a key role in assessing both vaccination effectiveness and the immune status of the population, and also to investigate disease prevalence in different geographical areas.[268]

Multiple serological test formats have been developed to meet this global demand. The most common ones comprise ELISA and fast lateral-flow immunoassays. ELISA-based assays are highly sensitive, but take from hours to days to deliver results and require centralized laboratory facilities and equipment not widely available.[268] Lateral-flow immunoassays, on the contrary, provide results in minutes and are simple to use, but their clinical performance is low compared to ELISA-based assays[269–272] and their costs still represent a concern for low-income countries.

To solve this issue, diverse groups developed assays to detect Ab against SARS-CoV-2 based on agglutination methods. Generally, these tests are performed in just minutes without complex equipment and offer an acceptable sensitivity for POC testing.[162,188,273] Furthermore, agglutination serological assays are isoform independent, meaning that they can produce agglutination in the presence of IgG, IgM, IgA or a combination of all of them, which could increase sensitivity compared to specific IgG or IgM ELISA-based assays. Moreover, although agglutination assays are usually read by the naked eye, the versatility of this technique makes it possible to use automated platforms for high-throughput screening in clinical laboratories as well.

Most of these tests detect IgG and/or IgM against the spike or the nucleocapsid proteins of SARS-CoV-2 virus. For example, Townsend and colleagues developed an HA test for rapid detection of Ab against spike protein of SARS-CoV-2.[274] They used a fusion protein formed by the Receptor Binding Domain (RBD) of the SARS-CoV-2 spike protein and a nanobody that recognized GYPA, which provided straightforward attachment of this construct on RBCs.

Thus, RBD was exposed in the RBCs surface and could be recognized by anti-spike Ab. If Ab were present in the sample, they bound the RBD-exhibiting RBC and formed a lattice that produced visible agglutination. This method achieved 90% sensitivity and 99% specificity at a reduced cost and in 1 h of assay time, although it did not comply the requirements of the Infectious Disease Society of America[275] for this type of tests. A similar strategy was attempted by Kruse,[276] who used two different fusion proteins containing RBD sequences in one end and a single-chain variable Ab fragment that bound RBCs in the other. While some agglutination was detected within 5 min of incubation with the RBCs, the final assay still required 1 h to provide reliable results.

Other approaches involved using latex particles directly coated with recombinant spike RBD or the nucleocapsid protein.[162] For example, Esmail and colleagues produced an assay with a sensitivity of 98% and a specificity of 100% in just 2 minutes of incubation with the plasma samples, but they required prior sample heat-inactivation for 30 min.

In this section, we will present a proof-of-concept of the potential use of synthrocytes for specific Ab recognition using SARS-CoV-2 as a model. All this experimental section has been performed thanks to the contribution of Biosystems, which kindly provided the proteins and samples used here.

9.2.1. Optimization of SARS-CoV-2 spike conjugation on the particles: production of spike-synthrocytes

In order to use synthrocytes as substitutes of erythrocytes or latex particles in agglutination assays, they were adapted specifically to expose trimeric SARS-CoV-2 spike protein in the surface. Spike protein is a homotrimeric glycoprotein responsible for virus binding to the host cell receptors and fusion of both membranes to promote virus entry. It comprises two subunits; S1, which contains the RBD, and S2. In order to drive fusion, this protein presents different conformational changes that could affect the recognition and affinity of the Ab. Most of the commercial serological tests detect anti-spike or anti-nucleocapsid Ab, but they use to be in fact Ab against only the specific subunits or parts of these proteins employed to produce the assay. Using the full trimeric protein should increase the recognition of a broader repertoire of Ab and improve the sensitivity and specificity of the assay.[277]

In brief, here trimeric spike protein was chemically conjugated to 10 µm amine Sicastar particles previously activated with glutaraldehyde, following the protocol described in Section 3.6.1. Then, coupled beads were washed and blocked to prevent nonspecific binding and inactivate the remaining reactive groups (Figure 9.3a). These SARS-CoV-2 adapted synthrocytes (spike-synthrocytes) we finally incubated for 5 min in the presence of a positive or negative serum sample (50 µL/well, diluted 1:100) and their sedimentation pattern was evaluated (Figure 9.3b).

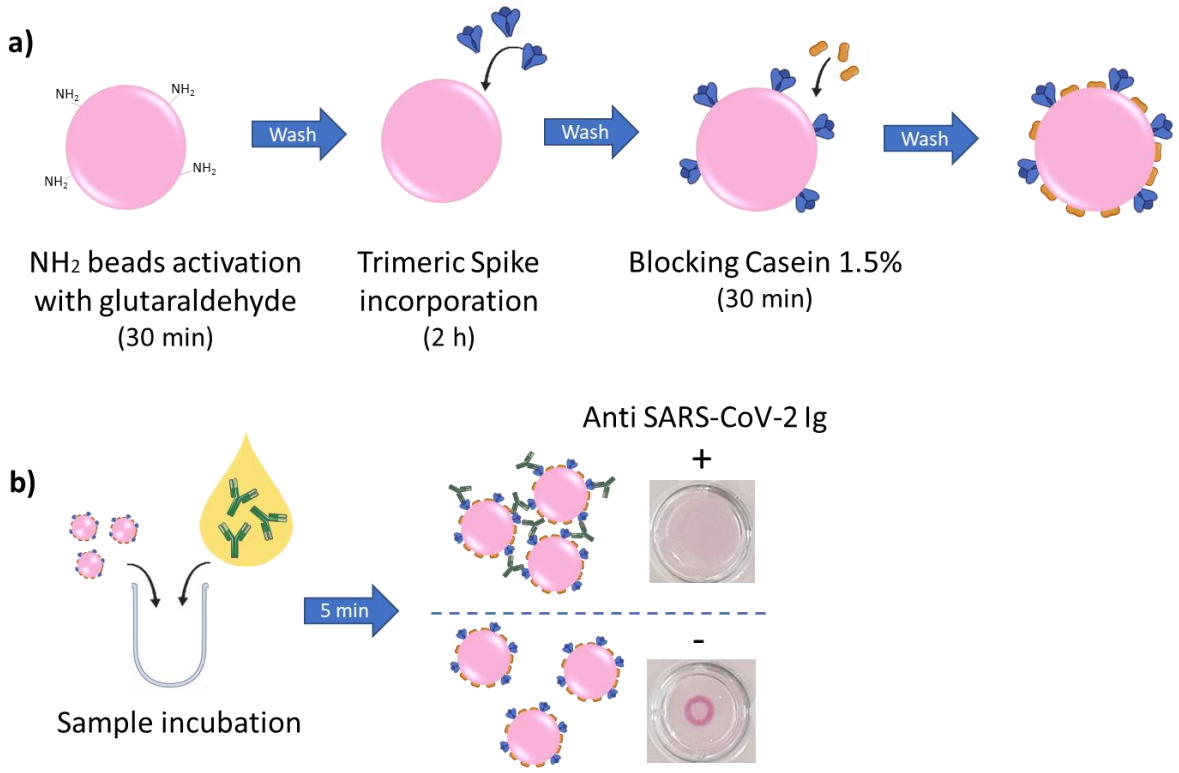

Figure 9.3 | a) Scheme of the incorporation of the trimeric spike protein in the surface of commercial 10 µm red Sicastar beads using glutaraldehyde. **b)** Diagram of SynA assay adapted to detect anti-spike Ab in serum samples. Ab binding to the spike-synthrocytes produced agglutination visible with naked eyes.

For this series of experiments, we employed commercially-dyed red Sicastar particles, instead of the blue ones used in the previous chapters, because we wanted to explore different dyes for different applications. Since our custom-dying protocol was still not developed, we were limited to the commercially available colors. We selected the red ones because of their availability and the high color intensity of that batch.

The first parameter optimized was the amount of protein required for particle conjugation. Concentrations were selected considering the size and charge of the trimeric spike protein and based on the previous results obtained with influenza-synthrocytes. As can be seen in Figure 9.4a, increasing by 25% the protein used to coat the particles did not improve their ability to agglutinate in the presence of anti-spike Ab. Therefore, 20 µg of trimeric spike was selected for the conjugation.

Next, we optimized the blocking step. Tris buffer was supplemented with different concentrations of casein or BSA, and beads were incubated with it in rotation to achieve a physical and chemical surface blocking. Figure 9.4b shows how casein produced a tighter bottom pellet in the negative controls in comparison with BSA blocking, which was easier to observe with naked eyes. Unfortunately, the agglutination pattern was also affected, producing a faint halo in the presence of Ab instead of the complete agglutination arrangement. Despite this, we selected casein as the blocking agent because tighter pellets allowed decreasing the number of particles/well necessary to perform the assay, enhancing assay sensitivity as previously seen with influenza-synthrocytes. Increasing the blocking concentration did not

impact the performance of these synthrocytes, and therefore 1.5% was selected as the blocking concentration.

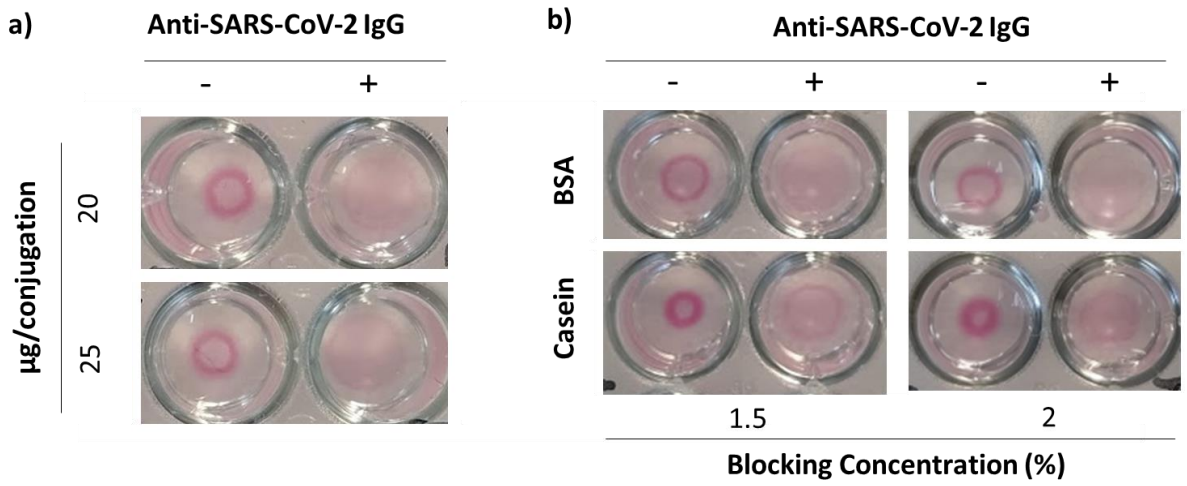

Figure 9.4 | Optimization of spike-synthrocytes production. SynA performed with a positive and a negative serum sample. Samples (diluted 1:100 with PBS) were incubated for 5 min with 150 µg of spike-synthrocytes produced with **a)** different amounts of trimeric spike protein or **b)** blocked with Tris supplemented with 1.5 or 2% of either BSA or casein.

9.2.2. Adaptation of SynA assay for anti-SARS-CoV-2 Ab detection

Once the conjugation protocol for production of spike-synthrocytes was defined, SynA was also adjusted for anti-SARS-CoV-2 Ab detection. We started with the processing of the serum sample, which needed to be diluted before being analyzed. Serial dilutions (ranging from 1:50 to 1:400) of one positive and one negative serum were incubated in U-shaped wells with spike-synthrocytes for 5 min. As can be seen in Figure 9.5a, the pellet formed with the negative sample was only affected at lower serum dilutions (i.e., 1:50), where a certain level of non-specific agglutination occurred, making the pellet faint. The positive sample, on the other side, produced a transient agglutination pattern that evolved over time to finally sediment when the serum was diluted over 1:200. This meant that, for this sample and dilutions, Ab were too diluted to form the agglutination lattice satisfactorily. Consequently, 1:100 was selected as the optimal dilution. This choice was confirmed by carrying further replicates with different Ab-containing serum samples, diluted 1:100, which produced slight agglutination pattern variations depending on the serum employed, ranging from complete agglutination to faint halos.

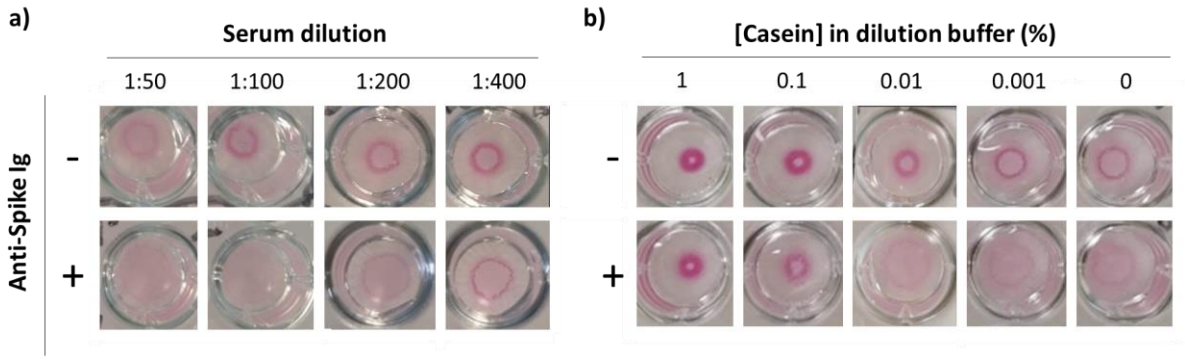

Figure 9.5 | Optimization of sample pretreatment and sample diluent. **a)** Effect of serum dilution in the agglutination and sedimentation patterns. **b)** SynA patterns after diluting the samples (1:100) with PBS supplemented with different concentrations of casein.

We next optimized the buffer used to dilute the samples. Usually, sample diluent buffers contain reagents that help to prevent non-specific interferences or preserve the target analyte. For this, we diluted the serum samples with either PBS or PBS supplemented with different concentrations of casein (ranging from 0.001% to 1%). Then, SynA was performed as usual. Figure 9.5b shows how high concentrations of casein in the diluting buffer increased the sedimentation of the particles, affecting both negative and positive patterns. For concentrations of casein 0.1% or higher, the agglutination was inhibited and spike-synthrocytes sedimented regardless of the presence/absence of anti-spike Ab. Using concentrations of casein of 0.01% improved the definition of the pellet in absence of anti-spike IgG without severely affecting the pattern of the agglutinated wells. Concentrations of 0.001% of casein produced no changes in the sedimentation patterns, both in positive and negative controls, when compared to non-supplemented medium. Therefore, we decided to use PBS with 0.01% of casein to ameliorate pellet definition in the negative controls.

Finally, we optimized the amount of synthrocytes per well to improve assay sensitivity. Based on influenza-synthrocytes, we expected that reducing the number of particles per well produced higher SynA titers. However, feasibility of decreasing the amount of synthrocytes was directly related to bead color intensity (in this case, the commercial red particles). We thus needed to assess the minimum amount of spike-synthrocytes that could be visually detected.

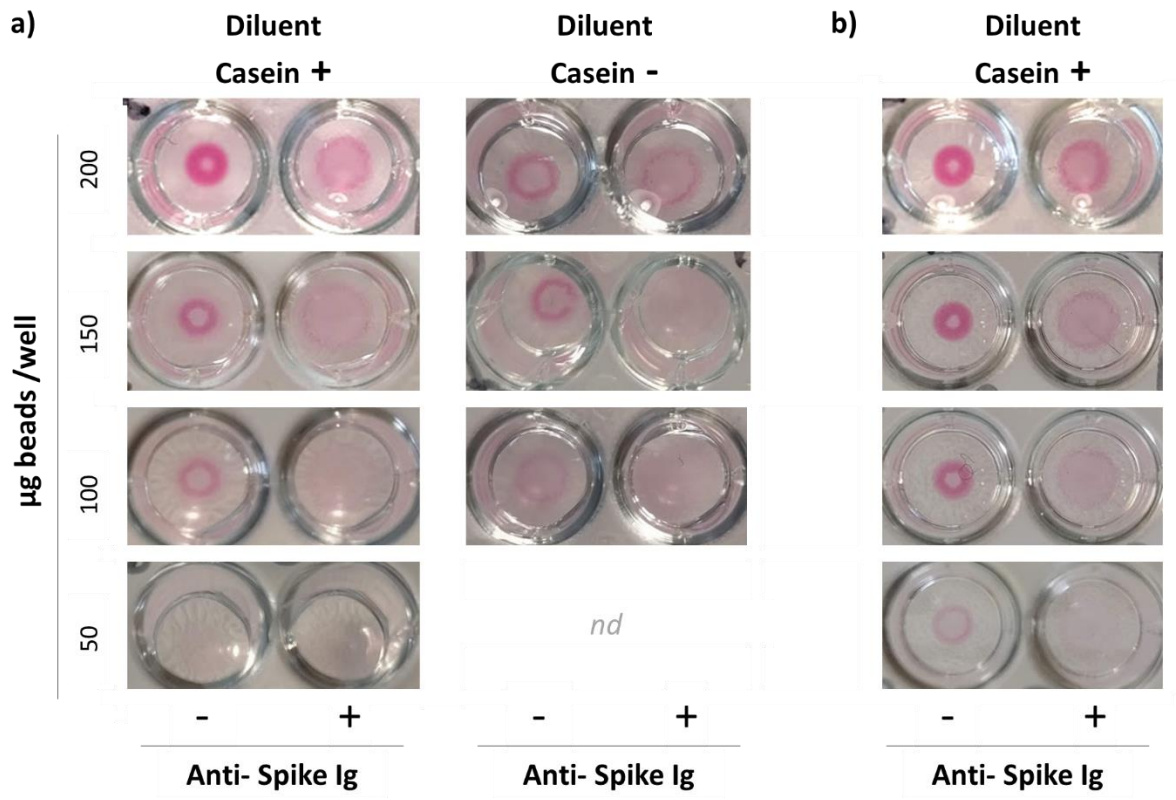

Figure 9.6 | Optimization of the amount of spike-synthrocytes used per well. **a)** SynA performed with different amounts of spike-synthrocytes with samples diluted 1:100 with or without the 0.01% casein supplemented diluent buffer. Results registered after a 5-min incubation. **b)** Same SynA showed in **a)** but after resting for 2 h.

As can be seen in Figure 9.6a, the amount of spike-synthrocytes could be reduced to 100 µg/well. The sedimentation pattern formed with negative samples was still noticeable with this amount of synthrocytes. Under these conditions, the agglutination pattern also improved, because the faint halo observable with 150-200 µg/well disappeared, producing a more uniform supernatant. Furthermore, we confirmed that using the sample diluent with casein contributed to reduce the amount of particles required per well by 30%. Discerning the different patterns using just 100 µg of synthrocytes/well without the supplemented diluent was possible, albeit considerably more difficult (Figure 9.6a, right images). Therefore, we selected 100 µg/well and 0.01% casein diluent buffer as the final settings for the assay.

Interestingly, when the time of the assay was extended to 2 h, the amount of synthrocytes used could be reduced even more (to 50 µg/well), decreasing the final cost of the assay by 50% (Figure 9.6b). However, the assay was not a fast method anymore.

To sum up, we developed and optimized spike-synthrocytes that produced visible agglutination in the presence of anti-SARS-CoV-2 Ab. To perform the SynA, we set the conditions of the assay to incubate serum diluted 1:100 (using a 0.01% casein supplemented sample dilution buffer) with 100 µg of synthrocytes/well, and to let them sediment for 5 min before assessing the sedimentation patterns.

9.2.3. Detection of anti-SARS-CoV-2 Ab in clinical serum samples

Finally, once we defined the optimal conditions for particle conjugation and SynA, assay performance was assessed in 31 patient and donor serum samples kindly provided by Biosystems. Negative serums had been obtained before the pandemic outbreak for other purposes. In parallel, we analyzed all the samples using a commercial ELISA able to quantify specifically anti-spike IgG. Samples were grouped according to the signals they produced by ELISA in three groups: negative, low and high titer, as shown in Figure 9.7a. Some representative examples of the sedimentation patterns obtained by SynA for each group are shown in Figure 9.7b, sorted from lower to higher anti-spike Ab concertation according to the ELISA absorbance signals. As can be seen in the top row, negative patterns were very consistent, forming a colored pellet similar in shape to the sediments formed by influenza-synthrocytes in previous chapters, albeit tighter due to the presence of the enriched sample dilution buffer. Of the 15 negative samples tested, just one of them produced a false positive result due nonspecific agglutination, resulting in 93% of specificity.

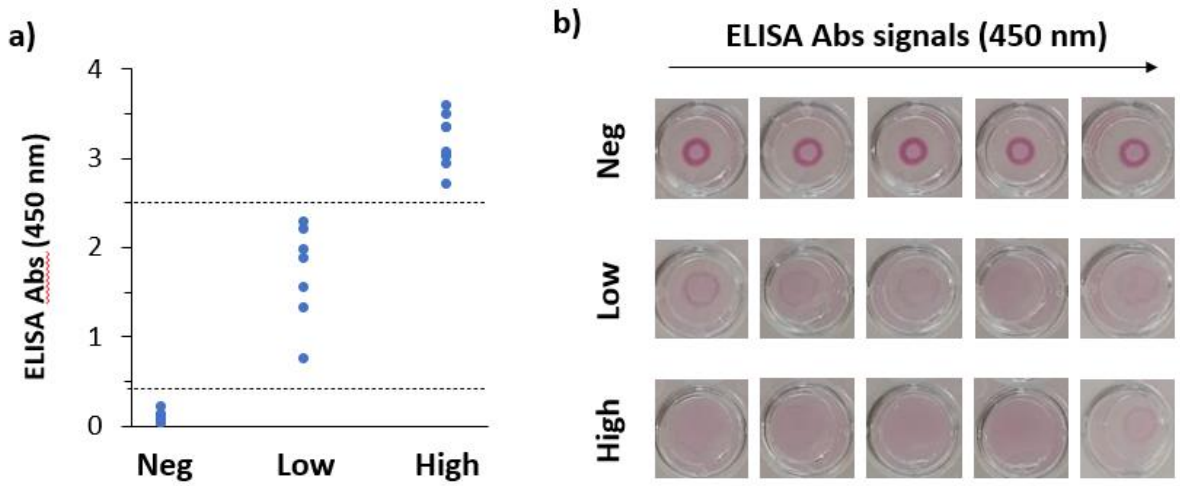

Figure 9.7 | a) Signals obtained for 31 samples using a commercially available ELISA for detection of anti-spike Ab. Samples were sorted in 3 groups depending on the obtained signals. Horizontal bars mark the limits for each group (samples generating signals below 0.45 AU were considered negative, "Neg" in the figure; signals between 0.45 and 2.5 AU signals corresponded to samples with low anti-spike Ab titers, "Low"; and the specimens generating signals above 2.5 were considered samples with high anti-spike Ab titers, "High"). **b)** Examples of the patterns obtained performing SynA with the same samples, also stratified by their assigned group.

Positive samples showed a clearly distinguishable pattern, although it not always corresponded to fully agglutinated spike-synthrocytes. This is, faint halos could be observed in some cases, especially in low Ab titer samples, and their intensity partially correlated with the absorbance signal obtained by ELISA. High Ab titer samples, on the other hand, showed a fully agglutinated well in most of the samples evaluated. The highest Ab titer sample produced a faint halo, similar to low titer serums, that could be explained by an excess of the target Ab that caused the prozone effect. Nonetheless, the 16 positive samples could be clearly differentiated from the negative ones. Discarding the lowest sample, which presented a more intense halo that could be mistaken, the assay sensitivity reached almost 94%.

9.3. Conclusions

These results suggested that synthrocytes could be adapted for alternative applications, and specially as a fast testing tool. In the first application shown, Ab-coated synthrocytes were used to detect PfLDH. In the second, synthrocytes were modified with trimeric SARS-CoV-2 spike protein for the detection of anti-SARS-CoV-2 Ab. The presence of these Ab triggered the formation of an agglutination pattern easily distinguishable with naked eyes, in just 5 min. Moreover, the assay also showed some correlation between the degree of agglutination in the wells and the concentration of anti-SARS-CoV-2 Ab in the patient sample. More samples are required to obtain consistent sensitivity and specificity numbers or asserting that SynA can provide semi quantitative results based on the halo intensity and diameter. Nevertheless, these results represent a successful proof-of-concept of synthrocyte versatility and possibility to be employed as a diagnostic tool, and not just for surveillance.

Chapter 10

Conclusions and future work

Chapter 10. Conclusions and future work

10.1. General conclusions

The overall aim of this PhD Thesis was the development of a synthetic reagent that could substitute animal erythrocytes in the HA/HAI assays used currently for global influenza surveillance.

Based on the work carried out to achieve the specific objectives defined in Chapter 2 and the results obtained along this PhD thesis, we can extract the conclusions summarized next:

1. **Synthrocytes are a synthetic reagent able to mimic RBCs behavior in classical HA/HAI assays and display differential sedimentation in the presence or absence of targeted agglutinating agents.** Synthrocytes are composed by dyed microparticles coated with receptors (natural or synthetic) by direct conjugation. The combination of size, density and material of the particles determines their ability to sediment differently when agglutinated. The type of receptor defines the reagent specificity, and thus detectable analyte. Particle staining allows visual result interpretation similar to that carried usually for RBCs, without requiring additional equipment or training compared to classical HA/HAI assays.

2. **When coated with appropriate sialylated receptors, synthrocytes can replace RBCs in HA-like SynA assays and bind targeted influenza viruses.** Synthrocyte-virus interaction triggers agglutination, producing changes in sedimentation in <25 min that resemble those generated by erythrocytes in 30-60 min.

3. **A combination of 6'-SL-BSA, 3'-SL-BSA and 3'-SLN-BSA synthetic receptors on the surface of 3 µm silica particles produced the best results**, achieving binding of the 4 influenza seasonal subtypes (A(H1N1)pdm09, A(H3N2), B/Yamagata and B/Victoria) and some avian influenza viruses (H5N1, H7N9).

4. **The changes in influenza-driven synthrocyte sedimentation are inhibited by anti-influenza antibodies in HAI-like SynAI assays**. This allows the use of synthrocytes to antigenically characterize influenza viruses using WHO reference reagents, and will allow carrying serological analysis when the problems of non-specific interactions observed in part of the serum samples are solved.

5. **Long-term storage of synthrocytes is possible through lyophilization**. This is a considerable improvement over RBCs, increasing the shelf-life from <2 weeks to several months when lyophilized, and to 1 month once resuspended.

6. **The first proof-of-concept of synthrocyte production scalability has been achieved**. Although more work will be required to reach an industrial level, the custom

dyeing protocol was escalated 20x and that for particle conjugation with receptors was escalated 40X.

7. **Synthrocytes and the protocols developed in this work have been tested in a real surveillance laboratory**, showing that synthrocytes can improve user experience and reproducibility of the assay. Albeit there was room for improvement, promising results were obtained together with positive feedback on their usability.

8. **A novel type of microfluidic device has been developed to improve SynA assays by providing handling automatization and more objective result readouts.** This low-cost device was made by assembling layers of hydrophilic polyester film intercalated with layers of double-sided adhesive to create microfluidic chambers and channels. Virus-agglutinated particles could be separated using the device and quantified employing an image software. Such quantitative readouts correlated with virus concentration and with the SynA titer obtained by microplate agglutination assay.

9. **Synthrocytes can be exploited in other applications, such as the ones that relay on Ab-Ag interactions.** We have proven that its feasible to use Ab-coated synthrocytes for visual detection of PfLDH of the malaria parasite and we obtained promising results using trimeric spike protein-coated synthrocytes for detection of anti-SARS-CoV-2 Ab. These results demonstrate the versatility of the synthrocyte technology and suggest that synthrocytes could be used as a fast diagnostic tool, and not just for surveillance.

10.2. Work in progress and future perspectives

Although we showed that synthrocytes can mimic RBCs in SynA and SynAI assays, some challenges should be overcome before having a real marketable product. Synthrocytes were envisioned to contribute to worldwide standardization of HAI tests, and thus should be a more stable, reproducible and mass-producible reagent than RBCs. Results obtained in this PhD thesis get us closer to this objective, but in order to achieve it, several issues should be addressed. It is worth noting that the group has continued working in the development of synthrocytes over 2022 and 2023, while this Thesis was being written and after I left the group to join Biosystems R&D Department. Hence, some of the issues will be discussed based on the results already obtained by my colleagues, which I could witness and to which I contributed in one or another way.

1. Synthrocyte sensitivity should be improved. Synthrocytes developed in this work recognized different influenza virus subtypes (including all the seasonal ones), but in some of the cases they showed a slightly decreased sensitivity compared to RBCs. For this reason, different strategies needed to be explored to improve their performance. The first one was testing alternative synthetic receptors for influenza binding. Promising results have been obtained by substituting 6'-SL-BSA by 6'-SLN-BSA, a conjugate that was custom-produced by Dextra after a year of development. Incorporating a new receptor required that the whole battery of receptors was

readjusted as well, but allowed detecting the 4 seasonal influenza viruses, and specially H1N1 ones, with enhanced sensitivity. These results demonstrated that synthrocytes could be potentially upgraded to detect fast evolving influenza viruses, but also evidenced the limitation imposed by having to use expensive receptor constructs of commercial origin. Accordingly, the second priority has been to explore other strategies for SA incorporation in an attempt to increase the number of SA available or to improve their orientation on the microparticle surface. Numerous chemical paths have been explored, both to incorporate SA directly to the particles or to produced cheaper customized SA-BSA conjugates. The second strategy has produced better results. By now, synthrocytes coated with these customized conjugates are up to 50-times cheaper, but less sensitive, showing that work has not finished yet. Finally, the results obtained in this work show that using lower amounts of microparticles/well lead to an increase in sensitivity. Therefore, reducing the number of microparticles/well in each assay, for example studying their performance in V-bottomed plates, could improve assay sensitivity. These microplates are already well-established for avian RBCs and, although they were discarded at the start of this work, this is an aspect worth considering due to all the optimization and improvements achieved with the synthrocytes (including custom-dyeing).

2. The cost of synthrocyte production and SynA/SynAI assays should be decreased. The cost of SynA/SynAI assays could be decreased by reducing the amount of microparticles and/or receptor required to perform the assays, or by changing their components for cheaper ones. The cost of producing synthrocytes has been heavily reduced between the first prototype using GYPA-coated microparticles and the current ones using synthetic SA-BSA (from >450 €/plate to 10-45 €/plate). But the SA-BSA receptors still constitute the most expensive element by far. SA-BSA receptors are currently purchased directly to the manufacturer, Dextra in UK, but their elevated cost, together with the importation taxes after the Brexit, made it necessary to explore the possibility to manufacture them ourselves. By producing customized receptors, we could also work to increase the number of SA-residues per molecule of BSA, potentially increasing the recognition efficiency and sensitivity of synthrocytes.

3. As shown in multiple sections of this work, SynAI with human serum samples still remains unsatisfactory, mostly because of non-specific agglutinating agents present in some samples. To solve this, implementation of serum pre-adsorption using synthrocytes should be achieved. This approach was tentatively explored during this work, but it required further optimization. Work has continued to produce a depletion reagent using unstained particles of smaller size (thus larger active surface) modified with SA-BSA. The team is currently testing different additives to minimize non-specific agglutination, optimize lyophilization and test performance in WHO reference reagents and serum samples.

4. Long-term stability of lyophilized synthrocytes and synthrocyte suspensions should be evaluated. It will be needed to carry out more long-term stability tests to evaluate the

real time stability of lyophilized and resuspended synthrocytes under different storing conditions, and specially at room temperature. This will allow defining the best strategy to guarantee the shelf-life of synthrocytes, including optimal packing and transport requirements. This includes increasing the size of the lyophilized vials to include the reagent needed to perform more than one plate with each of them, reducing the waste and potentially increasing even more the reproducibility.

5. Synthrocyte production should be scaled up further for industrial production. It will be necessary to continue optimizing the scale-up of synthrocytes, increasing the amount obtained in each production. Moreover, at the moment only fetuin-conjugation has been tested under scaled-up conditions due to its lower cost, but SA-BSA conjugation would also be tested and re-optimized as needed. Appropriate funding will be needed to support this type of experiments, which will be only feasible with the involvement of the industry.

6. Validation of the final prototype will be needed. Once all these modifications have been implemented, the final version of synthrocytes should be tested again to confirm their improved performance in a real environment and to obtain further feedback. This should be carried with the help of different centers of the international influenza control network, which could include the Valladolid NIC again, plus the WHO CCs center located at Atlanta, USA, which has been also contacted. In both cases, this validation should be performed through the shipment of lyophilized synthrocytes with just the instructions of how to use them. This will mimic the conditions of how the rest of the GISRS centers would receive this new reagent in the future, to ensure that the product is easy to use with minimum changes compared to classical HA/HAI.

7. Analyze if synthrocytes could be used with HA/HAI automatized machines. Because of the lack of automated machines in small and medium NICs, this will have to be performed in collaboration with the WHO CCs directly. Both the procedure of the assay and the automatic reading of the plates should be evaluated. In the lack of access to such equipment or in parallel to this testing, it could be interesting to confirm the usefulness of spectrophotometric reading to interpret the sedimentation patterns obtained, especially when a quantitative outcome is necessary. More samples should be studied to define the most appropriate protocol to interpret the size and color intensity of the halos formed in SynA wells and determine if they can provide a quantitative measure.

8. Regarding the low-cost microfluidic device developed in this thesis, next steps should include the incorporation of pre-loaded reagents. Examples of this are the synthrocytes themselves, that could be lyophilized and stored inside the device, or the PBS. This would reduce the handling of the device and contribute to obtain more homogenous data.

9. Study alternative applications. More samples are required specifically for the SARS-CoV-2 application, which seemed the most promising of the two evaluated. Nevertheless, this proof-of-concept opens the possibility of detection of other Ab or antigens of interest.

Bibliography

Bibliography

1. Estimating disease burden of influenza [Internet]. [cited 2023 Aug 6]. Available from: https://www.who.int/europe/activities/estimating-disease-burden-of-influenza

2. Uyeki TM, Hui DS, Zambon M, Wentworth DE, Monto AS. Influenza. The Lancet. 2022 Aug;400(10353):693–706.

3. Paget J, Danielle Iuliano A, Taylor RJ, Simonsen L, Viboud C, Spreeuwenberg P. Estimates of mortality associated with seasonal influenza for the European Union from the GLaMOR project. Vaccine. 2022 Feb 23;40(9):1361–9.

4. Factsheet about seasonal influenza [Internet]. 2017 [cited 2023 Aug 6]. Available from: https://www.ecdc.europa.eu/en/seasonal-influenza/facts/factsheet

5. Wallensten A. Influenza virus in wild birds and mammals other than man. Microbial Ecology in Health and Disease. 2007 Jan 1;19(2):122–39.

6. Reperant LA, Kuiken T, Osterhaus ADME. Influenza viruses: from birds to humans. Human Vaccines & Immunotherapeutics. 2012 Jan;8(1):7–16.

7. Caini S, Kusznierz G, Garate VV, Wangchuk S, Thapa B, de Paula Júnior FJ, et al. The epidemiological signature of influenza B virus and its B/Victoria and B/Yamagata lineages in the 21st century. PloS One. 2019;14(9):e0222381.

8. Caini S, Huang QS, Ciblak MA, Kusznierz G, Owen R, Wangchuk S, et al. Epidemiological and virological characteristics of influenza B: results of the Global Influenza B Study. Influenza and Other Respiratory Viruses. 2015 Aug;9(Suppl 1):3–12.

9. Sederdahl BK, Williams JV. Epidemiology and Clinical Characteristics of Influenza C Virus. Viruses. 2020 Jan 13;12(1):89.

10. Liu R, Sheng Z, Huang C, Wang D, Li F. Influenza D virus. Current Opinion in Virology. 2020 Oct 1;44:154–61.

11. Wu Y, Wu Y, Tefsen B, Shi Y, Gao GF. Bat-derived influenza-like viruses H17N10 and H18N11. Trends in Microbiology. 2014 Apr 1;22(4):183–91.

12. Soldevila N, Basile L, Martínez A, Torner N, Marcos MÁ, Mosquera M del M, et al. Surveillance of influenza B severe hospitalized cases during 10 seasons in Catalonia: Does the lineage make a difference? Journal of Medical Virology. 2022;94(9):4417–24.

13. Koutsakos M, Wheatley AK, Laurie K, Kent SJ, Rockman S. Influenza lineage extinction during the COVID-19 pandemic? Nature Reviews Microbiology. 2021 Dec;19(12):741–2.

14. Vajo Z, Torzsa P. Extinction of the Influenza B Yamagata Line during the COVID Pandemic—Implications for Vaccine Composition. Viruses. 2022 Aug 9;14(8):1745.

15. World Health Organization. A revision of the system of nomenclature for influenza viruses: a WHO Memorandum. Bulletin of the World Health Organization. 1980;58(4):585–91.

16. Kosik I, Yewdell JW. Influenza Hemagglutinin and Neuraminidase: Yin–Yang Proteins Coevolving to Thwart Immunity. Viruses. 2019 Apr 16;11(4):346.

17. Bouvier NM, Palese P. The biology of influenza viruses. Vaccine. 2008 Sep 12;26(Suppl 4):D49–53.

18. Dadonaite B, Vijayakrishnan S, Fodor E, Bhella D, Hutchinson EC. Filamentous influenza viruses. The Journal of General Virology. 2016 Aug;97(8):1755–64.

19. CDC. Images of Influenza Viruses [Internet]. Centers for Disease Control and Prevention. 2019 [cited 2023 Nov 26]. Available from: https://www.cdc.gov/flu/resource-center/freeresources/graphics/images.htm

20. Wilson IA, Skehel JJ, Wiley DC. Structure of the haemagglutinin membrane glycoprotein of influenza virus at 3 A resolution. Nature. 1981 Jan 29;289(5796):366–73.

21. Sakai T, Nishimura SI, Naito T, Saito M. Influenza A virus hemagglutinin and neuraminidase act as novel motile machinery. Scientific Reports. 2017 Mar 27;7(1):45043.

22. Sauter NK, Hanson JE, Glick GD, Brown JH, Crowther RL, Park SJ, et al. Binding of influenza virus hemagglutinin to analogs of its cell-surface receptor, sialic acid: analysis by proton nuclear magnetic resonance spectroscopy and x-ray crystallography. Biochemistry. 1992 Oct 13;31(40):9609–21.

23. McAuley JL, Gilbertson BP, Trifkovic S, Brown LE, McKimm-Breschkin JL. Influenza Virus Neuraminidase Structure and Functions. Frontiers in Microbiology. 2019;10.

24. Wilks S, Graaf MD, Smith DJ, Burke DF. A review of Influenza haemagglutinin receptor binding as it relates to pandemic properties. Vaccine. 2012 Jun 6;30(29):4369.

25. Varki A. Sialic acids in human health and disease. Trends in Molecular Medicine. 2008 Aug;14(8):351–60.

26. Kuchipudi SV, Nelli RK, Gontu A, Satyakumar R, Surendran Nair M, Subbiah M. Sialic Acid Receptors: The Key to Solving the Enigma of Zoonotic Virus Spillover. Viruses. 2021 Feb 8;13(2):262.

27. Lehmann F, Tiralongo E, Tiralongo J. Sialic acid-specific lectins: occurrence, specificity and function. Cellular and Molecular Life Sciences. 2006;63(12):1331–54.

28. Zhao C, Pu J. Influence of Host Sialic Acid Receptors Structure on the Host Specificity of Influenza Viruses. Viruses. 2022 Oct;14(10):2141.

29. Wu NC, Wilson IA. Influenza Hemagglutinin Structures and Antibody Recognition. Cold Spring Harbor Perspectives in Medicine. 2020 Aug;10(8):a038778.

30. Rogers GN, Paulson JC. Receptor determinants of human and animal influenza virus isolates: differences in receptor specificity of the H3 hemagglutinin based on species of origin. Virology. 1983 Jun;127(2):361–73.

31. Rogers GN, D'Souza BL. Receptor binding properties of human and animal H1 influenza virus isolates. Virology. 1989 Nov;173(1):317–22.

32. Connor RJ, Kawaoka Y, Webster RG, Paulson JC. Receptor specificity in human, avian, and equine H2 and H3 influenza virus isolates. Virology. 1994 Nov 15;205(1):17–23.

33. Matrosovich MN, Gambaryan AS, Teneberg S, Piskarev VE, Yamnikova SS, Lvov DK, et al. Avian influenza A viruses differ from human viruses by recognition of

sialyloligosaccharides and gangliosides and by a higher conservation of the HA receptor-binding site. Virology. 1997 Jun 23;233(1):224–34.

34. Shinya K, Ebina M, Yamada S, Ono M, Kasai N, Kawaoka Y. Influenza virus receptors in the human airway. Nature. 2006 Mar;440(7083):435–6.

35. Suzuki Y. Sialobiology of Influenza: Molecular Mechanism of Host Range Variation of Influenza Viruses. Biological & Pharmaceutical Bulletin. 2005;28(3):399–408.

36. Xu R, McBride R, Nycholat CM, Paulson JC, Wilson IA. Structural Characterization of the Hemagglutinin Receptor Specificity from the 2009 H1N1 Influenza Pandemic. Journal of Virology. 2012 Jan;86(2):982–90.

37. Walther T, Karamanska R, Chan RWY, Chan MCW, Jia N, Air G, et al. Glycomic Analysis of Human Respiratory Tract Tissues and Correlation with Influenza Virus Infection. PLOS Pathogens. 2013 Mar 14;9(3):e1003223.

38. Air GM. Influenza virus–glycan interactions. Current Opinion in Virology. 2014 Aug 1;7:128–33.

39. Shi Y, Wu Y, Zhang W, Qi J, Gao GF. Enabling the “host jump”: structural determinants of receptor-binding specificity in influenza A viruses. Nature Reviews Microbiology. 2014 Dec;12(12):822–31.

40. Long JS, Mistry B, Haslam SM, Barclay WS. Host and viral determinants of influenza A virus species specificity. Nature Reviews Microbiology. 2019 Feb;17(2):67–81.

41. Carrique L, Fan H, Walker AP, Keown JR, Sharps J, Staller E, et al. Host ANP32A mediates the assembly of the influenza virus replicase. Nature. 2020 Nov;587(7835):638–43.

42. Gambaryan A, Tuzikov A, Pazynina G, Bovin N, Balish A, Klimov A. Evolution of the receptor binding phenotype of influenza A (H5) viruses. Virology. 2006 Jan 20;344(2):432–8.

43. Gambaryan AS, Robertson JS, Matrosovich MN. Effects of egg-adaptation on the receptor-binding properties of human influenza A and B viruses. Virology. 1999 Jun 5;258(2):232–9.

44. Robertson JS, Bootman JS, Newman R, Oxford JS, Daniels RS, Webster RG, et al. Structural changes in the haemagglutinin which accompany egg adaptation of an influenza A(H1N1) virus. Virology. 1987 Sep;160(1):31–7.

45. Liang W, Tan TJC, Wang Y, Lv H, Sun Y, Bruzzone R, et al. Egg-adaptation pathway of human influenza H3N2 virus is contingent on natural evolution. bioRxiv; 2022. p. 2022.01.31.478576.

46. Kim H, Webster RG, Webby RJ. Influenza Virus: Dealing with a Drifting and Shifting Pathogen. Viral Immunology. 2018 Mar;31(2):174–83.

47. Shao W, Li X, Goraya MU, Wang S, Chen JL. Evolution of Influenza A Virus by Mutation and Re-Assortment. International Journal of Molecular Sciences. 2017 Aug 7;18(8):1650.

48. Jayaraman A, Pappas C, Raman R, Belser JA, Viswanathan K, Shriver Z, et al. A single base-pair change in 2009 H1N1 hemagglutinin increases human receptor affinity and leads to efficient airborne viral transmission in ferrets. PloS One. 2011 Mar 2;6(3):e17616.

49. Smith DJ, Lapedes AS, de Jong JC, Bestebroer TM, Rimmelzwaan GF, Osterhaus ADME, et al. Mapping the antigenic and genetic evolution of influenza virus. Science (New York, NY). 2004 Jul 16;305(5682):371–6.

50. Ferguson NM, Galvani AP, Bush RM. Ecological and immunological determinants of influenza evolution. Nature. 2003 Mar;422(6930):428–33.

51. Taubenberger JK, Kash JC. Influenza Virus Evolution, Host Adaptation and Pandemic Formation. Cell host & microbe. 2010 Jun 25;7(6):440–51.

52. Ma W, Kahn RE, Richt JA. The pig as a mixing vessel for influenza viruses: Human and veterinary implications. Journal of Molecular and Genetic Medicine: An International Journal of Biomedical Research. 2008 Nov 27;3(1):158–66.

53. Hampson AW, Mackenzie JS. The influenza viruses. Medical Journal of Australia. 2006;185(S10):S39–43.

54. Kilbourne ED. Influenza Pandemics of the 20th Century. [cited 2023 Aug 6]; Available from: https://wwwnc.cdc.gov/eid/article/12/1/05-1254_article

55. CDC. Key Facts About Influenza (Flu) [Internet]. Centers for Disease Control and Prevention. 2023 [cited 2023 Nov 26]. Available from: https://www.cdc.gov/flu/about/keyfacts.htm

56. Surveillance for seasonal influenza [Internet]. 2010 [cited 2023 Nov 26]. Available from: https://www.ecdc.europa.eu/en/seasonal-influenza/surveillance-reports-and-disease-data

57. Taubenberger JK. The Origin and Virulence of the 1918 “Spanish” Influenza Virus. Proceedings of the American Philosophical Society. 2006 Mar;150(1):86–112.

58. Reid AH, Fanning TG, Hultin JV, Taubenberger JK. Origin and evolution of the 1918 “Spanish” influenza virus hemagglutinin gene. Proceedings of the National Academy of Sciences of the United States of America. 1999 Feb 16;96(4):1651–6.

59. Tumpey TM, Maines TR, Van Hoeven N, Glaser L, Solórzano A, Pappas C, et al. A two-amino acid change in the hemagglutinin of the 1918 influenza virus abolishes transmission. Science (New York, NY). 2007 Feb 2;315(5812):655–9.

60. Glezen WP. Emerging Infections: Pandemic Influenza. Epidemiologic Reviews. 1996 Jan 1;18(1):64–76.

61. Viboud C, Simonsen L, Fuentes R, Flores J, Miller MA, Chowell G. Global Mortality Impact of the 1957-1959 Influenza Pandemic. The Journal of Infectious Diseases. 2016 Mar 1;213(5):738–45.

62. Kawaoka Y, Krauss S, Webster RG. Avian-to-human transmission of the PB1 gene of influenza A viruses in the 1957 and 1968 pandemics. Journal of Virology. 1989 Nov;63(11):4603–8.

63. Krause JC, Tsibane T, Tumpey TM, Huffman CJ, Albrecht R, Blum DL, et al. Human Monoclonal Antibodies to Pandemic 1957 H2N2 and Pandemic 1968 H3N2 Influenza Viruses. Journal of Virology. 2012 Jun;86(11):6334–40.

64. Jones JC, Baranovich T, Marathe BM, Danner AF, Seiler JP, Franks J, et al. Risk Assessment of H2N2 Influenza Viruses from the Avian Reservoir. Journal of Virology. 2014 Jan;88(2):1175–88.

65. Scholtissek C, Rohde W, Von Hoyningen V, Rott R. On the origin of the human influenza virus subtypes H2N2 and H3N2. Virology. 1978 Jun 1;87(1):13–20.

66. Van Poucke S, Doedt J, Baumann J, Qiu Y, Matrosovich T, Klenk HD, et al. Role of Substitutions in the Hemagglutinin in the Emergence of the 1968 Pandemic Influenza Virus. Journal of Virology. 2015 Sep 16;89(23):12211–6.

67. West J, Röder J, Matrosovich T, Beicht J, Baumann J, Mounogou Kouassi N, et al. Characterization of changes in the hemagglutinin that accompanied the emergence of H3N2/1968 pandemic influenza viruses. PLoS Pathogens. 2021 Sep 23;17(9):e1009566.

68. Jester BJ, Uyeki TM, Jernigan DB. Fifty Years of Influenza A(H3N2) Following the Pandemic of 1968. American Journal of Public Health. 2020 May;110(5):669–76.

69. Girard MP, Tam JS, Assossou OM, Kieny MP. The 2009 A (H1N1) influenza virus pandemic: A review. Vaccine. 2010 Jul 12;28(31):4895–902.

70. Short KR, Kedzierska K, van de Sandt CE. Back to the Future: Lessons Learned From the 1918 Influenza Pandemic. Frontiers in Cellular and Infection Microbiology. 2018;8.

71. Neumann G, Noda T, Kawaoka Y. Emergence and pandemic potential of swine-origin H1N1 influenza virus. Nature. 2009 Jun;459(7249):931–9.

72. Cohen J. Straight From the Pig's Mouth: Swine Research With Swine Influenzas. Science. 2009 Jul 10;325(5937):140–1.

73. Dawood FS, Iuliano AD, Reed C, Meltzer MI, Shay DK, Cheng PY, et al. Estimated global mortality associated with the first 12 months of 2009 pandemic influenza A H1N1 virus circulation: a modelling study. The Lancet Infectious Diseases. 2012 Sep 1;12(9):687–95.

74. Short KR, Richard M, Verhagen JH, van Riel D, Schrauwen EJA, van den Brand JMA, et al. One health, multiple challenges: The inter-species transmission of influenza A virus. One Health. 2015 Dec 1;1:1–13.

75. World Health Organization. Global Influenza Surveillance and Response System (GISRS) [Internet]. [cited 2023 Aug 6]. Available from: https://www.who.int/initiatives/global-influenza-surveillance-and-response-system

76. World Health Organization. History of GISRS [Internet]. 2022. Available from: https://www.who.int/images/default-source/departments/global-influenza-programme/gisrs-70th-images/history-of-gisrs-graphic-2022-revised-07.02.2022-v4.jpg?sfvrsn=44fe53f3_8

77. World Health Organization. Terms of Reference for National Influenza Centers of the Global Influenza Surveillance and Response System [Internet]. 2017. Available from: https://cdn.who.int/media/docs/default-source/influenza/national-influenza-centers-files/nic_tor_en.pdf?sfvrsn=93513e78_30

78. World Health Organization. CDC's World Health Organization Collaborating Center [Internet]. Centers for Disease Control and Prevention. 2021 [cited 2023 Aug 6]. Available from: https://www.cdc.gov/flu/weekly/who-collaboration.htm

79. Flunet [Internet]. [cited 2023 Dec 11]. Available from: https://www.who.int/tools/flunet

80. World Health Organization. Terms of reference for seasonal influenza for essential regulatory laboratories of the who global influenza surveillance and response system [Internet]. Available from: https://cdn.who.int/media/docs/default-source/influenza/erl_tor_seasonal_influenza.pdf?sfvrsn=4bd53f9_7

81. World Health Organization. Terms of Reference for WHO H5 Reference Laboratories [Internet]. Available from: https://cdn.who.int/media/docs/default-source/influenza/global-influenza-surveillance-and-response-system/h5-reference-labs/torh5reflab2006.pdf?sfvrsn=1c0a3004_5

82. World Health Organization. A Description of the Process of Seasonal and H5N1 Influenza Vaccine Virus Selection and Development [Internet]. 2007. Available from: https://apps.who.int/gb/pip/pdf_files/Fluvaccvirusselection.pdf

83. European Centre for Disease Prevention and Control. European Influenza Surveillance Network (EISN) [Internet]. 2017 [cited 2023 Aug 6]. Available from: https://www.ecdc.europa.eu/en/about-us/partnerships-and-networks/disease-and-laboratory-networks/eisn

84. Instituto de Salud Carlos III. Guía de procedimientos para la vigilancia de gripe en España [Internet]. 2019. Available from: https://www.isciii.es/QueHacemos/Servicios/VigilanciaSaludPublicaRENAVE/EnfermedadesTransmisibles/Documents/GRIPE/GUIAS/Guia_procedimientos_vigilancia_gripe_Octubre2019.pdf

85. Nuwarda RF, Alharbi AA, Kayser V. An Overview of Influenza Viruses and Vaccines. Vaccines. 2021 Sep 17;9(9):1032.

86. Centers for Disease Control and Prevention. Selecting Viruses for the Seasonal Flu Vaccine [Internet]. Centers for Disease Control and Prevention. 2022 [cited 2023 Aug 6]. Available from: https://www.cdc.gov/flu/prevent/vaccine-selection.htm

87. Belser JA, Katz JM, Tumpey TM. The ferret as a model organism to study influenza A virus infection. Disease Models & Mechanisms. 2011 Sep;4(5):575–9.

88. European Medicines Agency. Guideline on Influenza vaccines [Internet]. 2017. Available from: https://www.ema.europa.eu/en/documents/scientific-guideline/guideline-influenza-vaccines-quality-module-revision-1_en.pdf

89. Pérez Rubio A, Eiros JM. Cell culture-derived flu vaccine: Present and future. Human Vaccines & Immunotherapeutics. 2018 Jun 28;14(8):1874–82.

90. Lin Y, Wharton SA, Whittaker L, Dai M, Ermetal B, Lo J, et al. The characteristics and antigenic properties of recently emerged subclade 3C.3a and 3C.2a human influenza A(H3N2) viruses passaged in MDCK cells. Influenza and Other Respiratory Viruses. 2017 May;11(3):263–74.

91. Liang W, Tan TJC, Wang Y, Lv H, Sun Y, Bruzzone R, et al. Egg-adaptive mutations of human influenza H3N2 virus are contingent on natural evolution. PLoS Pathogens. 2022 Sep 26;18(9):e1010875.

92. Barr IG, Donis RO, Katz JM, McCauley JW, Odagiri T, Trusheim H, et al. Cell culture-derived influenza vaccines in the severe 2017–2018 epidemic season: a step towards improved influenza vaccine effectiveness. NPJ Vaccines. 2018 Oct 9;3:44.

93. Recommended composition of influenza virus vaccines for use in the 2022-2023 northern hemisphere influenza season [Internet]. [cited 2023 Aug 6]. Available from: https://www.who.int/publications/m/item/recommended-composition-of-influenza-virus-vaccines-for-use-in-the-2022-2023-northern-hemisphere-influenza-season

94. Nichol KL, Treanor JJ. Vaccines for seasonal and pandemic influenza. The Journal of Infectious Diseases. 2006 Nov 1;194 Suppl 2:S111-118.

95. Candidate vaccine viruses [Internet]. [cited 2023 Aug 6]. Available from: https://www.who.int/teams/global-influenza-programme/vaccines/who-recommendations/candidate-vaccine-viruses

96. Dwyer DE, Smith DW, Catton MG, Barr IG. Laboratory diagnosis of human seasonal and pandemic influenza virus infection. Medical Journal of Australia. 2006;185(S10):S48–53.

97. Warren L. The thiobarbituric acid assay of sialic acids. The Journal of Biological Chemistry. 1959 Aug;234(8):1971–5.

98. Aymard-Henry M, Coleman MT, Dowdle WR, Laver WG, Schild GC, Webster RG. Influenzavirus neuraminidase and neuraminidase-inhibition test procedures. Bulletin of the World Health Organization. 1973;48(2):199–202.

99. Pedersen JC. Neuraminidase-Inhibition Assay for the Identification of Influenza A Virus Neuraminidase Subtype or Neuraminidase Antibody Specificity. In: Spackman E, editor. Avian Influenza Virus. Totowa, NJ: Humana Press; 2008. p. 67–75. (Methods in Molecular Biology™).

100. Eisfeld AJ, Neumann G, Kawaoka Y. Influenza A virus isolation, culture and identification. Nature Protocols. 2014 Nov;9(11):2663–81.

101. Karakus U, Crameri M, Lanz C, Yángüez E. Propagation and Titration of Influenza Viruses. Methods in Molecular Biology (Clifton, NJ). 2018;1836:59–88.

102. Hirst GK. Adsorption of influenza hemagglutinins and virus by red blood cells. The Journal of Experimental Medicine. 1942 Aug 1;76(2):195–209.

103. Norrby E. Hemagglutination by Measles Virus. 4. A Simple Procedure for Production of High Potency Antigen for Hemagglutination-Inhibition (HI) Tests. Proceedings of the Society for Experimental Biology and Medicine. 1962 Dec 1;111(3):814–8.

104. Stewart GL, Parkman PD, Hopps HE, Douglas RD, Hamilton JP, Meyer HM. Rubella-virus hemagglutination-inhibition test. The New England Journal of Medicine. 1967 Mar 9;276(10):554–7.

105. Rosen L. Hemagglutination by adenoviruses. Virology. 1958 Jun;5(3):574–7.

106. Mutanda LN, Munube GM. Agglutination of African primate and rodent erythrocytes by adenoviruses, reoviruses, and enteroviruses. Applied Microbiology. 1972 Dec;24(6):939–42.

107. Koransky JR, Scales RW, Kraus SJ. Bacterial hemagglutination by Neisseria gonorrhoeae. Infection and Immunity. 1975 Sep;12(3):495–8.

108. Klimov A, Balish A, Veguilla V, Sun H, Schiffer J, Lu X, et al. Influenza virus titration, antigenic characterization, and serological methods for antibody detection. Methods in Molecular Biology (Clifton, NJ). 2012;865:25–51.

109. Fernandes HP, Cesar CL, Barjas-Castro M de L. Electrical properties of the red blood cell membrane and immunohematological investigation. Revista brasileira de hematologia e hemoterapia. 2011;33(4):297–301.

110. Kaufmann L, Syedbasha M, Vogt D, Hollenstein Y, Hartmann J, Linnik JE, et al. An Optimized Hemagglutination Inhibition (HI) Assay to Quantify Influenza-specific Antibody Titers. Journal of Visualized Experiments : JoVE. 2017 Dec 1;(130):55833.

111. Aminoff D, Anderson J, Dabich L, Gathmann WD. Sialic acid content of erythrocytes in normal individuals and patients with certain hematologic disorders. American Journal of Hematology. 1980 Dec;9(4):381–9.

112. Ito T, Suzuki Y, Mitnaul L, Vines A, Kida H, Kawaoka Y. Receptor specificity of influenza A viruses correlates with the agglutination of erythrocytes from different animal species. Virology. 1997 Jan 20;227(2):493–9.

113. Louisirirotchanakul S, Lerdsamran H, Wiriyarat W, Sangsiriwut K, Chaichoune K, Pooruk P, et al. Erythrocyte binding preference of avian influenza H5N1 viruses. Journal of Clinical Microbiology. 2007 Jul;45(7):2284–6.

114. Trombetta CM. Impact of erythrocyte species on assays for influenza serology. Journal of Preventive Medicine and Hygiene. 2018 Mar 29;59(1):E1–E1.

115. World Health Organization. Manual for the laboratory diagnosis and virological surveillance of influenza. Geneva: World Health Organization; 2011.

116. Nobusawa E, Ishihara H, Morishita T, Sato K, Nakajima K. Change in Receptor-Binding Specificity of Recent Human Influenza A Viruses (H3N2): A Single Amino Acid Change in Hemagglutinin Altered Its Recognition of Sialyloligosaccharides. Virology. 2000 Dec 20;278(2):587–96.

117. Medeiros R, Escriou N, Naffakh N, Manuguerra JC, van der Werf S. Hemagglutinin Residues of Recent Human A(H3N2) Influenza Viruses That Contribute to the Inability to Agglutinate Chicken Erythrocytes. Virology. 2001 Oct 10;289(1):74–85.

118. Byrd-Leotis L, Gao C, Jia N, Mehta AY, Trost J, Cummings SF, et al. Antigenic Pressure on H3N2 Influenza Virus Drift Strains Imposes Constraints on Binding to Sialylated Receptors but Not Phosphorylated Glycans. Schultz-Cherry S, editor. Journal of Virology. 2019 Nov 15;93(22):e01178-19.

119. Peck H, Laurie KL, Rockman S, Leung V, Lau H, Soppe S, et al. Enhanced isolation of influenza viruses in qualified cells improves the probability of well-matched vaccines. npj Vaccines. 2021 Dec 9;6(1):1–9.

120. Kahane I, Polliack A, Rachmilewitz EA, Bayer EA, Skutelsky E. Distribution of sialic acids on the red blood cell membrane in β thalassaemia. Nature. 1978 Feb;271(5646):674–5.

121. Durocher JR, Payne RC, Conrad ME. Role of sialic acid in erythrocyte survival. Blood. 1975 Jan;45(1):11–20.

122. Kumar D, Rizvi SI. Erythrocyte membrane bound and plasma sialic acid during aging. Biologia. 2013 Aug 1;68(4):762–5.

123. Diez-Silva M, Dao M, Han J, Lim CT, Suresh S. Shape and Biomechanical Characteristics of Human Red Blood Cells in Health and Disease. MRS bulletin / Materials Research Society. 2010 May;35(5):382–8.

124. Gregory TR. Nucleotypic effects without nuclei: Genome size and erythrocyte size in mammals. Genome. 2000 Oct;43(5):895–901.

125. Scanes CG. Chapter 10 - Blood. In: Scanes CG, editor. Sturkie's Avian Physiology (Sixth Edition). San Diego: Academic Press; 2015. p. 167–91.

126. Hartman FA, Lessler MA. Erythrocyte Measurements in Birds. The Auk. 1963 Oct;80(4):467–73.

127. Jonges M, Liu WM, van der Vries E, Jacobi R, Pronk I, Boog C, et al. Influenza Virus Inactivation for Studies of Antigenicity and Phenotypic Neuraminidase Inhibitor Resistance Profiling. Journal of Clinical Microbiology. 2010 Mar;48(3):928–40.

128. Goldstein MA, Tauraso NM. Effect of Formalin, β-Propiolactone, Merthiolate, and Ultraviolet Light Upon Influenza Virus Infectivity, Chicken Cell Agglutination, Hemagglutination, and Antigenicity. Applied Microbiology. 1970 Feb;19(2):290–4.

129. Elveborg S, Monteil VM, Mirazimi A. Methods of Inactivation of Highly Pathogenic Viruses for Molecular, Serology or Vaccine Development Purposes. Pathogens. 2022 Feb;11(2):271.

130. Bonnafous P, Nicolaï MC, Taveau JC, Chevalier M, Barrière F, Medina J, et al. Treatment of influenza virus with Beta-propiolactone alters viral membrane fusion. Biochimica et Biophysica Acta (BBA) - Biomembranes. 2014 Jan 1;1838(1, Part B):355–63.

131. Ananthanarayan R, Paniker CKJ. Non-specific inhibitors of influenza viruses in normal sera. Bulletin of the World Health Organization. 1960;22(3–4):409–19.

132. Ryan-Poirier KA, Kawaoka Y. Distinct glycoprotein inhibitors of influenza A virus in different animal sera. Journal of Virology. 1991 Jan;65(1):389–95.

133. Isaacs A, Bozzo A. The Use of V. cholerae Filtrates in the Destruction of Non-Specific Inhibitor in Ferret Sera. British Journal of Experimental Pathology. 1951 Aug;32(4):325–35.

134. Fedorov AY, Zhirnov OP. Method for evaluating the neuraminidase activity of receptordestroying enzyme (RDE) compounds using the influenza virus. Voprosy Virusologii. 2020;65(2):113–8.

135. Kim HR, Lee KK, Kwon YK, Kang MS, Moon OK, Park CK. Comparison of serum treatments to remove nonspecific inhibitors from chicken sera for the hemagglutination inhibition test with inactivated H5N1 and H9N2 avian Influenza A virus subtypes. Journal of Veterinary Diagnostic Investigation. 2012 Sep 1;24(5):954–8.

136. CDC. Modified hemagglutination inhibition (hi) assay using horse rbcs for serologic detection of antibodies to h7 subtype avian influenza virus in human sera (Version 1) [Internet]. 2013 [cited 2023 Nov 26]. Available from: https://media.tghn.org/articles/160713_Modified_Hemagglutination_Inhibition_Assay_Using_Horse_RBCs.pdf

137. Spackman E, Sitaras I. Hemagglutination Inhibition Assay. In: Spackman E, editor. Animal Influenza Virus: Methods and Protocols. New York, NY: Springer US; 2020. p. 11–28. (Methods in Molecular Biology).

138. FLUCOP Training module [Internet]. figshare. figshare; 2021 [cited 2023 Nov 26]. Available from: https://figshare.com/articles/media/FLUCOP_Training_module/14822475/1

139. Waldock J, Zheng L, Remarque EJ, Civet A, Hu B, Jalloh SL, et al. Assay Harmonization and Use of Biological Standards To Improve the Reproducibility of the Hemagglutination Inhibition Assay: a FLUCOP Collaborative Study. mSphere. 2021 Jul 28;6(4):10.1128/msphere.00567-21.

140. Antigenic Characterization | CDC [Internet]. 2023 [cited 2023 Dec 7]. Available from: https://www.cdc.gov/flu/about/professionals/antigenic.htm

141. Monto AS, Maassab HF. Ether treatment of type B influenza virus antigen for the hemagglutination inhibition test. Journal of Clinical Microbiology. 1981 Jan;13(1):54–7.

142. Carnell GW, Trombetta CM, Ferrara F, Montomoli E, Temperton NJ. Correlation of Influenza B Haemagglutination Inhibiton, Single-Radial Haemolysis and Pseudotype-Based Microneutralisation Assays for Immunogenicity Testing of Seasonal Vaccines. Vaccines. 2021 Feb;9(2):100.

143. Kendal AP, Cate TR. Increased sensitivity and reduced specificity of hemagglutination inhibition tests with ether-treated influenza B/Singapore/222/79. Journal of Clinical Microbiology. 1983 Oct;18(4):930–4.

144. Noah DL, Hill H, Hines D, White EL, Wolff MC. Qualification of the Hemagglutination Inhibition Assay in Support of Pandemic Influenza Vaccine Licensure. Clinical and Vaccine Immunology : CVI. 2009 Apr;16(4):558–66.

145. Coudeville L, Bailleux F, Riche B, Megas F, Andre P, Ecochard R. Relationship between haemagglutination-inhibiting antibody titres and clinical protection against influenza: development and application of a bayesian random-effects model. BMC Medical Research Methodology. 2010 Mar 8;10:18.

146. Trombetta CM, Perini D, Mather S, Temperton N, Montomoli E. Overview of Serological Techniques for Influenza Vaccine Evaluation: Past, Present and Future. Vaccines. 2014 Oct 13;2(4):707–34.

147. Veguilla V, Hancock K, Schiffer J, Gargiullo P, Lu X, Aranio D, et al. Sensitivity and specificity of serologic assays for detection of human infection with 2009 pandemic H1N1 virus in U.S. populations. Journal of Clinical Microbiology. 2011 Jun;49(6):2210–5.

148. Matrosovich M, Matrosovich T, Carr J, Roberts NA, Klenk HD. Overexpression of the α-2,6-Sialyltransferase in MDCK Cells Increases Influenza Virus Sensitivity to Neuraminidase Inhibitors. Journal of Virology. 2003 Aug;77(15):8418–25.

149. Mögling R, Richard MJ, van der Vliet S, van Beek R, Schrauwen EJA, Spronken MI, et al. Neuraminidase-mediated haemagglutination of recent human influenza A(H3N2) viruses is determined by arginine 150 flanking the neuraminidase catalytic site. The Journal of General Virology. 2017 Jun;98(6):1274–81.

150. Childs RA, Palma AS, Wharton S, Matrosovich T, Liu Y, Chai W, et al. Receptor-binding specificity of pandemic influenza A (H1N1) 2009 virus determined by carbohydrate microarray. Nature biotechnology. 2009 Sep;27(9):797–9.

151. Jorquera PA, Mishin VP, Chesnokov A, Nguyen HT, Mann B, Garten R, et al. Insights into the antigenic advancement of influenza A(H3N2) viruses, 2011–2018. Scientific Reports. 2019 Feb 25;9:2676.

152. Wood JM, Major D, Heath A, Newman RW, Höschler K, Stephenson I, et al. Reproducibility of serology assays for pandemic influenza H1N1: collaborative study to evaluate a candidate WHO International Standard. Vaccine. 2012 Jan 5;30(2):210–7.

153. Wood JM, Gaines-Das RE, Taylor J, Chakraverty P. Comparison of influenza serological techniques by international collaborative study. Vaccine. 1994 Jan 1;12(2):167–74.

154. Innovative Medicines Initiative. 10th Call for Proposals 2013 (Version 2) [Internet]. 2013 [cited 2023 Nov 26]. Available from: https://www.imi.europa.eu/sites/default/files/uploads/documents/apply-for-funding/call-documents/imi1/Call10_final_text.pdf

155. Van Kerkhove MD, Broberg E, Engelhardt OG, Wood J, Nicoll A. The consortium for the standardization of influenza seroepidemiology (CONSISE): a global partnership to standardize influenza seroepidemiology and develop influenza investigation protocols to inform public health policy. Influenza and Other Respiratory Viruses. 2013 May;7(3):231–4.

156. FLUCOP [Internet]. FLUCOP. [cited 2023 Nov 26]. Available from: https://flucop.eu/about-flucop/project-description/

157. Zacour M, Ward BJ, Brewer A, Tang P, Boivin G, Li Y, et al. Standardization of Hemagglutination Inhibition Assay for Influenza Serology Allows for High Reproducibility between Laboratories. Hodinka RL, editor. Clinical and Vaccine Immunology. 2016 Mar;23(3):236–42.

158. Wagner R, Göpfert C, Hammann J, Neumann B, Wood J, Newman R, et al. Enhancing the reproducibility of serological methods used to evaluate immunogenicity of pandemic H1N1 influenza vaccines—An effective EU regulatory approach. Vaccine. 2012 Jun 8;30(27):4113–22.

159. Wood JM, Montomoli E, Newman RW, Daas A, Buchheit KH, Terao E. Collaborative study on influenza vaccine clinical trial serology - part 2: reproducibility study. Pharmeuropa Bio & Scientific Notes. 2011 Jun;2011(1):36–54.

160. Carbosynth LLC. Glutaraldehyde-stabilized freshly prepared Turkey Red Blood Cells [Internet]. [cited 2023 Dec 4]. Available from: https://www.fishersci.com/shop/products/turkey-red-blood-cells-2/501253514

161. Kode SS, Pawar SD, Tare DS, Mullick J. Application of frozen and stored glutaraldehyde-fixed turkey red blood cells for hemagglutination and hemagglutination inhibition assays for the detection and identification of influenza viruses. Journal of Virological Methods. 2021 Mar;289:114046.

162. Esmail S, Knauer MJ, Abdoh H, Voss C, Chin-Yee B, Stogios P, et al. Rapid and accurate agglutination-based testing for SARS-CoV-2 antibodies. Cell Reports Methods. 2021 May 12;1(2):100011.

163. Xu X, Jin M, Yu Z, Li H, Qiu D, Tan Y, et al. Latex Agglutination Test for Monitoring Antibodies to Avian Influenza Virus Subtype H5N1. Journal of Clinical Microbiology. 2005 Apr;43(4):1953–5.

164. Grace MR, Chauhan J, Suman Kumar M, Kumar A, Bhilegaonkar KN, Singh M, et al. Evaluation of carboxyl beads based latex agglutination test for rapid sero-diagnosis of Japanese encephalitis. Biologicals. 2019 Nov 1;62:72–6.

165. Hosaka S, Murao Y, Masuko S, Miura K. Preparation of Microspheres of Poly(Glycidyl Methacrylate) and its Derivatives as Carriers for Immobilized Proteins. Immunological Communications. 1983 Jan 1;12(5):509–17.

166. Driskell JD, Jones CA, Tompkins SM, Tripp RA. One-step assay for detecting influenza virus using dynamic light scattering and gold nanoparticles. The Analyst. 2011 Aug 7;136(15):3083–90.

167. Chen J, Jin M, Yu Z, Dan H, Zhang A, Song Y, et al. A latex agglutination test for the rapid detection of avian influenza virus subtype H5N1 and its clinical application. Journal of Veterinary Diagnostic Investigation: Official Publication of the American Association of Veterinary Laboratory Diagnosticians, Inc. 2007 Mar;19(2):155–60.

168. Buffin S, Ikhelef N, Prudent J, Dubayle J, Nougarede N, Varenne MP, et al. A latex agglutination assay to quantify the amount of hemagglutinin protein in adjuvanted low-dose influenza monovalent vaccines. Journal of Virological Methods. 2018 Jan;251:46–53.

169. Poonthiyil V, Nagesh PT, Husain M, Golovko VB, Fairbanks AJ. Gold Nanoparticles Decorated with Sialic Acid Terminated Bi-antennary N-Glycans for the Detection of Influenza Virus at Nanomolar Concentrations. ChemistryOpen. 2015;4(6):708–16.

170. Lee C, Gaston MA, Weiss AA, Zhang P. Colorimetric viral detection based on sialic acid stabilized goldnanoparticles. Biosensors and Bioelectronics. 2013 Apr 15;42:236–41.

171. Richards SJ, Baker AN, Walker M, Gibson MI. Polymer-Stabilized Sialylated Nanoparticles: Synthesis, Optimization, and Differential Binding to Influenza Hemagglutinins. Biomacromolecules. 2020 Apr 13;21(4):1604–12.

172. Marín MJ, Rashid A, Rejzek M, Fairhurst SA, Wharton SA, Martin SR, et al. Glyconanoparticles for the plasmonic detection and discrimination between human and avian influenza virus. Organic & Biomolecular Chemistry. 2013 Oct 1;11(41):7101–7.

173. Papp I, Sieben C, Ludwig K, Roskamp M, Böttcher C, Schlecht S, et al. Inhibition of influenza virus infection by multivalent sialic-acid-functionalized gold nanoparticles. Small (Weinheim an Der Bergstrasse, Germany). 2010 Dec 20;6(24):2900–6.

174. Papp I, Sieben C, Sisson AL, Kostka J, Böttcher C, Ludwig K, et al. Inhibition of influenza virus activity by multivalent glycoarchitectures with matched sizes. Chembiochem: A European Journal of Chemical Biology. 2011 Apr 11;12(6):887–95.

175. Lee C, Wang P, Gaston MA, Weiss AA, Zhang P. Plasmonics-Based Detection of Virus Using Sialic Acid Functionalized Gold Nanoparticles. Biosensors and Biodetection. 2017 Mar 10;1571:109–16.

176. Tayyab S, Qasim MA. Biochemistry and roles of glycophorin A. Biochemical Education. 1988;16(2):63–6.

177. Marchesi VT, Furthmayr H, Tomita M. The red cell membrane. Annual Review of Biochemistry. 1976;45:667–98.

178. Aoki T. A Comprehensive Review of Our Current Understanding of Red Blood Cell (RBC) Glycoproteins. Membranes. 2017 Dec;7(4):56.

179. Vesterberg O, Breig U. Quantitative analysis of multiple molecular forms of transferrin using isoelectric focusing and zone immunoelectrophoresis assay (ZIA). Journal of Immunological Methods. 1981 Oct 15;46(1):53–62.

180. Uittenbogaard JP, Zomer B, Hoogerhout P, Metz B. Reactions of β-Propiolactone with Nucleobase Analogues, Nucleosides, and Peptides: Implications for the inactivation of viruses. Journal of Biological Chemistry. 2011 Oct 21;286(42):36198–214.

181. Doshi N, Zahr AS, Bhaskar S, Lahann J, Mitragotri S. Red blood cell-mimicking synthetic biomaterial particles. Proceedings of the National Academy of Sciences of the United States of America. 2009 Dec;106(51):21495.

182. Guo J, Agola JO, Serda R, Franco S, Lei Q, Wang L, et al. Biomimetic Rebuilding of Multifunctional Red Blood Cells: Modular Design Using Functional Components. ACS Nano. 2020 Jul;14(7):7847–59.

183. Trakarnsanga K, Griffiths RE, Wilson MC, Blair A, Satchwell TJ, Meinders M, et al. An immortalized adult human erythroid line facilitates sustainable and scalable generation of functional red cells. Nature Communications. 2017 Mar 14;8(1):14750.

184. Zheng L, Wei J, Lv X, Bi Y, Wu P, Zhang Z, et al. Detection and differentiation of influenza viruses with glycan-functionalized gold nanoparticles. Biosensors & bioelectronics. 2017 May;91:46–52.

185. Horiguchi Y, Goda T, Matsumoto A, Takeuchi H, Yamaoka S, Miyahara Y. Direct and label-free influenza virus detection based on multisite binding to sialic acid receptors. Biosensors & Bioelectronics. 2017 Jun;92:234.

186. Courtney SJ, Stromberg ZR, Kubicek-Sutherland JZ. Nucleic Acid-Based Sensing Techniques for Diagnostics and Surveillance of Influenza. Biosensors. 2021 Feb;11(2):47.

187. Norouzi N, Bhakta HC, Grover WH. Sorting cells by their density. PLoS ONE. 2017 Jul 19;12(7):e0180520.

188. Alves D, Curvello R, Henderson E, Kesarwani V, Walker JA, Leguizamon SC, et al. Rapid Gel Card Agglutination Assays for Serological Analysis following SARS-CoV-2 Infection in Humans. ACS Sensors. 2020;

189. Bruce-Staskal PJ, Woods RM, Borisov OV, Massare MJ, Hahn TJ. Hemagglutinin from multiple divergent influenza A and B viruses bind to a distinct branched, sialylated poly-LacNAc glycan by surface plasmon resonance. Vaccine. 2020 Oct 7;38(43):6757–65.

190. Meng B, Marriott AC, Dimmock NJ. The receptor preference of influenza viruses. Influenza and other Respiratory Viruses. 2010 May;4(3):147–53.

191. Guo H, Vries E de, McBride R, Dekkers J, Peng W, Bouwman KM, et al. Highly Pathogenic Influenza A(H5Nx) Viruses with Altered H5 Receptor-Binding Specificity. Emerging Infectious Diseases. 2017 Feb;23(2):220–30.

192. Du W, Guo H, Nijman VS, Doedt J, Vries E van der, Lee J van der, et al. The 2nd sialic acid-binding site of influenza A virus neuraminidase is an important determinant of the hemagglutinin-neuraminidase-receptor balance. PLOS Pathogens. 2019 Jun;15(6):e1007860.

193. Spik G, Bayard B, Fournet B, Strecker G, Bouquelet S, Montreuil J. Studies on glycoconjugates. LXIV. Complete structure of two carbohydrate units of human serotransferrin. FEBS Letters. 1975 Feb;50(3):296–9.

194. Baenziger JU, Fiete D. Structure of the complex oligosaccharides of fetuin. The Journal of Biological Chemistry. 1979 Feb 10;254(3):789–95.

195. Hoshi K, Kariya Y, Nara K, Ito H, Matsumoto K, Nagae M, et al. Lectin-dependent inhibition of antigen–antibody reaction: application for measuring α2,6-sialylated glycoforms of transferrin. The Journal of Biochemistry. 2013 Sep 1;154(3):229–32.

196. López-Gallego F, Betancor L, Mateo C, Hidalgo A, Alonso-Morales N, Dellamora-Ortiz G, et al. Enzyme stabilization by glutaraldehyde crosslinking of adsorbed proteins on aminated supports. Journal of biotechnology. 2005 Sep;119(1):70–5.

197. Spiro RG. Studies on Fetuin, a Glycoprotein of Fetal Serum: I. Isolation, chemical composition, and physiocochemical properties. Journal of Biological Chemistry. 1960 Oct;235(10):2860–9.

198. Mu B, Huang X, Bu P, Zhuang J, Cheng Z, Feng J, et al. Influenza virus detection with pentabody-activated nanoparticles. Journal of Virological Methods. 2010 Nov;169(2):282–9.

199. Chou TC, Hsu W, Wang CH, Chen YJ, Fang JM. Rapid and specific influenza virus detection by functionalized magnetic nanoparticles and mass spectrometry. Journal of Nanobiotechnology. 2011 Nov 16;9:52.

200. Matrosovich MN, Mochalova LV, Marinina VP, Byramova NE, Bovin NV. Synthetic polymeric sialoside inhibitors of influenza virus receptor-binding activity. FEBS letters. 1990 Oct 15;272(1–2):209–12.

201. Matrosovich M, Klenk HD. Natural and synthetic sialic acid-containing inhibitors of influenza virus receptor binding. Reviews in Medical Virology. 2003;13(2):85–97.

202. Bhatia S, Dimde M, Haag R. Multivalent glycoconjugates as vaccines and potential drug candidates. MedChemComm. 2014;5(7):862–78.

203. Carlescu I, Scutaru D, Popa M, Uglea CV. Synthetic sialic-acid-containing polyvalent antiviral inhibitors. Medicinal Chemistry Research. 2009 Jul 1;18(6):477–94.

204. Fernandes AI, Gregoriadis G. The effect of polysialylation on the immunogenicity and antigenicity of asparaginase: implication in its pharmacokinetics. International Journal of Pharmaceutics. 2001 Apr 17;217(1–2):215–24.

205. Ogata M, Murata T, Murakami K, Suzuki T, Hidari KIPJ, Suzuki Y, et al. Chemoenzymatic synthesis of artificial glycopolypeptides containing multivalent sialyloligosaccharides with a gamma-polyglutamic acid backbone and their effect on inhibition of infection by influenza viruses. Bioorganic & Medicinal Chemistry. 2007 Feb 1;15(3):1383–93.

206. Whitesides GM, Mathias JP, Seto CT. Molecular Self-Assembly and Nanochemistry: a Chemical Strategy for the Synthesis of Nanostructures. Science. 1991 Nov 29;254(5036):1312–9.

207. Sigal GB, Mammen M, Dahmann G, Whitesides GM. Polyacrylamides Bearing Pendant α-Sialoside Groups Strongly Inhibit Agglutination of Erythrocytes by Influenza Virus: The Strong Inhibition Reflects Enhanced Binding through Cooperative Polyvalent Interactions. Journal of the American Chemical Society. 1996 Apr 24;118(16):3789–800.

208. Totani K, Kubota T, Kuroda T, Murata T, Hidari KIPJ, Suzuki T, et al. Chemoenzymatic synthesis and application of glycopolymers containing multivalent sialyloligosaccharides with a poly(L-glutamic acid) backbone for inhibition of infection by influenza viruses. Glycobiology. 2003 May 1;13(5):315–26.

209. Otsuka I, Blanchard B, Borsali R, Imberty A, Kakuchi T. Enhancement of plant and bacterial lectin binding affinities by three-dimensional organized cluster glycosides constructed on helical poly(phenylacetylene) backbones. Chembiochem: A European Journal of Chemical Biology. 2010 Nov 22;11(17):2399–408.

210. Roy R, Zanini D, Meunier SJ, Romanowska A. Solid-phase synthesis of dendritic sialoside inhibitors of influenza A virus haemagglutinin. Journal of the Chemical Society, Chemical Communications. 1993 Jan 1;(24):1869–72.

211. Reuter JD, Myc A, Hayes MM, Gan Z, Roy R, Qin D, et al. Inhibition of Viral Adhesion and Infection by Sialic-Acid-Conjugated Dendritic Polymers. Bioconjugate Chemistry. 1999 Mar 1;10(2):271–8.

212. Sashiwa H, Shigemasa Y, Roy R. Chemical Modification of Chitosan. 10. Synthesis of Dendronized Chitosan−Sialic Acid Hybrid Using Convergent Grafting of Preassembled Dendrons Built on Gallic Acid and Tri(ethylene glycol) Backbone. Macromolecules. 2001 Jun 1;34(12):3905–9.

213. Kingery-Wood JE, Williams KW, Sigal GB, Whitesides GM. The agglutination of erythrocytes by influenza virus is strongly inhibited by liposomes incorporating an analog of sialyl gangliosides. Journal of the American Chemical Society. 1992 Aug 1;114(18):7303–5.

214. Guo CT, Sun XL, Kanie O, Shortridge KF, Suzuki T, Miyamoto D, et al. An O-glycoside of sialic acid derivative that inhibits both hemagglutinin and sialidase activities of influenza viruses. Glycobiology. 2002 Mar 1;12(3):183–90.

215. Losada-Garcia N, Garcia-Sanz C, Andreu A, Velasco-Torrijos T, Palomo JM. Glyconanomaterials for Human Virus Detection and Inhibition. Nanomaterials. 2021 Jun 26;11(7):1684.

216. Benton DJ, Martin SR, Wharton SA, McCauley JW. Biophysical Measurement of the Balance of Influenza A Hemagglutinin and Neuraminidase Activities. The Journal of Biological Chemistry. 2015 Mar 6;290(10):6516–21.

217. Sauter NK, Bednarski MD, Wurzburg BA, Hanson JE, Whitesides GM, Skehel JJ, et al. Hemagglutinins from two influenza virus variants bind to sialic acid derivatives with millimolar dissociation constants: a 500-MHz proton nuclear magnetic resonance study. Biochemistry. 1989 Oct 17;28(21):8388–96.

218. Cuellar-Camacho JL, Bhatia S, Reiter-Scherer V, Lauster D, Liese S, Rabe JP, et al. Quantification of Multivalent Interactions between Sialic Acid and Influenza A Virus Spike Proteins by Single-Molecule Force Spectroscopy. Journal of the American Chemical Society. 2020 Jul 15;142(28):12181–92.

219. Worldwide Influenza Center, The Francis Crick Institute. Report prepared for the WHO annual consultation on the composition of influenza vaccines for the Southern Hemisphere 2023 [Internet]. 2022 [cited 2023 Dec 5]. Available from: https://www.crick.ac.uk/sites/default/files/2022-10/Crick%20report%20Sep2022%20for%20SH2023_to%20post.pdf

220. Stencel-Baerenwald JE, Reiss K, Reiter DM, Stehle T, Dermody TS. The sweet spot: defining virus–sialic acid interactions. Nature reviews Microbiology. 2014 Nov;12(11):739–49.

221. Soundararajan V, Tharakaraman K, Raman R, Raguram S, Shriver Z, Sasisekharan V, et al. Extrapolating from sequence--the 2009 H1N1 “swine” influenza virus. Nature Biotechnology. 2009 Jun;27(6):510–3.

222. Cheng VCC, To KKW, Tse H, Hung IFN, Yuen KY. Two Years after Pandemic Influenza A/2009/H1N1: What Have We Learned? Clinical Microbiology Reviews. 2012 Apr;25(2):223–63.

223. Bradley KC, Jones CA, Tompkins SM, Tripp RA, Russell RJ, Gramer MR, et al. Comparison of the receptor binding properties of contemporary swine isolates and early human pandemic H1N1 isolates (Novel 2009 H1N1). Virology. 2011 May 10;413(2):169–82.

224. Chen LM, Rivailler P, Hossain J, Carney P, Balish A, Perry I, et al. Receptor specificity of subtype H1 influenza A viruses isolated from swine and humans in the United States. Virology. 2011 Apr 10;412(2):401–10.

225. Ovsyannikova IG, White SJ, Albrecht RA, García-Sastre A, Poland GA. Turkey Versus Guinea Pig Red Blood Cells: Hemagglutination Differences Alter Hemagglutination Inhibition Responses Against Influenza A/H1N1. Viral Immunology. 2014 May;27(4):174–8.

226. Farnsworth A, Cyr TD, Li C, Wang J, Li X. Antigenic stability of H1N1 pandemic vaccines correlates with vaccine strain. Vaccine. 2011 Feb 11;29(8):1529–33.

227. Creanga A, Hang NLK, Cuong VD, Nguyen HT, Phuong HVM, Thanh LT, et al. Highly Pathogenic Avian Influenza A(H5N1) Viruses at the Animal–Human Interface in Vietnam, 2003–2010. The Journal of Infectious Diseases. 2017 Sep 15;216(suppl_4):S529–38.

228. Kayali G, Setterquist SF, Capuano AW, Myers KP, Gill JS, Gray GC. Testing Human Sera for Antibodies against Avian Influenza Viruses. Journal of clinical virology : the official publication of the Pan American Society for Clinical Virology. 2008 Sep;43(1):73–8.

229. Jankowski MD, Glaberman SR, Kimball DB, Taylor-McCabe KJ, Fair JM. Sialic acid on avian erythrocytes. Comparative Biochemistry and Physiology Part B: Biochemistry and Molecular Biology. 2019 Dec 1;238:110336.

230. Ramachandran S, Fu E, Lutz B, Yager P. Long-term dry storage of an enzyme-based reagent system for ELISA in point-of-care devices. The Analyst. 2014 Mar 21;139(6):1456–62.

231. Huang Y, Tuo W, Wang D, Kang L, Chen X, Luo M. Restoring the youth of aged red blood cells and extending their lifespan in circulation by remodelling membrane sialic acid. Journal of Cellular and Molecular Medicine. 2016 Feb;20(2):294–301.

232. Huang YX, Wu ZJ, Mehrishi J, Huang BT, Chen XY, Zheng XJ, et al. Human red blood cell aging: correlative changes in surface charge and cell properties. Journal of Cellular and Molecular Medicine. 2011 Dec;15(12):2634–42.

233. Sut C, Tariket S, Chou ML, Garraud O, Laradi S, Hamzeh-Cognasse H, et al. Duration of red blood cell storage and inflammatory marker generation. Blood Transfusion. 2017 Mar;15(2):145–52.

234. Dalen AB. The effect of glutaraldehyde on the stability of erythrocytes and on virus receptor substances. Acta Pathologica Et Microbiologica Scandinavica Section B, Microbiology. 1976 Aug;84(4):196–200.

235. Lim YA. Preparation of Glutaraldehyde-Treated Red Blood Cells Expressing Weak ABO and RhD Antigens for Use in Tube Methods. Journal of Laboratory Medicine and Quality Assurance. 2020 Jun 30;42(2):84–90.

236. Han Y, Quan GB, Liu XZ, Ma EP, Liu A, Jin P, et al. Improved preservation of human red blood cells by lyophilization. Cryobiology. 2005 Oct 1;51(2):152–64.

237. Xu SZ, Bode AP. Stabilization of Human Erythrocytes for Lyophilization: Recovery of Biochemical Activities and Membrane Filterability. Blood. 2004 Nov 16;104(11):3670.

238. Arav A, Natan D. Freeze Drying of Red Blood Cells: The Use of Directional Freezing and a New Radio Frequency Lyophilization Device. Biopreservation and Biobanking. 2012 Aug;10(4):386–94.

239. Zhu W, Chen X, Yuan L, Wu J, Yao J. Degradation Kinetics and Shelf Life of N-acetylneuraminic Acid at Different pH Values. Molecules. 2020 Jan;25(21):5141.

240. Kawasaki H, Shimanouchi T, Kimura Y. Recent Development of Optimization of Lyophilization Process. Journal of Chemistry. 2019 May 5;2019:e9502856.

241. Laidler KJ. The development of the Arrhenius equation. Journal of Chemical Education. 1984 Jun 1;61(6):494.

242. Bell TA. Challenges in the scale-up of particulate processes—an industrial perspective. Powder Technology. 2005 Feb 16;150(2):60–71.

243. European Commission Decision C(2020)6320. Horizon 2020 – Work Programme 2018-2020 - Technology readiness levels [Internet]. 2020. Available from: https://ec.europa.eu/research/participants/data/ref/h2020/other/wp/2018-2020/annexes/h2020-wp1820-annex-g-trl_en.pdf

244. Chambers BS, Li Y, Hodinka RL, Hensley SE. Recent H3N2 Influenza Virus Clinical Isolates Rapidly Acquire Hemagglutinin or Neuraminidase Mutations When Propagated for Antigenic Analyses. Journal of Virology. 2014 Sep;88(18):10986–9.

245. Sklavounos AA, Lamanna J, Modi D, Gupta S, Mariakakis A, Callum J, et al. Digital Microfluidic Hemagglutination Assays for Blood Typing, Donor Compatibility Testing, and Hematocrit Analysis. Clinical Chemistry. 2021 Dec 1;67(12):1699–708.

246. Nguyen M, Fries K, Khoury R, Zheng L, Hu B, Hildreth SW, et al. Automated Imaging and Analysis of the Hemagglutination Inhibition Assay. SLAS Technology. 2016 Apr 1;21(2):287–96.

247. Park J, Park JK. Finger-Actuated Microfluidic Display for Smart Blood Typing. Analytical Chemistry. 2019 Sep 17;91(18):11636–42.

248. Ramasubramanian M, Anthony S, Lambert J. Simplified spectraphotometric method for the detection of red blood cell agglutination. Applied Optics. 2008 Aug 1;47(22):4094–105.

249. Jang I, Kang H, Song S, Dandy DS, Geiss BJ, Henry CS. Flow control in a laminate capillary-driven microfluidic device. Analyst. 2021 Mar 22;146(6):1932–9.

250. Weigl BH, Bardell R, Schulte T, Battrell F, Hayenga J. Design and Rapid Prototyping of Thin-Film Laminate-Based Microfluidic Devices. Biomedical Microdevices. 2001 Dec 1;3(4):267–74.

251. Samae M, Chatpun S, Chirasatitsin S. Hemagglutination Detection with Paper–Plastic Hybrid Passive Microfluidic Chip. Micromachines. 2021 Dec 9;12(12):1533.

252. FluHema [Internet]. SciRobotics. [cited 2023 Nov 29]. Available from: https://scirobotics.com/fluhema/

253. Wilson G, Ye Z, Xie H, Vahl S, Dawson E, Rowlen K. Automated interpretation of influenza hemagglutination inhibition (HAI) assays: Is plate tilting necessary? PLoS ONE. 2017 Jun 29;12(6):e0179939.

254. Ives, J.T., Woodward, C. Manual versus Automated Readers for Hemagglutination Assays [Internet]. 2017 [cited 2023 Nov 29]. Available from: https://www.indevr.com/wp-content/uploads/2020/05/CypherOne-Application-Note-Manual-versus-Automated-Readers-for-Hemagglutination-Assays-CF-0142-R002.pdf

255. Zhao W, Baldwin E, Cameron R. A digital data interpretation method for hemagglutination inhibition assay by using a plate reader. Analytical Biochemistry. 2019 Apr 15;571:37–9.

256. Samper IC, Sánchez-Cano A, Khamcharoen W, Jang I, Siangproh W, Baldrich E, et al. Electrochemical Capillary-Flow Immunoassay for Detecting Anti-SARS-CoV-2 Nucleocapsid Protein Antibodies at the Point of Care. ACS Sensors. 2021 Nov 26;6(11):4067–75.

257. Carrell C, Jang I, Link J, Terry JS, Call Z, Panraksa Y, et al. Capillary driven microfluidic sequential flow device for point-of-need ELISA: COVID-19 serology testing. Analytical Methods. 15(22):2721–8.

258. Adkins JA, Noviana E, Henry CS. Development of a Quasi-Steady Flow Electrochemical Paper-Based Analytical Device. Analytical Chemistry. 2016 Nov 1;88(21):10639–47.

259. Polpanich D, Tangboriboonrat P, Elaissari A, Udomsangpetch R. Detection of Malaria Infection via Latex Agglutination Assay. Analytical Chemistry. 2007 Jun 1;79(12):4690–5.

260. Salam MA, Khan MGM, Mondal D. Urine antigen detection by latex agglutination test for diagnosis and assessment of initial cure of visceral leishmaniasis. Transactions of the Royal Society of Tropical Medicine and Hygiene. 2011 May;105(5):269–72.

261. Cruz CJG, Kil R, Wong S, Dacquay LC, Mirano-Bascos D, Rivera PT, et al. Malarial Antibody Detection with an Engineered Yeast Agglutination Assay. ACS Synthetic Biology. 2022 Sep 16;11(9):2938–46.

262. Molina-Bolívar JA, Galisteo-González F. Latex Immunoagglutination Assays. Journal of Macromolecular Science, Part C: Polymer Reviews. 2005 Jan;45(1):59–98.

263. Mathison BA, Pritt BS. Update on Malaria Diagnostics and Test Utilization. Journal of Clinical Microbiology. 2017 Jul;55(7):2009–17.

264. de la Serna E, Arias-Alpízar K, Borgheti-Cardoso LN, Sanchez-Cano A, Sulleiro E, Zarzuela F, et al. Detection of Plasmodium falciparum malaria in 1 h using a simplified enzyme-linked immunosorbent assay. Analytica Chimica Acta. 2021 Apr 1;1152:338254.

265. Ruiz-Vega G, Arias-Alpízar K, de la Serna E, Borgheti-Cardoso LN, Sulleiro E, Molina I, et al. Electrochemical POC device for fast malaria quantitative diagnosis in whole blood by using magnetic beads, Poly-HRP and microfluidic paper electrodes. Biosensors and Bioelectronics. 2020 Feb 15;150:111925.

266. Sánchez-Cano A, Ruiz-Vega G, Vicente-Gómez S, de la Serna E, Sulleiro E, Molina I, et al. Development of a Fast Chemiluminescent Magneto-Immunoassay for Sensitive Plasmodium falciparum Detection in Whole Blood. Analytical Chemistry. 2021 Sep 21;93(37):12793–800.

267. Tangpukdee N, Duangdee C, Wilairatana P, Krudsood S. Malaria Diagnosis: A Brief Review. The Korean Journal of Parasitology. 2009 Jun;47(2):93–102.

268. Emanuel EJ, Persad G, Upshur R, Thome B, Parker M, Glickman A, et al. Fair Allocation of Scarce Medical Resources in the Time of Covid-19. The New England Journal of Medicine. 2020 May 21;382(21):2049–55.

269. Li Z, Yi Y, Luo X, Xiong N, Liu Y, Li S, et al. Development and clinical application of a rapid IgM-IgG combined antibody test for SARS-CoV-2 infection diagnosis. Journal of Medical Virology. 2020;92(9):1518–24.

270. Pavlova IP, Nair SS, Kyprianou N, Tewari AK. The Rapid Coronavirus Antibody Test: Can We Improve Accuracy? Frontiers in Medicine. 2020 Sep 2;7:569.

271. Peeling RW, Wedderburn CJ, Garcia PJ, Boeras D, Fongwen N, Nkengasong J, et al. Serology testing in the COVID-19 pandemic response. The Lancet Infectious Diseases. 2020 Sep 1;20(9):e245–9.

272. Whitman JD, Hiatt J, Mowery CT, Shy BR, Yu R, Yamamoto TN, et al. Test performance evaluation of SARS-CoV-2 serological assays. medRxiv; 2020. p. 2020.04.25.20074856.

273. Kobayashi J, Matsuyama S, Shirakura M, Arita T, Suzuki Y, Asanuma H, et al. Use of the particle agglutination/particle agglutination inhibition test for antigenic analysis of SARS-CoV-2. Influenza and Other Respiratory Viruses. 2023;17(2):e13093.

274. Townsend A, Rijal P, Xiao J, Tan TK, Huang KYA, Schimanski L, et al. A haemagglutination test for rapid detection of antibodies to SARS-CoV-2. Nature Communications. 2021 Mar 29;12(1):1951.

275. Hanson KE, Caliendo AM, Arias CA, Englund JA, Hayden MK, Lee MJ, et al. Infectious Diseases Society of America Guidelines on the Diagnosis of COVID-19:Serologic Testing. Clinical Infectious Diseases: An Official Publication of the Infectious Diseases Society of America. 2020 Sep 12;ciaa1343.

276. Kruse RL, Huang Y, Smetana H, Gehrie EA, Amukele TK, Tobian AAR, et al. A rapid, point-of-care red blood cell agglutination assay detecting antibodies against SARS-CoV-2. Biochemical and Biophysical Research Communications. 2021 May 14;553:165–71.

277. Pino P, Kint J, Kiseljak D, Agnolon V, Corradin G, Kajava AV, et al. Trimeric SARS-CoV-2 Spike Proteins Produced from CHO Cells in Bioreactors Are High-Quality Antigens. Processes. 2020 Dec;8(12):1539.

Annex A1

Publications produced as a result of this PhD Thesis

Detection of viruses and virus-neutralizing antibodies using synthetic erythrocytes: towards a tuneable tool for virus surveillance

Ana Sánchez-Cano[1,2], Cristina Andrés[3], José R. Herance[4], Tomás Pumarola[2,3], Andrés Antón[2,3], Eva Baldrich*[1,5]

1 Diagnostic Nanotools Group, CIBBIM - Nanomedicine, Vall d'Hebron Institut de Recerca (VHIR), Vall d'Hebron Barcelona Hospital Campus, Barcelona, Spain.

2 Universitat Autònoma de Barcelona (UAB), Bellaterra, Spain.

3 Respiratory Viruses Unit, Microbiology Department, Vall d'Hebron Hospital Universitari, Vall d'Hebron Barcelona Hospital Campus, Barcelona, Spain.

4 Medical Molecular Imaging Group, CIBBIM - Nanomedicine, Vall d'Hebron Institut de Recerca (VHIR), Vall d'Hebron Barcelona Hospital Campus, Barcelona, Spain.

5 CIBER de Bioingeniería, Biomateriales y Nanomedicina (CIBER-BBN), Spain.

ABSTRACT: The hemagglutination inhibition assay (HAI) is a classical method used worldwide in many analytical applications, including pathogen identification, vaccine production monitoring, and detection and characterization of pathogen-neutralizing antibodies (n-Ab). This is also a World Health Organization (WHO) reference method for the global surveillance of influenza viruses, which provides the information needed for the annual reformulation of the flu vaccine. HAI is a simple and inexpensive method that is performed without sophisticated equipment. However, it has to be carried out with fresh red blood cells (RBCs), a highly variable, unstable and hard to mass-produce reagent, which impairs assay reproducibility. Here, we used the tests employed for influenza surveillance as a model to develop s*ynthrocytes*, a synthetic reagent that could substitute animal erythrocytes in HAI. Contrary to previous examples exploiting sophisticated production paths to generate therapeutic synthetic RBCs, we founded production on the identification of microparticles able to generate different sedimentation patters when agglutinated or no, which is the main requirement for HAI testing. Upon incorporation of influenza-binding receptors and optimization of production and assay conditions, synthrocytes succeeded binding influenza A(H1N1) and B viruses as erythrocytes do, but were faster and more stable. Synthrocytes were finally employed in a HAI-like assay to detect the WHO reference reagents for influenza surveillance. Our results show that it is possible to substitute erythrocytes in classical HAI by a highly tuneable and potentially mass-produced synthetic reagent, which should facilitate worldwide HAI standardization with minimal equipment or training requirements.

KEYWORDS: synthetic erythrocyte; influenza surveillance; flu viruses; hemagglutination inhibition assay (HAI); characterization of virus-neutralizing antibodies; fast detection tests; method standardization.

Hemagglutination (HA) and hemagglutination inhibition assays (HAI) have been reference serological techniques for decades and are still used extensively to probe glycan-lectin interactions.[1,2] Among others, HA and HAI are employed for blood typing, virus antigenic characterization, determination of immunity to recent infection or vaccination, monitoring vaccine production and, eventually, with diagnostic purposes.[3] These are also World Health Organization (WHO) reference techniques for the permanent and global virological surveillance of influenza viruses, which is crucial to establish the annual reformulation of the flu vaccine.[4–6]

HA and HAI were originally described by Hirst in 1942 based on the ability of influenza viruses to bind red blood cells (RBCs), causing hemagglutination and altering RBC sedimentation.[7] Hirst observed as well that hemagglutination was inhibited in the presence of antibodies with virus-neutralizing capacity (n-Ab), an effect that was strain-specific and allowed virus classification and n-Ab titration. It is now known that this behaviour is caused by hemagglutinin, one of the main glycoproteins and leading antigenic determinants of the influenza viral envelope, which binds to terminal sialic acids of glycoprotein and glycolipid cell membrane receptors.[8] This interaction, which is driven by a combination of hydrophobic, electrostatic and hydrogen bonds, counteracts the repulsion imposed normally between individual RBCs by the negative charges of the sialylated proteins, producing RBCs agglutination.[9] The list of pathogens possessing hemagglutinin-like proteins that could be studied by HA and HAI was soon extended to embrace coronaviruses, paramyxoviruses, adenoviruses, enteroviruses, reoviruses, myxoviruses, poxviruses and flaviviruses (causing cold, rubella, measles, smallpox, Newcastle disease and Dengue), and some strains of *Escherichia coli*, *Salmonella*, *Vibrio*, *Pseudomonas*, *Haemophilus*, *Bacillus*, *Brucella*, *Corynebacterium diphtheria*, *Clostridium botulinum* and *Clostridium septicum* bacteria (producing food-poisoning, diphtheria, botulism and gas gangrene, among others).[10,11] Besides, carbohydrate-binding lectins exist in plants and animals and have been involved in physiological processes such as cell adhesion, migration, proliferation, apoptosis and differentiation, playing key roles in tumour cell metastasis, autoimmune diseases, inflammation, and atherosclerosis.[12]

HA assays are performed in microtiter plates by mixing dilutions of virus-containing samples with a fixed amount of RBCs.[13] For HAI, a fixed amount of virus is preincubated with a dilution series of the n-Ab-containing sample, which is followed by the addition of the RBCs. In both cases, the mixtures and then incubated for 30-60 min, depending on the RBC type, and cell sedimentation is interpreted by visual examination. RBCs alone settle to the bottom of the wells forming defined red buttons (for nucleated avian RBCs) or halos (for anucleated mammalian RBCs) (**Scheme 1**).

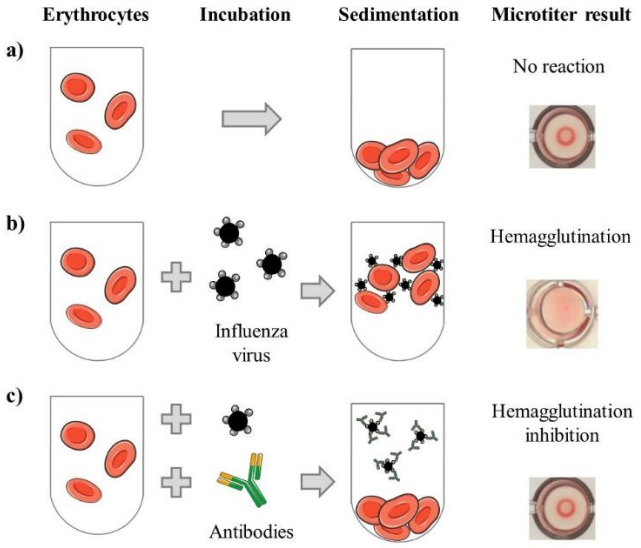

Scheme 1. Classical HA and HAI tests. a) RBCs sediment over time due to gravity, producing characteristic sedimentation patterns in the wells of a microtiter plate. b) In HA, hemagglutinating agents, such as influenza viruses, bind to the RBCs, producing agglutination and altering RBCs sedimentation. c) In HAI, the presence of virus n-Ab produces inhibition of RBC agglutination.

In contrast, agglutinated RBCs form a 3D network or lattice structure that gives the solution a cloudy or turbulent appearance. The experimentalist identifies the wells showing the transition from agglutinated to non-agglutinated RBCs, and the activity of the analyte is expressed as the lowest dilution that causes complete agglutination or agglutination inhibition.

HA and HAI are relatively simple and inexpensive, do not require sophisticated facilities or equipment, generate results in hours and have been improved at many levels, including handling automation and result objectivization through image data analysis.[14–16] However, these methods have to be carried out on fresh erythrocytes, a biological reagent that is variable, displays short half-life (<2 weeks), and is hard to mass-produce for its global distribution. This places RBCs as the main source of variability of HA and HAI.[17] Some authors have suggested alternatives to this classical method. For example, Zheng and coworkers used glycan-functionalized gold nanoparticles to produce an agglutination method for influenza identification.[18] In a different approach, Horiguchi *et al*. detected influenza virus using gold electrodes modified with sialic acid receptors and either a quartz crystal microbalance or an electrochemical sensor.[19] Nevertheless, implementing a completely different method to substitute HA and HAI worldwide faces the resiliency of the National Health Systems. In the case of influenza surveillance, this would require providing appropriate training and measuring equipment to all the laboratories of the global network as well, which would be expensive.

In this work, we developed *synthrocytes*, a synthetic reagent that could mimic erythrocytes in HA and HAI. We took as a model the methods employed for worldwide influenza surveillance, in which the lack of a standard reagent has global consequences. To carry out this task, the WHO distributes to the requesting centres (through the International Reagent Resource, IRR, established by the CDC, Atlanta, USA), a kit that includes most of the reagents needed for influenza HAI typing, subtyping and antigenic characterization. However, this kit does not contain the RBCs, which are acquired by each of the centres of the global surveillance network by its own means. This introduces high intra- and inter-laboratory variability when generating results that must be analysed globally.[17]

The idea of producing synthetic RBCs is not new and has been pursued as the holy grail of materials science.[20] However, previous attempts envisioned the fabrication of an artificial material that could fully mimic the broad properties of native human RBCs: size, biconcave shape, deformability, oxygen-carrying capacity, and long circulation time. Designed mostly as drug delivery carriers, these examples entailed micro- and nano-scale processing steps that are too complex and expensive to fabricate a high-throughput laboratory reagent for HAI.[21–23] Here, we explore a simpler and cheaper alternative to develop synthrocytes able to fit the main HAI requirement. This is, generation of differential sedimentation patterns in the presence and absence of agglutinating agents, which could be visually interpreted in <1 h. Taking into account that avian RBCs are also used in HAI and are spherical nucleated cells, we evaluated as the starting material spherical microparticles of different materials, size and surface properties. Those exhibiting different sedimentation when agglutinated or not were then chemically modified with influenza-binding sialylated receptors. Upon optimization of the production and assay conditions, the resulting synthetic reagent was used in a HAI-like assay to detect the reference strains provided by the WHO for influenza surveillance. As it will be shown, synthrocytes recognize influenza A(H1N1) and B viruses faster than native RBCs and are more stable. These results show that RBCs could be substituted in HAI by a synthetic reagent, which would be potentially tuneable, mass-produced for global distribution, and used without altering the established methodology.

EXPERIMENTAL SECTION

Reagents. Glutaraldehyde, 4-Morpholineethanesulfonic acid (MES), N-hydroxysuccinimide (NHS) and bovine serum albumin (BSA) were obtained from Merck (Missouri, USA). 1-ethyl-3-(-3-dimethylaminopropyl) carbodiimide hydrochloride (EDC) and phosphate-buffered saline (PBS; 11.9 mM sodium phosphate, 137 mM NaCl, 2.7 mM KCl, pH 7.4) were from Fisher Scientific (New Hampshire, USA). TRIS Buffered Saline (TBS; 25 mM Tris, 140 mM NaCl, 3.0 mM KCl) was from VWR Life Science.

Twelve types of particles were tested that are summarized in **Table S1**.

Four highly sialylated proteins (glycophorin A (GYPA), bovine mucin (BM), avidin (Av) and porcine mucin (PM)) were tested as potential bioreceptors for influenza binding (**Table S2**). Neutravidin (NeuAv), a deglycosylated protein, was used as a negative control.

Inactivated influenza viruses were provided by Hytest (Turku, Finland), including influenza A(H1N1), strains A/New Caledonia/20/99, A/Solomon Islands/03/06, A/Taiwan/1/86, and A/Beijing/262/95; influenza A(H3N2), strains A/Brisbane/10/07 and A/Panama/2007/99; and influenza B, strain B/Victoria/504/00.

Reference viral antigens and antisera were obtained from the 2018-2019 WHO influenza reagents' kit for identification of influenza isolates through the Influenza Reagent Resource (Influenza Division; WHO collaborating center for the surveillance, epidemiology and control of Influenza; Centers for Disease Control and Prevention, Atlanta, USA). Chicken and guinea pig RBCs were obtained from Innovative Grade US Origin (MI,

USA). Human RBCs were obtained locally from residual samples from anonymized O- individuals and approval from the Ethical Committee was not required.

Characterization of bioreceptor candidates by ELISA. The ability of bioreceptor candidates to recognize different influenza types was assessed by enzyme-linked immunosorbent assay (ELISA; **Fig. S1**). Unless otherwise stated, incubations were performed in 100-µL volumes, for 1 h at 34ºC, and were followed by three consecutive washes with PBS, 0.05% Tween20 (200 µL/well). Briefly, 50 µL/well of bioreceptor was immobilized overnight at 4ºC in a 96-well high–binding plate (Corning, Glendale, USA). The wells were then blocked for 1 h at room temperature (RT) with 200 µL of BSA 1%. Three consecutive incubations, with the corresponding washing steps, followed, the first with a serial dilution of influenza virus for 90 min, the second with primary Ab (Ref. 3AH1, Hytest; diluted 1:10000), and the third with secondary peroxidase-labelled Ab (Ab-HRP, Ref. A9044, Merck; diluted 1:30000). The plate was washed 4 times and was incubated for 20 min with 100 µL/well of substrate solution (3,3′,5,5′-tetramethylbenzidine Liquid Substrate, Supersensitive, TMB; Merck). Stop solution was added (50 µL of 1 M H_2SO_4) and the plate was read at 450 nm.

Determination of beads displaying agglutination-dependent sedimentation. Particle sedimentation was studied using alternatively flat-, U- and V-bottomed 96-well microtiter plates (NUNC). For this, microparticles were washed once with PBS and were serially diluted on plate in PBS with or without a chemical crosslinker. Agglutination of amine bearing particles was induced with bis[sulfosuccinimidyl] suberate (BS3; Thermo Fisher). For the agglutination of carboxyl particles, a mixture of EDC and Poly(ethylene glycol) diamine (Merck) was added. The plate was mixed by pipetting and was incubated for 30 min at RT, while registering the sedimentation pattern every 5 min with a digital camera (Sony G Exmor R 20.4).

Bead chemical modification. The modification of Sicastar-blue particles with sialylated proteins was performed using glutaraldehyde for amine-bearing beads and EDC for carboxylated particles. Unless otherwise stated, all incubations were carried out in Eppendorf tubes, at RT, protected from light, and under end-to-end mixing using a Mini LabRoller rotator (Labnet International, NJ; USA).

For glutaraldehyde cross-linking, 12.5 mg of beads were centrifuged for 3 min at 100 XG, were washed 3 times with PBS, and were incubated in 0.5 mL of 8% glutaraldehyde for 30 min. Glutaraldehyde-activated beads were washed twice with PBS and were incubated for 2 h in 0.5 mL of PBS with 150 µg of sialylated protein at 950 rpm in a thermoshaker (Thermal Shake Lite, VWR). Protein-modified beads were then centrifuged, the supernatant was removed, and the beads were incubated for 30 min with blocking buffer (TBS, 0.5% BSA). The resulting microparticles were washed once more with PBS and were finally stored in PBS, 0.1% BSA, 0.1% of sodium azide at 4ºC.

For EDC conjugation, 25 mg of COOH-beads were washed twice with 1 mL of MES 0.5 M and were incubated in 500 µL of MES, 20 mM EDC, 69 mM NHS for 45 min. EDC-activated particles were washed once with PBS and were incubated for 3 h with 200 µg of sialylated protein in PBS. After washing once with PBS, the beads were incubated in 1 mL of blocking buffer for 30 min. Finally, the conjugated beads were washed 3 times with PBS and were stored as above. Modified beads were counted with a Neubauer chamber and adjusted to a final concentration of ~$1.1x10^8$ or ~$9.5x10^8$ beads/mL for 10-µm and 5-µm particles, respectively.

Bead agglutination assays. Three lectins displaying different affinity for sialic acids were used as models to simulate virus-induced agglutination. Wheat germ agglutinin from *Triticum vulgaris* (WGA) has affinity mainly for N-acetyl-β-D-glucosamine oligomers, although it also recognizes Neu5Ac. Lectin from *Sambuccus nigra* (SNA) interacts mostly with Neu5Acα2-6Gal(NAc), the same receptor as human influenza viruses. Lectin from *Maackia amurensis* (MAA) interacts mostly with Neu5Acα2-3Gal(Nac), a similar receptor than avian influenza viruses.[24] For the assay, lectin 10-fold dilutions were pipetted in a 96-well plate (50 µL/well in PBS) and modified beads were added (50 µL/well, containing 7.5 µL of bead stock solution and 42.5 µL of PBS). The plate was mixed by pipetting and was incubated for 15 min for sedimentation evaluation.

For influenza-mediated agglutination, virus dilutions were incubated on plate (50 µL/well in PBS) for 15 min with 10-µm conjugated microparticles (7.5 µL of stock solution diluted with 42.5 µL of PBS).

Bead agglutination characterization by optical microscopy. In order to confirm lectin- and virus-induced agglutination, 3.5 µL of modified beads were mixed with 25 µL of lectin or virus and were incubated for 5 min on a glass slide. The slide was covered and observed by microscopy (20x) using a Nikon TE2000 microscope.

Agglutination inhibition by n-Ab. Synthrocytes (GYPA-conjugated 10-µm beads) were used to carry out a serological agglutination inhibition assay. Two monoclonal Ab specific for influenza A hemagglutinin were tested, Ab1 and Ab2 (Refs. ABIN1605067 and ABIN284533, respectively; Antibodies online, Aachen, Germany). While Ab1 had been produced against influenza A/NewCaledonia/20/99, Ab2 had been raised against A/Taiwan/1/86.

A/NewCaledonia virus (50 µL/well, 2.5 µg/mL) was added to the wells of a U-bottomed microtiter plate and was incubated for 30 min with 10-fold dilutions of either Ab1 or Ab2. Synthrocytes were then added (30 µL/well of a 1:4 stock dilution prepared in PBS) and sedimentation proceeded for 10 min.

(Hem)agglutination inhibition assay with WHO reference reagents. HAI and HAI-like assays were carried with a fixed amount of virus, usually 4 or 8 hemagglutination units (HAU) per well for RBCs and synthrocytes, respectively, which were determined by titrating each viral isolate for each RBC/synthrocyte preparation according to the WHO standards.[4] For this, 2-fold serial dilutions of each virus (50 µL/well) were mixed in the wells of a microtiter plate with 50 µL of RBCs (washed 4 times with PBS and resuspended in PBS to a final concentration of 0.75% prior to use) or synthrocytes ($8.25x10^5$ beads) in PBS. These mixtures were then incubated for 60 (human or guinea pig RBCs), 30 (chicken RBCs) or 10 min (synthrocytes). The highest dilution of virus showing complete (hema)agglutination was considered 1 HAU.

Antisera provided by WHO were pre-treated with receptor destroying enzyme (RDE, Ref. C8772, Merck) as described in [4]. Two-fold serial dilutions of each serum (25 µL/well) were mixed with 4 or 8 HAU of the corresponding virus (in 25 µL of PBS) and the plates were incubated for 30 min at RT. Then, 50 µL of RBCs (0.75%) or synthrocytes ($6.05x10^5$ beads) were added and incubated for 60 or 10 min, respectively. The HAI titter was the reciprocal of the highest serum dilution at which the agglutination was inhibited.

RESULTS AND DISCUSSION

The objective of this work was the production of *synthrocytes*, a synthetic reagent that could substitute animal RBCs in the HAI assays currently used for, among others, influenza monitoring. Synthrocyte development included 4 main work packages that were completed over time. First, the identification of commercial beads displaying different sedimentation patterns when agglutinated or not. Second, the selection of potential bioreceptors for influenza binding. Third, the production of bioreceptor-modified beads exhibiting sedimentation changes upon influenza binding. And fourth, the evaluation of these modified beads in HAI-like assays.

Identification of beads displaying agglutination-dependent sedimentation. Particle sedimentation in a given liquid is mainly affected by three factors, particle size, shape and density.[25] In the case of RBCs, surface charge has been also shown to be crucial for HA and HAI to occur.[9] Here, work started with the study of a battery of commercial microparticles displaying a range of sizes and densities (Table S1). The objective was to identify beads able to produce different sedimentation patterns when free or agglutinated. For this, beads displaying on surface amino or carboxyl groups were serially diluted in PBS with/without a chemical cross-linker and were allowed to settle down in the wells of a microtiter plate (**Figures 1a and S2**).

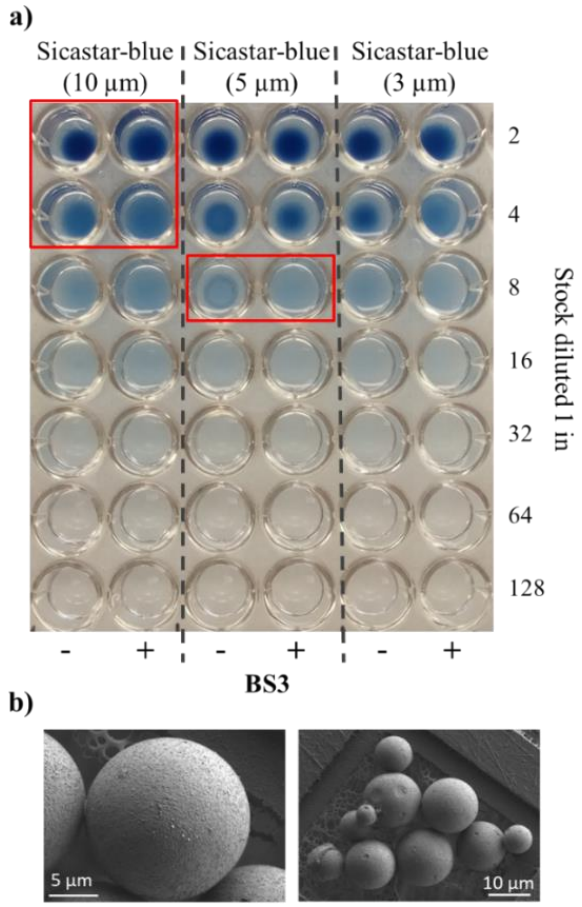

Figure 1. a) Sedimentation of 3 types of beads displaying amino groups on surface. Beads were serially diluted with PBS in the absence (-) or presence (+) of a chemical agglutinating agent (BS3 2.5 mM) and were allowed to settle down in U-shaped wells. Red squares highlight the changes in sedimentation observed. b) SEM images of Sycastar-blue (10 µm) particles.

Only two of the beads studied changed their sedimentation pattern upon agglutination, Sicastar-blue 5- and 10-µm in diameter (**Figure 1b**). These were spherical particles made of silica that exhibited a density of 1.8 g/ccm, which placed them close to the characteristics of human RBCs (6–8 µm in diameter and a density of 1.1 g/ccm). In the absence of any agglutinating agent, a dilution 1:8 of the 5-µm Sicastar-blue stock (equivalent to 625 µg/well) sedimented forming a halo at the bottom of the well. The presence of the chemical crosslinker prevented bead sedimentation and the solution remained turbulent. The 10-µm Sicastar-blue beads showed also a tight sediment when non-agglutinated, but only for dilutions 1:2 and 1:4 (equivalent to 1.25 and 2.5 mg/well).

Sicastar-blue 5- and 10-µm beads were additionally tested in 3 types of microtiter plates, which had flat-, U- or V-bottomed wells (**Fig. S3**). The difference in sedimentation between agglutinated and non-agglutinated 5-µm beads was only evident at U-shaped wells, in which they formed a ring. In the case of the 10-µm beads, their sedimentation changed upon agglutination both in U- and V-shaped wells, but the assay was more sensitive in U-wells. No distinction could be made in flat-bottomed plates. This result was unexpected, because spherical avian RBCs use to produce more sensitive HAI assays in V-shaped plates, while discoidal human RBCs work better in U-shaped plates, suggesting that shape is not the origin of this difference.

Selection of influenza-binding bioreceptors. Influenza interacts with RBCs through the hemagglutinin of the viral envelop, which binds the sialic acids exposed on RBC surface. Avian and mammalian viruses recognize preferentially sialic acids interacting with galactose residues through α(2→3) and α(2→6) bounds, respectively.[8] Here, we studied the ability of 4 proteins that are known to be highly sialylated to bind influenza viruses (Table S2). A deglycosylated protein, NeuAv, was used in parallel as the negative control. A sandwich ELISA was optimized for this purpose, in which each bioreceptor candidate was immobilised on surface, followed by blocking to prevent non-specific adsorption, incubation with the virus, and indirect immunodetection (**Fig. S1 and S4**).

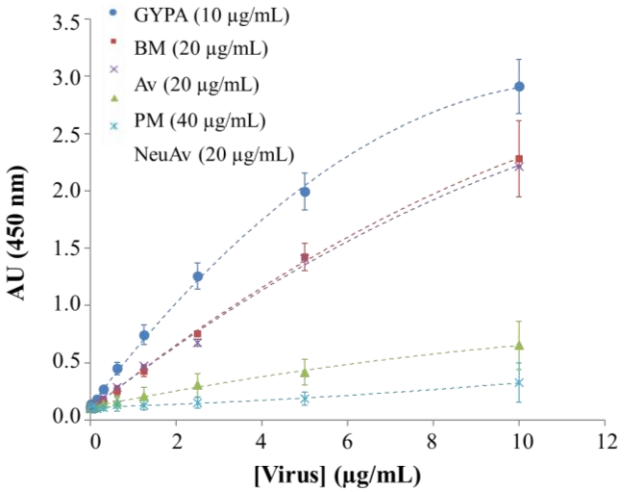

Figure 2. Binding of influenza A(H1N1) A/NewCaledonia/20/99 by 5 different bioreceptor candidates. ELISA in which each candidate was immobilized on surface (optimal concentration in brackets; optimization in Figure S4), followed by incubation with increasing concentrations of influenza A(H1N1) and indirect immunodetection.

As it can be observed, in the presence of influenza A(H1N1), the signals registered for GYPA, BM and Av were proportional to the concentration of virus, showing that the 3 proteins bound it (**Fig. 2 and S5a**). In contrast, PM (that displayed a lower sialic acid content) and NeuAv (which is deglycosylated) provided no binding at all. The best response was observed for GYPA, which provided the highest signals registered at a lower concentration (10 µg/mL of GYPA on plate). This is consistent with reports that indicate that GYPA has a carbohydrate content ranging 40-80%[26] and accounts for 75% of the total sialic acid exhibited on the RBCs membrane.[27,28] Similar trends were observed for the 4 strains of influenza A(H1N1) tested (A/New Caledonia/20/99; A/Solomon Islands/03/06; A/Taiwan/1/86; and A/Beijing/262/95), a certain degree of binding was observed for influenza B, but none of the proteins evaluated recognized influenza A(H3N2). Virus binding was efficient at RT and only improved slightly at 34°C for high virus concentrations (**Fig. S5b**). On the other hand, binding was fast and occurred in about 30 min, but ameliorated if the incubation was extended to 90 min, especially for high virus loads (**Fig. S5c**).

Production of sialylated beads and behaviour after lectin-mediated agglutination. Sicastar-blue beads, 5- and 10-µm in diameter, were next employed to produce sialylated beads. For this, each bioreceptor candidate (PM, BM, GYPA and Av) was chemically conjugated to beads displaying on surface amino or carboxyl groups, using glutaraldehyde or EDC, respectively. The modification protocol finished with extensive washing and a blocking step in order to remove poorly bound molecules, inactivate any remaining crosslinker reactive groups, cover the beads' surface, and prevent subsequent non-specific binding.

PM-, BM- and GYPA-particles sedimented in PBS pH 7.4 forming evident pellets (**Fig. 3 and S6**). In contrast, Av-particles did not settle down under similar conditions. This was attributed to the isoelectric point (Ip) of the conjugated protein (Ip of 10-10.5 for Av; 3-4 for mucins; and approximately 6 for GYPA). Accordingly, the beads sedimented only in buffers of pH higher than the Ip of the surface-displayed sialylated protein, when they were negatively charged (**Fig. S7**). This behaviour reminded RBCs, in which membrane sialylated glycoproteins are negatively charged at neutral pH, producing repulsion between individual RBCs and preventing their agglutination.[9] In this context, Av-conjugated particles would not be useful for virus detection, which is performed at neutral pH.

The difference in sedimentation between free and agglutinated beads was next studied. A fixed concentration of modified beads was allowed to settle down for 10 min in the presence or in the absence of an agglutinating protein. Three plant lectins were used for this purpose, SNA, WGA and MAA, which had different carbohydrate-binding tropism. In all cases, the presence of increasing concentrations of lectin prevented bead sedimentation (**Fig. 3a, Fig. S6, Video 1**). This change was lectin-dependent, demonstrating that it was induced by lectin binding and not randomly. For instance, while GYPA-beads detected lower concentrations of SNA, the beads modified with BM and PM were more sensitive for WGA (**Fig. 3b**). A similar pattern was observed for 5- and 10-µm particles, but bigger particles seemed more sensitive and detected lectin concentrations 10 times lower (**Fig S6**). On the other hand, bead size had a profound effect in sedimentation speed, with bigger beads sedimenting faster (**Fig. S8**).

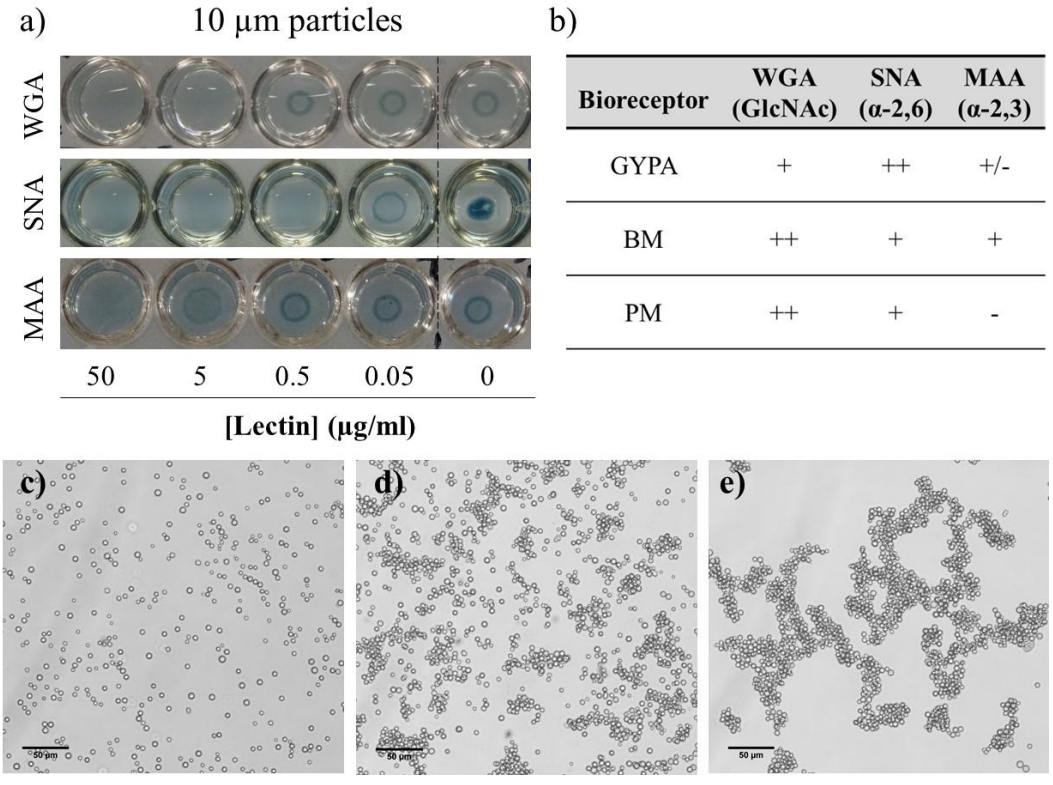

Bioreceptor	WGA (GlcNAc)	SNA (α-2,6)	MAA (α-2,3)
GYPA	+	++	+/-
BM	++	+	+
PM	++	+	-

Figure 3. a) Sedimentation of 10-µm GYPA-beads in the presence of three different lectins, WGA, SNA and MAA ($8.25x10^5$ beads per U-shaped well). b) Response of 10-µm particles displaying on surface PM, BM or GYPA for the different lectins. c-e) Microscopic images of BM-conjugated 10-µm particles incubated in PBS (c), 1 µg/mL (d) and 10 µg/mL of WGA (e).

The microscopic characterization revealed that, while the beads alone remained individualized in PBS, the presence of lectin resulted in the formation of aggregates (**Fig. 3c-e**). The size of these aggregates increased proportionally to the concentration of lectin, confirming that the changes in sedimentation correlated to lectin-mediated agglutination. While carboxylated beads conjugated using EDC were lighter in colour and produced wide ring-like sediments, amine-beads conjugated through glutaraldehyde chemistry had a darker colour and generated tighter pellets that were easier to interpret (**Fig. S9**). Other parameters that affected the performance of sialylated beads were the amount of protein used for bead modification (**Fig. S9**), the type of agitation imposed during conjugation (**Fig. S10a**), the volume of the conjugation reaction (**Fig. S10b**), and the number of beads per well (**Fig. S10c**).

Behaviour of sialylated beads in the presence of influenza virus. The results obtained indicated that GYPA- and BM-conjugated 10-µm particles were the best candidates for influenza virus detection. First, GYPA and BM recognized influenza A(H1N1) efficiently by ELISA. Second, GPYA- and BM-beads formed evident sediments at pH 7.4 and changed their sedimentation after lectin-agglutination. Finally, 10-µm particles were in general more sensitive than 5-µm beads.

As shown in **Figure 4a** and Video 2 (Supplementary material), GYPA-particles changed their sedimentation pattern in the presence of A(H1N1) virus. This behaviour reversed in the presence of high concentrations of free GYPA, which competed for the interaction with influenza and inhibited viral-induced bead agglutination (**Fig. 4b**). In contrast, BM-particles did not change their behaviour in the presence of influenza (**Fig. 4a**). This was attributed to the lower content of sialic acids of BM, which was consistent with reports claiming that a high virus-receptor load is required for RBCs to agglutinate.[29] The microscopy study confirmed that GYPA-beads agglutinated in the presence of influenza (**Fig. 4c-d**), while BM-particles displayed only mild virus-induced agglutination.

In view of these results, 10-µm GYPA-particles were selected to produce synthrocytes. As summarized in **Figure 5a**, synthrocytes recognized different influenza A(H1N1) and B strains, exhibiting a sedimentation pattern similar to animal RBCs, but did not detect influenza A(H3N2). Compared to RBCs, synthrocytes were slightly less sensitive, requiring a higher concentration of virus to produce changes in sedimentation. In contrast, synthrocytes were significantly faster. Whereas RBCs had to be incubated for 30-60 min to display their characteristic sedimentation pattern, synthrocytes provided results in <5 min, which was attributed to their spherical shape and bigger size and density (1.8 g/ccm for 10-µm synthrocytes, compared to 1.1 g/ccm for 6–8 µm human RBC, which are discoidal).[30] Synthrocytes were also more stable and could be used after 3 weeks of storage at 4ºC, while erythrocytes had lost performance after 2 weeks at 4ºC and did not recognize the virus one week later (**Fig. 5b**).

These results indicated that synthrocytes could mimic animal RBCs in classical HA assays, providing a faster readout and expanded lifespan.

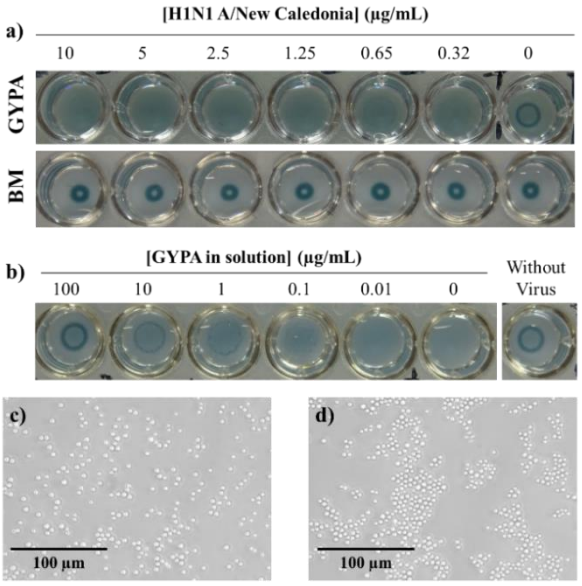

Figure 4. a) Sedimentation of GYPA- and BM-particles in U-shaped wells in the presence of increasing concentrations of influenza A(H1N1). b) Competition assay performed by incubating GYPA-particles with 2.5 µg/mL of A(H1N1) and increasing concentrations of free GYPA. c-d) Microscopic images of GYPA-particles incubated in PBS (c) or 5 µg/mL of A(H1N1) virus (d).

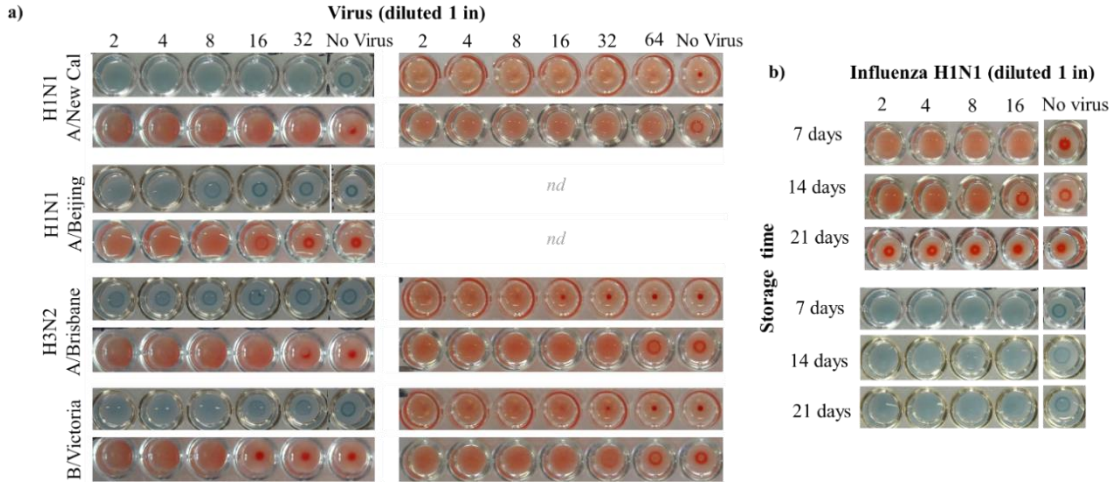

Figure 5. a) Sedimentation of synthrocytes and RBCs from (clockwise for each virus strain) chicken, guinea pig and human in the presence of increasing dilutions of A(H1N1). Changes were visually observable after 60 (human and guinea pig), 30 (chicken) or 5 min (synthrocytes) of incubation. *nd* stands for not determined. b) Performance of RBCs (left) and synthrocytes (right) after storage at 4ºC.

Agglutination inhibition assays using synthrocytes. We finally investigated if synthrocytes would be useful for the optimization of HAI-like assays. Two commercial n-Ab were employed for this purpose. Both n-Ab were specific for influenza A(H1N1) viruses and one of them had been raised against A/New Caledonia/20/99. In these experiments, a fixed amount of A(H1N1) A/New Caledonia/20/99 virus was incubated for 30 min in the wells of a plate with increasing concentrations of n-Ab. Synthrocytes were then added and their sedimentation pattern was studied over time. **Figure 6a** shows that virus-induced agglutination was abolished by concentrations of n-Ab higher than 1 μg/mL, producing synthrocyte sedimentation. As expected, this effect was more pronounced for Ab1, which had been raised specifically for the virus strain that was used in these experiments and displayed higher affinity for it.

Synthrocytes were next tested with the reference reagents included in the kit provided by the WHO for influenza surveillance (season 2018-2019). This kit contained 4 inactivated viral strains (A(H1N1)pdm09 A/Michigan/45/2015 NYMC X-275; A(H3N2) A/Singapore/INFIMH-16-0019/2016; Influenza B/Yamagata lineage B/Phuket/3073/2013; and B/Victoria lineage B/Colorado/06/2017), 4 antisera raised against these 4 strains, and a negative control serum.

The 4 influenza strains were first titrated to determine the virus dilution needed to perform agglutination inhibition assays (equivalent to 4 and 8 HAU for RBCs and synthrocytes). Synthrocytes were able to recognize all the reference isolates except A(H3N2) A/Singapore, which was also poorly recognized by human RBCs (**Fig. S11**). HAI and HAI-like assays were finally carried out using a fixed amount of virus and a dilution series of the corresponding positive and negative control kit antisera. As shown in **Figure 6b**, the presence of n-Ab specific against a viral strain prevented its binding to both RBCs and synthrocytes, inhibiting their agglutination. On the contrary, the incubation with the negative control antisera, which did not contain specific n-Ab, did not prevent agglutination. As before, synthrocytes were less sensitive than RBCs, but still displayed differential sedimentation in the presence of positive and negative antisera. These results confirmed that synthrocytes could be used to mimic RBCs in HAI-like assays.

CONCLUSIONS

As noted before, HA and HAI are classical methods that have been used for decades and are still in use. Their relative simplicity and the fact that they are operated with minimal equipment and technical requirements has perpetuated their use worldwide. Nevertheless, having to employ fresh erythrocytes imposes to these methods a high level of variability and faces also the increasing ethical and safety concerns raised by the use of animal-derived products. This is remarkable if we take into account that these are the WHO reference methods for the antigenic characterization of circulating influenza viruses and for the titration of specific n-Ab against them, two tasks crucial to determine the annual reformulation of the flu vaccine.

In this work we developed synthrocytes, a synthetic reagent that is able to bind to influenza A(H1N1) and B viruses, mimicking RBCs in classical HA assays. This interaction triggers synthrocytes' agglutination, producing changes in the sedimentation pattern that can be observed by the naked eye in less than 5 min, and that resemble those generated by animal RBCs in 30-60 min. Furthermore, the interaction between synthrocytes and influenza can be inhibited by specific n-Ab, which allows performing HAI-like assays for antigenic characterization and serological studies. This has been demonstrated here by carrying HAI-like assays using synthrocytes and the reference reagents provided by the WHO for influenza surveillance.

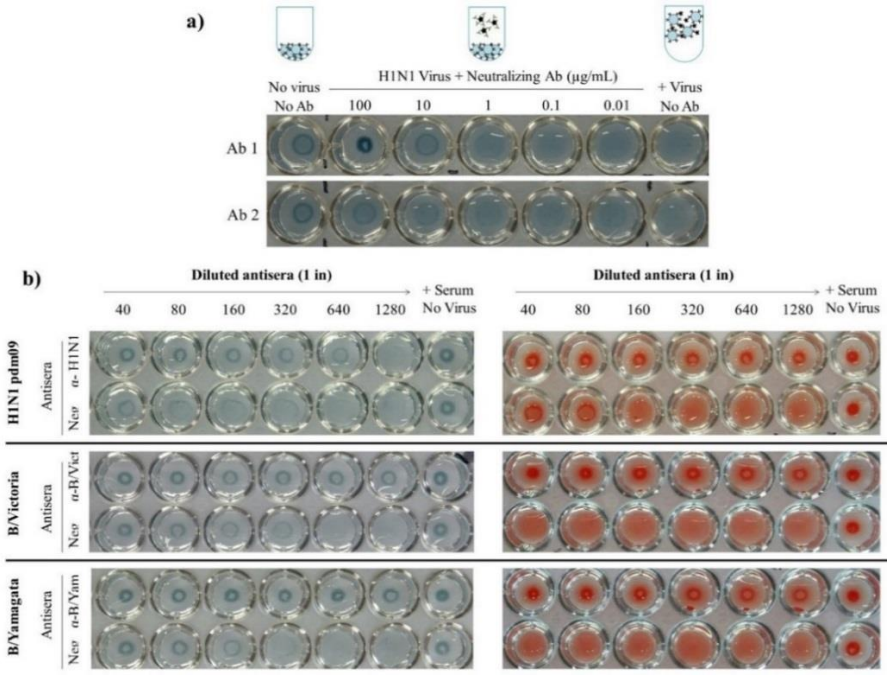

Figure 6. a) Agglutination inhibition assay in the presence of increasing concentrations of two neutralizing Ab (Ab1 and Ab2). Each well contained 2.5 μg/mL of A(H1N1) A/New Caledonia/20/99 virus and 8.25×10^5 synthrocytes. **b)** Agglutination inhibition assay performed with synthrocytes (left, 5 min) or human RBCs (right, 60 min), using WHO reference viruses and antisera.

Although sensitivity, selectivity and stability should be improved, these results demonstrate that it is possible to substitute RBCs in the HA and HAI assays currently used for, among others, global influenza surveillance. Compared to RBCs, a synthetic reagent would display a number of advantages. Synthrocytes produce results significantly faster. Production of a synthetic reagent is compatible with the customized incorporation of selected bioreceptors and surface fine-tuning, which would impart specificity and prevent the unwanted non-specific interactions displayed by native RBCs. Finally, a synthetic reagent could be also mass-produced and stabilized for global distribution, which would facilitate the standardization of HAI-like methods worldwide, providing enhanced tools for pathogen surveillance and vaccine evaluation.

ASSOCIATED CONTENT

Supporting Information

Methodology and description of particle and bioreceptor candidates tested. Results of bead bioengineering optimization. Results of the titration of WHO antigens. Videos showing synthrocyte sedimentation in the absence and in the presence of agglutinating agents.

AUTHOR INFORMATION

Corresponding Author

* E-mail: eva.baldrich@vhir.org.

ORCID.

E. Baldrich: 0000-0003-1393-215X. A. Anton: 0000-0002-1476-0815. J.R. Herance: 0000-0001-7178-3290. T. Pumarola: 0000-0002-5171-7461.

ACKNOWLEDGMENT

Work funded by the Spanish Ministry of Economy (BIO2015-72401-EXP) and Instituto de Salud Carlos III (CPII18/00025 and IFI18/00020, cofinanced by the European Regional Development Fund). Diagnostic Nanotools is a Consolidated Group of Secretaria d'Universitats i Recerca, Generalitat de Catalunya (2017 SGR 240).

REFERENCES

(1) Trombetta, C. M.; Perini, D.; Mather, S.; Temperton, N.; Montomoli, E. Overview of Serological Techniques for Influenza Vaccine Evaluation: Past, Present and Future. *Vaccines* **2014**, *2*, 707–734.

(2) Kumar, S.; Henrickson, K. J. Update on Influenza Diagnostics: Lessons from the Novel H1N1 Influenza A Pandemic. *Clinical Microbiology Reviews* **2012**, *25*, 344–361.

(3) Katz, J. M.; Hancock, K.; Xu, X. Serologic Assays for Influenza Surveillance, Diagnosis and Vaccine Evaluation. *Expert Review of Anti-Infective Therapy* **2011**, *9*, 669–683.

(4) World Health Organization. WHO Global Influenza Surveillance Network Manual for the Laboratory Diagnosis and Virological Surveillance of Influenza; **2011**.

(5) Trucchi, C.; Paganino, C.; Amicizia, D.; Orsi, A.; Tisa, V.; Piazza, M. F.; Icardi, G.; Ansaldi, F. Universal Influenza Virus Vaccines: What Needs to Happen Next? *Expert Opinion on Biological Therapy* **2019**, *19*, 671–683.

(6) Yamayoshi, S.; Kawaoka, Y. Current and Future Influenza Vaccines. *Nature Medicine* **2019**, *25*, 212–220.

(7) Hirst, G. K. The Quantitative Determination of Influenza Virus and Antibodies by Means of Red Cell Agglutination. *J. Exp. Med.* **1942**, *75*, 49–64.

(8) De Graaf, M.; Fouchier, R. A. M. Role of Receptor Binding Specificity in Influenza A Virus Transmission and Pathogenesis. *EMBO Journal*. **2014**, *33*, 823–841.

(9) Fernandes, H. P.; Cesar, C. L.; Barjas-Castro, M. de L. Electrical Properties of the Red Blood Cell Membrane and Immunohematological Investigation. *Rev Bras Hematol Hemoter* **2011**, *33*, 297–301.

(10) Hierholzer, J. C.; Suggs, M. T. Standardized Viral Hemagglutination and Hemagglutination-Inhibition Tests. I. Standardization of Erythrocyte Suspensions. *Appl. Microbiol.* **1969**, *18*, 816–823.

(11) Neter, E. Bacterial Hemagglutination and Hemolysis. *Bacteriol. Rev.* **1956**, *20*, 166–188.

(12) Ghazarian, H.; Idoni, B.; Oppenheimer, S. B. A Glycobiology Review: Carbohydrates, Lectins and Implications in Cancer Therapeutics. *Acta Histochem.* **2011**, *113*, 236–247.

(13) Eisfeld, A. J.; Neumann, G.; Kawaoka, Y. Influenza A Virus Isolation, Culture and Identification. *Nat. Protoc.* **2014**, *9*, 2663–2681.

(14) Nguyen, M.; Fries, K.; Khoury, R.; Zheng, L.; Hu, B.; Hildreth, S. W.; Parkhill, R.; Warren, W. Automated Imaging and Analysis of the Hemagglutination Inhibition Assay. *J. Lab. Autom.* **2016**, *21*, 287–296.

(15) Zacour, M.; Ward, B. J.; Brewer, A.; Tang, P.; Boivin, G.; Li, Y.; Warhuus, M.; McNeil, S. A.; LeBlanc, J. J.; Hatchette, T. F. Standardization of Hemagglutination Inhibition Assay for Influenza Serology Allows for High Reproducibility between Laboratories. *Clin. Vaccine Immunol.* **2016**, *23*, 236–242.

(16) Zhao, W.; Baldwin, E.; Cameron, R. A Digital Data Interpretation Method for Hemagglutination Inhibition Assay by Using a Plate Reader. *Anal. Biochem.* **2019**, *571*, 37–39.

(17) Wood, J. M.; Montomoli, E.; Newman, R. W.; Daas, A.; Buchheit, K. H.; Terao, E. Collaborative Study on Influenza Vaccine Clinical Trial Serology - Part 2: Reproducibility Study. *Pharmeur. Bio Sci. Notes* **2011**, *2011*, 36–54.

(18) Zheng, L.; Wei, J.; Lv, X.; Bi, Y.; Wu, P.; Zhang, Z.; Wang, P.; Liu, R.; Jiang, J.; Cong, H.; *et al*. Detection and Differentiation of Influenza Viruses with Glycan-Functionalized Gold Nanoparticles. *Biosens. Bioelectron.* **2017**, *91*, 46–52.

(19) Horiguchi, Y.; Goda, T.; Matsumoto, A.; Takeuchi, H.; Yamaoka, S.; Miyahara, Y. Direct and Label-Free Influenza Virus Detection Based on Multisite Binding to Sialic Acid Receptors. *Biosens. Bioelectron.* **2017**, *92*, 234–240.

(20) Yang, J.; Wang, F.; Lu, Y.; Qi, J.; Deng, L.; Sousa, F.; Sarmento, B.; Xu, X.; Cui, W. Recent Advance of Erythrocyte-Mimicking Nanovehicles: From Bench to Bedside. *Journal of Controlled Release*. **2019**, *314*, 81–91.

(21) Guo, J.; Agola, J. O.; Serda, R.; Franco, S.; Lei, Q.; Wang, L.; Minster, J.; Croissant, J. G.; Butler, K. S.; Zhu, W.; *et al.* Biomimetic Rebuilding of Multifunctional Red Blood Cells: Modular Design Using Functional Components. *ACS Nano* **2020**, *14*, 7847-7859.

(22) Ou, W.; Nam, K. S.; Park, D. H.; Hwang, J.; Ku, S. K.; Yong, C. S.; Kim, J. O.; Byeon, J. H. Artificial Nanoscale Erythrocytes from Clinically Relevant Compounds for Enhancing Cancer Immunotherapy. *Nano-Micro Lett.* **2020**, *12*, 90.

(23) Doshi, N.; Zahr, A. S.; Bhaskar, S.; Lahann, J.; Mitragotri, S. Red Blood Cell-Mimicking Synthetic Biomaterial Particles. *Proc. Natl. Acad. Sci. U. S. A.* **2009**, *106*, 21495–21499.

(24) Suzuki, Y.; Ito, T.; Suzuki, T.; Holland, R. E.; Chambers, T. M.; Kiso, M.; Ishida, H.; Kawaoka, Y. Sialic Acid Species as a Determinant of the Host Range of Influenza A Viruses. *J. Virol.* **2000**, *74*, 11825–11831.

(25) Chen, J.; Li, J. Prediction of Drag Coefficient and Ultimate Settling Velocity for High-Density Spherical Particles in a Cylindrical Pipe. *Phys. Fluids* **2020**, *32*, 053303.

(26) Tayyab, S.; Qasim, M. A. Biochemistry and Roles of Glycophorin A. *Biochem. Educ.* **1988**, *16*, 63–66.

(27) Marchesi, V. T.; Furthmayr, H.; Tomita, M. The Red Cell Membrane. *Annu. Rev. Biochem.* **1976**, *45*, 667–698.

(28) Aoki, T. A Comprehensive Review of Our Current Understanding of Red Blood Cell (RBC) Glycoproteins. *Membranes (Basel).* **2017**, *7*, 56.

(29) Alves, D.; Curvello, R.; Henderson, E.; Kesarwani, V.; Walker, J. A.; Leguizamon, S. C.; McLiesh, H.; Raghuwanshi, V. S.; Samadian, H.; Wood, E. M.; *et al*. Rapid Gel Card Agglutination Assays for Serological Analysis Following SARS-CoV-2 Infection in Humans. *ACS sensors* **2020**. https://doi.org/10.1021/acssensors.0c01050.

(30) Grover, W. H.; Bryan, A. K.; Diez-Silva, M.; Suresh, S.; Higgins, J. M.; Manalis, S. R. Measuring Single-Cell Density. *Proc. Natl. Acad. Sci. U. S. A.* **2011**, *108*, 10992–10996.

Annex A2

Publications with results not included in this Thesis

1. **Sánchez-Cano A**, Ruiz-Vega G, Vicente-Gómez S, de la Serna E, Sulleiro E, Molina I, Sánchez-Montalvá A, Baldrich E. Development of a Fast Chemiluminescent Magneto-Immunoassay for Sensitive *Plasmodium falciparum* Detection in Whole Blood. *Anal. Chem.* 2021, 93, 37, 12793–12800.

pubs.acs.org/ac Article

Development of a Fast Chemiluminescent Magneto-Immunoassay for Sensitive *Plasmodium falciparum* Detection in Whole Blood

Ana Sánchez-Cano, Gisela Ruiz-Vega,* Sergi Vicente-Gómez, Erica de la Serna, Elena Sulleiro, Israel Molina, Adrián Sánchez-Montalvá, and Eva Baldrich*

Cite This: *Anal. Chem.* 2021, 93, 12793–12800 Read Online

2. Samper IC, **Sánchez-Cano A**, Khamcharoen W, Jang I, Siangproh W, Baldrich E, Geiss BJ, Dandy DS, Henry CS. Electrochemical Capillary-Flow Immunoassay for Detecting Anti-SARS-CoV-2 Nucleocapsid Protein Antibodies at the Point of Care. *ACS Sens*. 2021, 6, 11, 4067–4075

pubs.acs.org/acssensors Article

Electrochemical Capillary-Flow Immunoassay for Detecting Anti-SARS-CoV-2 Nucleocapsid Protein Antibodies at the Point of Care

Isabelle C. Samper,♦ Ana Sánchez-Cano,♦ Wisarut Khamcharoen,♦ Ilhoon Jang, Weena Siangproh, Eva Baldrich, Brian J. Geiss, David S. Dandy, and Charles S. Henry*

Cite This: *ACS Sens.* 2021, 6, 4067–4075 Read Online

3. Arias-Alpízar K, **Sánchez-Cano A**, Prat-Trunas J, de la Serna E, Alonso O, Sulleiro E, Sánchez-Montalvá A, Diéguez A, Baldrich E. Malaria quantitative POC testing using magnetic particles, a paper microfluidic device and a hand-held fluorescence reader, Biosens Bioelectron. 2022, 215, 1, 114513

Biosensors and Bioelectronics 215 (2022) 114513

Contents lists available at ScienceDirect

Biosensors and Bioelectronics

journal homepage: www.elsevier.com/locate/bios

Malaria quantitative POC testing using magnetic particles, a paper microfluidic device and a hand-held fluorescence reader

K. Arias-Alpízar [a,b], A. Sánchez-Cano [a,b], J. Prat-Trunas [a], E. de la Serna Serna [a], O. Alonso [c,g], E. Sulleiro [b,d,e], A. Sánchez-Montalvá [b,e,f], A. Diéguez [c,g], E. Baldrich [a,e,*]

4. Arias-Alpízar K, **Sánchez-Cano A**, Prat-Trunas J, Sulleiro E, Bosch-Nicolau P, Salvador F, Oliveira I, Molina I, Sánchez-Montalvá A, Baldrich E. Magnetic Bead Handling Using a Paper-Based Device for Quantitative Point-of-Care Testing. *Biosensors*. 2022, 12, 9, 680.

biosensors

MDPI

Article

Magnetic Bead Handling Using a Paper-Based Device for Quantitative Point-of-Care Testing

Kevin Arias-Alpízar [1,2], Ana Sánchez-Cano [1,2], Judit Prat-Trunas [1], Elena Sulleiro [2,3,4], Pau Bosch-Nicolau [3,4], Fernando Salvador [3,4], Inés Oliveira [3,4], Israel Molina [3,4], Adrián Sánchez-Montalvá [2,3,4] and Eva Baldrich [1,4,*]

5. de la Serna E, Arias-Alpízar K, Borgheti-Cardoso LN, **Sánchez-Cano A**, Sulleiro E, Zarzuela F, Bosch-Nicolau P, Salvador F, Molina I, Ramírez M, Fernàndez-Busquets X, Sánchez-Montalvá A, Baldrich E. Detection of *Plasmodium falciparum* malaria in 1 h using a simplified enzyme-linked immunosorbent assay, Anal Chim Acta, 2021, 1152, 338254

Analytica Chimica Acta 1152 (2021) 338254

Contents lists available at ScienceDirect

Analytica Chimica Acta

journal homepage: www.elsevier.com/locate/aca

Detection of *Plasmodium falciparum* malaria in 1 h using a simplified enzyme-linked immunosorbent assay

Erica de la Serna [a], Kevin Arias-Alpízar [a, b], Livia Neves Borgheti-Cardoso [c, d], Ana Sanchez-Cano [a, b], Elena Sulleiro [b, e, f], Francesc Zarzuela [e, f], Pau Bosch-Nicolau [f, g], Fernando Salvador [f, g], Israel Molina [f, g], Miriam Ramírez [d], Xavier Fernàndez-Busquets [c, d, h], Adrián Sánchez-Montalvá [b, f, g], Eva Baldrich [a, i, *]